The Flux and Dissipation of Energy in the LET Theory of Turbulence

Matthew Salewski

A thesis submitted in fulfilment of the requirements
for the degree of Doctor of Philosophy
to the
University of Edinburgh
2010

Abstract

The first part of this thesis examines and compares the separate closure formalisms of Wyld and Martin, Siggia, and Rose (MSR). The simplicity of Wyld's perturbation scheme is offset by an incorrect renormalisation, this contrasts with the formally exact analysis of MSR. The work here shows that a slight change in Wyld's renormalisation keeps the main results intact and, in doing so, demonstrates that this formalism is equivalent to MSR.

The remainder of the thesis is concerned with turbulent dissipation. A numerical solution of the Local Energy Transfer theory, or LET, is reworked and extended to compute decaying and forced turbulence at large Reynolds numbers. Using this numerical simulation, the phenomenon of turbulent dissipation is investigated.

In order to use decaying turbulence to study the turbulent dissipation rate as a function of Reynolds number, it is necessary to choose an appropriate time with which a measurement can be taken. Using phenomenological arguments of the evolution of a turbulent fluid, criteria for establishing such a time are developed.

An important study in turbulence is the dissipation rate in the limit of vanishing viscosity, also known as the dissipation anomaly. This thesis derives an equation for the dissipation rate from the spectral energy balance equation. Using the LET computation for both decaying and forced turbulence, results are obtained that can be used along with the equation to study the mechanisms behind the dissipation anomaly. It is found that there is a difference in the behaviour of the normalised dissipation rate between decaying and forced turbulence and, for both cases, it is largely controlled by the energy flux.

Declaration

I declare that this thesis was composed by myself and that, except where explicitly stated otherwise in the text, the work contained therein is my own or was carried out in collaboration with Professor W. D. McComb, Dr. Arjun Berera, and Sam Yoffe.

The LET2008 code used for computing the LET was constructed from the LET2000 code created by A. P. Quinn.

All results generated from Direct Numerical Simulation (DNS) found in chapters 3 and 6 were computed by Sam Yoffe.

Some of the results of Chapter 6 were presented at the EUROMECH European Turbulence Conference, ETC 12, 7-10, September 2009.

M. Salewski
August 2010

Acknowledgements

Firstly, i would like to express my appreciation to my supervisors, Professors Arjun Berera and W. David McComb. Prof Berera's kind cheerfulness and keen intellect made working with him very rewarding. The patience and guidance of Prof McComb has had a profound impact on me and has directed me towards better ideals.

Exceptional grattitude is due to Sam Yoffe, who provided the DNS results that appear in this thesis, for the innumerable and invaluable hours spent in discussion about the work we struggled through.

Dr. Alexander Morozov is also due his share of thanks for his advice and mentoring in all things turbulent. His enthusiam and commitment to science i found inspirational in the many discussions we had. I am particularly grateful to him for opening me up to a greater world of turbulence.

I would like to extend my thanks to Professor Yukio Kaneda, for his invitation to visit him at the Newton Institute, and Professor Bruno Eckhardt, for an invitation to visit him and his group in the Philipps-Universität Marburg.

The funding of my PhD was provided by the School of Physics and Astronomy, and i would like to give my thanks to those who granted me this award and afforded me this oppourtunity.

I would like to give special thanks to the administrative staff in the School, especially Jane Patterson for her kind and diligent efforts to help the process of being a postgrad run smoothly.

Contents

List of Figures

Chapter 1

Introduction to Turbulence

1.1 Introduction

Turbulence is claimed to be the last unsolved problem of classical physics [1–3]. This statement is appropriately justified by numerous attempts made over the past century to understand how a simple system such as a near-continuous, incompressible fluid can exhibit such complex behaviours. In addition, the equations used to describe fluid motion are equally complex. The Navier-Stokes equations (NSE) have existed for well over one hundred years, but there has been little in the way of general solutions to these highly nonlinear equations. Questions arise over whether to solve these equations to help understand turbulence, or to solve turbulence to help understand the Navier-Stokes equations.

The extent of turbulence is wide and has applications ranging from human physiology [4–6], to weather and climate modelling [7, 7–9], to aero/hydrodynamic engineering [10–13]. Turbulent phenomena are also found beyond the atmosphere of Earth as the surface of the sun expels turbulent plumes; understanding how these dissipate may aid in predicting how they will affect the earth [14, 15].

The persistence of the Great Red Spot in Jupiter's southern hemisphere, and indeed its entire surface, also illustrates the complex motion of turbulent flows [16]. Beyond the solar system, the stars making up the galaxy swirl in a vortex familiar to scientists studying turbulence. Even cosmological models seeking to understand the dynamics of the early universe have been known to employ turbulence [17, 18], demonstrating its far-reaching extent.

In this introductory chapter, concepts and ideas relevant to the scope of this thesis are presented. Most are well documented and generally accepted in the turbulence community. Further detail can be found in texts that focus on the Navier-Stokes equations [19, 20], fluid motion [21–23], and turbulence [24–28]. At the end of this

chapter, there is an outline of the remaining chapters of the thesis.

1.2 The Dynamical Equations of Fluid Turbulence

The study of fluid motion has a long history and there is a wealth of scientific effort that attests to this [29]. From that endeavour comes such concepts as continuum systems, vector fields, convection, and viscosity which are used to define and describe a fluid. Using these concepts in a first-principles derivation of a fluid and its dynamics [21, 30] is too involved for this present work. Instead, the use of the Navier-Stokes and continuity equations presented here imply these foundations.

1.2.1 The Navier-Stokes Equations

In this thesis, a fluid is described by a velocity vector field that is space- and time-dependent, $\mathbf{u}(\mathbf{x}, t)$. The Navier-Stokes and continuity equations,

$$\frac{\partial}{\partial t}u_\alpha(\mathbf{x},t) + \big(\mathbf{u}(\mathbf{x},t)\cdot\nabla\big)u_\alpha(\mathbf{x},t) \;=\; -\frac{1}{\rho}\big[\nabla p(\mathbf{x},t)\big]_\alpha - \nu\nabla^2 u_\alpha(\mathbf{x},t) + f_\alpha(\mathbf{x},t) \tag{1.1}$$

and

$$\nabla\cdot\big(\rho(\mathbf{x},t)\mathbf{u}(\mathbf{x},t)\big) = 0 \tag{1.2}$$

explain the conservation of momentum and mass of a (flowing) fluid. The first equation connects the rate of change of the fluid at a point in space and time to its being convected by the fluid surrounding it, the pressure forces acting upon it, the viscous strains and stresses applied to it, and other external forces such as gravity or the Coriolis force. The continuity equation demands that the fluid contained within an arbitrary volume depend on the flow into and out-of the volume's boundary. In the case of the present work where the fluid is incompressible, the continuity equation further reduces to

$$\frac{\partial}{\partial \mathrm{x}_\alpha}u_\alpha(\mathbf{x},t) = 0, \tag{1.3}$$

where the mass density is then implied to be a constant. The Einstein summation convention is introduced here and used throughout the thesis.

Of great interest to the study of turbulence is the nonlinear term, $\mathbf{u}\cdot\nabla\mathbf{u}$. This term contains much of the complexity that underlies turbulent motion. Attempts to determine whether solutions mathematically exist for the Navier-Stokes equation have been undermined by this complicated term [19, 20, 31]. Among more pure mathematical open problems, the NSE holds its status as one the Millennium Prizes [32] to be solved.

1.2.2 The Reynolds Number

Of particular importance to turbulence is the comparison of the non-linear and viscous terms. Turbulence is found to occur when the strength of the inertial forces are large compared to those of viscous dissipation, and the Reynolds number provides a measure of this. It is a dimensionless parameter that weighs the inertial forces against the viscous. It can be derived from the NSE by considering dimensionless variables,

$$x^*_\alpha \equiv \frac{1}{l}\mathrm{x}_\alpha, \tag{1.4}$$

$$u^*_\alpha(x,T) \equiv \frac{1}{U}u_\alpha(\mathbf{x},t), \tag{1.5}$$

scaled by reference lengthscale, l, and velocity U (a time scale, T , can be constructed from these $T = l/U$). Using these to scale the pressure, density, and force terms, and then substituting all into the NSE

$$\frac{U^2}{l}\frac{\partial}{\partial T}u^*_\alpha + \frac{U^2}{l}\big(\mathbf{u}^*\cdot\nabla_l\big)u^*_\alpha = -\frac{\rho^* U^2}{\rho^* l}\big[\nabla_l p^*\big]_\alpha - \frac{\nu U}{l^2}\nabla^2_l u^*_\alpha + \frac{U^2}{l}f^*_\alpha, \tag{1.6}$$

which simplifies to

$$\frac{\partial}{\partial T}u^*_\alpha + \big(\mathbf{u}^*\cdot\nabla_l\big)u^*_\alpha = -\big[\nabla_l p^*\big]_\alpha - \left(\frac{\nu}{Ul}\right)\nabla^2_l u^*_\alpha + f^*_\alpha. \tag{1.7}$$

Considering the ratio of dimensionless inertial and viscous terms gives

$$\frac{\big(\mathbf{u}^*\cdot\nabla_l\big)u^*_\alpha}{\nabla^2_l u^*_\alpha} = \frac{Ul}{\nu}, \tag{1.8}$$

which is the Reynolds number, R. When the Reynolds number is large, which can typically be made to occur by increasing the (mean) velocity or decreasing the viscosity, the inertial interactions are much stronger than the dissipative, and turbulent motion ensues.

A final word about the lengthscales commonly used for the Reynolds number. For the turbulence considered in this reseach, there are two lengthscales that are used in for the Reynolds numbers, the integral lengthscale, L, and the Taylor lengthscale λ. The integral lengthscale gives the scale at which energy is injected into a flow, for example the diameter of a pipe or the size of a grid. The Taylor lengthscale, or Taylor microscale, is an estimate of the largest eddy to be affected by viscosity. Reynolds

numbers defined by these quantities will be denoted with relevant subscripts:

$$R_L \equiv \frac{UL}{\nu}, \tag{1.9}$$

and

$$R_\lambda \equiv \frac{U\lambda}{\nu}. \tag{1.10}$$

These will be referred to here as the Integral-lengthscale Reynolds and Taylor-Reynolds numbers, respectively.

1.2.3 Statistical Methods and Turbulence

The intractability of the NSE or the inherent complexity of turbulent fluid motion does not preclude advances in understanding either. As a tool for furthering understanding, statistical methods are used to decipher fluid motion. One could argue that theoretical description, like experimental description, must also employ statistics to make connections between prediction and realisation.

However, the nonlinearity contained in the NSE leads to additional problems. To illustrate this, one can consider the time evolution of the mean velocity field, given here in schematic form

$$\Big(\partial_t + \nu\nabla^2\Big)\big\langle U\big\rangle = -\nabla\cdot\Big(\big\langle UU\big\rangle\Big) - \nabla\langle P\rangle \tag{1.11}$$

The correlation of two velocity fields, where $\langle\cdots\rangle$ is used to denote averages, gives the connection to the average kinetic energy contained in a turbulent fluid in a domain $\mathcal{V}$

$$\int_{\mathcal{V}} d\mathbf{x}\; tr\big\{\big\langle \mathbf{u}(\mathbf{x},t)\otimes\mathbf{u}(\mathbf{x},t)\big\rangle\big\} \propto \mathrm{u}(t)^2 \propto E(t). \tag{1.12}$$

The notation $tr\{\cdots\}$ denotes the trace over vector indices. This shows that knowledge of the correlation of three velocity fields is needed,

$$\Big(\partial_t + \nu\nabla^2\Big)\big\langle UU\big\rangle \;=\; -\nabla\cdot\Big(\big\langle UUU\big\rangle\Big) - \nabla\langle PU\rangle. \tag{1.13}$$

This is an example of the so-called closure problem where statistical quantities of a given order are dependent on quantities of higher order,

$$\Big(\partial_t + \nu\nabla^2\Big)\big\langle U^n\big\rangle \;=\; -\nabla\cdot\Big(\big\langle U^{n+1}\big\rangle\Big) - \nabla\big\langle P(U^{n-1})\big\rangle. \tag{1.14}$$

Unless additional equations are introduced that can make approximate connections between low- and high-order correlations, this open set of equations offers little in the way of a solution.

1.2.4 Homogeneous Isotropic Turbulence

A quote from Sir S. F. Edwards referring to the use of homogeneous isotropic turbulence [33] reads,

> The problem of understanding the statistical dynamics of turbulence is a difficult one for many reasons. It is reasonable to study the problem under the simplest non-trivial conditions and enquire whether if, under any physically possible conditions, solutions describing the statistical distribution of fluid velocities of a turbulent system can be obtained, even if by 'physically possible' one may mean situations which, though conceivable, are not obtainable in a laboratory.

Idealisations are ubiquitous in science; the study of turbulence is no different. Homogeneous Isotropic Turbulence (HIT), gives a turbulent velocity field in an infinite, or periodic, domain free of boundary conditions. Such a system allows major simplifications to the NSE with reasonable returns.

The use of homogeneity and isotropy bring some constraints to the NSE that allow for some simplifications to be made on statistical quantities of interest.

The 2-point, 2-time correlation tensor,

$$\begin{aligned} C_{\alpha\beta}(\mathbf{x},\mathbf{x}';t,t') &\equiv \left\langle u_\alpha(\mathbf{x},t)u_\beta(\mathbf{x}',t')\right\rangle \\ &= \left\langle u_\alpha(\mathbf{x},t)u_\beta(\mathbf{x}+\mathbf{r},t')\right\rangle \end{aligned} \tag{1.15}$$

for a (statistically) homogeneous turbulent environment becomes a function only of the separation vector, $\mathbf{r}$ as the velocity-components are invariant to their position in space. Adding to it the constraint of isotropy gives the correlation tensor invariance under rotation and reflection operations. The combination of these allows a decoupling of the tensors from the correlation, leaving a scalar function of the separation distance multiplied by a general isotropic tensor $P_{\alpha\beta}(\mathbf{r})$,

$$\begin{aligned} \left\langle u_\alpha(\mathbf{x},t)u_\beta(\mathbf{x}',t')\right\rangle &= C(\mathrm{r};t,t')\Big(\delta_{\alpha\beta}-\frac{\mathrm{r}_\alpha\mathrm{r}_\beta}{\mathrm{r}^2}\Big) \\ &= C(\mathrm{r};t,t')P_{\alpha\beta}(\mathbf{r}). \end{aligned} \tag{1.16}$$

This, and its wave-vector analogue, is found in many calculations considering isotropic turbulence.

Time Dependence in Turbulence

Levying a further constraint of stationarity, taking the NSE and statistical quantities to be independent of time, additionally simplifies the equations. However, the viscous

forces remove energy from the fluid and this drain needs to be offset by the introduction of an external mechanism to drive the system. External sources force the system to behave in a manner that reflects the external input rather than the intrinsic properties of the turbulence. Choosing instead the time-dependent case, usually in the form of freely-decaying or decaying turbulence allows the non-linear nature of the fluid system to be more observable [3, 24, 34]. It is common practise to distinguish between the cases of time-dependent and time-independent as freely-decaying and forced turbulence respectively.

1.2.5 The Spectral Dynamics of Turbulence

The use of spectral methods is of great importance in describing turbulence and proves its worth time and again in a vast majority of computational models wishing to solve the NSE for a turbulent (and otherwise) fluids [35, 36]. Spectrally transformed systems can have properties that help in finding solutions to some differential equations [37, 38]. They also provide a different perspective with how the energy is organised, for example in various length-scales, and how it changes within a system.

Spectral Navier-Stokes Equations

Using the following spectral conventions for the velocity field, the pressure, and the forcing field,

$$u_\alpha(\mathbf{x},t) = \int d\mathbf{k}\, u_\alpha(\mathbf{k},t)e^{i\mathbf{k}\cdot\mathbf{x}}, \qquad u_\alpha(\mathbf{k},t) = \frac{1}{(2\pi)^3}\int d\mathbf{x}\, u_\alpha(\mathbf{x},t)e^{-i\mathbf{k}\cdot\mathbf{x}} \tag{1.17}$$

$$p(\mathbf{x},t) = \int d\mathbf{k}\, p(\mathbf{k},t)e^{i\mathbf{k}\cdot\mathbf{x}}, \qquad p(\mathbf{k},t) = \frac{1}{(2\pi)^3}\int d\mathbf{x}\, p(\mathbf{x},t)e^{-i\mathbf{k}\cdot\mathbf{x}} \tag{1.18}$$

$$f_\alpha(\mathbf{x},t) = \int d\mathbf{k}\, f_\alpha(\mathbf{k},t)e^{i\mathbf{k}\cdot\mathbf{x}}, \qquad f_\alpha(\mathbf{k},t) = \frac{1}{(2\pi)^3}\int d\mathbf{x}\, f_\alpha(\mathbf{x},t)e^{-i\mathbf{k}\cdot\mathbf{x}} \tag{1.19}$$

the Fourier-space or spectral Navier-Stokes equations become

$$\left(\partial_t + \nu \mathrm{k}^2\right) u_\alpha(\mathbf{k},t) = M_{\alpha\beta\gamma}(\mathbf{k}) \iint\limits_{\mathbf{j}+\mathbf{l}=\mathbf{k}} d\mathbf{j}\, d\mathbf{l}\, u_\beta(\mathbf{j},t) u_\gamma(\mathbf{l},t) + f_\alpha(\mathbf{k},t) \tag{1.20}$$

$$\mathrm{k}_\alpha u_\alpha(\mathbf{k},t) = 0. \tag{1.21}$$

The notation $\mathbf{j}+\mathbf{l}=\mathbf{k}$ under the integral signs indicates that the integration variables must obey this constraint due to the convolution. The pressure term has been removed using the analogue of the continuity equation, (1.21) (see [35]). The tensor $M_{\alpha\beta\gamma}(\mathbf{k})$ is

the momentum transfer operator and is defined by

$$M_{\alpha\beta\gamma}(\mathbf{k}) \equiv \frac{1}{2i}\left(\mathrm{k}_\beta\delta_{\alpha\gamma} - \frac{\mathrm{k}_\alpha\mathrm{k}_\beta\mathrm{k}_\gamma}{\mathrm{k}^2} + \mathrm{k}_\gamma\delta_{\alpha\beta} - \frac{\mathrm{k}_\alpha\mathrm{k}_\beta\mathrm{k}_\gamma}{\mathrm{k}^2}\right) \tag{1.22}$$

$$\equiv \frac{1}{2i}\Big(\mathrm{k}_\beta P_{\alpha\gamma}(\mathbf{k}) + \mathrm{k}_\gamma P_{\alpha\beta}(\mathbf{k})\Big). \tag{1.23}$$

The tensors that show up in the last line are those referred to earlier in (1.16).

The Spectral Distribution of Energy

The spectral NSE can be used along with an averaging procedure to derive a dynamical equation for the spectral energy density of a turbulent fluid,

$$\partial_t E(\mathrm{k},t) = T(\mathrm{k},t) + W(\mathrm{k},t) - D(\mathrm{k},t). \tag{1.24}$$

Note that this is a 1-D projection in wavenumber-space. This equation is commonly referred to as the 'Spectral Energy-balance Equation'.

Similar to the NSE itself, this equation describes how the energy contained in a particular mode k changes via the input work done on the fluid, $W(\mathrm{k},t)$, adding energy into k; the transfer, $T(\mathrm{k},t)$, of energy to k from all other modes and vice versa; and the removal of energy via dissipation, $D(\mathrm{k},t)$. It is instructive to consider a schematic representation of these quantities in terms of their 1-D spectral projection as given in fig. 1.1 which shows the general forms of these functions. The total energy is shown with its maximum in the lower wavenumber region; this is due to the dissipation of energy which by virtue of its definition,

$$D(\mathrm{k},t) \equiv 2\nu\mathrm{k}^2 E(\mathrm{k},t), \tag{1.25}$$

has a greater influence in the higher wavenumbers, essentially damping out all but the lowest and most energetic modes.. In order to conserve the total energy, an inertial transfer mechanism exists that takes the energy out of the low wavenumber, or 'low-k', region and effectively delivers it to the dissipation region. Finally, the energy in the low-k either decreases from an initial state, or is maintained by a steady or time-varying input, $W(\mathrm{k},t)$. The region of small wavenumbers corresponds to large (macroscopic) scales where the typical instigators of fluid motion exist.

The dissipation and transfer of energy play a fundamental and important role in turbulence; to stress this, the following subsections are given to them.

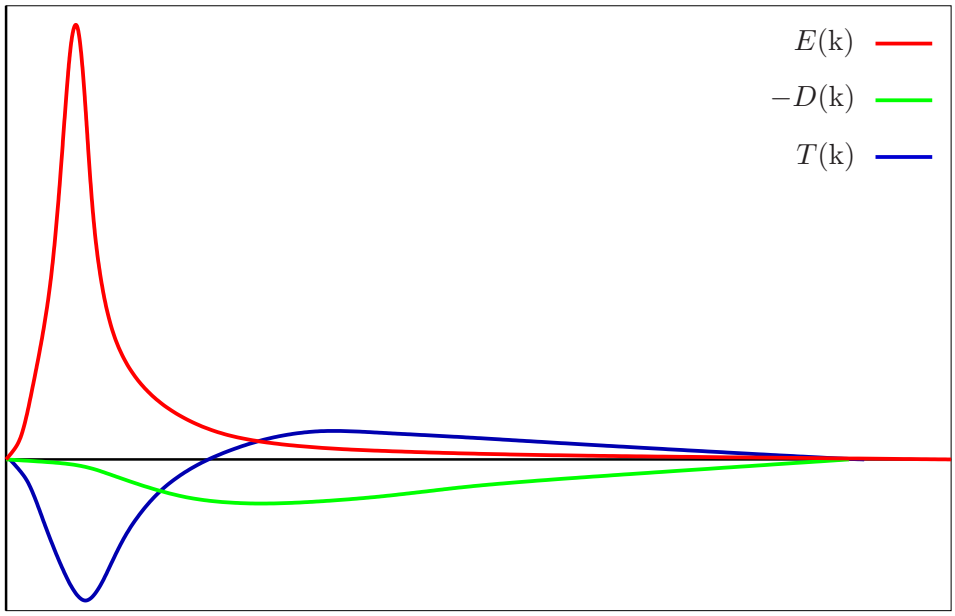

Figure 1.1: A schematic plot of the spectral energy density, $E(\mathrm{k})$, spectral energy-dissipation density, $D(\mathrm{k})$, and the spectral energy-transfer density, $T(\mathrm{k})$. It is usual that $E(\mathrm{k})$ is peaked in the low-k region as representing an amount of energy that will freely decay or that is injected via external forcing. The negative of the dissipation spectrum is given to emphasise its role in the removing energy in the large-k region. The characteristic shape of the transfer spectrum illustrates its role in absorbing energy in the low-k region and emitting it in the high-k region.

Energy Dissipation and the Universal Equilibrium Range

The dissipation of energy occurs most prominently on the smallest of scales where the molecular forces of viscosity are comparable to the size and mean free-path lengthscale of the fluid's constituent particles [24]. On the continuum scale of the fluid, the sum of these interactions creates a considerable drain of energy for the entire fluid.

The idea that all fluids behave similarly under the influence of viscosity has led the way to some important theories in the study of turbulence. Most notably among these are those of Kolmogorov [39, 40]. In two papers from 1941, Kolmogorov made two hypotheses and derived some of the longest standing results available to turbulence knowledge. The first hypothesis is based on the notion that at small scales where dissipation is most apparent, there is a significant separation from the activities of the large scales.

The decoupling of these two scales implies that they do not influence each other. Large-scale motion does not directly feed into small scales but rather advects regions of small-scale motion. Likewise, the dissipative forces in the small scale are not significant

enough to impede upon the large scales. The relatively quick dynamics of the dissipative scales ensures that they are in a statistical equilibrium compared to the large scales and therefore, they destroy any anisotropy imparted to them from the large scales. These arguments paraphrase §5.2 in Davidson [24] where further details can be found. What is important is that this decoupling allows a description of the energy spectrum in this region to be based solely on parameters of the energy input/destruction rate ε and the viscosity ν [25].

A similarity hypothesis is given for the energy spectrum in the dissipation region [27],

$$E_{\text{eq.}}(\mathrm{k}) = v^2 l f(\mathrm{k}l). \tag{1.26}$$

where v and l are arbitrary velocity- and length-scales and f is a dimensionless function; the 'eq.' subscript on the energy spectrum denotes it as in statistical equilibrium.. As v and l are determined by ν and ε, dimensional arguments can be used to construct them as

$$v \to \mathrm{v}_D \equiv (\nu\varepsilon)^{1/4}, \qquad l \to \eta \equiv \left(\frac{\nu^3}{\varepsilon}\right)^{1/4}, \tag{1.27}$$

the dissipation velocity- and length-scales respectively. The inverse of η is often used as the dissipation wave-vector,

$$\mathrm{k}_D \equiv \left(\frac{\varepsilon}{\nu^3}\right)^{1/4} \tag{1.28}$$

Inserting these into (1.26) gives

$$E_{\text{eq.}}(\mathrm{k}) = \nu^{5/4}\varepsilon^{1/4} f(\mathrm{k}\eta). \tag{1.29}$$

The proof of the universality and the similarity of this dissipation scales can be seen in fig. 1.2; when appropriately scaled using the dissipation parameters, ε and ν, the energy spectra of various experimental observations begin to collapse onto the same curve.

Energy Conservation and the Inertial Range

As energy is created in the large scales and then dissipated in the small scales, there exists a mechanism to transfer the energy among these scales called the energy cascade [41]. This has been alluded to previously and is due to the non-linear terms.

It can be shown that this transfer conserves energy, resulting in the vanishing of the transfer spectrum,

$$\int_0^\infty d\mathrm{k}\, T(\mathrm{k}, t) = 0. \tag{1.30}$$

The equation below demonstrates the relation of the transfer spectrum to the triple-correlation of the velocity field,

$$\begin{aligned}\int_0^\infty d\mathrm{k}\, T(\mathrm{k},t) &= \int_0^\infty d\mathrm{k}\, 2\pi\mathrm{k}^2 M_{\alpha\beta\gamma}(\mathbf{k}) \int_0^\infty d\mathbf{j} \times \\ &\quad \Big(\langle u_\beta(\mathbf{j},t) u_\gamma(\mathbf{k}-\mathbf{j},t) u_\alpha(-\mathbf{k},t)\rangle \\ &- \langle u_\beta(-\mathbf{j},t) u_\gamma(-\mathbf{k}+\mathbf{j},t) u_\alpha(\mathbf{k},t)\rangle \Big). \end{aligned} \tag{1.31}$$

Using the properties of the momentum-transfer operator, $M_{\alpha\beta\gamma}(\mathbf{k})$ defined in (1.22), and the continuity relation, $(\mathrm{k}-\mathrm{j})_\gamma u_\gamma(\mathbf{k}-\mathbf{j},t) = 0$, the interchange of the wave-vectors $\mathbf{k}$ and $\mathbf{j}$, shows the transfer spectrum is anti-symmetric and must therefore vanish. Thus, the transfer term neither adds nor subtracts energy from the system, but instead recycles it throughout all wave-numbers; the viscosity is the only drain of energy.

As the transfer spectrum only shuffles energy throughout k-space, it can be said to connect various scales. In fully turbulent systems with large Reynolds number, though, the scales can become separated. The low-k region which contains all the energy is not affected by the high-k properties, namely viscosity; nor does the high-k region feel the effects of the large-energy fluctuations below, except where they enter the equilibrium range after traversing the energy cascade [24, 25].

A second similarity hypothesis is given for this region and the result is the most famous of Kolmogorov's results [39]. It is the derivation of the inertial range spectrum. Using simple dimensional arguments and the hypotheses outlined above, Kolmogorov found that the energy spectrum should only depend on the dissipation rate and the wavenumber.

Recalling that the equilibrium range where dissipation is relevant can be described using

$$E_{\mathrm{eq.}}(\mathrm{k}) = \nu^{5/4}\varepsilon^{1/4} f(\mathrm{k}\eta) \tag{1.32}$$

where $f(\mathrm{k}\eta)$ is a non-dimensional function of the wavenumber and the dissipation length-scale. Matching this against inertial range where the viscosity is to be negligible requires

$$f(\mathrm{k}\eta) \propto (\mathrm{k}\eta)^c \tag{1.33}$$

where the exponent, c, is determined by requiring that the form of this inertial region does not depend on viscosity. Inserting this into the above and employing the constraint

that the viscosity vanish from this equation ($\nu \to 1$),

$$\begin{aligned} E_I(\mathrm{k}) &= \nu^{5/4}\varepsilon^{1/4}\alpha(\mathrm{k}\eta)^c \\ &= \alpha\nu^{5/4}\varepsilon^{1/4}\mathrm{k}^c\nu^{3c/4}\varepsilon^{-c/4} \qquad (1.34) \\ \nu^{-5/4+3c/4=0} &\Rightarrow c = -5/3 \\ &\Rightarrow E_I(\mathrm{k}) = \alpha\varepsilon^{2/3}\mathrm{k}^{-5/3}. \qquad (1.35) \end{aligned}$$

This result, often referred to as the "five-thirds" law, is among the most well-known in turbulence. Indeed, this results has long-standing experimental evidence supporting and is even viewed as a benchmark in numerical studies. Figure 1.2 is often cited as a testament to the five-thirds law, and can be found in many texts.

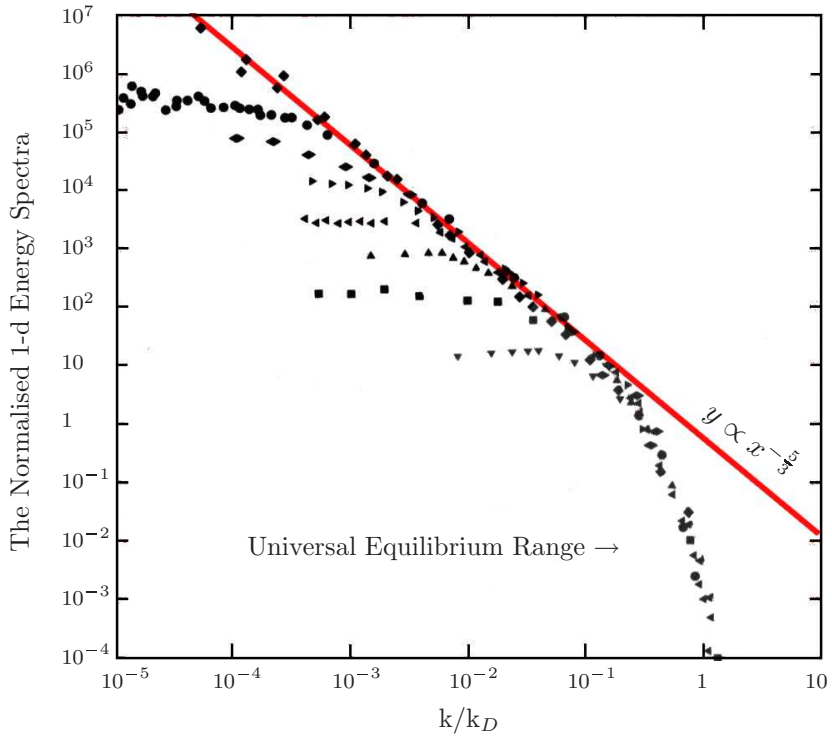

Figure 1.2: Experimental evidence supporting Kolmogorov (adapted from McComb [35]). These results show a variety of Reynolds numbers in different experimental set-ups, including a tidal channel. The red line shows the $k^{-5/3}$ scaling predicted for the inertial ranges. The collapse of data-points onto a similar curve labelled as the 'Universal equilibrium range' suggests the universality of the high-end wavenumbers in turbulent systems.

When R is large, the energy in the low-k scales is relatively larger than that in the

viscous scales. Increasing the amount of energy in the low-k region increases the rate at which it enters the cascade and, as it is conserved, the rate at which it will be transferred to the dissipation region. However, decreasing the viscosity will not have this effect; the amount in the large scales does not change, nor does its rate passing into and through the energy cascade. In any case, the rate of energy leaving the cascade must equal the rate at which energy is dissipated; therefore, one can argue that even in the limit where viscosity is reduced to an infinitesimal amount, there will be a non-vanishing dissipation rate equal to the rate of energy moving through the cascade.

The matter of intermittency with relation to Kolmogorov's theories also needs addressing. This was first brought about by Kolmogorov's contemporary Landau [21, 42] and was enough to cause Kolmogorov to revise his theory some twenty years later [43]. Landau's objection relates to primarily using ε which is the global average of the dissipation, rather than the more relevant locally averaged dissipation rate, which will fluctuate, hence intermittency, much more than its global cousin leading to what are referred to as 'intermittency corrections' to the inertial range of energy spectra. Useful information on Kolmogorov and intermittency can be found in Frisch [44], and for more recent work see [45]. For the purposes of this thesis, the contribution of intermittency corrections will be ignored when evaluating the energy spectra encountered later.

1.2.6 The Flow of Energy in Spectral Space

Another spectral quantity of importance is the transport energy flux, or 'flux'. It is defined as a partial integration of the transfer spectrum,

$$\Pi(\mathrm{k},t) \equiv -\int_0^{\mathrm{k}} d\mathrm{j}\, T(\mathrm{j},t) \quad = \quad \int_k^{\infty} d\mathrm{j}\, T(\mathrm{j},t) \tag{1.36}$$

This dual definition is provided by the anti-symmetry of the transfer spectrum. The spectral flux is then a measure of the rate of energy being transferred through a particular wavenumber k. Differentiating both sides of this definition leads to an alternate equation,

$$T(\mathrm{k},t) \equiv -\frac{\partial \Pi(\mathrm{k},t)}{\partial \mathrm{k}}, \tag{1.37}$$

which shows that the transfer spectrum is slope of the flux spectrum. The particular shape and the anti-symmetry of the transfer spectrum tells that the flux is always positive or zero, thus the rate, $T(\mathrm{k},t)$, of energy entering a given wavenumber is such that the flow of energy goes from low to high wavenumbers.

At this point it is worth noting a few more aspects about the flux. As it is the flow of energy from modes $\mathrm{j} < \mathrm{k}$ to modes $\mathrm{j} > k$, the anti-symmetry of $T(\mathrm{k},t)$, guarantees

two characteristics of the flux: (1) the amount of energy coming from modes $\mathrm{j} < \mathrm{k}$ is equal to that going to modes $\mathrm{j} > \mathrm{k}$; (2) the flux is maximal when the largest amount of energy can be transferred which occurs for $\Pi(\mathrm{k}_0, t)$ where k_0 is the zero-crossing point of the transfer spectrum, $T(\mathrm{k}_0, t) = 0$.

The first remark reiterates the property of energy conservation of the transfer spectrum; the second remark requires further clarity. For $\Pi(\mathrm{k}, t)$ to be a maximum point, this entails that

$$\frac{\partial \Pi(\mathrm{k}, t)}{\partial \mathrm{k}} = -T(\mathrm{k}, t) = 0, \tag{1.38}$$

and this occurs at exactly three points, $\mathrm{k} = 0, \mathrm{k}_0$ and $\mathrm{k} \to \infty$. Furthermore,

$$\frac{\partial^2 \Pi(\mathrm{k}, t)}{\partial \mathrm{k}} < 0 \quad \Rightarrow \quad \frac{\partial T(\mathrm{k}, t)}{\partial \mathrm{k}} > 0, \tag{1.39}$$

only occurs, by inspection of the schematic in figure 1.1, at the zero-crossing wavenumber, $\mathrm{k} = \mathrm{k}_0$. Physically, for a given wavenumber k, $T(\mathrm{k}, t)$ is negative when the net flow of energy leaves k, and requiring $\Pi(\mathrm{k}, t)$ to be maximal implies the integral over j must capture the largest amount of energy leaving all wavenumbers $\mathrm{j} < \mathrm{k}$. Thus the range of wavenumbers is given by $\mathrm{j} = [0, \mathrm{k}_0]$.

A new quantity can be defined which denotes the maximal flux,

$$\Pi_{\max}(t) \equiv -\int_0^{\mathrm{k}_0} d\mathrm{j}\, T(\mathrm{j}, t) \;\; = \;\; \int_{\mathrm{k}_0}^{\infty} d\mathrm{j}\, T(\mathrm{j}, t). \tag{1.40}$$

The maximum-flux will be seen as an important quantity in what is to come in later chapters.

1.3 Thesis Overview

This thesis can be divided into two main parts: The first part is chapter 2 while the second consist of chapters 3-6. Chapter 2 deals with statistical methods devised to get around the closure problem. Two formalisms employing renormalisation, one perturbative and the other non-perturbative, are explored in detail and compared against each other. Understanding how these approaches differ is beneficial to devising a closure based on first principles.

The second part deals primarily with a numerical investigation of turbulent dissipation. Chapter 3 gives an account of a numerical solution based on a particular closure, the Local Energy Transfer (LET), which is used to model moderately turbulent systems in both freely decaying and forced scenarios.

Chapter 5 explores the measurement times of turbulent paragraphmeters needed to investigate dissipation in decaying turbulence. Using the time dependent properties of turbulent paragraphmeters may help in finding times within which measurements can be made that indicate the dynamics of decaying turbulence.

Finally, chapter 6 investigates turbulent dissipation, most notably its dependence on the Reynolds number in both freely-decaying and forced turbulence. It will be shown that there are intrinsic differences in the behaviour of the normalised dissipation rate for decaying and forced turbulence with supporting evidence from the numerical work using the LET-model.

Chapter 2

Field-Theoretic Closure Formalisms for Eulerian Fluid Turbulence

2.1 Statistical Closures in Turbulence

In turbulence, statistical closures are, in a general sense, techniques employed to close the moment-hierarchy established in a statistical treatment of the Navier-Stokes equation. These theories postulate a relationship between high- and low-order moments by way of physical arguments. The goal is to accurately describe and predict the statistics of a turbulent system while maintaining a strong connection to the underlying dynamics of the NSE. Closure theories can, in principle, allow efficient computation of turbulent statistics without the computationally intensive demands of Direct Numerical Simulation (DNS). This quality makes closure theories particularly attractive when computational power is severely limited. Although the ability to compute the full Navier-Stokes equations using DNS is currently and increasingly more tractable, closure-based computations are still able to provide useful insights into turbulent systems at a smaller computational cost.

There are a number of closure theories to be found in turbulence and no one closure seems adequate to cover the standard turbulent systems, whether bounded-flows or HIT. For the latter, it is possible to classify these closures into two main groups distinguished by dynamics with respect to a reference frame, Eulerian and Lagrangian closures. The former case focuses on describing a fluid from a 'lab' frame of reference, where the fluid moves relative to a fixed frame of reference outside the fluid, as in the Navier-Stokes equations. The Lagrangian description is in fact a re-formulation of fluid dynamics that calculates statistics by following fluid particle dynamics; closures similar

to those developed for Eulerian systems are then applied to these formulations. While it is a recognisable study, the work presented here does not consider the Lagrangian closures but instead focuses on those of the standard Eulerian formulation.

The quasi-normal approximation was one of the ealiest closures to be applied to homogeneous isotropic turbulence. Treating the velocity field as a random-Gaussian variable, the quasi-normal approximation allows the fourth-order correlation to be written in terms of products of second-order correlations [46, 47]. The primary problem in such a procedure is that turbulence is highly non-Gaussian [44] and the resultant predictions for the total kinetic energy take on negative values [48]. The failure of quasi-normality triggered research that made improvements upon it, resulting in the EDQNM-methods (see for example [27]). The focus here will be on a subset of this latter direction, Renormalised Perturbation Theories.

Renormalised Perturbation Theories, or RPTs, take conventional perturbation expansions and re-sum the infinite terms generated in such expansions into a more tractable form while keeping the necessary details. There is a body of literature that has grown up around this work and some principle sources elaborating these directions are Leslie [49] and McComb [35]. There is one RPT that deserves to be mentioned, on historical grounds but also in terms of what is to follow later in this chapter.

2.1.1 The Direct Interaction Approximation

Kraichnan's Direct Interaction Approximation (DIA) [50–52] is perhaps one of the best known renormalised perturbation theories of homogeneous isotropic turbulence. To understand the basis for the DIA it is helpful to consider the spectral NSE,

$$\left[R^{(0)}(\mathbf{k},t,s)\right]^{-1}u_\alpha(\mathbf{k},s) = M_{\alpha\beta\gamma}(\mathbf{k})\int\limits_{\mathbf{j}+\mathbf{l}=\mathbf{k}} d^3\mathrm{j}\, d^3\mathrm{l}\, u_\beta(\mathbf{j},t)u_\gamma(\mathbf{l},t), \tag{2.1}$$

where

$$\left[R^{(0)}(\mathbf{k},t,s)\right]^{-1} \equiv \partial_t + \nu\mathrm{k}^2. \tag{2.2}$$

A general solution for $u_\alpha(\mathbf{l},t)$ is

$$u_\alpha(\mathbf{l},t) = \int\limits_{-\infty}^{t} ds\, R^{(0)}(\mathbf{l},t,s)\, M_{\alpha\beta\gamma}(\mathbf{l}) \int\limits_{\mathbf{m}+\mathbf{n}=\mathbf{l}} d^3\mathrm{m}\, d^3\mathrm{n}\, u_\beta(\mathbf{m},s)u_\gamma(\mathbf{n},s). \tag{2.3}$$

The product of velocity-field coefficients in the integrand of (2.1) can be written as

$$\left[R^{(0)}(\mathbf{k},t,s)\right]^{-1}u_\alpha(\mathbf{k},t) \;=\; M_{\alpha\beta\gamma}(\mathbf{k})\int\limits_{\mathbf{j}+\mathbf{m}+\mathbf{n}=\mathbf{k}} d^3\mathrm{j}\,d^3\mathrm{l}\,d^3\mathrm{m}\,d^3\mathrm{n}\,R^{(0)}(\mathbf{l},t)M_{\gamma\delta\epsilon}(\mathbf{l})\times \left(u_\beta(\mathbf{j},t)u_\delta(\mathbf{m},t)u_\epsilon(\mathbf{n},t)\right), \tag{2.4}$$

It can be seen that while the original velocity coefficients $u_\beta(\mathbf{j},t)$ and $u_\gamma(\mathbf{l},t)$ are directly coupled to $u_\alpha(\mathbf{k},t)$, the two new velocity coefficients in the integrand of (2.4) are only indirectly coupled, via $R^{(0)}(\mathbf{l},t)$ and $M_{\gamma\delta\epsilon}(\mathbf{l})$, to $u_\alpha(\mathbf{k},t)$. These define what Kraichnan called the 'direct' and 'indirect interactions'.

These interactions are characterised by their wave-vector couplings and can be seen graphically as in fig. 2.1 where examples of direct and indirect couplings are given. The direct interactions only form triangles whereas the indirect interactions form polygons of greater order, though in general the indirectly interacting wave-vectors are not constrained to the same plane as the directly interacting wave-vectors.

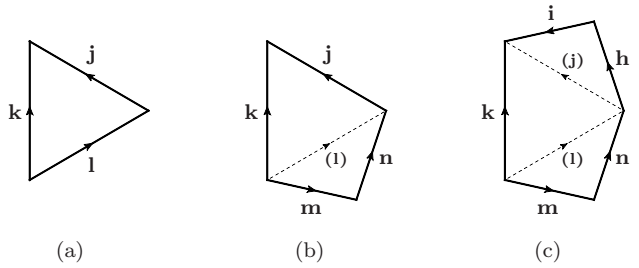

Figure 2.1: A direct interaction (a) and indirect interactions (b, c).

Kraichnan exploited this concept and used it to create a somewhat unique perturbation expansion that could be used to bring about a closure to the statistical hierarchy and derive an equation of motion for the correlation of velocity-field coefficients,

$$\begin{aligned}\left(\partial_t+\nu\mathrm{k}^2\right)C_{\alpha\alpha'}(\mathbf{k};t,t') = M_{\alpha\beta\gamma}(\mathbf{k})\int\limits_{\mathbf{j}+\mathbf{l}=\mathbf{k}} d^3\mathrm{j}\,d^3\mathrm{l}\,\times \\ \left\{2\int\limits_{-\infty}^{t} ds\; R_{\beta\beta'}(\mathbf{j};t,s)M_{\beta'\delta\epsilon}(\mathbf{j})C_{\gamma\delta}(\mathbf{l};t,s)C_{\epsilon\alpha'}(\mathbf{k};s,t')\right\} \\ -\int\limits_{-\infty}^{t'} ds\; R_{\alpha'\bar{\alpha}}(\mathbf{k};t',s)M_{\bar{\alpha}\beta'\gamma'}(\mathbf{k})C_{\gamma\gamma'}(\mathbf{l};t,s)C_{\beta\beta'}(\mathbf{j};t,s)\Bigg\}\end{aligned} \tag{2.5}$$

along with an equation of motion for the response function or propagator,

$$\Big(\partial_t + \nu \mathrm{k}^2\Big) R_{\alpha\alpha'}(\mathbf{k};t,t') - 4M_{\alpha\beta\gamma}(\mathbf{k}) \int_{\mathbf{j}+\mathbf{l}=\mathbf{k}} d^3\mathrm{j}\, d^3\mathrm{l}\, \times$$
$$\left\{ \int_{t'}^{t} ds\; R_{\beta\beta'}(\mathbf{j};t,s) M_{\beta'\gamma'\bar{\alpha}}(\mathbf{j}) C_{\gamma\gamma'}(\mathbf{l};t,s) R_{\alpha'\bar{\alpha}}(\mathbf{k};s,t') \right\}$$
$$= P_{\alpha\alpha'}(\mathbf{k})\delta(t-t'). \tag{2.6}$$

The derivation of the DIA for homogeneous isotropic turbulence is beyond the scope of the current chapter; some useful references found to be the most faithful to the original derivation of the DIA are Beran[53], Kida and Gotoh [54], and Krommes [55]. Leslie's book [49] is largely dedicated to Kraichnan's works and provides many insights.

The DIA, although successful in low- to moderate-Reynolds numbers fails to produce a Kolmogorov inertial range. Kraichnan himself showed that the DIA gives an inertial range with $\mathrm{k}^{-3/2}$ [51] and associated it with the DIA's not properly dealing with the indirect interactions [56, 57], manifest by the DIA's inability to decouple the large-scales from the viscous scales [27]. As will later be seen the momentum transfer terms are in effect vertex functions. The indirect interactions are intrinsically associated with these vertex functions leading to the notion that "the whole problem of strong turbulence is contained in a proper treatment of vertex renormalisation"[58].

The success and failings of the DIA led to further closures based on renormalised perturbation theories. Notable ones are those of Wyld [59], Herring [60, 61], Nakano [62], and McComb [35]. Convinced of the perceived intrinsic failings of the DIA based on an Eulerian framework, Kraichnan reformulated fluid dynamics to use Lagrangian variables and produced the Lagrangian-DIA [63]. This also led to many off-shoots notably those of Kraichnan [35, 49, 64] and the LRA of Kaneda [54, 65, 66]. The Eulerian-DIA still enjoys some use notably in the regularised-DIA (RDIA) of Frederiksen [67–70]

The sections to follow detail two formalisms that aim to achieve a statistical closure that properly deals with both the direct and indirect interactions. These formalisms are more general in their respective approaches to classical dynamics, but were applied to turbulence in their original sources. It will be shown that both formalisms are equivalent in their reproduction of the DIA result at lowest order, but differ in their treatments of higher-orders where vertex renormalisation occurs.

2.2 The Wyld Formalism

The Wyld formalism [59] is a perturbative analysis of the statistical turbulence. It represents one of the earlier attempts [62, 71] to extend the methods of quantum field theory, specifically those of diagrammatic representation, to the problem of classical turbulence.

In the approach used by Wyld, a statistical average is taken of two velocity-fields which are expanded as diagrammatic perturbation series, thus establishing a two-point velocity correlation function. As the perturbation series are in fact infinite, a systematic renormalisation method is employed to reduce the series into a more manageable format. This results in integral equations that, which at lowest non-trivial order, reproduce the Kraichnan DIA result.

While being formally correct, the method breaks down in the renormalisation process where different choices in the diagrammatic resummations result in different outcomes to the exact propagator function. Wyld's original method was updated in a later paper by Lee, who corrected some of the problems with an *ad hoc* fix.

2.2.1 Wyld's Perturbation Method

The main focus in examining Wyld's method is the renormalisation procedure. However, the fundamental or 'bare' equations must be established prior to renormalisation. The following account briefly explains Wyld's construction of the velocity correlation function via a perturbation expansion of the velocity field.

There are a few points in which the following summary of Wyld's method deviates from Wyld's original work; these deviations are trivial in the sense that they do not obscure the method under investigation.

Wyld's perturbation expansion

The NSE in Fourier space, but without the Fourier transform of the time variable, is:

$$\Big(\partial_t + \nu \mathrm{k}^2\Big) u_\alpha(\mathbf{k},t) = f_\alpha(\mathbf{k},t) + \frac{1}{(2\pi)^3} M^0_{\alpha\beta\gamma}(\mathbf{k}) \int d^3\mathrm{j}\; u_\beta(\mathbf{j},t) u_\gamma(\mathbf{k}-\mathbf{j},t). \tag{2.7}$$

Already this is different than Wyld in that the time variable is Fourier-transformed as well. The wave-vector $\mathbf{k}$ and wave-frequency ω are then lumped together into a 4-vector $k \equiv (\mathbf{k}, -\omega)$ and the tensorial NSE is abandoned in favour of a simpler one-dimensional 'model' equation. These changes do not affect the overall analysis and will not be implemented here.

Inverting the linear differential operator on the LHS of (2.7) to the RHS results

in a form of the NSE that is more amenable to the ensuing analysis,

$$\begin{aligned} u_\alpha(\mathbf{k},t) &= \int_{-\infty}^{t} dt' R^{(0)}_{\alpha\alpha'}(\mathbf{k};\, t,t') f_{\alpha'}(\mathbf{k},t') \\ &+ \lambda \frac{1}{(2\pi)^3} \int_{-\infty}^{t} dt' R^{(0)}_{\alpha\alpha'}(\mathbf{k};\, t,t') M^0_{\alpha'\beta\gamma}(\mathbf{k}) \int d^3\mathrm{j}\; u_\beta(\mathbf{j},t') u_\gamma(\mathbf{k}-\mathbf{j},t'). \end{aligned} \tag{2.8}$$

A bookkeeping parameter, $\lambda < 1$, has been multiplied to the nonlinear term for the purposes of the perturbation expansion; it will later be set equal to unity.

The next step is to consider a perturbation expansion of the NSE,

$$u_\alpha(\mathbf{k},t) = u^{(0)}_\alpha(\mathbf{k},t) + \lambda u^{(1)}_\alpha(\mathbf{k},t) + \lambda^2 u^{(2)}_\alpha(\mathbf{k},t) + \ldots, \tag{2.9}$$

This can be substituted for each velocity field in (2.8) and then expressions can be matched by powers of λ. At the lowest order,

$$u^{(0)}_\alpha(\mathbf{k},t) = \int_{-\infty}^{t} dt' R^{(0)}_{\alpha\alpha'}(\mathbf{k};\, t,t') f_{\alpha'}(\mathbf{k},t'), \tag{2.10}$$

and one can establish a response function $R^{(0)}_{\alpha\beta}(\mathbf{k};\, t,t')$ such that

$$\Big(\partial_t + \nu \mathrm{k}^2\Big)\Big[R^{(0)}_{\alpha\beta}(\mathbf{k};\, t,t')\Big] = P_{\alpha\beta}(\mathbf{k})\delta(t-t'). \tag{2.11}$$

Already, it may be seen that there are many variables, arguments, and indices to keep track of, therefore it is useful here to introduce a reduced notation:

$$u^{(0)}_\alpha(\mathbf{k},t) \;\rightarrow\; u^{(0)}_{\mathbf{k}} \tag{2.12a}$$

$$R^{(0)}_{\alpha\beta}(\mathbf{k};\, t,t') \;\rightarrow\; R^{(0)}_{\mathbf{k}} \tag{2.12b}$$

$$\frac{1}{(2\pi)^3} M^0_{\alpha\beta\gamma}(\mathbf{k}) \int d^3\mathrm{j} \;\rightarrow\; M^0_{\mathbf{k}}. \tag{2.12c}$$

This notation provides a more-intuitive format for the reader to follow; vector indices and time arguments can be determined secondarily where needed. The spectral NSE in the new notation becomes

$$(\partial_t + \nu \mathrm{k}^2) u_{\mathbf{k}} = f_{\mathbf{k}} + \lambda M^0_{\mathbf{k}} u_{\mathbf{j}} u_{\mathbf{k}-\mathbf{j}}, \tag{2.13}$$

and the perturbation equations are similarly

$$u_{\mathbf{k}} = R^{(0)}_{\mathbf{k}} f_{\mathbf{k}} + \lambda R^{(0)}_{\mathbf{k}} M^0_{\mathbf{k}} u_{\mathbf{j}} u_{\mathbf{k}-\mathbf{j}} \tag{2.14}$$

$$u_{\mathbf{k}} = u^{(0)}_{\mathbf{k}} + \lambda u^{(1)}_{\mathbf{k}} + \lambda^2 u^{(2)}_{\mathbf{k}} + \lambda^3 u^{(3)}_{\mathbf{k}} \ldots \tag{2.15}$$

In using this notation, the integral following the momentum transfer operator is always a convolution where the wave-vector arguments of the convoluted functions must add up to the wave-vector of the momentum transfer operator immediately preceding them. Some care may be initially needed to keep track of these integrated wave-vectors; a simple rule that adjusts for this is that all non-$\mathbf{k}$ wave-vectors are integrated out.

The perturbation terms by order in λ are

$$\lambda^0 : \quad u^{(0)}_{\mathbf{k}} = R^{(0)}_{\mathbf{k}} f_{\mathbf{k}} \tag{2.16a}$$

$$\lambda^1 : \quad u^{(1)}_{\mathbf{k}} = \lambda R^{(0)}_{\mathbf{k}} M^0_{\mathbf{k}} u^{(0)}_{\mathbf{j}} u^{(0)}_{\mathbf{k}-\mathbf{j}} \tag{2.16b}$$

$$\lambda^2 : \quad u^{(2)}_{\mathbf{k}} = \lambda^2 R^{(0)}_{\mathbf{k}} M^0_{\mathbf{k}} \left(2 u^{(0)}_{\mathbf{j}} u^{(1)}_{\mathbf{k}-\mathbf{j}}\right) \tag{2.16c}$$

$$\vdots$$

The term $u^{(1)}_{\mathbf{k}-\mathbf{j}}$ in the integrand of the expression for $u^{(2)}_{\mathbf{k}}$ can be replaced by its definition, leaving $u^{(2)}_{\mathbf{k}}$ written only in terms of $u^{(0)}$. In fact, any order $u^{(n)}$ may be written as product of $(n+1)$ $u^{(0)}$'s. For example, the last term in the above equation for the perturbation expansion of $u^{(2)}_{\mathbf{k}}$ can now be written as

$$\lambda^2 : \; u^{(2)}_{\mathbf{k}} = 2\lambda^2 R^{(0)}_{\mathbf{k}} M^0_{\mathbf{k}} R^{(0)}_{\mathbf{k}-\mathbf{j}} M^0_{\mathbf{k}-\mathbf{j}} u^{(0)}_{\mathbf{j}} u^{(0)}_{\mathbf{l}} u^{(0)}_{\mathbf{k}-\mathbf{j}-\mathbf{l}}. \tag{2.17}$$

This provides a major simplification that will help to enable the closure of the correlation equations.

Wyld's correlation

Wyld approaches the correlation of two velocity fields very simply by considering the average of the product of two velocity field expansions of u's:

$$\left\langle u_\alpha(\mathbf{k},t) u_\omega(\mathbf{k}',t') \right\rangle = \left\langle \left(u^{(0)}_\alpha(\mathbf{k},t) + \lambda u^{(1)}_\alpha(\mathbf{k},t) + \cdots \right) \times \left(u^{(0)}_\omega(\mathbf{k}',t') + \lambda u^{(1)}_\omega(\mathbf{k}',t') + \cdots \right) \right\rangle \tag{2.18}$$

The functions for the zeroth-order and exact correlators are given respectively by

$$C^{(0)}_{\alpha\omega}(\mathbf{k};t,t')\delta(\mathbf{k}'+\mathbf{k}) \equiv \langle u^{(0)}_\alpha(\mathbf{k},t)u^{(0)}_\omega(\mathbf{k}',t')\rangle = \langle u^{(0)}_{\mathbf{k}}u^{(0)}_{\mathbf{k}'}\rangle, \tag{2.19}$$

$$C_{\alpha\omega}(\mathbf{k};t,t')\delta(\mathbf{k}'+\mathbf{k}) \equiv \langle u_\alpha(\mathbf{k},t)u_\omega(\mathbf{k}',t')\rangle = \langle u_{\mathbf{k}}u_{\mathbf{k}'}\rangle; \tag{2.20}$$

and their reduced-notation counterparts are

$$C^{(0)}_{\alpha\omega}(\mathbf{k};t,t')\delta_{\mathbf{k}+\mathbf{k}'} \rightarrow C^{(0)}_{\mathbf{k}}\delta_{\mathbf{k}+\mathbf{k}'}, \tag{2.21}$$

$$C_{\alpha\omega}(\mathbf{k};t,t')\delta_{\mathbf{k}+\mathbf{k}'} \rightarrow C_{\mathbf{k}}\delta_{\mathbf{k}+\mathbf{k}'}. \tag{2.22}$$

The delta-function on the LHS of these definitions is a result of the construction of the Fourier-transform of the real-space correlation equation,

$$\begin{aligned}
\langle u_\alpha(\mathbf{k},t)u_\omega(\mathbf{k}',t')\rangle &= \left\langle \int d^3\mathrm{x}\int d^3\mathrm{r}\, u_\alpha(\mathbf{x},t)u_\omega(\mathbf{x}+\mathbf{r},t')e^{-i\mathbf{k}'\cdot\mathbf{x}}e^{-i\mathbf{k}\cdot(\mathbf{x}+\mathbf{r})}\right\rangle \\
&= \int d^3\mathrm{x}\int d^3\mathrm{r}\,\big\langle u_\alpha(\mathbf{0},t)u_\omega(\mathbf{r},t')\big\rangle e^{-i(\mathbf{k}'+\mathbf{k})\cdot\mathbf{x}}e^{-i\mathbf{k}\cdot\mathbf{r}} \\
&= \int d^3\mathrm{r}\, C_{\alpha\omega}(\mathbf{r};t,t')e^{-i\mathbf{k}\cdot\mathbf{r}}\delta(\mathbf{k}'+\mathbf{k}) \\
&= C_{\alpha\omega}(\mathbf{k};t,t')\delta(\mathbf{k}'+\mathbf{k}).
\end{aligned} \tag{2.23}$$

The second line uses the homogeneity constraint, $\big\langle u_\alpha(\mathbf{x},t)u_\omega(\mathbf{x}+\mathbf{r},t')\big\rangle = \big\langle u_\alpha(\mathbf{0},t)u_\omega(\mathbf{r},t')\big\rangle$.

It is appropriate to point out here that the zeroth-order velocity field expansion terms are random-Gaussian functions; this is implied in (2.11) by their being delta-function correlated in time. A well-known and easily proved fact of random-Gaussian variables is that correlations of odd-numbered products of them vanish. Fortunately, the present analysis has been fashioned such that correlations of odd-numbered products of velocity fields correspond to odd-orders in λ. These odd-ordered correlations can be excluded.

Continuing in reduced notation (without odd-order moments), a series-expansion

for the exact correlator is obtained,

$$\begin{aligned}
\langle u_{\mathbf{k}} u_{\mathbf{k}'} \rangle &= \\
C_{\mathbf{k}} \delta_{\mathbf{k}+\mathbf{k}'} &= C^{(0)}_{\mathbf{k}} \delta_{\mathbf{k}+\mathbf{k}'} \\
&+ \lambda^2 \big(\langle u^{(0)}_{\mathbf{k}} u^{(2)}_{\mathbf{k}'} \rangle + \langle u^{(1)}_{\mathbf{k}} u^{(1)}_{\mathbf{k}'} \rangle + \langle u^{(2)}_{\mathbf{k}} u^{(0)}_{\mathbf{k}'} \rangle \big) \\
&+ \lambda^4 \big(\langle u^{(0)}_{\mathbf{k}} u^{(4)}_{\mathbf{k}'} \rangle + \langle u^{(1)}_{\mathbf{k}} u^{(3)}_{\mathbf{k}'} \rangle + \langle u^{(2)}_{\mathbf{k}} u^{(2)}_{\mathbf{k}'} \rangle + \langle u^{(3)}_{\mathbf{k}} u^{(1)}_{\mathbf{k}'} \rangle + \langle u^{(0)}_{\mathbf{k}} u^{(4)}_{\mathbf{k}'} \rangle \big) \\
&+ \mathcal{O}(\lambda^6). \qquad (2.24)
\end{aligned}$$

As mentioned above, all terms can be written as products of zeroth-order velocity field terms. For example consider the last of the second-order correlations or moments:

$$\langle u^{(2)}_{\mathbf{k}} u^{(0)}_{\mathbf{k}'} \rangle = 2 R^{(0)}_{\mathbf{k}} M^0_{\mathbf{k}} R^{(0)}_{\mathbf{k}-\mathbf{j}} M^0_{\mathbf{k}-\mathbf{j}} \langle u^{(0)}_{\mathbf{j}} u^{(0)}_{\mathbf{l}} u^{(0)}_{\mathbf{k}-\mathbf{j}-\mathbf{l}} u^{(0)}_{\mathbf{k}'} \rangle \qquad (2.25)$$

Another property of random-Gaussian variables is that any n-th order moment may be decomposed into a sum of products of lesser-order moments. In the example, the fourth-order moment is decomposed into three pairs of second-order moments,

$$\begin{aligned}
\langle u^{(2)}_{\mathbf{k}} u^{(0)}_{\mathbf{k}'} \rangle &= 2 R^{(0)}_{\mathbf{k}} M^0_{\mathbf{k}} R^{(0)}_{\mathbf{k}-\mathbf{j}} M^0_{\mathbf{k}-\mathbf{j}} \times \\
&\Big(\langle u^{(0)}_{\mathbf{j}} u^{(0)}_{\mathbf{l}} \rangle \langle u^{(0)}_{\mathbf{k}-\mathbf{j}-\mathbf{l}} u^{(0)}_{\mathbf{k}'} \rangle + \langle u^{(0)}_{\mathbf{j}} u^{(0)}_{\mathbf{k}-\mathbf{j}-\mathbf{l}} \rangle \langle u^{(0)}_{\mathbf{l}} u^{(0)}_{\mathbf{k}'} \rangle + \langle u^{(0)}_{\mathbf{l}} u^{(0)}_{\mathbf{k}-\mathbf{j}-\mathbf{l}} \rangle \langle u^{(0)}_{\mathbf{j}} u^{(0)}_{\mathbf{k}'} \rangle \Big). \qquad (2.26)
\end{aligned}$$

Note that all possible combinations of second-order moments are created in this decomposition. What is immediately useful here is that the fourth-order moment can be written as pairs of second-order moments or more importantly, zeroth-order correlation functions.

Using the definition of the (zeroth-order) correlator, the above equation becomes

$$\langle u^{(2)}_{\mathbf{k}} u^{(0)}_{\mathbf{k}'} \rangle = 2 R^{(0)}_{\mathbf{k}} M^0_{\mathbf{k}} R^{(0)}_{\mathbf{k}-\mathbf{j}} M^0_{\mathbf{k}-\mathbf{j}} \Big(C^{(0)}_{\mathbf{j}} C^{(0)}_{\mathbf{k}} \delta_{\mathbf{k}+\mathbf{k}'} + C^{(0)}_{\mathbf{j}} C^{(0)}_{\mathbf{k}} \delta_{\mathbf{k}+\mathbf{k}'} + 0 \Big). \qquad (2.27)$$

The last term vanishes as it implies $M^0_{\mathbf{k}-\mathbf{j}} \delta_{\mathbf{k}-\mathbf{j}}$, which vanishes by definition. Cleaning up leaves

$$\langle u^{(2)}_{\mathbf{k}} u^{(0)}_{\mathbf{k}'} \rangle = 4 R^{(0)}_{\mathbf{k}} M^0_{\mathbf{k}} R^{(0)}_{\mathbf{k}-\mathbf{j}} M^0_{\mathbf{k}-\mathbf{j}} C^{(0)}_{\mathbf{j}} C^{(0)}_{\mathbf{k}} \delta_{\mathbf{k}+\mathbf{k}'}. \qquad (2.28)$$

A similar calculation can be made for the other terms, giving the correlation equation

to second-order,

$$\begin{aligned} C_{\mathbf{k}}\delta_{\mathbf{k}+\mathbf{k}'} &= C^{(0)}_{\mathbf{k}}\delta_{\mathbf{k}+\mathbf{k}'} \\ &+ 4R^{(0)}_{\mathbf{k}}M^{0}_{\mathbf{k}}R^{(0)}_{\mathbf{k}-\mathbf{j}}M^{0}_{\mathbf{k}-\mathbf{j}}C^{(0)}_{\mathbf{j}}C^{(0)}_{\mathbf{k}}\delta_{\mathbf{k}+\mathbf{k}'} \\ &+ 4R^{(0)}_{\mathbf{k}'}M^{0}_{\mathbf{k}'}R^{(0)}_{\mathbf{k}'-\mathbf{j}'}M^{0}_{\mathbf{k}'-\mathbf{j}'}C^{(0)}_{\mathbf{k}}C^{(0)}_{\mathbf{j}'}\delta_{\mathbf{k}+\mathbf{k}'} \\ &+ 2R^{(0)}_{\mathbf{k}}M^{0}_{\mathbf{k}}R^{(0)}_{\mathbf{k}'}M^{0}_{\mathbf{k}'}C^{(0)}_{\mathbf{j}}C^{(0)}_{\mathbf{k}-\mathbf{j}}\delta_{\mathbf{k}+\mathbf{k}'} \\ &+ \mathcal{O}(\lambda^4). \end{aligned} \tag{2.29}$$

This can be applied to all orders; however, as this is an infinite expansion, a full calculation will be intractable. This led Wyld to use a diagrammatic resummation, an approach that would contain the effects of all orders generated by the perturbation expansions into a more manageable set of equations.

2.2.2 Wyld's Diagrammatic Method

Wyld introduced a set of diagrams relating to the terms of the perturbation expansion. The diagrams generated could then be combined amongst themselves in forming the correlations of velocity expansion terms. These combinations resulted in a new set of diagrams, a graphical expansion for the exact correlator function. The assignment of diagrams to functions is presented for the perturbation and the formation of correlations from these is demonstrated.

Defining diagrams

Wyld begins his diagrammatic notation by assigning symbols to the various terms obtained in the perturbation expansion of the velocity field:

$$\underset{\alpha}{\overset{\mathbf{k},t}{\frac{\quad}{\quad}}} \quad \leftrightarrow \quad u^{(0)}_{\alpha}(\mathbf{k},t) \quad \rightarrow \quad u^{(0)}_{\mathbf{k}} \qquad \begin{array}{l}\text{Zeroth-order}\\ \text{velocity term}\end{array} \tag{2.30}$$

$$\underset{\alpha}{\overset{t}{\bullet}}\!\!\text{- - -}\overset{\mathbf{k}}{\text{- - -}}\!\!\underset{\beta}{\overset{t'}{\bullet}} \quad \leftrightarrow \quad R^{(0)}_{\alpha\beta}(\mathbf{k};\,t,t') \quad \rightarrow \quad R^{(0)}_{\mathbf{k}} \qquad \text{Bare propagator} \tag{2.31}$$

$$\mathbf{k}\,\overset{\beta}{\underset{\alpha}{\bullet}}\!\!\overset{\mathbf{j}}{\underset{\gamma}{<}}\,\mathbf{k}-\mathbf{j} \quad \leftrightarrow \quad M^{0}_{\alpha\beta\gamma}(\mathbf{k}) \quad \rightarrow \quad M^{0}_{\mathbf{k}} \qquad \text{Bare vertex} \tag{2.32}$$

These are placed into the relevant equations for the perturbed expressions.

Following the examples given previously, the second-order velocity term in the perturbation expansion,

$$u^{(2)}_{\mathbf{k}} = 2R^{(0)}_{\mathbf{k}}M^{0}_{\mathbf{k}}u^{(0)}_{\mathbf{j}}R^{(0)}_{\mathbf{k}\text{-}\mathbf{j}}M^{0}_{\mathbf{k}\text{-}\mathbf{j}}\left(u^{(0)}_{\mathbf{l}}u^{(0)}_{\mathbf{k}\text{-}\mathbf{j}\text{-}\mathbf{l}}\right), \tag{2.33}$$

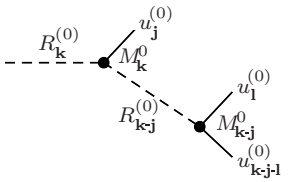

Temporarily breaking away from the reduced notation, the effectiveness of this diagrammatic approach is highlighted by seeing it with all variables, arguments, and indices restored:

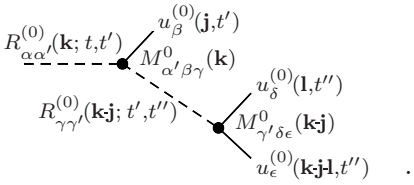

.

For completeness, the analytic form of this equation is

$$\begin{aligned} u^{(2)}_{\alpha}(\mathbf{k},t) \;=\; & \lambda^2 2 \int_{-\infty}^{t} dt' R^{(0)}_{\alpha\alpha'}(\mathbf{k};\, t,t') M_{\alpha'\beta\gamma}(\mathbf{k}) \times \\ & \int d^3\mathrm{j}\; u^{(0)}_{\beta}(\mathbf{j},t') \int_{-\infty}^{t'} dt'' R^{(0)}_{\gamma\gamma'}(\mathbf{k}-\mathbf{j};\, t',t'') M^0_{\gamma'\delta\epsilon}(\mathbf{k}-\mathbf{j}) \times \\ & \int d^3\mathrm{l} \left(u^{(0)}_{\delta}(\mathbf{l},t'')\, u^{(0)}_{\epsilon}(\mathbf{k}-\mathbf{j}-\mathbf{l},t'') \right). \end{aligned} \tag{2.34}$$

Perturbation or 'Tree' Diagrams

The terms of the perturbation expansion diagrams begin on a propagator and end in the zeroth-order velocity terms. The equations and their diagrammatic representations for these terms are given below to fourth-order:

$$u^{(1)}_{\mathbf{k}} = R^{(0)}_{\mathbf{k}} M^0_{\mathbf{k}} u^{(0)}_{\mathbf{j}} u^{(0)}_{\mathbf{k\text{-}j}} \qquad \text{ 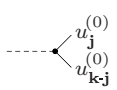 } \tag{2.35}$$

$$u^{(2)}_{\mathbf{k}} = 2 R^{(0)}_{\mathbf{k}} M^0_{\mathbf{k}} R^{(0)}_{\mathbf{k\text{-}j}} M^0_{\mathbf{k\text{-}j}} u^{(0)}_{\mathbf{j}} \left(u^{(0)}_{\mathbf{l}} u^{(0)}_{\mathbf{k\text{-}j\text{-}l}} \right) \qquad \text{ 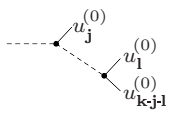 } \tag{2.36}$$

$$
\begin{aligned}
u^{(3)}_{\mathbf{k}} &= R^{(0)}_{\mathbf{k}} M^0_{\mathbf{k}} R^{(0)}_{\mathbf{j}} M^0_{\mathbf{j}} R^{(0)}_{\mathbf{k\text{-}j}} M^0_{\mathbf{k\text{-}j}} \times \\
&\qquad \left(u^{(0)}_{\mathbf{g}} u^{(0)}_{\mathbf{j\text{-}g}} u^{(0)}_{\mathbf{l}} u^{(0)}_{\mathbf{k\text{-}j\text{-}l}} \right) \\
&\quad + 4 R^{(0)}_{\mathbf{k}} M^0_{\mathbf{k}} R^{(0)}_{\mathbf{k\text{-}j}} M^0_{\mathbf{k\text{-}j}} R^{(0)}_{\mathbf{k\text{-}j\text{-}l}} M^0_{\mathbf{k\text{-}j\text{-}l}} \times \\
&\qquad \left(u^{(0)}_{\mathbf{j}} u^{(0)}_{\mathbf{l}} u^{(0)}_{\mathbf{m}} u^{(0)}_{\mathbf{k\text{-}j\text{-}l\text{-}m}} \right) \\
u^{(4)}_{\mathbf{k}} &= 2 R^{(0)}_{\mathbf{k}} M^0_{\mathbf{k}} R^{(0)}_{\mathbf{k\text{-}j}} M^0_{\mathbf{k\text{-}j}} R^{(0)}_{\mathbf{l}} M^0_{\mathbf{l}} R^{(0)}_{\mathbf{k\text{-}j\text{-}l}} M^0_{\mathbf{k\text{-}j\text{-}l}} \times \\
&\qquad \left(u^{(0)}_{\mathbf{j}} u^{(0)}_{\mathbf{h}} u^{(0)}_{\mathbf{l\text{-}h}} u^{(0)}_{\mathbf{m}} u^{(0)}_{\mathbf{k\text{-}j\text{-}l\text{-}m}} \right) \\
&\quad + 4 R^{(0)}_{\mathbf{k}} M^0_{\mathbf{k}} R^{(0)}_{\mathbf{j}} M^0_{\mathbf{j}} R^{(0)}_{\mathbf{k\text{-}j}} M^0_{\mathbf{k\text{-}j}} R^{(0)}_{\mathbf{k\text{-}j\text{-}l}} M^0_{\mathbf{k\text{-}j\text{-}l}} \times \\
&\qquad \left(u^{(0)}_{\mathbf{g}} u^{(0)}_{\mathbf{j\text{-}g}} u^{(0)}_{\mathbf{l}} u^{(0)}_{\mathbf{m}} u^{(0)}_{\mathbf{k\text{-}j\text{-}l\text{-}m}} \right) \\
&\quad + 8 R^{(0)}_{\mathbf{k}} M^0_{\mathbf{k}} R^{(0)}_{\mathbf{k\text{-}j}} M^0_{\mathbf{k\text{-}j}} R^{(0)}_{\mathbf{k\text{-}j\text{-}l}} M^0_{\mathbf{k\text{-}j\text{-}l}} R^{(0)}_{\mathbf{k\text{-}j\text{-}l\text{-}m}} M^0_{\mathbf{k\text{-}j\text{-}l\text{-}m}} \times \\
&\qquad \left(u^{(0)}_{\mathbf{j}} u^{(0)}_{\mathbf{l}} u^{(0)}_{\mathbf{m}} u^{(0)}_{\mathbf{n}} u^{(0)}_{\mathbf{k\text{-}j\text{-}l\text{-}m\text{-}n}} \right)
\end{aligned}
\tag{2.37, 2.38}
$$

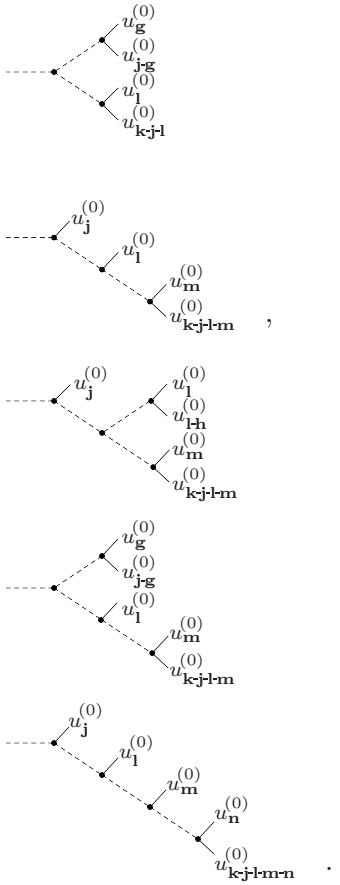

These are the so-called "tree-level" diagrams.

Correlation diagrams

Correlation diagrams arise from attaching tree-level diagrams together by fusing the velocity field terms at the ends of branches. These become the zeroth-order correlation functions.

The diagram for the zeroth-order correlation term or 'bare correlator' is given by

$$
\overset{t}{\underset{\alpha}{\bullet}} \xrightarrow{\mathbf{k}} \overset{t'}{\underset{\beta}{\bullet}} \quad \leftrightarrow \; C^{(0)}_{\alpha\beta}(\mathbf{k}; t, t') \;\; \rightarrow \;\; C^{(0)}_{\mathbf{k}}
\tag{2.39}
$$

To see how the diagrams operate in place of the traditional mathematics, it is instructive to examine the construction of second-order correlation terms from the tree-level diagrams.

The first term considered here is the last of the second-order terms in (2.24),

$$
\begin{aligned}
\langle u^{(2)}_{\mathbf{k}} u^{(0)}_{\mathbf{k}'} \rangle &= 2 R^{(0)}_{\mathbf{k}} M^0_{\mathbf{k}} R^{(0)}_{\mathbf{k\text{-}j}} M^0_{\mathbf{k\text{-}j}} \langle u^{(0)}_{\mathbf{j}} u^{(0)}_{\mathbf{l}} u^{(0)}_{\mathbf{k\text{-}j\text{-}l}} u^{(0)}_{\mathbf{k}'} \rangle \\
&= 4 R^{(0)}_{\mathbf{k}} M^0_{\mathbf{k}} R^{(0)}_{\mathbf{k\text{-}j}} M^0_{\mathbf{k\text{-}j}} C^{(0)}_{\mathbf{j}} C^{(0)}_{\mathbf{k}'} \delta_{\mathbf{k}+\mathbf{k}'} .
\end{aligned}
\tag{2.40}
$$

Diagrammatically this corresponds to

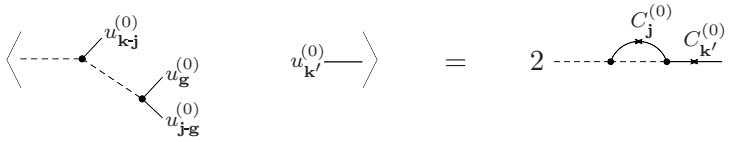

(2.41)

An extra factor of 2 arises from the combinatorics, analogous to the Wick contractions of the fourth-order moment into products of second-order moments,

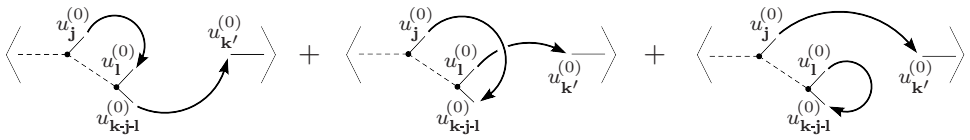

$$\langle u^{(0)}_{\mathbf{j}} u^{(0)}_{\mathbf{l}} \rangle \langle u^{(0)}_{\mathbf{k-j-l}} u^{(0)}_{\mathbf{k'}} \rangle \quad + \quad \langle u^{(0)}_{\mathbf{j}} u^{(0)}_{\mathbf{k-j-l}} \rangle \langle u^{(0)}_{\mathbf{l}} u^{(0)}_{\mathbf{k'}} \rangle \quad + \quad \langle u^{(0)}_{\mathbf{j}} u^{(0)}_{\mathbf{k'}} \rangle \langle u^{(0)}_{\mathbf{l}} u^{(0)}_{\mathbf{k-j-l}} \rangle$$

The last term above vanishes as in (2.27) thereby establishing a rule that any diagram with a closed loop that is connected to the diagram by a single propagator line will vanish.

The other diagrams in the second-order terms are obtained by a similar construction,

$$\begin{aligned} \langle u^{(0)}_{\mathbf{k}} u^{(2)}_{\mathbf{k'}} \rangle &= 2R^{(0)}_{\mathbf{k}} M^0_{\mathbf{k}} R^{(0)}_{\mathbf{k'-j'}} M^0_{\mathbf{k'-j'}} \langle u^{(0)}_{\mathbf{k}} u^{(0)}_{\mathbf{j'}} u^{(0)}_{\mathbf{l'}} u^{(0)}_{\mathbf{k'-j'-l'}} \rangle \\ &= 4R^{(0)}_{\mathbf{k}} M^0_{\mathbf{k}} R^{(0)}_{\mathbf{k'-j'}} M^0_{\mathbf{k'-j'}} C^{(0)}_{\mathbf{k}} C^{(0)}_{\mathbf{k'-j'}} \delta_{\mathbf{k+k'}} \end{aligned} \tag{2.42}$$

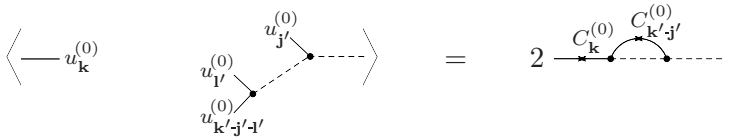

(2.43)

$$\begin{aligned} \langle u^{(1)}_{\mathbf{k}} u^{(1)}_{\mathbf{k'}} \rangle &= R^{(0)}_{\mathbf{k}} M^0_{\mathbf{k}} R^{(0)}_{\mathbf{k'}} M^0_{\mathbf{k'}} \langle u^{(0)}_{\mathbf{j}} u^{(0)}_{\mathbf{k\text{-}j}} u^{(0)}_{\mathbf{j'}} u^{(0)}_{\mathbf{k'\text{-}j'}} \rangle \\ &= 2R^{(0)}_{\mathbf{k}} M^0_{\mathbf{k}} R^{(0)}_{\mathbf{k'}} M^0_{\mathbf{k'}} C^{(0)}_{\mathbf{j}} C^{(0)}_{\mathbf{k\text{-}j}} \delta_{\mathbf{k+k'}} \end{aligned} \tag{2.44}$$

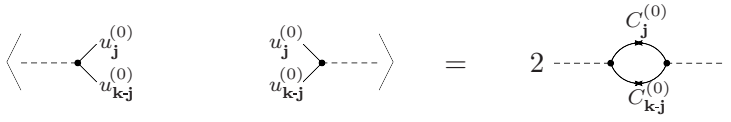

(2.45)

This procedure can be applied to all orders, and it can be shown that a one-to-one correspondence is established between diagrams and their analytical counterparts, with

the correct numerical prefactors. A reproduction of primitive correlator diagrams to fourth-order is given in the figure below.

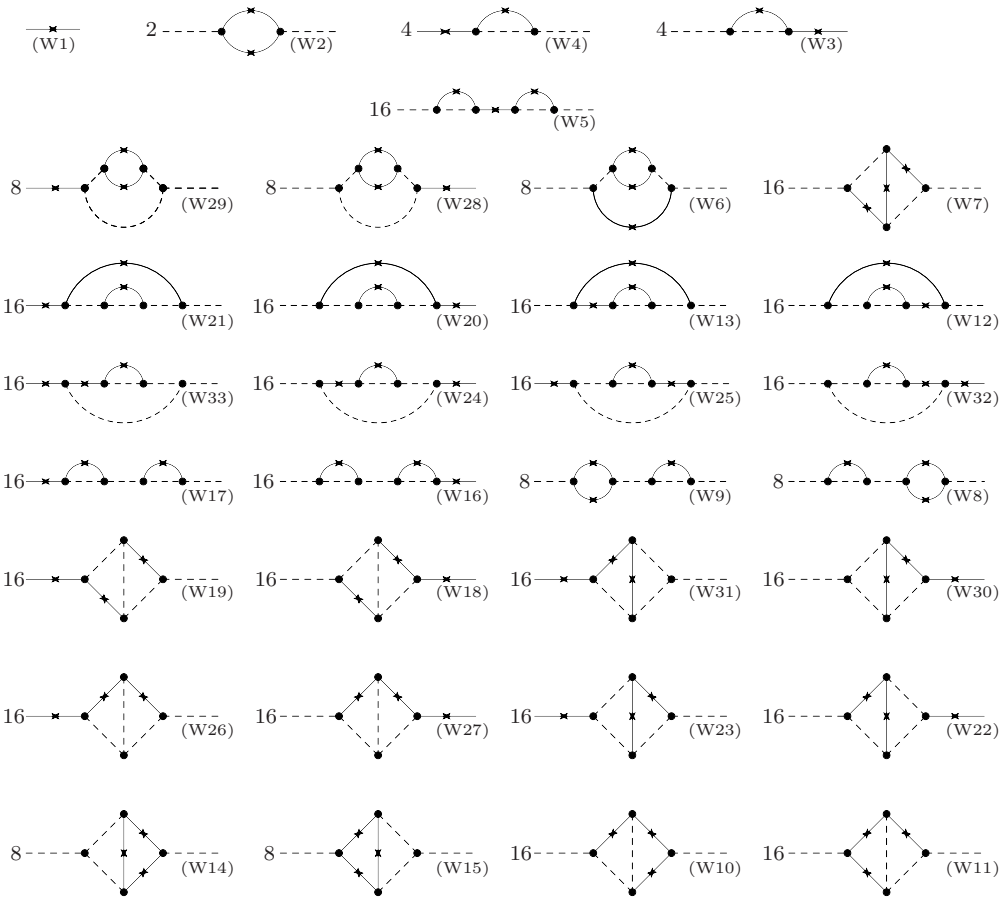

Figure 2.2: Wyld's diagrams representing the correlator expansion up to and including the fourth-order terms. The labels shown on each diagram correspond to those given in figure 2 of the original paper.

Wyld's perturbation method is formally exact and uses Gaussian statistics to enable the closure; it does however retain an infinite number of terms in the expansion of the correlation function. The next subsection sees the systematic renormalisation of these terms into a more manageable formula.

2.2.3 Wyld's Renormalisation

Wyld's method of renormalisation is a resummation of diagrams based on the emergence and recurrence of fundamental, irreducible diagram units. An analogy can be made with finding the irreducible diagrams in other diagrammatic methods, most appropriately those in particle physics [72].

The main controversies associated with Wyld's formalism are due to the renormalisation, and therefore, the procedure here will be different than Wyld's. Explanations will be given at points where it differs from the Wyld method.

The new starting point is the spectral NSE which multiplied by a second velocity-field coefficient, $u_{\alpha'}(-\mathbf{k},t')$ and then averaged,

$$\Big(\frac{\partial}{\partial t}+\nu \mathrm{k}^2\Big)\big\langle u_\alpha(\mathbf{k},t)u_{\alpha'}(-\mathbf{k},t')\big\rangle = \big\langle f_\alpha(\mathbf{k},t)u_{\alpha'}(-\mathbf{k},t')\big\rangle + \frac{1}{(2\pi)^3}M^0_{\alpha\beta\gamma}(\mathbf{k})\int d^3\mathrm{j}\,\big\langle u_\beta(\mathbf{j},t)u_\gamma(\mathbf{k}-\mathbf{j},t)u_{\alpha'}(-\mathbf{k},t')\big\rangle. \tag{2.46}$$

This formulation has been used by Kraichnan [50] and also for the LET [35]. It must be noted that this formulation gives exactly the same result as Wyld's formulation when the velocity-field coefficient on the RHS are expanded perturbatively, thus the terms given in fig. 2.2 can be obtained from the above equation.

There are two reasons why this formulation will be considered. The first is that the bare propagator (see on the LHS of (2.46) in its inverted form) will remain unrenormalised. The second point is that the vertex associated with the momentum-transfer operator $M^0_{\alpha\beta\gamma}(\mathbf{k})$ is outside of the average, and will also not be included in the resummation. These points are more explicit in the formulation considered here rather than being embedded in Wyld's method.

The first criterion by which to classify diagrams is the ability to separate a diagram into two parts by severing a single correlator. Diagrams that can be split into two separate diagrams by cutting a single correlator are labelled by Wyld as 'Class-A'. The procedure here will further distinguish two types of Class-A diagrams: those diagrams with the correlators on the LHS of the left-most vertex, and those with separable diagrams connected by a single bare correlator that occurs on the RHS of the left-most vertex. These are labelled Class-A$_L$ and Class-A$_R$, respectively.

The classification for Class-A$_R$ includes diagrams with an internal correlator line, such as

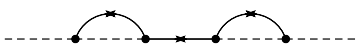

Bare correlators are given analytically by

$$\langle u^{(0)}_\alpha(\mathbf{k},t)u^{(0)}_\omega(\mathbf{k}',t')\rangle = \big\langle R^{(0)}_{\alpha\alpha'}(\mathbf{k};\,t,s)f_{\alpha'}(\mathbf{k},s)f_{\omega'}(\mathbf{k}',s')R^{(0)}_{\omega'\omega}(\mathbf{k};\,s',t')\big\rangle, \tag{2.47}$$

which reveals the propagators within each. This identification is what will allow the derivation of the propagator diagrams to come. Cutting of an external correlator differs from field theoretic methods of particle physics as external lines are typically not cut, for details see [72, 73]. An example of cutting an external correlator is given

diagrammatically by

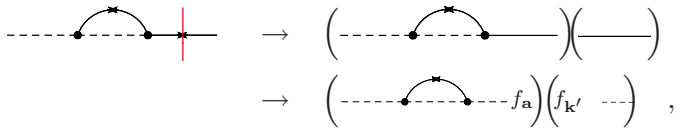

with its analytic counterpart given by

$$\begin{aligned} R^{(0)}_{\mathbf{k}} M^{0}_{\mathbf{k}} R^{(0)}_{\mathbf{j}} M^{0}_{\mathbf{j}} C^{(0)}_{\mathbf{k\text{-}j}} C^{(0)}_{\mathbf{k}'} \rightarrow & \quad \left(R^{(0)}_{\mathbf{k}} M^{0}_{\mathbf{k}} R^{(0)}_{\mathbf{j}} M^{0}_{\mathbf{j}} C^{(0)}_{\mathbf{k\text{-}j}} u^{(0)}_{\mathbf{a}} \right) \left(u^{(0)}_{\mathbf{k}'} \right) \\ \rightarrow & \quad \left(R^{(0)}_{\mathbf{k}} M^{0}_{\mathbf{k}} R^{(0)}_{\mathbf{j}} M^{0}_{\mathbf{j}} C^{(0)}_{\mathbf{k\text{-}j}} R^{(0)}_{\mathbf{a}} f_{\mathbf{a}} \right) \left(f_{\mathbf{k}'} R^{(0)}_{\mathbf{k}'} \right). \end{aligned}$$

The same can be applied to diagram (W4), a member of the Class-A$_L$ diagrams, and in general to any diagram with an external correlator. Using fig. 2.2 as a reference, the Class-A$_L$ diagrams are: 4, 17-25(odd), 26, 29-33(odd); and the Class-A$_R$ diagrams are: 3, 5, 16-24(even),27, 28-32(even).

It can now be seen that these diagrams can be written with the correlation in the form of a force-force correlation. For example,

$$\langle f_{\mathbf{k}} f_{\mathbf{k}'} \rangle = \langle f_{\mathbf{k}} f_{\mathbf{k}'} \rangle + 4 \langle f_{\mathbf{k}} f_{\mathbf{k}'} \rangle + \mathcal{O}(\lambda^4), \tag{2.48}$$

$$R^{(0)}_{\mathbf{k}} \langle f_{\mathbf{k}} f_{\mathbf{k}'} \rangle R_{\mathbf{k}'} = R^{(0)}_{\mathbf{k}} \langle f_{\mathbf{k}} f_{\mathbf{k}'} \rangle R^{(0)}_{\mathbf{k}'} + 4 R^{(0)}_{\mathbf{k}} \langle f_{\mathbf{k}} f_{\mathbf{k}'} \rangle R^{(0)}_{\mathbf{k}'} R^{(0)}_{\mathbf{k}'} M^{0}_{\mathbf{k}} R_{\mathbf{j}} M^{0}_{\mathbf{j}} C^{(0)}_{\mathbf{k}'} + \mathcal{O}(\lambda^4). \tag{2.49}$$

A new function, the exact propagator, has been established as well as a new diagram associated with it,

$$= + 4 + \mathcal{O}(\lambda^4), \tag{2.50}$$

$$R_{\mathbf{k}} = R^{(0)}_{\mathbf{k}} + 4\lambda^2 R^{(0)}_{\mathbf{k}} M^{0}_{\mathbf{j}} C^{(0)}_{\mathbf{j}} R^{(0)}_{\mathbf{k\text{-}j}} M^{0}_{\mathbf{k}} R^{(0)}_{\mathbf{k}} + \mathcal{O}(\lambda^4). \tag{2.51}$$

The complete expansion to fourth-order is given below:

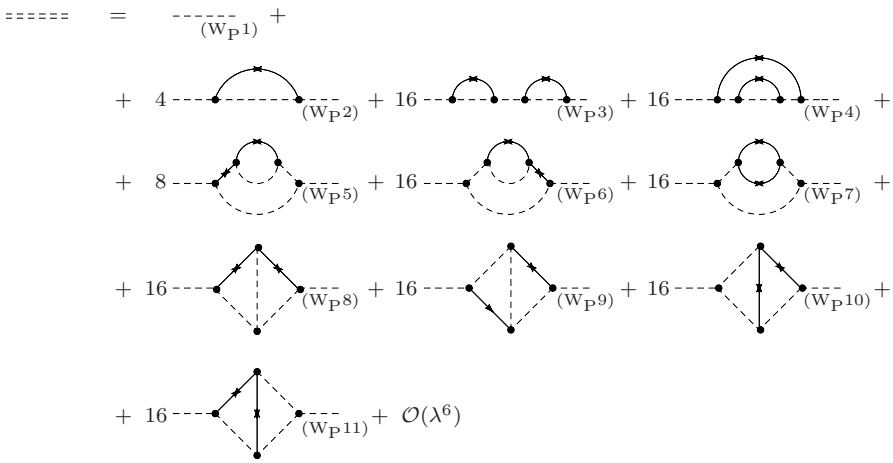

(2.52)

Note that while the method used here to obtain these terms is different from Wyld's, the same terms are obtained for the expansion.

The procedure for dealing with Class-A$_R$ diagrams will be postponed as it is similar to that used to re-sum the remaining diagrams. Diagrams not classified as Class-A are designated as Class-B diagrams; these are further classified into reducible and irreducible based on finding embedded elements of low-order within diagrams of higher-order. An example of this can be seen by examining the diagram W6 in fig. 2.2,

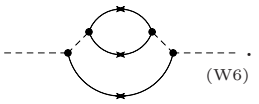

It is readily seen that the elements between the two outermost vertices is the diagram W2 in fig. 2.2; this is also equivalent to the W2 diagram by replacing the top correlator with itself. This will be given in more detail below however it will be useful to include another function at this time.

Wyld introduced an exact vertex function as an expansion without giving a detailed method of how it was dervied but instead wrote a diagram series expansion for the exact vertex function,

(2.53)

$$\begin{aligned} M_{\mathbf{k}} &= M^0_{\mathbf{k}} + 4M^0_{\mathbf{k}} C^{(0)}_{\mathbf{j}} R^{(0)}_{\mathbf{k\text{-}j}} M^0_{\mathbf{a}} R^{(0)}_{\mathbf{a}} M^0_{\mathbf{b}} \\ &+ 4M^0_{\mathbf{k}} C^{(0)}_{\mathbf{k\text{-}j}} R^{(0)}_{\mathbf{j}} M^0_{\mathbf{a}} R^{(0)}_{\mathbf{a}} M^0_{\mathbf{b}} + 4M^0_{\mathbf{k}} R^{(0)}_{\mathbf{j}} R^{(0)}_{\mathbf{k\text{-}j}} M^0_{\mathbf{a}} C^{(0)}_{\mathbf{a}} M^0_{\mathbf{b}} + \mathcal{O}(\lambda^5). \end{aligned} \tag{2.54}$$

Starting with these irreducible diagrams, Wyld generated the full expansion by replacing any of the constituent elements with a higher-order element. For example, replacing the correlator, a propagator, or a vertex in the first term of (2.53) results in the following terms, respectively:

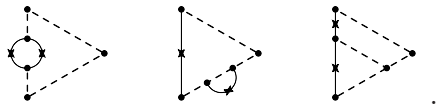

Irreducible diagrams can then be found by selectively removing correlators, propagators, and vertex corrections from Class-B diagrams. The set is left with diagrams that cannot be constructed from non-trivial (bare correlators, propagators, or vertices) elements. Under this classification, there are two up to fourth order,

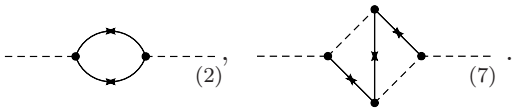

Starting with the second-order Class-B irreducible diagrams, all Class-B diagrams (except the Class-B irreducible diagrams that arise at higher orders) can be generated by replacing the appropriate correlator, propagator, and vertex corrections with their respective expansions. This is demonstrated by considering three correlator diagrams as examples,

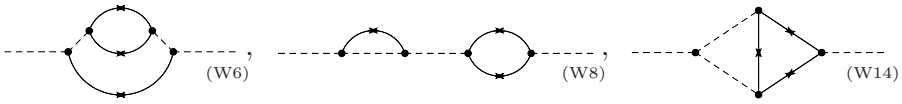

and examining their construction.

1. Construction with a Correlator Correction

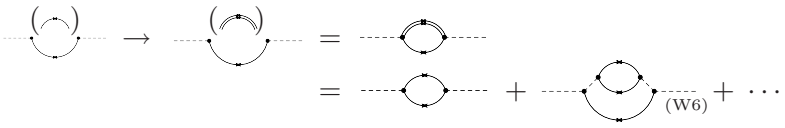

(2.55)

Replacing a bare correlator with an exact one in the irreducible second-order correlator diagram is equivalent to inserting the series for the correlator, giving rise to the

anticipated diagram as well as others.

2. Construction with a Propagator Correction

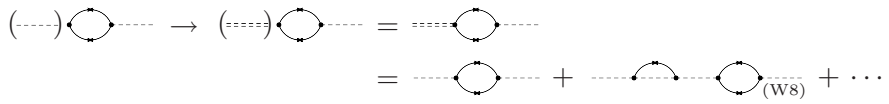

(2.56)

Inserting the exact propagator and its expansion obtains the desired term, (W8).

3. Construction with a Vertex Correction

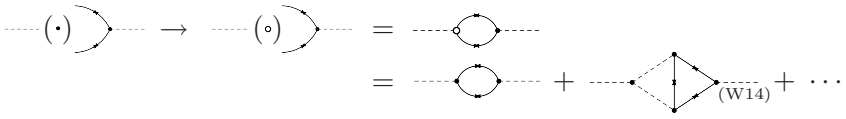

(2.57)

As with the others, the inclusion of the vertex expansion in this case produces (W14) and (W15), not shown, plus others at higher orders.

Taking this one step further, all bare quantities in the irreducible second-order correlator can be replaced by their exact counterparts,

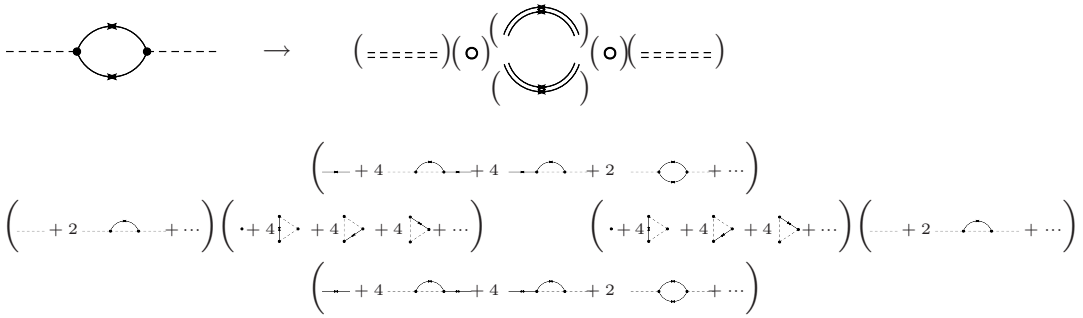

This procedure generates all Class-A$_R$ terms and Class-B reducible terms given in fig. 2.2.

Collecting the irreducibles, where each bare term is replaced with its respective exact term, together with the Class-A$_L$ terms expressed in (2.52) leads to an equation for the exact correlator,

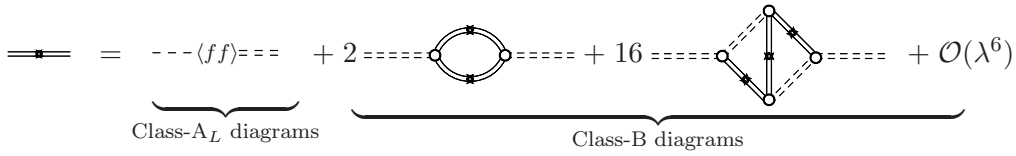

$$+ \text{ Class-A}_R \text{ diagrams} \quad . \tag{2.58}$$

This is similar to Wyld's exact correlator equation,

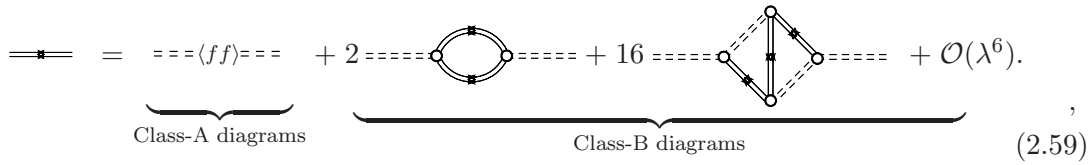

(2.59)

where the first term on the RHS contains both A_L and A_R diagrams. Further remarks about the exact correlator will be made later in this section; at this point it is more pertinent to deal with the exact propagator.

The approach Wyld used to determine an equation for the exact correlator could not be used for the exact propagator. Using both Classes A_L and A_R, the result is a primitive expansion for the propagator with some of the terms redundantly generated, specifically diagrams ($\mathrm{W_P}3$), ($\mathrm{W_P}6$), and ($\mathrm{W_P}7$) in (2.52). Wyld circumvented this by using a Dyson equation for the propagator, expressing his arguments only mathematically and without a diagram equation for the exact propagator. The result was to introduce modified vertex functions and use the Ward-Takashi identities to relate these to the propagators, as in quantum field theory [72]. Wyld's final complete set of equations has a diagrammatic expansion for the exact correlator, two diagram series for the exact and modified-exact vertex functions, and the Ward-Takashi identities.

It was however argued by Lee that the method using the Dyson equation and Ward-Takashi identities cannot be applied to the full 3-dimensional NSE as they were to Wyld's scalar model [74]. Lee had adapted Wyld's method to magnetohydrodynamic (MHD) turbulence and found the same problem but introduced the following equation for the exact propagator:

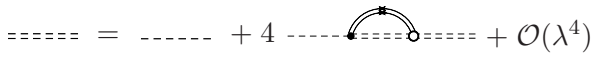

(2.60)

The left-most propagator and vertex have both been left bare. The former clears the redundant generation of propagator diagram ($\mathrm{W_P}3$); while the latter does the same for diagrams ($\mathrm{W_P}6$) and ($\mathrm{W_P}7$). This equation for the propagator does correct the redundancies, however, the asymmetry introduced by Lee also does not generate Wyld's diagram (W10) hence the inclusion of a fourth-order irreducible propagator term not found in Wyld. Lee's exact propagator is

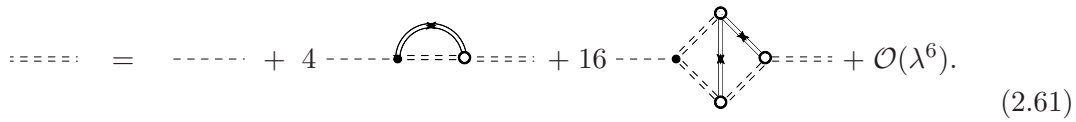

(2.61)

Lee introduced this as an *ad hoc* fix, however the above equation can be derived by adopting a scheme where the left-most propagator and vertex stay unrenormalised when

constructing the exact diagrams. Finding the irreducible propagator diagrams from the set of Class-A_L diagrams while maintaining that the left-most propagator and vertex remain unrenormalised results in (2.61). This can be applied to classes A_R and B. The result is the following subset of diagrams,

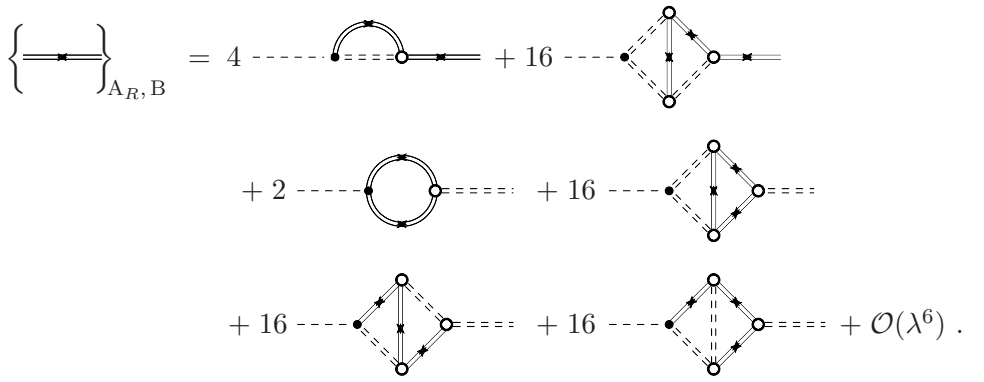

(2.62)

The brackets with subscripts denote the terms of the exact correlator from classes A_R and B. The classes have been segregated by line with the top line containing those of Class-A_R. The vertices postulated by Wyld, given in (2.53), have been used in constructing these sets. The exact vertex expansion from Wyld is still valid to $\mathcal{O}(\lambda^5)$ and can be used here,

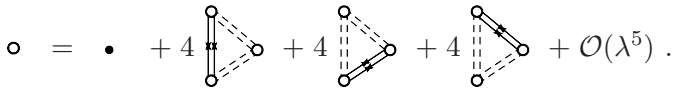

(2.63)

Using all classes together, the expansion for the exact correlator can now be given

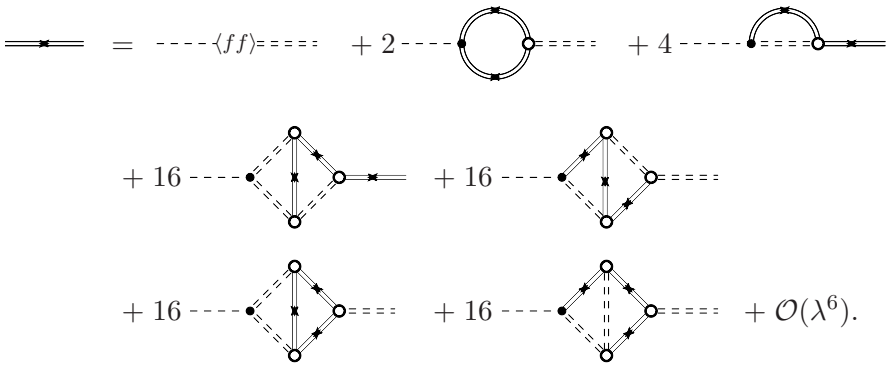

(2.64)

This equation is very different from Wyld's equation for the exact correlator, (2.59); the

inclusion of these terms will prove an important feature of the new renormalisation when comparing the the method of MSR in the following section. Considering only terms up to second-order and noting that the bare propagator is equivalent to $(\partial_t + \nu \mathrm{k}^2)^{-1}$, the equation above and the equation for the propagator (2.61) give the result of the DIA, (2.5) and (2.6), given earlier. Wyld required some rearrangement of his exact correlator equation, (2.59), and was able show the same result diagrammatically in his paper.

The set of equations, (2.61), (2.63), and (2.64), contains the same information of the correlator expansion up to fourth-order, fig. 2.2, and describes turbulence insofar as the NSE can be treated perturbatively, with the Gaussian statistics assumed in the external forcing introduced to facilitate the closure. The above equations are still, in principle, infinite series however the resummation contains the detail of a greater number of terms and allows a truncation that retains more of this information."

Ignoring the perturbative treatment of a strongly-coupled system, Wyld's formalism and diagrammatic treatment of the initial correlator expansion is rigorous and can be extended to the 3-dimensional NSE. The renormalisation procedure is systematic and though it formally works for Wyld's model-NSE, it cannot be generalised to the actual NSE. Lee's reworking of the formalism to MHD fixed the issue of the propagator but did so with an *ad hoc* choice without a systematic derivation as in the correlator or vertex terms.

It has been found here that a different resummation method, which maintains that the left-most propagator and vertex be kept out of the resummation, is suitable in obtaining a set of closed equations. The equations and methods here have only been used to fourth-order and are correct under this constraint. The approach borrowed ideas from both the Kraichnan and Wyld formalisms, and successfully derived the DIA. It also derived the correct propagator expansion found empirically by Lee.

As the DIA does not give the Kolmogorov spectrum, it is thought that the Wyld formalism is incorrect. The exclusion of the renormalised vertex terms, which are said to contain the information of the nonlinear couplings in the NSE, is thought to be responsible [58]. The Class-A_R terms of (2.64) are additional terms which were not part of Wyld's original derivation; these extra terms will be important in the following section.

2.3 The Martin-Siggia-Rose Formalism

The MSR Formalism [58] is by now a well-known theory that can be used to calculate the "statistical dynamics of classical systems." The formalism establishes a operator theory where the observables are defined as Heisenberg operators. This permits a

non-perturbative treatment akin to the Schwinger formalism [75–77] in quantum field theory which formally closes the statistical moment hierarchy. The operator formalism introduces an adjoint operator which can be used in the construction of nontrivial commutation relations leading to correlation and response functions [55]. Employing the Schwinger formalism for statistical closure involves the use of a generating or characteristic functional. An alternative to the construction of such operators comes from functional or path integrals [78].

Notable sources providing detailed information on MSR are works by Rose [79], Phythian [80–82], Andersen [83] and Krommes [55]. As demonstrated in their original paper, the formalism is applicable to the turbulence problem which has inspired further work in the analysis of least-action principles [84, 85] and gauge symmetries [86–88] in the study of turbulence.

MSR is by their own account comparable to perturbative formalisms of Kraichnan and Wyld. However, it is their claim supported by Kraichnan (see footnote 11 in in their paper) that Wyld is incorrect in his renormalisation procedure specifically with regard to his vertex corrections. As it is possible to work directly from their diagrammatic interpretation and compare it to Wyld, it is shown here that this assertion is not accurate and that both formalisms are equivalent to fourth order.

2.3.1 Setting up the Formalism

It has been seen already that the velocity field $u_\alpha(\mathbf{x}, t)$ is a fundamental observeable in fluid dynamics. The MSR formalism extends the common notion of it to that of a classical statistical operator [80, 83]. In the language of quantum field theory, it is similar to a Heisenberg operator, in that it is time dependent [72]. This is an essential first-step in establishing the formalism.

A remark about notation is in order. MSR use a single variable to stand for all space and time arguments, as well as indices. Their notation will not be employed here, rather, their formalism will be written in the notation used in earlier chapters. To see how their notation is set-up, consider the following example

$$u_\alpha(\mathbf{x}, t) \;\rightarrow\; u_{\alpha_1}(\mathbf{x}_1, t_1) \;\rightarrow\; u(1). \tag{2.65}$$

It can easily be seen that their notation is much more compact and is helpful in working through their paper.

Dynamical Equations

A generalised equation of motion for a field variable, $u_\alpha(\mathbf{x},t)$ is introduced,

$$\begin{aligned}\partial_t u_\alpha(\mathbf{x},t) &= \widehat{U}_\alpha(\mathbf{x};t) + \widehat{U}_{\alpha\beta}(\mathbf{x},\mathbf{x}';t,t')u_\beta(\mathbf{x}',t') \\ &+ \widehat{U}_{\alpha\beta\gamma}(\mathbf{x},\mathbf{x}',\mathbf{x}'';t,t',t'')u_\beta(\mathbf{x}',t')u_\gamma(\mathbf{x}'',t''). \end{aligned} \tag{2.66}$$

The quantities defined within,

$$\widehat{U}_\alpha(\mathbf{x};t) \leftrightarrow \text{0-point potential/external force} \tag{2.67}$$

$$\widehat{U}_{\alpha\beta}(\mathbf{x},\mathbf{x}';t,t') \leftrightarrow \text{1-point potential} \tag{2.68}$$

$$\widehat{U}_{\alpha\beta\gamma}(\mathbf{x},\mathbf{x}',\mathbf{x}'';t,t',t'') \leftrightarrow \text{2-point potential,} \tag{2.69}$$

are the generalised interaction potential functions. Integration of repeated arguments and summation of indices are implied.

It is argued that (2.66) can accommodate many dynamical systems, and in principle, can be generalised to higher orders of interaction. MSR cite several example systems and demonstrate how the interaction potential functions may be written to adapt to these examples. One such example is the Navier Stokes Equation, where,

$$\widehat{U}_\alpha(\mathbf{x};t) \rightarrow \widehat{F} \quad \text{external forcing} \tag{2.70}$$

$$\widehat{U}_{\alpha\beta}(\mathbf{x},\mathbf{x}';t,t') \rightarrow \widehat{D} \quad \text{dissipation term} \tag{2.71}$$

$$\widehat{U}_{\alpha\beta\gamma}(\mathbf{x},\mathbf{x}',\mathbf{x}'';t,t',t'') \rightarrow \widehat{T} \quad \text{inertial term.} \tag{2.72}$$

To see this, the nonlinear inertial term in the NSE can be written as

$$\begin{aligned}&\widehat{T}_{\alpha\beta\gamma}(\mathbf{x},\mathbf{x}',\mathbf{x}'';t,t',t'')u_\beta(\mathbf{x}',t')u_\gamma(\mathbf{x}'',t'') \\ &\equiv \int d^3\mathrm{x}' \int d^3\mathrm{x}'' \int dt' \int dt''\ \widehat{T}_{\alpha\beta\gamma}(\mathbf{x},\mathbf{x}',\mathbf{x}'';t,t',t'')u_\beta(\mathbf{x}',t')u_\gamma(\mathbf{x}'',t'') \\ &= \int d^3\mathrm{x}' \int d^3\mathrm{x}'' \int dt' \int dt''\ \frac{\partial}{\partial x'_\beta}\delta_{\alpha\gamma}\delta(\mathbf{x}-\mathbf{x}')\delta(\mathbf{x}-\mathbf{x}'')\delta(t-t')\delta(t-t'') \\ &\quad \times\Big(u_\beta(\mathbf{x}',t')u_\gamma(\mathbf{x}'',t'')\Big) \\ &= u_\beta(\mathbf{x},t)\frac{\partial}{\partial x_\beta}u_\alpha(\mathbf{x},t). \end{aligned} \tag{2.73}$$

The last step uses the incompressibility condition, $\nabla\cdot\mathbf{u}=0$.

In keeping the goal of an analogous formalism to QFT, an adjoint operator is

introduced by way of a commutation relation,

$$\left[u_\alpha(\mathbf{x},t),\widehat{u}_\beta(\mathbf{x}',t)\right] = \delta_{\alpha\beta}\,\delta(\mathbf{x}-\mathbf{x}'). \tag{2.74}$$

which defines the adjoint operator accordingly,

$$\widehat{u}_\alpha(\mathbf{x},t) \;\equiv\; \frac{-\delta}{\delta u_\alpha(\mathbf{x},t)}. \tag{2.75}$$

In the path-integral formalism, the Fourier conjugate of the adjoint field readily occurs in the treatment of the delta-functional (see for example Jensen [78] and Krommes [55]).

An equation of motion for the adjoint field,

$$\begin{aligned} -\partial_t\widehat{u}_\alpha(\mathbf{x},t) &= \widehat{D}_{\beta\alpha}(\mathbf{x}',\mathbf{x};t',t)\widehat{u}_\beta(\mathbf{x}',t') \\ &+ \widehat{T}_{\alpha\beta\gamma}(\mathbf{x}',\mathbf{x}'',\mathbf{x};t,t',t'')\widehat{u}_\beta(\mathbf{x}',t')u_\gamma(\mathbf{x}'',t''), \end{aligned} \tag{2.76}$$

may be constructed using (2.66) and the commutation relation, (2.74).

Both fields are collected together in what Krommes calls an 'extended field vector',

$$U_\alpha(\mathbf{x};t) = \left[\begin{array}{c} u_\alpha(\mathbf{x},t) \\ \widehat{u}_\alpha(\mathbf{x},t) \end{array}\right]. \tag{2.77}$$

The commutator for the 'extended field vector' is

$$\Big[U_\alpha(\mathbf{x};t),U_\beta(\mathbf{x}';t)\Big] = i\sigma_2\delta_{\alpha\beta}\,\delta(\mathbf{x}-\mathbf{x}'), \tag{2.78}$$

where

$$\sigma_2 \equiv \left[\begin{array}{cc} 0 & -i \\ i & 0 \end{array}\right]. \tag{2.79}$$

As argument labels are about to increase, a new notation will been used where all arguments are combined into the spatial argument and placed in the subscript, $U_\alpha(\mathbf{x};t) \to U_{\mathbf{x}}$. One can begin to appreciate how the MSR single-variable notation was so useful.

An equation of motion for the 'extended field vector' is then simply constructed from the dynamical equations of $\mathbf{u}$ and $\widehat{\mathbf{u}}$,

$$-i\sigma_2\partial_t U_{\mathbf{x}} \;=\; \widehat{\mathcal{F}}_{\mathbf{x}} + \widehat{\mathcal{D}}_{\mathbf{x},\mathbf{x}'}U_{\mathbf{x}'} + \frac{1}{2}\widehat{\mathcal{T}}_{\mathbf{x},\mathbf{x}',\mathbf{x}''}U_{\mathbf{x}'}U_{\mathbf{x}''}. \tag{2.80}$$

The curly-script used for the potentials distinguishes them from their predecessors.

Statistics

A generating functional is introduced and used to create all statistical quantities,

$$\mathcal{Z} \;=\; \Big\{ \exp\big[\int_{t_i}^{t_f} U_{\mathbf{x}} \eta_{\mathbf{x}} \big] \Big\}_{\mathrm{T}}, \tag{2.81}$$

where $\{\cdots\}_{\mathrm{T}}$ denotes time-ordering. The term $\eta_{\mathbf{x}} \equiv \eta(\mathbf{x},t)$ plays the role of the source term that is standard to these techniques; it is in effect a perturbation to the 0-point potential.

Using the generating functional, one can find the statistical moments or cumulants as needed through functional differentiation of the generating functional with respect to the source term. In practise, the cumulants are obtained by functionally differentiating the logarithm of the generating functional, returning what are called the connected Green's functions [72]. As an example, the first- and second-order cumulants are produced respectively via

$$\begin{aligned} G(\mathbf{x},t) &= \frac{\delta}{\delta\eta(\mathbf{x},t)} \ln\langle \mathcal{Z} \rangle \\ &= \frac{\big\langle \big\{ \mathcal{Z} U(\mathbf{x},t) \big\}_{\mathrm{T}} \big\rangle}{\langle \mathcal{Z} \rangle}, \end{aligned} \tag{2.82}$$

$$\begin{aligned} G(\mathbf{x},\mathbf{x}';t,t') &= \frac{\delta^2}{\delta\eta(\mathbf{x},t)\eta(\mathbf{x}',t')} \ln\langle \mathcal{Z} \rangle \\ &= \frac{\delta}{\delta\eta(\mathbf{x},t)} G_1(\mathbf{x}',t'). \end{aligned} \tag{2.83}$$

In the reduced notation, $G(\mathbf{x};t) \to G_{\mathbf{x}}$ and $G(\mathbf{x},\mathbf{x}';t,t') \to G_{\mathbf{x},\mathbf{x}'}$.

A pause is needed here to consider what has been achieved at this point; the correlator and propagator functions are contained within the second-order cumulant of the extended field vector,

$$\begin{aligned} G(\mathbf{x},\mathbf{x}';t,t')\Big|_{\eta=0} &= \begin{bmatrix} \langle u_\alpha(\mathbf{x},t) u_\beta(\mathbf{x}',t') \rangle & \langle u_\alpha(\mathbf{x},t) \widehat{u}_\beta(\mathbf{x}',t') \rangle \\ \langle \widehat{u}_\alpha(\mathbf{x},t) u_\beta(\mathbf{x}',t') \rangle & 0 \end{bmatrix} \\ &= \begin{bmatrix} C_{\alpha\beta}(\mathbf{x},\mathbf{x}';t,t') & R_{\alpha\beta}(\mathbf{x},\mathbf{x}';t,t') \\ R_{\beta\alpha}(\mathbf{x}',\mathbf{x};t',t) & 0 \end{bmatrix}. \end{aligned} \tag{2.84}$$

The interest is in obtaining a dynamical equation for a particular statistical quantity, which for example can be the second-order correlation function of two velocity fields

of a turbulent fluid. Using (2.80), (2.82), and (2.83), one can construct an equation of motion for the mean-field,

$$-i\sigma_2\partial_t G_{\mathbf{x}} = \widehat{\mathcal{F}}_{\mathbf{x}} + \eta_{\mathbf{x}} + \widehat{\mathcal{D}}_{\mathbf{x},\mathbf{y}} G_{\mathbf{y}} + \frac{1}{2}\widehat{\mathcal{T}}_{\mathbf{x},\mathbf{y},\mathbf{z}}\Big(G_{\mathbf{y},\mathbf{z}} + G_{\mathbf{y}} G_{\mathbf{z}}\Big). \tag{2.85}$$

Note that a second-order cumulant is present in this equation, suggesting the problem of statistical closure. Differentiating (2.85) by $\eta_{\mathbf{x}'}$ gives

$$-i\sigma_2\partial_t G_{\mathbf{x},\mathbf{x}'} = \delta_{\mathbf{x},\mathbf{x}'} + \widehat{\mathcal{D}}_{\mathbf{x},\mathbf{y}} G_{\mathbf{y},\mathbf{x}'} + \widehat{\mathcal{T}}_{\mathbf{x},\mathbf{y},\mathbf{z}}\Big(G_{\mathbf{y}} G_{\mathbf{z},\mathbf{x}'} + \frac{1}{2}\frac{\delta G_{\mathbf{y},\mathbf{z}}}{\delta \eta_{\mathbf{x}'}}\Big). \tag{2.86}$$

In this case, the problem of closure occurs with the last term where a third-order cumulant is introduced,

$$\frac{\delta G_{\mathbf{x},\mathbf{y}}}{\delta \eta_{\mathbf{z}}} = G_{\mathbf{x},\mathbf{y},\mathbf{z}}. \tag{2.87}$$

A method is needed to proceed further without the introduction of *ad hoc* hypotheses to link various moments or cumulants.

Closure

The problem of closure can now be addressed. The method employed by MSR, the Schwinger-Dyson formalism, which has been used to deal with the closure problem in QFT [72], closes the hierarchy of successive statistical quantities. By way of a Legendre transform,

$$\mathcal{L}[G_{\mathbf{y}}] = \ln \mathcal{Z}[\eta_{\mathbf{y}}] - G_{\mathbf{x}}\eta_{\mathbf{x}}, \tag{2.88}$$

a closure can be found through the introduction of vertex functions that can be related to cumulants of various orders. Obtaining functional derivatives with respect to $G_{\mathbf{y}}$ of this equation results in terms that can be related to the triple-order cumulant. It is a straight-forward calculation to determine that the three-point vertex function is

$$\Gamma_{\mathrm{ABC}}(\mathbf{x},\mathbf{y},\mathbf{z};t,t',t'') = \frac{\delta^3 \mathcal{L}[G_{\mathrm{A}'}(\mathbf{x}';s')]}{\delta G_{\mathrm{A}}(\mathbf{x};t)\delta G_{\mathrm{B}}(\mathbf{y};t')\delta G_{\mathrm{C}}(\mathbf{z};t'')} \tag{2.89}$$

$$= -\frac{\delta}{\delta G_{\mathrm{A}}(\mathbf{x};t)}\Big[G_{\mathrm{BC}}(\mathbf{y},\mathbf{z};t',t'')\Big]^{-1}. \tag{2.90}$$

In a less straight-forward calculation, the last term in (2.86) may be rewritten to

contain the three-point vertex

$$\begin{aligned}\frac{1}{2}\widehat{\mathcal{T}}_{\mathbf{x},\mathbf{y},\mathbf{z}}\frac{\delta G_{\mathbf{y},\mathbf{z}}}{\delta\eta_{\mathbf{x}'}} &= \frac{1}{2}\widehat{\mathcal{T}}_{\mathbf{x},\mathbf{y},\mathbf{z}}G_{\mathbf{y},\mathbf{y}'}G_{\mathbf{z},\mathbf{z}'}\left(\frac{-\delta\left[G_{\mathbf{y}',\mathbf{z}'}\right]^{-1}}{\delta G_{\mathbf{w}}}\right)G_{\mathbf{w},\mathbf{x}'} \\ &= \frac{1}{2}\widehat{\mathcal{T}}_{\mathbf{x},\mathbf{y},\mathbf{z}}G_{\mathbf{y},\mathbf{y}'}G_{\mathbf{z},\mathbf{z}'}\Gamma_{\mathbf{w},\mathbf{y}',\mathbf{z}'}G_{\mathbf{w},\mathbf{x}'}. \end{aligned} \tag{2.91}$$

Another function that has proved useful in QFT in concept and calculation is the self-energy function [89]. The self-energy is responsible for attributing a particle with a 'dressed' or renormalised mass, which is an observable quantity. In the present calculation, the self-energy is defined using the three-point vertex,

$$\Sigma_{\mathbf{x},\mathbf{x}'} \equiv \frac{1}{2}\widehat{\mathcal{T}}_{\mathbf{x},\mathbf{y},\mathbf{z}}G_{\mathbf{y},\mathbf{y}'}G_{\mathbf{z},\mathbf{z}'}\Gamma_{\mathbf{x}',\mathbf{y}',\mathbf{z}'}. \tag{2.92}$$

Now the dynamical equation for the second-order cumulant, (2.86), can be rewritten with the self-energy term,

$$-i\sigma_2\partial_t G_{\mathbf{x},\mathbf{x}'} = \delta_{\mathbf{x},\mathbf{x}'} + \widehat{\mathcal{D}}_{\mathbf{x},\mathbf{y}}G_{\mathbf{y},\mathbf{x}'} + \widehat{\mathcal{T}}_{\mathbf{x},\mathbf{y},\mathbf{z}}G_{\mathbf{y}}G_{\mathbf{z},\mathbf{x}'} + \Sigma_{\mathbf{x},\mathbf{y}}G_{\mathbf{y},\mathbf{x}'}. \tag{2.93}$$

The inclusion of the self-energy leads to the establishment of the well-known Dyson equation [90]

$$\left[G^0_{\mathbf{x},\mathbf{y}}\right]^{-1}G_{\mathbf{y},\mathbf{x}'} = \delta_{\mathbf{x},\mathbf{x}'} + \Sigma_{\mathbf{x},\mathbf{y}}G_{\mathbf{y},\mathbf{x}'}. \tag{2.94}$$

The Dyson equation is an equation of motion for the second-order cumulant, which is directly obtained from (2.92). It necessitates the addition of the inverse bare second-order cumulant, defined by

$$\left[G^0_{\mathbf{x},\mathbf{x}'}\right]^{-1} \equiv -i\sigma_2\partial_t\delta_{\mathbf{x},\mathbf{x}'} - \widehat{\mathcal{D}}_{\mathbf{x},\mathbf{x}'} - \widehat{\mathcal{T}}_{\mathbf{x},\mathbf{y},\mathbf{x}'}G_{\mathbf{y}}. \tag{2.95}$$

Written in a different way,

$$\left[G_{\mathbf{x},\mathbf{x}'}\right]^{-1} = \left[G^0_{\mathbf{x},\mathbf{x}'}\right]^{-1} - \Sigma_{\mathbf{x},\mathbf{x}'}, \tag{2.96}$$

this equation gives (Dyson) equations relating the bare and exact propagators,

$$\left[R_{\mathbf{x},\mathbf{x}'}\right]^{-1} = \left[R^0_{\mathbf{x},\mathbf{x}'}\right]^{-1} - \left[\Sigma_{\mathbf{x},\mathbf{x}'}\right]_{\pm\mp}, \tag{2.97}$$

which are the off-diagonal components in $\left[G_{\mathbf{x},\mathbf{x}'}\right]^{-1}$. This equation can be inverted to give

$$R_{\mathbf{x},\mathbf{x}'} = R^0_{\mathbf{x},\mathbf{x}'} + R^0_{\mathbf{x},\mathbf{y}}\left[\Sigma_{\mathbf{y},\mathbf{y}'}\right]^{-1}_{\pm\mp}R_{\mathbf{y}',\mathbf{x}'}. \tag{2.98}$$

Immediately, one can see that the renormalisation is carried in this term by the self-

energy term. Furthermore, this can be compared to the 'Kraichnan-Wyld propagator' to second order,

$$\begin{aligned} R_{\alpha\beta}(\mathbf{k};t,t') &= R^{(0)}_{\alpha\beta}(\mathbf{k};\,t,t') \\ &\quad + R^{(0)}_{\alpha\beta}(\mathbf{k};\,t,t'')\Big(M_{\alpha\delta\gamma}(\mathbf{k}) R_{\delta\delta'}(\mathbf{k}-\mathbf{j};t'',t''-s) \\ &\quad \times C_{\gamma\gamma'}(\mathbf{j};t'',s) M_{\beta'\delta'\gamma'}(-\mathbf{k})\Big) R_{\beta'\beta}(-\mathbf{k};s,t'). \end{aligned} \tag{2.99}$$

Returning to the vertex function which can be rewritten in terms of the self-energy and itself:

$$\Gamma_{\mathbf{x},\mathbf{y},\mathbf{z}} = \widehat{\mathcal{T}}_{\mathbf{x},\mathbf{y},\mathbf{z}} + \frac{\delta\Sigma_{\mathbf{x},\mathbf{y}}}{\delta G_{\mathbf{x}',\mathbf{y}'}}\Big(G_{\mathbf{x}',\mathbf{x}''} G_{\mathbf{y}',\mathbf{y}''} \Gamma_{\mathbf{x}'',\mathbf{y}'',\mathbf{z}}\Big). \tag{2.100}$$

This effectively completes this brief exposition of the MSR formalism. However, in their present form, the set of equations employing the Dyson equations require mutual iterations which can extend to infinite orders. Truncations are then necessary to deliver practical results. The first approximation is given with a first order truncation of the vertex function

$$\Gamma_{\mathbf{x},\mathbf{y},\mathbf{z}} \approx \widehat{\mathcal{T}}_{\mathbf{x},\mathbf{y},\mathbf{z}} \tag{2.101}$$

with the self-energy as

$$\Sigma_{\mathbf{x},\mathbf{x}'} = \frac{1}{2}\widehat{\mathcal{T}}_{\mathbf{x},\mathbf{y},\mathbf{z}} G_{\mathbf{y},\mathbf{y}'} G_{\mathbf{z},\mathbf{z}'} \widehat{\mathcal{T}}_{\mathbf{y}',\mathbf{z}',\mathbf{x}'} \tag{2.102}$$

While it may not be evident in this form, this approximation gives the DIA; this will become more apparent when the diagrammatic representation of MSR is given.

The next order of approximation is given with a third order truncation of the vertex function,

$$\Gamma_{\mathbf{x},\mathbf{y},\mathbf{z}} \approx \widehat{\mathcal{T}}_{\mathbf{x},\mathbf{y},\mathbf{z}} + \widehat{\mathcal{T}}_{\mathbf{x},\mathbf{x}',\mathbf{j}''} G_{\mathbf{j}'',\mathbf{k}''} \widehat{\mathcal{T}}_{\mathbf{y},\mathbf{y}',\mathbf{k}''} G_{\mathbf{y}',\mathbf{y}''} G_{\mathbf{x}',\mathbf{x}''} \widehat{\mathcal{T}}_{\mathbf{x}'',\mathbf{y}'',\mathbf{z}}, \tag{2.103}$$

and the self-energy as

$$\begin{aligned} \Sigma_{\mathbf{x},\mathbf{x}'} &= \frac{1}{2}\widehat{\mathcal{T}}_{\mathbf{x},\mathbf{y},\mathbf{z}} G_{\mathbf{y},\mathbf{y}'} G_{\mathbf{z},\mathbf{z}'} \widehat{\mathcal{T}}_{\mathbf{y}',\mathbf{z}',\mathbf{x}'} \\ &+ \frac{1}{2}\widehat{\mathcal{T}}_{\mathbf{x},\mathbf{y},\mathbf{z}} G_{\mathbf{y},\mathbf{y}'} G_{\mathbf{z},\mathbf{z}'} \widehat{\mathcal{T}}_{\mathbf{y}',\mathbf{v}',\mathbf{v}''} G_{\mathbf{v}'',\mathbf{w}''} \widehat{\mathcal{T}}_{\mathbf{z}',\mathbf{w}',\mathbf{w}''} G_{\mathbf{w}',\mathbf{w}''} G_{\mathbf{v}',\mathbf{v}''} \widehat{\mathcal{T}}_{\mathbf{v}'',\mathbf{w}'',\mathbf{x}'}. \end{aligned} \tag{2.104}$$

Similarly, this approximation generates fourth-order terms given in Wyld, as will be seen in the following section.

2.3.2 The Diagrammatic Representation of MSR

The formalism invented by Martin, Siggia, and Rose was directly demonstrated to be applicable to the turbulence problem, and is by their account comparable to that of Wyld. It is possible to work directly from their diagrammatic interpretation and make a direct comparison to Wyld.

The second-order cumulant diagrams

The correlator and propagators are obtained from the second-order cumulant tensor,

$$G(\mathbf{x},\mathbf{x}';t,t')\Big|_{\eta=0} = \begin{bmatrix} C_{\alpha\beta}(\mathbf{x},\mathbf{x}';t,t') & R_{\alpha\beta}(\mathbf{x},\mathbf{x}';t,t') \\ R_{\beta\alpha}(\mathbf{x}',\mathbf{x};t',t) & 0 \end{bmatrix}. \tag{2.105}$$

Borrowing the same notation for exact correlators and propagators from the Wyld analysis, this can be transcribed diagrammatically as

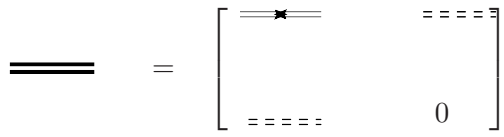

(2.106)

Several points need to be addressed before continuing. The first is quite simply that though the current derivation has been worked out in real space, there is no problem that prevents redoing it in spectral space. Real space has been used here in order for one to follow MSR's original paper. The remainder of the analysis will switch to Fourier space in order to facilitate a comparison with Wyld's diagrammatic method.

A second point is while the external force was introduced as $\widehat{\mathcal{F}}$, this term would not survive in the second-order cumulant equation, (2.86). This term is needed for stationary turbulence, as was shown in Wyld though its presence there was primarily for generating the statistics. MSR avoids this difficulty by introducing the forcing into the 1-point potential, $\widehat{\mathcal{D}}$. This may be justified by noting that the forcing can be constructed as a linear function of the velocity field, see for example [91, 92].

The final point is that in the case of turbulence considered here, the mean field is considered to be zero, hence $G_{\mathbf{k}} = 0$. These points are included in a new form of (2.95),

$$\left[G^0_{\mathbf{k},\mathbf{k}'}\right]^{-1} = -i\sigma_2\partial_t\delta_{\mathbf{k},\mathbf{k}'} - \widehat{\mathcal{D}}_{\mathbf{k},\mathbf{k}'} - \widehat{f}_{\mathbf{k},\mathbf{k}'}. \tag{2.107}$$

It is important to note that all arguments have been changed to their Fourier counterparts, the 1-point forcing potential $\widehat{f}_{\mathbf{k},\mathbf{k}'}$ where only $\left[\widehat{f}_{\mathbf{k},\mathbf{k}'}\right]_{--} = \langle f_\alpha(\mathbf{k},t) f_{\alpha'}(\mathbf{k}',t')\rangle$ is nonzero has been introduced, and the mean-field has been set to zero.

Using (2.96), an equation for $G_{\mathbf{k},\mathbf{k}'}$ can be constructed,

$$G_{\mathbf{k},\mathbf{k}'} = G_{\mathbf{k},\mathbf{j}}\left[G^0_{\mathbf{j},\mathbf{j}'}\right]^{-1} G_{\mathbf{j}',\mathbf{k}'} - G_{\mathbf{k},\mathbf{j}}\Sigma_{\mathbf{j},\mathbf{j}'}G_{\mathbf{j}',\mathbf{k}'}. \tag{2.108}$$

From the architecture of these matrices and using the Dyson equation for the propagator given in (2.98) one can construct a graphical interpretation for the second-order cumulant equation,

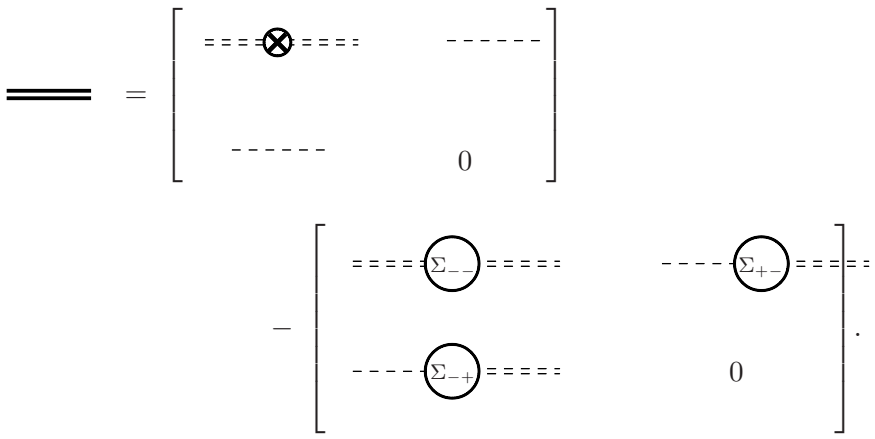

(2.109)

Equating (2.106) and (2.109), one can obtain a diagrammatic equation for the exact correlator

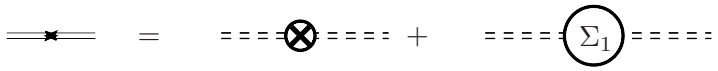

, (2.110)

where

$$\Sigma_1 \equiv \left[\Sigma_{\mathbf{k},\mathbf{k}'}\right]_{--}. \tag{2.111}$$

and

$$= \left\langle \mathbf{f}(\mathbf{k},t) \otimes \mathbf{f}(\mathbf{k}',t') \right\rangle \tag{2.112}$$

is the external force contribution, which in the case of NSE turbulence is the correlation of two random forces. The mathematical formula for this is then

$$C_{\mathbf{k},\mathbf{k}'} = R_{\mathbf{k},\mathbf{j}}\left\langle \mathbf{f}(\mathbf{j},t) \otimes \mathbf{f}(\mathbf{j}',t') \right\rangle R_{\mathbf{j}',\mathbf{k}'} - R_{\mathbf{k},\mathbf{j}}\left[\Sigma_{\mathbf{j},\mathbf{j}'}\right]_{--} R_{\mathbf{j}',\mathbf{k}'}. \tag{2.113}$$

The graphical equation for the exact propagator can likewise be extracted from (2.109),

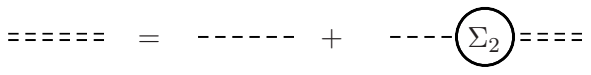

, (2.114)

with its analytic counterpart

$$R_{\mathbf{k},\mathbf{k}'} = R^0_{\mathbf{k},\mathbf{k}'} - R^0_{\mathbf{k},\mathbf{j}}\left[\Sigma_{\mathbf{j},\mathbf{j}'}\right]_{\mp\pm} R_{\mathbf{j}',\mathbf{k}'}. \tag{2.115}$$

The lowest order correlator term can be constructed from the bare propagators and the correlation of the forcing functions,

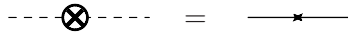

(2.116)

To proceed further, the self-energy equations must be expressed in diagrams. From (2.92) and, borrowing from previous section, the graphical notation for the bare and exact vertices, the self-energy can be presented as

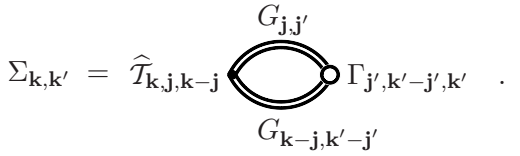

(2.117)

The diagrammatic analogue of the exact vertex function of (2.100), is

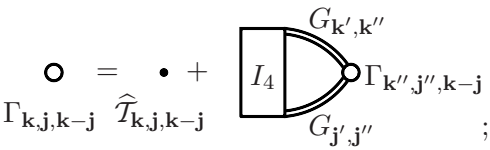

(2.118)

the quantity I_4 is used here in place of $\delta\Sigma_{\mathbf{k},\mathbf{j}}/\delta G_{\mathbf{k}',\mathbf{j}'}$. This equation can be substituted into the vertex term of (2.117), giving

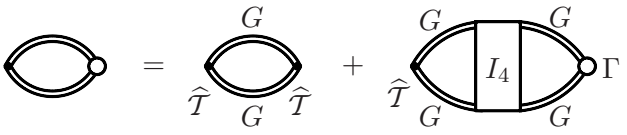

(2.119)

where wave-vector labels have been suppressed; the analogous equation to this diagram is

$$\Sigma_{\mathbf{k},\mathbf{k}'} = \frac{1}{2}\widehat{\mathcal{T}}_{\mathbf{k},\mathbf{j},\mathbf{l}} G_{\mathbf{j},\mathbf{j}'} G_{\mathbf{l},\mathbf{l}'} \widehat{\mathcal{T}}_{\mathbf{k}',\mathbf{j}',\mathbf{l}'} + \frac{1}{2}\widehat{\mathcal{T}}_{\mathbf{k},\mathbf{j},\mathbf{l}} G_{\mathbf{j},\mathbf{j}'} G_{\mathbf{l},\mathbf{l}'} \left[\frac{\delta\Sigma_{\mathbf{j}',\mathbf{l}'}}{\delta G_{\mathbf{m},\mathbf{n}}}\right] G_{\mathbf{m},\mathbf{m}'} G_{\mathbf{n},\mathbf{n}'} \Gamma_{\mathbf{k}',\mathbf{m}',\mathbf{n}'}. \tag{2.120}$$

The four-point term I_4 can be written as

$$\begin{aligned} I_4 &= \frac{\delta}{\delta G_{\mathbf{m},\mathbf{n}}}\left(\frac{1}{2}\widehat{\mathcal{T}}_{\mathbf{j}',\mathbf{g},\mathbf{h}} G_{\mathbf{g},\mathbf{g}'} G_{\mathbf{h},\mathbf{h}'} \Gamma_{\mathbf{l}',\mathbf{g}',\mathbf{h}'}\right) \\ &= \frac{1}{2}\widehat{\mathcal{T}}_{\mathbf{j}',\mathbf{m},\mathbf{h}} G_{\mathbf{h},\mathbf{h}'} \Gamma_{\mathbf{l}',\mathbf{n},\mathbf{h}'} + \frac{1}{2}\widehat{\mathcal{T}}_{\mathbf{j}',\mathbf{g},\mathbf{m}} G_{\mathbf{g},\mathbf{g}'} \Gamma_{\mathbf{l}',\mathbf{g}',\mathbf{n}} \\ &\quad + \frac{1}{2}\widehat{\mathcal{T}}_{\mathbf{j}',\mathbf{g},\mathbf{h}} G_{\mathbf{g},\mathbf{g}'} G_{\mathbf{h},\mathbf{h}'} \frac{\delta}{\delta G_{\mathbf{m},\mathbf{n}}}\left(\Gamma_{\mathbf{l}',\mathbf{g}',\mathbf{h}'}\right), \end{aligned} \tag{2.121}$$

with the corresponding diagram

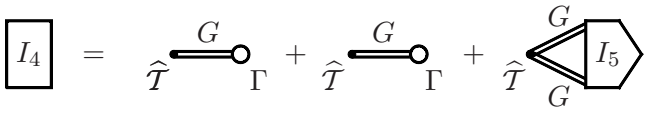

. (2.122)

The term $I_5 \equiv \delta\Gamma_{\mathbf{l}',\mathbf{g}',\mathbf{h}'}/\delta G_{\mathbf{m},\mathbf{n}}$ has been introduced merely as a label. Temporarily abandoning all labels, it can be seen that by inserting this term into (2.119) results in

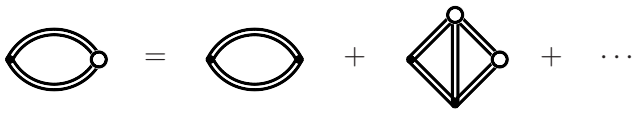

; (2.123)

which can be further written with the bare vertices as

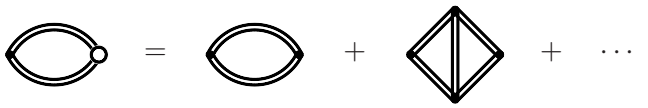

. (2.124)

Note that $\widehat{\mathcal{T}}$ is a $2 \times 2 \times 2$ tensor, and it can be shown [55, 79] to be symmetric with three nonzero entries, labelled here with its "extended field vector" indices,

$$\left[\widehat{\mathcal{T}}_{\mathbf{k},\mathbf{j},\mathbf{l}}\right]_{++-} = \left[\widehat{\mathcal{T}}_{\mathbf{k},\mathbf{j},\mathbf{l}}\right]_{+-+} = \left[\widehat{\mathcal{T}}_{\mathbf{k},\mathbf{j},\mathbf{l}}\right]_{-++}. \tag{2.125}$$

Using this and noting that only $[G_{\mathbf{a},\mathbf{b}}]_{--}$ vanishes, the self-energy is constrained to have only one zero component, $[\Sigma_{\mathbf{a},\mathbf{b}}]_{++}$. The remaining terms of the self-energy are found

to be

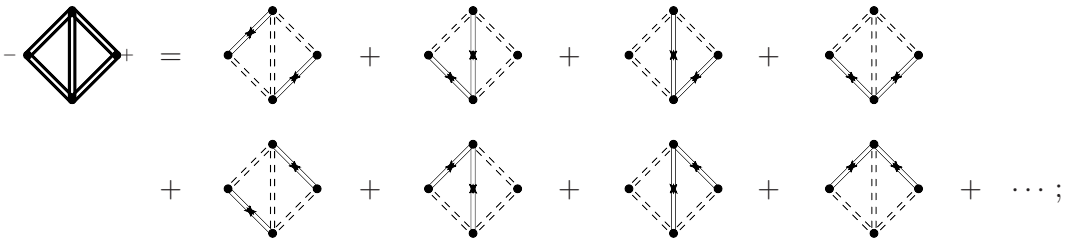

(2.126)

for the off-diagonal terms (recall that $\Sigma_{\mathbf{a},\mathbf{b}}$ is a 2×2 tensor), and

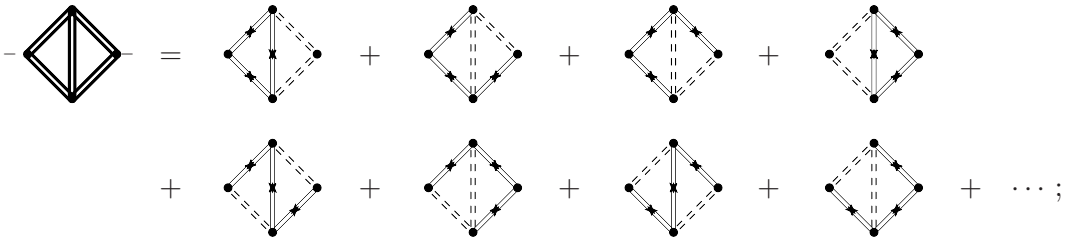

(2.127)

as the non-vanishing diagonal component. Both of these equations have been shown only to fourth-order in $\widehat{\mathcal{T}}$ as this is the extent of this study.

To make a connection to the original work of MSR, note that the non-vanishing elements of the self-energy tensor obtained above can be written as

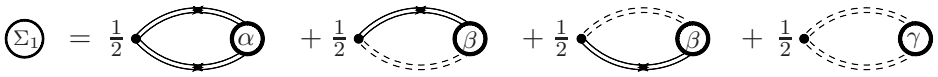

(2.128)

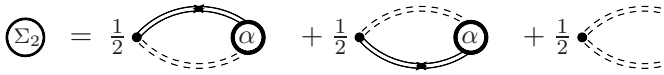

(2.129)

where α, β, and γ are arbitrary labels for the vertex corrections,

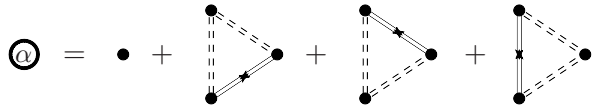

(2.130)

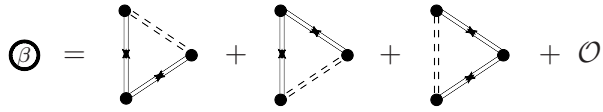

(2.131)

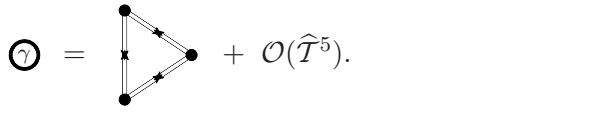

(2.132)

These three terms correspond to the non-vanishing elements of Γ, which are Γ_{-++},

Γ_{--+}, and Γ_{---}, again using the extended field-vector indices. In their paper, (2.128) and (2.129) are given as

(2.133)

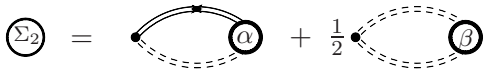

(2.134)

with a slightly different set of vertices, namely

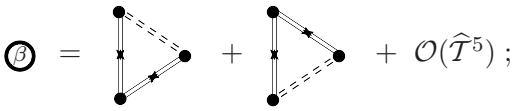

(2.135)

only a term has been removed from the β-correction and all other corrections are the same. While their analytic formalism is intact, this mis-interpretation into diagrams leads to some confusion in the number of diagrams present and seemingly results in the absence of a particular diagram; these issues are addressed in the next section.

The nonzero entries of G connect to those of $\widehat{\mathcal{T}}$ to give expressions for the three nonzero vertex corrections of Γ. Inserting these into their respective positions in the self-energy diagrams (2.133) and (2.134) gives the self-energy diagrams to fourth-order. Then, the expanded self-energies are inserted into (2.114) to obtain the propagator diagrams to fourth-order,

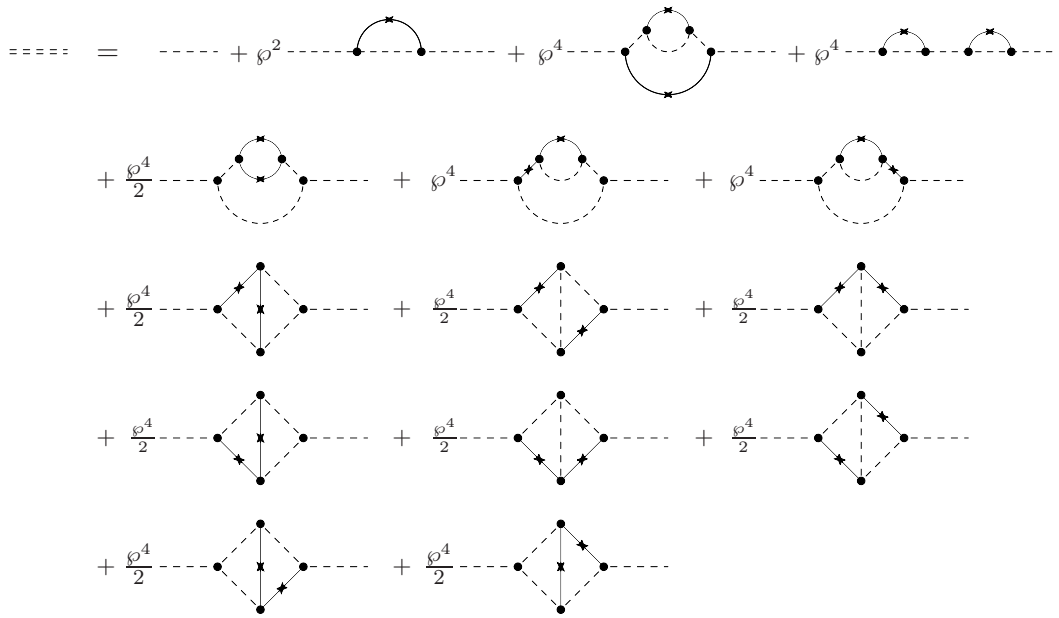

.

(2.136)

A factor $\wp$ has been introduced for each vertex as the relative weightings of these terms are different between MSR and Wyld.

Using this propagator expansion, the terms in (2.110) for the exact correlator may now be determined. Those terms obtained from the forcing function are

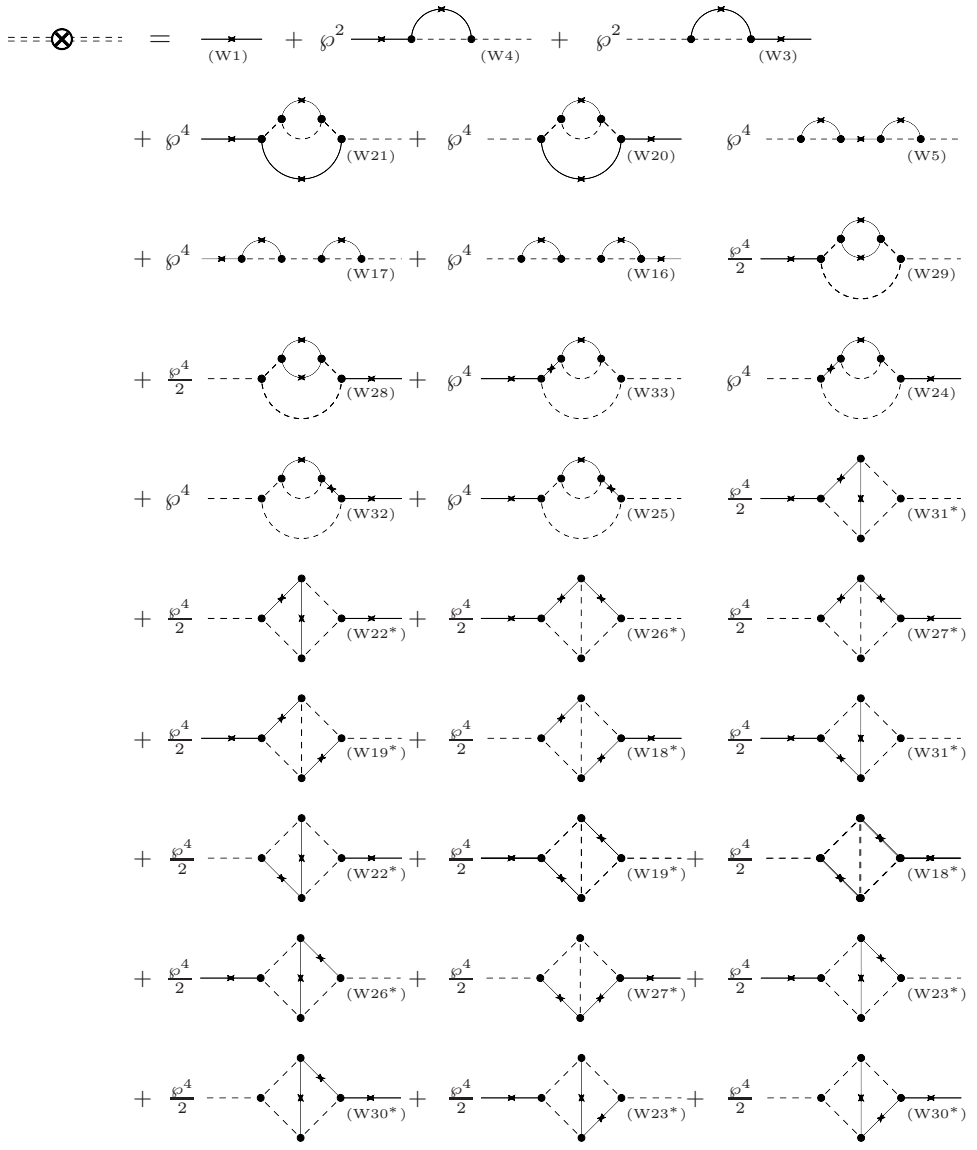

(2.137)

The labels (Wn) correspond to Wyld's diagrams as seen in fig. 2.2. Additionally, the diagrams whose labels contain an asterisk denote diagrams which have half the weighting as their Wyld counterparts but for a given (Wn), there are two such diagrams in this equation and their sum gives the correct weighting. The reason for this can be seen in that the diagrams are symmetric when reflected about a horizontal line. In Wyld's formalism such diagrams are equivalent.

Those diagrams representing the self-energy interaction are expressed by

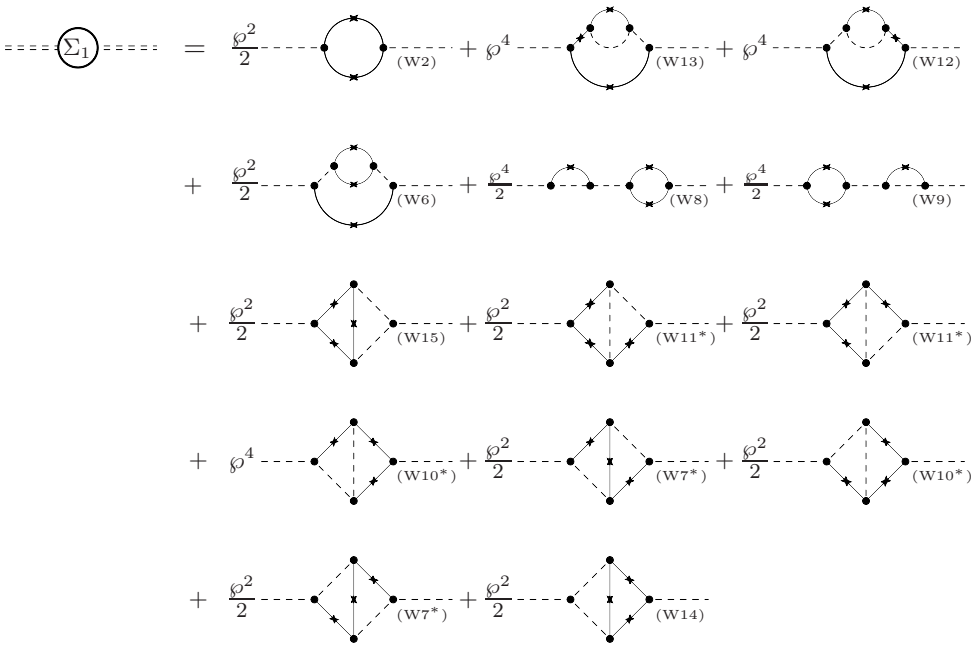

(2.138)

Combining (2.137) and (2.138) together gives the diagrammatic equation for the exact correlator function expanded to fourth-order in the bare vertex as obtained via the MSR formalism. There are 44 diagrams counted in these two equations, confirming a statement made by the authors. Note that some of the diagrams are repeated but these are still accounted for by their adjusted weighting factors. Comparing these two equations to the diagrams given in fig. 2.2, it can be concluded that the MSR formalism gives the primitive correlator expansion of Wyld provided the factor $\wp = 2$.

2.4 Comparison

The renormalised diagrammatic expressions for homogeneous isotropic turbulence have been presented here according to the formalisms of Wyld (sections §2.2.2, 2.2.3) and Martin, Siggia, and Rose (§2.3.2). It is at this stage that some comparisons between the two formalisms can be made. The first of the following sections compares the new resummation of Wyld presented in section §2.2.3 to the exact expressions for the self-energy and vertex diagrams derived in MSR. The next section follows with a few remarks on MSR's original expansion for the correlator in terms of bare diagrams.

2.4.1 The Resummation of Wyld

In order to make a better comparison of the diagram equations as obtained in their respective formalisms, some rearrangement of terms is necessary.

Looking again at the propagator expression of Wyld in (2.61), this equation can be written in such a way as to anticipate the MSR form of the propagator with the self-energy term

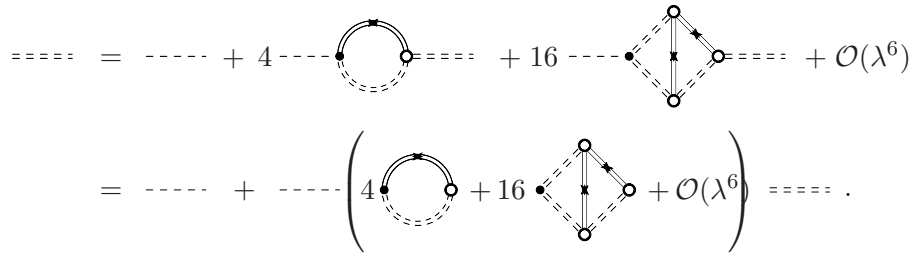

(2.139)

This can be done since the construction of the propagator expansion from the $\langle \mathbf{f} \otimes \mathbf{u} \rangle$-term maintains the left-most propagator and vertex remain unrenormalised. Noting the reflection-symmetry of Wyld diagrams, the fourth-order term in (2.139) can be written as a sum of two terms,

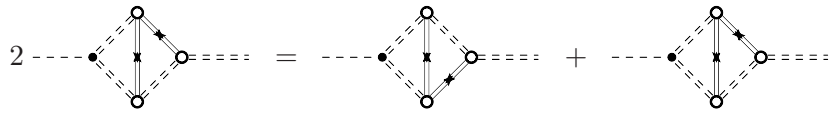

(2.140)

This allows the above equation for the propagator, (2.139), to be written using two of the MSR-vertex terms, $\Gamma_{(\alpha)}$ and $\Gamma_{(\beta)}$ (see (2.130) and (2.135)):

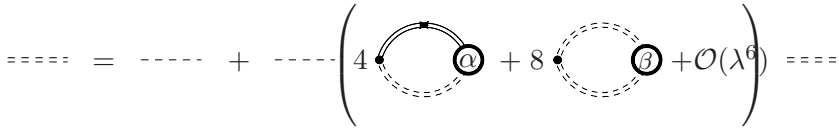

(2.141)

In all further diagrams of both formalisms, diagrams that are equivalent through this symmetry will be combined.

The "$\mathcal{O}(\lambda^6)$" has been kept explicit as the above only applies to fourth-order; the next order has not been analysed. If however, all terms of $\mathcal{O}(\lambda^6)$ can be contained in either of these two self-energy components, the MSR propagator given in (2.114) is recovered,

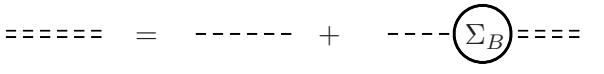

Before continuing with Wyld, it will be helpful to rewrite the diagram equation for the exact MSR-correlator, seen in (2.110) and reproduced here,

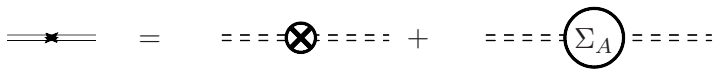

.

It is this equation that MSR give as part of their DIA equation (see fig. 8 in [58]). However, it requires some slight modification to accurately depict the DIA-correlator. Substituting the propagator equation given above (from (2.114)) for the exact propagator on the left of the force-force correlation, $\langle \mathbf{f} \otimes \mathbf{f} \rangle$ and the self-energy term, Σ_{--}, the correlator equation can be made to resemble the DIA equation more accurately,

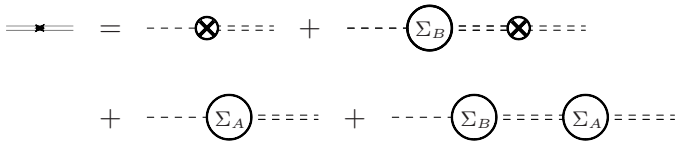

. (2.142)

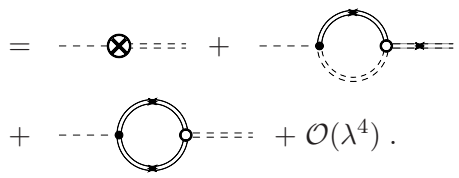

(2.143)

However, in making the comparison with Wyld, it will be better to use (2.142). The self-energy terms Σ_A and Σ_B can be written explicitly as

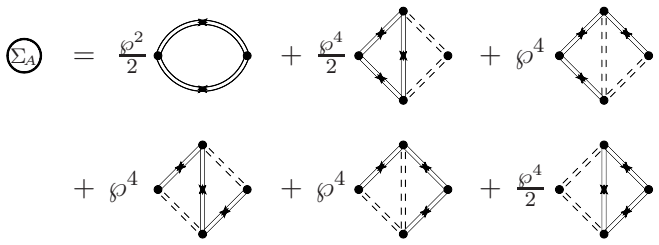

, (2.144)

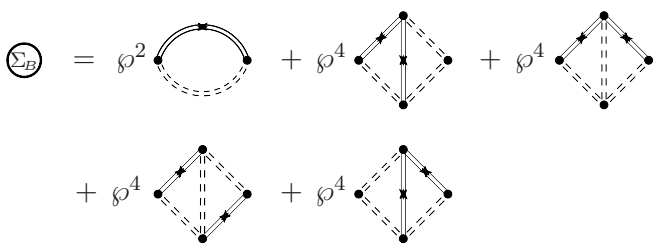

. (2.145)

The factor $\wp$, associated with each vertex, has been included for convenience.

The terms with only one self-energy component are given as

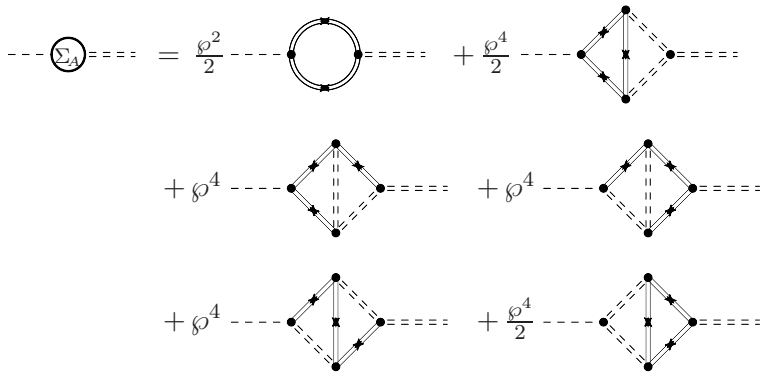

, (2.146)

and

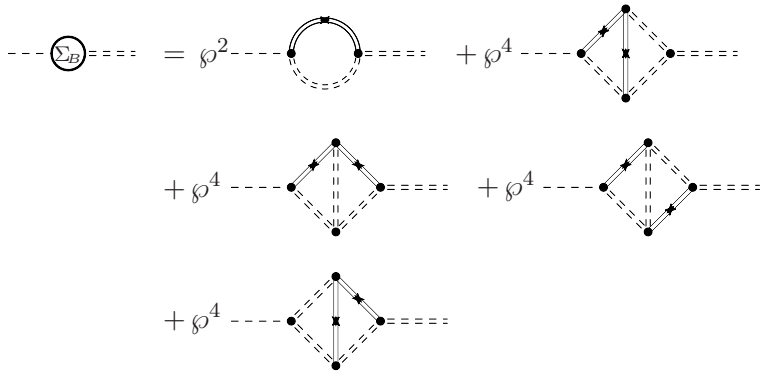

. (2.147)

The term with both Σ_A and Σ_B will not be expanded. This term can be combined with (2.147) to give

. (2.148)

Using the expressions (2.146)-(2.148), these equations can be substituted back into

(2.142),

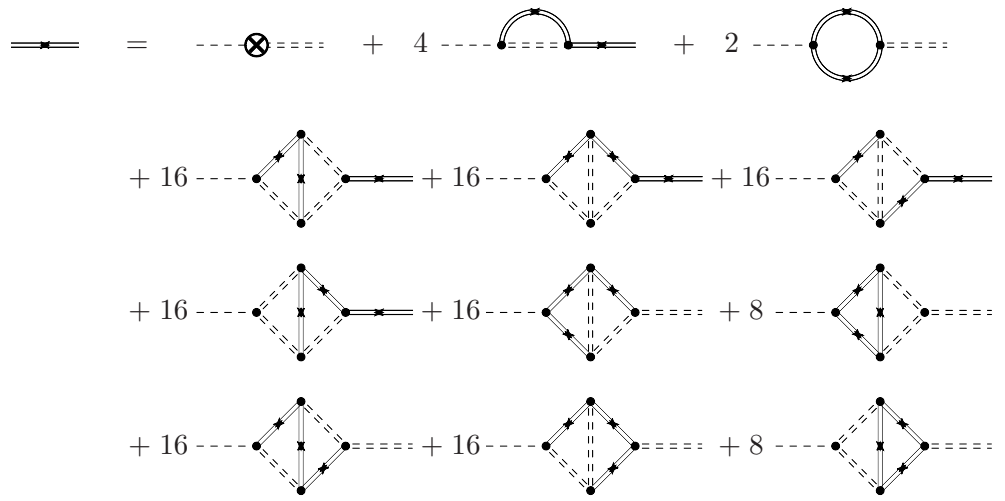

(2.149)

The term $\wp = 2$ has been used; this will enable the comparison with Wyld. To make a comparison with this correlator, some adjustment is required for the Wyld correlator.

The equation for the correlator given in (2.64),

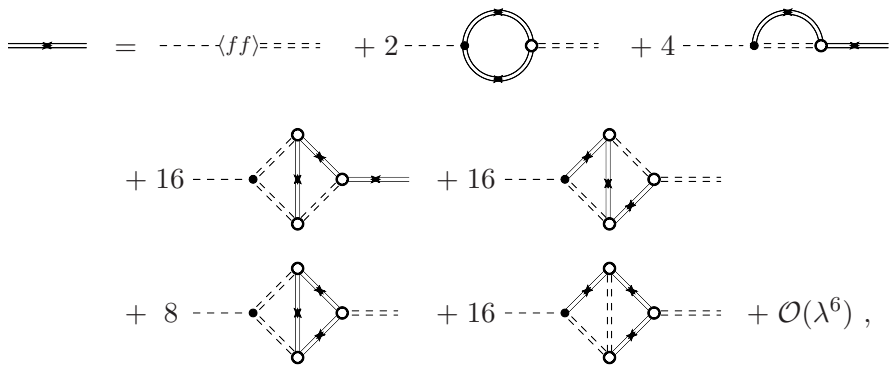

(2.150)

can be expanded using the renormalised vertex expansion of (2.53) and truncated to

fourth-order, leaving

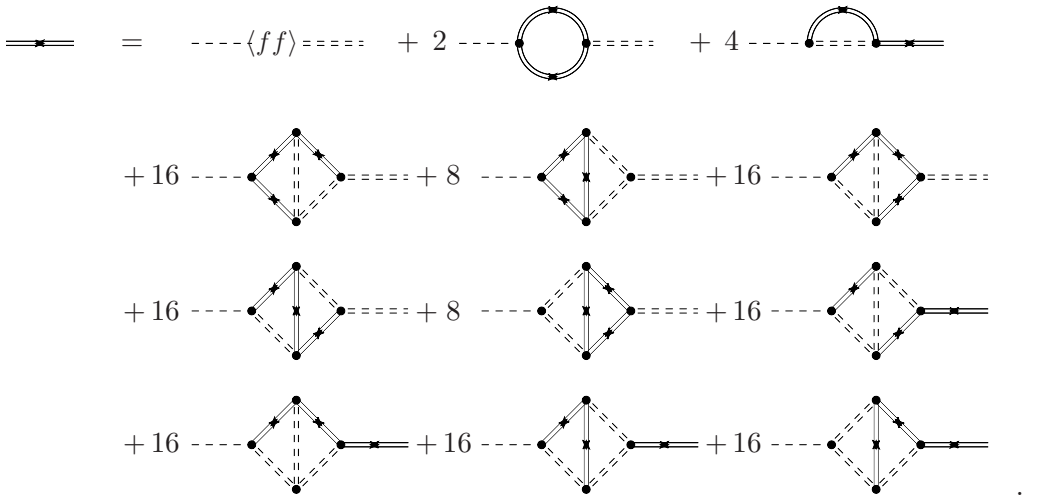

(2.151)

This equation can be readily compared to (2.149). The double-force correlation term in Wyld can be connected with that given in MSR (see (2.116)), $\langle ff \rangle =$ ⊗ .

The equations (2.149) and (2.151) are equivalent. It can be said that the results produced by both formalisms are equivalent to fourth-order. This raises questions on the claims by MSR and Kraichnan over the mistreatment of the vertex renormalisation by Wyld. Their claim was that Wyld was missing certain classes of vertex corrections, namely (2.132) and (2.135). It was shown that 'new' irreducible diagrams were found by applying a different resummation method, resulting in (2.64). Therefore, their claim is somewhat substantiated as Wyld's original resummation did not distinguish these terms.

2.4.2 Remarks on the Primitive Correlator Expansion of MSR

At the end of the last section, it was shown that the primitive correlator expansion of MSR is indeed equivalent to that of Wyld up to and including fourth-order. While the exposition here has taken care to demonstrate all steps in the MSR diagrammatic treatment of homogeneous, isotropic turbulence, it must be noted that it is not immediately obvious from their paper that they are able to reproduce the Wyld diagrams for the primitive correlator expansion.

The main problem that has been found in this study is their equations for the vertex corrections, which are seen here in (2.130), (2.132), and (2.135). It was noted previously that (2.135) lacks a particular diagram which can be seen by comparing this equation to (2.131). These vertex corrections along with the self-energy equations, (2.133) and

(2.134), and the diagrams for the exact correlator and propagator, (2.110) and (2.114), respectively, are those found in their paper. Using these, one will find that all diagrams of the primitive correlator expansion of Wyld are not reproduced. This is not to suggest that Wyld's equation is a benchmark, but obtaining the primitive correlator expansion is expected.

The result of their vertex corrections is the absence of

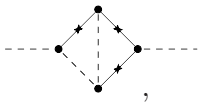

which is diagram (W10) in fig. 2.2. This diagram cannot in general occur according to the original MSR diagrams. Thus it appears that there has been a slight misinterpretation of their formalism for HIT to diagrams.

Additionally, the proper-weighting is left to confusion as there is no specification of it within the paper itself. It has been assumed here that one exists, to which $\wp$ has been used. Setting $\wp = 2$ does give the proper Wyld weightings but this cannot be known *a priori*.

None of these remarks are meant to discredit the MSR formalism as these are not serious flaws of their work. For the purposes of using it for homogeneous, isotropic turbulence with Gaussian statistics, it appears to work very well. The problems mentioned here only refer to the transposition of their formalism to diagrams as presented in their original work.

2.5 Discussion

The formalisms of Wyld and Martin, Siggia, and Rose have been presented in detail is this chapter. Specific attention has been given to the diagrammatic interpretations of both formalisms, as this is where the primary discrepancies occur.

2.5.1 Conclusions

A new derivation of the propagator for the Wyld formalism has been demonstrated that obtains the propagator proposed by Lee. The main feature of this resummation is that the left-most propagator and left-most vertex remain unrenormalised; these quantities are by construction not included in the correlation of the triple-moment of (2.46) and are effectively not part of the closure. Applying this method for the propagator, one directly obtains the DIA results when truncated to lowest nontrivial order but finds additional irreducible diagrams. These irreducible diagrams have counterparts in the MSR equation for the exact correlator.

The MSR formalism was also presented here with a detailed the diagrammatic application to homogeneous isotropic turbulence. It has been found here that the diagrams given in their original paper correctly give the Wyld results as MSR claim. Following the diagrammatic treatment demonstrated here, their formalism produces a correlator expansion that is a one-to-one correspondence with that of Wyld to fourth-order.

Furthermore, using the resummation introduced here, the Wyld equations for the exact correlator and propagator have been shown to be those of MSR. The 'missing' vertex corrections were found in the new irreducible terms generated by the new resummation.

It is therefore the conclusion of this work that both formalisms agree to fourth-order. This means that the Wyld formalism with the diagrammatic resummation used here produces equations for the exact correlator, propagator, and vertex corrections that are the same as those obtained using the formalism of MSR.

2.5.2 Further Work

A primary motivation in this chapter has been to attempt to resolve a long-standing debate on why these formalisms clashed. There seems to have been a complete rejection of Wyld's method on the basis of his failure to renormalise the propagator correctly. It has been shown here that Wyld's method is nearly equivalent to that of MSR. If the Wyld formalism can be brought to the sort of acceptance that the MSR formalism enjoys, then it could offer turbulence some of the usefulness of diagram equations found in high-energy physics.

It is not fully understood whether such diagrammatic representations in turbulence can be related to the physical system it is constructed to represent, as in the case of particle physics where the diagrams create a conceptual analogue [93]. As in particle physics, the diagrams of these formalisms convey a sense of histories embedded in the network of propagators and correlations found in higher-order diagrams. This does help in illustrating the dynamics the diagrams are meant to convey but it is not clear what role the topology plays. Furthermore, the resummation of propagators and vertices can be said to account for the short memory of the collective interactions of a turbulent fluid, allowing meaningful truncations to be applied. Analogous to mass and charge renormalisation in QED [89], one may consider this to be 'viscosity' and 'interaction' renormalisation, though further work is needed to establish this firmly.

In attempting to resolve the discrepancy here, it is believed that these formalisms can offer a stronger foundation of the Local Energy Transfer (LET) theory of McComb,

which is the subject of the following chapter and is used in subsequent chapters of this thesis. In its present state, the LET-correlator equation uses diagrammatic resummation much like that of Wyld but postulates a relationship between the correlators and propagators using a fluctuation-dissipation relation. It is thought that studying these formalisms will offer insight on how to derive the correlator-propagator relationship that is essential to the LET.

Chapter 3

LET Theory of Turbulence and its Numerical Solution

This chapter summarises the construction and operation of the LET2008 code, a numerical solution of the Local Energy Transfer (LET) theory of turbulence. A brief overview of the LET is discussed, focusing on the equations that are key to the theory and the method of numerical solution. Results comparing the current code to results of direct numerical simulation (DNS) as well as to past versions show that the current code's operation is in order for decaying turbulence. Similar comparisons against a past version for forced turbulence show adequate results. Details are also given for a new time-truncation method employed in the current code.

3.1 The Local Energy Transfer Theory of Turbulence

The Local Energy Transfer theory is a statistical closure for homogeneous, isotropic turbulence. It uses a closure based on the hypothesis that the dominant interactions of the mode-coupled velocity field coefficients in the nonlinear term are local in wavenumber space. This was originally created in the 1970s as an eddy-viscosity model of turbulence [94, 95]. It has since been redeveloped [96–98] as a renormalised perturbation theory like the early Eulerian theories of Kraichnan [50–52].

The LET's most important feature is its use of a fluctuation-dissipation relation; this was introduced in the earlier versions to connect the Fourier coefficients of the velocity field at different times via a propagator function,

$$u_\alpha(\mathbf{k}, t) = R_{\alpha\beta}(\mathbf{k}; t, t')u_\beta(\mathbf{k}, t'). \tag{3.1}$$

However, defined in this way, unphysical mathematical constraints were imposed on

them. The breakthrough [35, 98, 99] came in noting that the problems associated with the velocity field coefficients were alleviated when the fluctuation-dissipation relationship was applied to the correlation of the velocity field coefficients:

$$\underbrace{u_\alpha(\mathbf{k},t) = R_{\alpha\beta}(\mathbf{k};t,t')u_\beta(\mathbf{k},t')}_{\text{LET ca. 1978}} \;\rightarrow\; \underbrace{C_{\alpha\beta}(\mathbf{k};t,t') = R_{\alpha\gamma}(\mathbf{k};t,t')C_{\gamma\beta}(\mathbf{k};t',t')}_{\text{LET ca. 1992}}. \quad (3.2)$$

This addressed the problem of unphysical fixed-phase relationships expressed in the early derivations; for a full discussion see [35].

The LET claims successes in producing satisfactory results in decaying and forced turbulence. In the past, it has been shown to display the correct turbulent phenomenology for decaying turbulence and compared well to Kraichnan's DIA [100]. It has succeeded in producing proper velocity-field statistics [97] and has been used in investigating the passive scalar convection [98]. In more recent times it has been tested against DNS and adapted to incorporate forced turbulence, also tested against DNS [101, 102]. It is considered the only Eulerian closure capable of producing a Kolmogorov inertial range [103]. Further developments have seen the LET reformulated and re-derived to obtain more computationally tractable Markovian versions, see [104–108].

3.1.1 The LET Equations

It is generally the case that when dealing with closure models, the primary quantity of interest in homogeneous isotropic turbulence is the correlation, or correlator, of the velocity field. The LET is no exception to this but does make the point of using both single- and two-time correlators, which distinguishes it from other closures. According to the LET, the time-evolution of these quantities is given by

$$\partial_t C(\mathrm{k};t,t) = -2\nu\mathrm{k}^2 C(\mathrm{k};t,t) + 2P(\mathrm{k};t,t) \quad (3.3)$$

$$\partial_t C(\mathrm{k};t,t') = -\nu\mathrm{k}^2 C(\mathrm{k};t,t') + P(\mathrm{k};t,t') \quad (3.4)$$

where

$$
\begin{aligned}
P(\mathrm{k};t,t') \;=\; & \int_0^\infty d\mathrm{j}\, 2\pi \mathrm{j}^2 \int_1^{-1} d\mu L(\mathrm{k},\mathrm{j},\mu) \times \\
& \Bigg(\int_0^{t'} ds R(\mathrm{k};t',s) C(\mathrm{j};t,s) C(|\mathbf{k}-\mathbf{j}|;t,s) \\
& - \int_0^{t} ds R(\mathrm{j};t,s) C(\mathrm{k};s,t') C(|\mathbf{k}-\mathbf{j}|;t,s) \Bigg).
\end{aligned} \tag{3.5}
$$

As in most closure hypotheses, an additional function, the propagator or response function $R(\mathrm{k};t',s)$, is included to effect the closing of the statistical hierarchy. For the LET this is the addition of a fluctuation-dissipation relation to connect the single- and two-time correlators via the response function,

$$C(\mathrm{k};t,t') = R(\mathrm{k};t,t')C(\mathrm{k};t',t'). \tag{3.6}$$

As the response functions in the time-evolution equations can be replaced by a ratio of two- and single-time correlators, a closed set of equations is now achieved. This set of equations, (3.3)-(3.6), is called the LET equations. A summary derivation of (3.3) is given in the chapter appendix 3.A.

Given the form of these equations, they may be numerically integrated forward in time from an initial condition, in the form of a energy spectrum, to give a dynamical simulation for the statistics of a turbulent fluid. They may also be adapted to include an external forcing term to compute for stationary systems.

3.1.2 Decaying Turbulence versus Forced Turbulence in the LET

The investigation of homogeneous isotropic turbulence is generally split among two canonical directions: freely-decaying turbulence and externally-forced turbulence. The case of decaying turbulence has a unique position in that it gives access to studying the effects of the inertial transfer mechanisms first-hand, without the encumbrances of boundary conditions and/or external forces which may skew the dynamics thereby masking the true mechanisms at work [3]. Examination of this kind of turbulence requires an initial condition strong enough to induce turbulence from which the system decays. Conversely, the use of external forcing intentionally perturbs the system to study the response of the inertial mechanisms to continual or periodic energy injection. This effect biases the observable parameters of the system based on how and where (in terms of the physical length scales or wavenumber spectrum) the forcing is implemented

[24].

The current numerical solution of the LET has been constructed to deal with both cases. The very early instances of the computation were developed solely for decaying turbulence [97, 98, 100], and only rather recently has it been extended to forced turbulence [101]. The current LET code computes both freely-decaying and forced turbulence, and extends the Reynolds number in both cases. These results are given in the next chapter.

3.2 Numerical Analysis of the LET

The LET has been computed previously, most notably in 1984 [100], 1989 [97], 1992 [98], and most recently in 2000 [101]. The current code, hereafter called 'LET2008', is a re-build of the previous code, LET2000 from [101]. LET2000 was itself a rebuild of LET1984 and included the functionality to directly compute and compare the results of both codes. In addition, LET2000 provides functionality to compute Kraichnan's DIA equations. The LET2000 code has shown its robustness in handling both decaying and forced turbulence with successful comparisons to DNS of up to Taylor-Reynolds numbers of $R_\lambda \sim 129$ and $R_\lambda \sim 230$ for decaying and forced turbulence, respectively.

3.2.1 Numerical Solution Method

The solution of the LET equations is the numerical integration of the discretised single- and two-time LET equations of the form

$$\begin{aligned} C(\mathrm{k};t_i,t_i) &= e^{-2\nu\mathrm{k}^2\Delta t}C(\mathrm{k};t_{i-1},t_{i-1}) + \frac{1}{2\nu\mathrm{k}^2}\big(1-e^{-2\nu\mathrm{k}^2\Delta t}\big)\times \\ &\quad \Big(P(\mathrm{k};t_{i-1},t_{i-1}) + P(\mathrm{k};t_i,t_i)\Big), \end{aligned} \tag{3.7}$$

$$\begin{aligned} C(\mathrm{k};t_i,t_j) &= e^{-\nu\mathrm{k}^2\Delta t}C(\mathrm{k};t_{i-1},t_j) + \frac{1}{2\nu\mathrm{k}^2}\big(1-e^{-\nu\mathrm{k}^2\Delta t}\big)\times \\ &\quad \Big(P(\mathrm{k};t_{i-1},t_j) + P(\mathrm{k};t_i,t_j)\Big), \end{aligned} \tag{3.8}$$

with the response functions contained within the functions $P(\mathrm{k};t_i,t_j)$ being replaced by

$$R(\mathrm{k};t_i,t_j) = \frac{C(\mathrm{k};t_i,t_j)}{C(\mathrm{k};t_j,t_j)}. \tag{3.9}$$

The complete derivation of these equations may be found in [101].

Discretised Equations of Motion

As implied in the equations given above, the domain used for computation is discretised in both time and wavenumber space. Though past versions of the LET have employed both variable and logarithmic time- and wavenumber-stepping, see for example [100], the current code uses fixed, linear stepping in both domains.

The time discretisation uses a physical time appropriate for a physical system to evolve which in the present case ranges from 1.5-15 s. This length of time is divided into a number of timesteps of length Δt with the constraints that $\Delta t \lesssim 1/U(t)\mathrm{k_{top}}, 1/\nu\mathrm{k_{top}^2}$, depending on which is smaller. These represent the characteristic convection and decay times, respectively. The quantity $\mathrm{k_{top}}$ marks the largest wavenumber used in the computation; it also resolves the dynamics of lengthscales on the order of $1/\mathrm{k_{top}}$. Ideally an adaptive algorithm would be applied at all times to ensure Δt conforms to the convection constraints, however it has been found that ensuring $\Delta t \lesssim 1/U(0)\mathrm{k_{top}}$ is sufficient for present purposes.

The discretisation of the wavenumber range takes a similar approach. However, rather than using the endpoint values as in the time-discretisation, a midpoint method is used such that for an array of wavenumbers k_i separated by a stepsize of $\Delta\mathrm{k}$, the value for a wavenumber used in the computation is $\mathrm{k_n} = (\mathrm{k}_i + \mathrm{k}_{i+1})/2$. This definition sidesteps possible divide-by-zero errors when $\mathrm{k}_{i=0} = 0$.

In making the projection from the 3-dimensional to a 1-dimensional system, the parameter $\mu \equiv (\mathbf{k} \cdot \mathbf{j})/\mathrm{kj}$ has been introduced (see (3.43) and (3.44) in the appendix 3.A to ths chapter). This parameter is the cosine of the angle between the two wave-vectors $\mathbf{k}$ and $\mathbf{j}$ and ranges from [1,-1]; it occurs in the so-called "L-coefficient" as well as in the computation of $C(|\mathbf{k} - \mathbf{j}|; t, t')$. There is a singularity in the L-coefficient corresponding to $\mu = 1$ and $\mathbf{k} \parallel \mathbf{j}$ which is navigated by choosing the midpoints on the μ-array as was done in the case of the array of wave-vectors. It is important to point out that an analytical or empirical relationship exists linking the stepsizes $\Delta\mathrm{k}$ and $\Delta\mu$ to ensure maximum coverage of the wave-vector space with a minimum of computation. No investigation was made into the relationship between the stepsizes $\Delta\mathrm{k}$ and $\Delta\mu$; Quinn used a standard $\Delta\mu = .02$ for all computations where $\Delta\mathrm{k} = 1$ and this has been followed here.

3.2.2 The Time Integration Algorithm

The well-known predictor-corrector algorithm [109, 110] was employed to create and use this information to step the system forward in time.

The predictor-corrector method involves the use of an initial condition or known solution for functions of t_{i-1} to be used in the place of t_i in the equation(s) that relates functions of t_{i-1} to those of t_i. More specifically, in (3.7) and (3.8), the functions $P(\mathrm{k}, t_i, *)$ depend on correlations $C(\mathrm{j}, t_i, *)$; these transfer-correlation function terms are replaced with their t_{i-1}-values, giving a 'predicted' value for $C(\mathrm{k}, t_i, *)$. The predicted correlators are then used in the transfer-correlation, leading to a prediction for those terms. The process is iterated with the predicted functions being replaced by 'corrected' functions. Further corrector iterations are used if needed for convergence upon a solution.

Decreasing the Memory Kernel

Noting that for a given time, t_i, (3.7) and (3.8) depend on functions of all previous time points. This can be explicitly seen in the time integrals of $P(\mathrm{k}; t_i, t_i)$ in (3.5) which involve correlation functions of all times $0 \leq t \leq t_i$; this is referred to as the "memory kernel" as it comprises all information about the system's evolution in time.

As the system evolves this information increases. In practise, this implies that the amount of memory needed and the number of computations required will increase exponentially with time. A method for memory truncation developed by Quinn in the LET2000 code called the "Time History Integral Truncation" (THIT). It reduces the number of computations by eliminating elements from the two-time P-transfer function, $P(\mathrm{k}; t_i, t_j)$. The truncation resets the lower limits on the time-integrals in (3.5) to a value that is a fixed number of timesteps below the larger of the two times t_i and t_j. For $t_i > t_j$, the new limit would be $t_i - N_\mathrm{T}$:

$$\begin{aligned} P^\mathrm{T}(\mathrm{k}; t_i, t_j) &= \int d^3\mathrm{j} L(\mathrm{k}, \mathrm{j}, \mu) \Bigg(\int_{t_i - N_\mathrm{T}}^{t_j} ds R(\mathrm{k}; t_j, s) C(\mathrm{j}; t_i, s) C(|\mathbf{k} - \mathbf{j}|; t_i, s) \\ &- \int_{t_i - N_\mathrm{T}}^{t_i} ds R(\mathrm{j}; t_i, s) C(\mathrm{k}; s, t_j) C(|\mathbf{k} - \mathbf{j}|; t_i, s) \Bigg). \end{aligned} \tag{3.10}$$

The effect is that the turbulence remembers only N timesteps, thereby reducing the number of calculations significantly.

This may be seen as retaining some of the near neighbours of the time diagonal. One may consider a $N \times N = 5 \times 5$ array $P_{i,j}$ such that

$$P_{i,j} = \begin{bmatrix} P_{0,0} & P_{0,1} & P_{0,2} & P_{0,3} & P_{0,4} \\ P_{1,0} & P_{1,1} & P_{1,2} & P_{1,3} & P_{1,4} \\ P_{2,0} & P_{2,1} & P_{2,2} & P_{2,3} & P_{2,4} \\ P_{3,0} & P_{3,1} & P_{3,2} & P_{3,3} & P_{3,4} \\ P_{4,0} & P_{4,1} & P_{4,2} & P_{4,3} & P_{4,4} \end{bmatrix}.$$

This array corresponds with the P-transfer function for a particular wavenumber $P(\mathrm{k}; t_i, t_j)$. Keeping only $N_\mathrm{T} = 3$ timesteps, the array reduces to

$$P^\mathrm{T}_{i,j} = \begin{bmatrix} P_{0,0} & P_{0,1} & P_{0,2} & & \\ P_{1,0} & P_{1,1} & P_{1,2} & P_{1,3} & \\ P_{2,0} & P_{2,1} & P_{2,2} & P_{2,3} & \\ & P_{3,1} & P_{3,2} & P_{3,3} & P_{3,4} \\ & & P_{4,2} & P_{4,3} & P_{4,4} \end{bmatrix},$$

which is a calculation involving $(N - N_\mathrm{T})(N_\mathrm{T} - 1) + NN_\mathrm{T}$-terms rather than N^2 (for the present case of $N = 5$ and $N_\mathrm{T} = 3$, 25 terms are reduced to 19).

The LET2000 code truncation reduces only the P-transfer functions while still computing all two-time correlators; the LET2008 code truncation does not compute those correlators which do not occur in the time kernel of the P-transfer function eliminating further computations. The result is a negligible difference in all parameters showing this truncation to be useful. Examples of the effectiveness of this method are given later in this chapter. It is interesting to note that through the fluctuation-dissipation relation, there exist versions of the LET that are Markovian, eliminating the need for such truncations; for details see Oberlack *et al* [104], and the work of McComb and Kiyani [105, 108].

3.3 Benchmarking the LET2008 Code

The original codes of 1984, and in 1992, were contructed using Fortran-77. Later, in 2000, the code was rebuilt using the Fortran-90 architecture and was benchmarked against its precursors. Detailed comparisons were made showing the new LET2000 code's ability to reproduce the workings of the LET1984 code with success. In addition, the LET2000 was also the first to be tested directly against DNS for decaying and forced turbulence. All details of this testing are given in Quinn [101].

3.3.1 Turbulence Quantities

For what is to follow, it is useful to define various quantities that will be presented in the plots. As given in the previous section, there are two quantities that are directly computed in the LET2008 code, the correlation $C(\mathrm{k};t,t)$ and transfer-correlation function $P(\mathrm{k};t,t)$.

Spectral Quantities

There are four spectral quantities that will be presented below. These have been seen in the first chapter and are given here using $C(\mathrm{k};t,t)$ and $P(\mathrm{k};t,t)$:

$$\begin{aligned} \text{Energy Spectrum} \quad E(\mathrm{k},t) &= 4\pi\mathrm{k}^2 C(\mathrm{k};t,t), && (3.11)\\ \text{Dissipation Spectrum} \quad D(\mathrm{k},t) &= 2\nu\mathrm{k}^2 E(\mathrm{k};t) \\ &= 8\pi\nu\mathrm{k}^4 C(\mathrm{k};t,t), && (3.12)\\ \text{Energy Transfer Spectrum} \quad T(\mathrm{k},t) &= 8\pi\mathrm{k}^2 P(\mathrm{k};t,t). && (3.13) \end{aligned}$$

The factor $4\pi\mathrm{k}^2$ that arises in each of these definitions is due to the total energy being related to the velocity correlation (see chapter appendix 3.B). The fourth spectral quantity used is the flux,

$$\Pi(\mathrm{k},t) \equiv -\int_0^{\mathrm{k}} d\mathrm{j}\, T(\mathrm{j},t) \;=\; \int_k^{\infty} d\mathrm{j}\, T(\mathrm{j},t), \tag{3.14}$$

also defined in chapter 1.

Integral Parameters

The integral parameters include the mean total kinetic energy, the rms velocity, the mean dissipation rate two lengthscales. These are computed from the spectral quantities defined above. Thus, the mean total kinetic energy and mean dissipation rate are defined by integrating the spectral quantities over the whole of wavenumber space,

$$E(t) \equiv \int_0^{\infty} d\mathrm{k}\, E(\mathrm{k},t), \tag{3.15}$$

and

$$\varepsilon(t) \equiv \int_0^{\infty} d\mathrm{k}\, D(\mathrm{k},t) = \int_0^{\infty} d\mathrm{k}\, 2\nu\mathrm{k}^2 E(\mathrm{k},t). \tag{3.16}$$

The rms-velocity is obtained from the mean total kinetic energy using

$$E(t) \equiv \frac{3}{2}U(t)^2. \tag{3.17}$$

There are two lengthscales commonly encountered in the turbulence community: the integral lengthscale, $L(t)$ and the Taylor lengthscale, $\lambda(t)$ [111]. These are defined as follows:

$$L(t) \equiv \frac{3\pi}{4E(t)^2}\int_0^\infty d\mathrm{k}\,\mathrm{k}^{-1}E(\mathrm{k},t), \tag{3.18}$$

and

$$\lambda(t) \equiv \left(\frac{15\nu U(t)^2}{\varepsilon(t)}\right)^{1/2}. \tag{3.19}$$

Note that the integrals here span the full wavenumber range, however this is not possible in practise as the limits are bounded by the lowest and largest wavenumbers specified by the computation parameters. Therefore, the limits in the integral are set to $\mathrm{k}_{\mathrm{bottom}}$ and $\mathrm{k}_{\mathrm{top}}$.

One further quantity used here is the velocity derivative skewness,

$$S(t) \equiv -\frac{\left\langle(\partial u_1(\mathrm{x},t)/\partial \mathrm{x}_1)^3\right\rangle}{\left\langle(\partial u_1(\mathrm{x},t)/\partial \mathrm{x}_1)^2\right\rangle^{3/2}}. \tag{3.20}$$

The notation here may be misleading as the velocity skewness, similarly defined [28], can be found with the same notation. An alternate definition [25] that utilises the spectral equations used in the computations here is

$$S(t) \equiv -\frac{2}{35}\left(\frac{15\nu}{\varepsilon(t)}\right)^{3/2}\int_0^\infty d\mathrm{k}\,\mathrm{k}^2T(\mathrm{k},t). \tag{3.21}$$

The velocity-derivative skewness offers an important quantity for the comparison of computational models based on the DIA or LET theories as it is considered a sensitive measure of turbulence (see [112]). The skewness was used frequently in Quinn to check the resolution and memory-kernel truncation.

3.3.2 Initial Energy Spectra

In computations of decaying turbulence, an initial state with nonzero energy is needed from which the system will evolve. All spectra used have the same general form:

$$E(\mathrm{k},0) = c_1\mathrm{k}^{c_2}\exp(-c_3\mathrm{k}^{c_4}) \tag{3.22}$$

where the constants are given in Table 3.1. The spectra are given labels that roughly

Spectrum	c_1	c_2	c_3	c_4
I	0.00524169	4	0.088388	2
II	0.0662912	1	0.022097	2
III	0.0662912	1	0.210224	1
IV	0.4	1	0.5	1
V	0.001702	4	0.08	2
VI	0.031913	2	0.08	2

Table 3.1: Initial energy spectra parameter values

correspond to their chronology. Spectra I and II were originally found in Ogura [48], and reused in Kraichnan along with Spectrum III [113]. All three of these spectra were used for the LET1984 code in [100], which also introduced Spectrum IV. Quinn [101] added an additional spectrum, V. All spectra with the exception of Spectra V and VI may be integrated analytically to give the initial total kinetic energy density 1.5 m^2/s^2, which implies an initial rms velocity $U(0) = 1\ m/s$. The following figure shows the shape of all initial energy spectra.

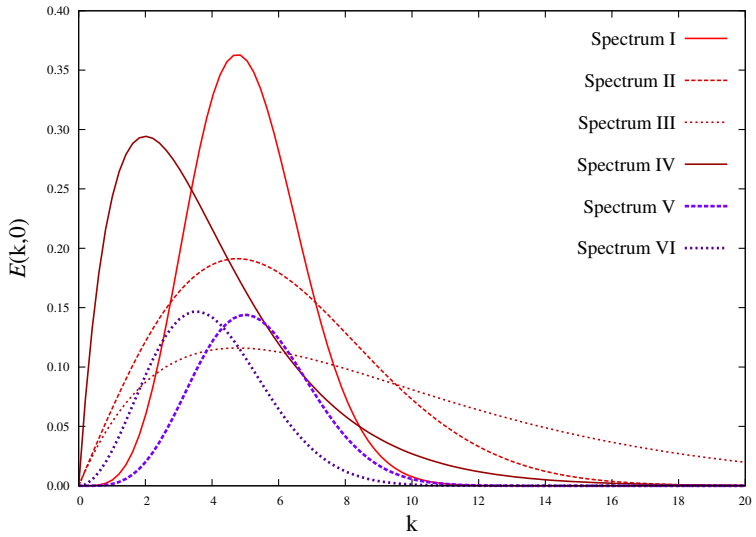

Figure 3.1: The six initial spectra used in the computation of LET2008. Spectra V and VI were extended to higher Reynolds numbers for freely-decaying turbulence, and Spectrum I was extended to higher Reynolds numbers for forced turbulence (see next chapter).

In forced turbulence, the initial energy spectrum is wiped away by the effects of the forcing, which after some time establishes a steady-state with a new (constant)

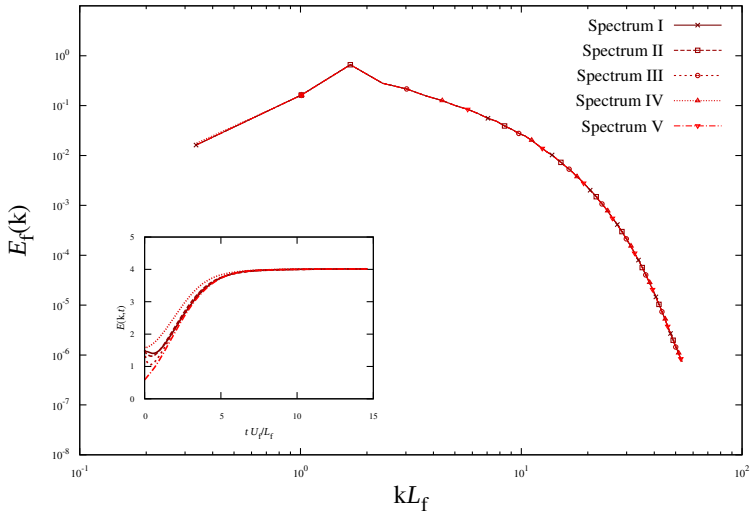

Figure 3.2: Forced turbulence using the LET2008 computation. The initial spectra I-V are evolved in time to become the same energy spectrum; this is confirmed by the total kinetic energies of the different spectra converging to the same point (inset). Final values are denoted by a subscript 'f'.

energy spectrum that takes shape according to the intensity, the injection rate, and wavenumber(s) in which the energy is input. Figure 3.2 shows the same final steady-state energy spectrum dictated by the forcing using different initial spectra I-V (compare to the initial shapes in fig. 3.1). Correspondingly, the inset gives the total kinetic energy density of the same initial spectra, showing how they evolve over time to the same final state.

3.3.3 Decaying Turbulence with the LET

In this section, the LET2008 code is used to investigate the LET's ability to reproduce appropriate turbulent quantities for the case of free-decay. Some results can be checked against the LET2000 code, which, as noted earlier, has been checked against the LET1984 code and DNS computations using the same initial energy spectra. This includes computations using initial spectra I-V, which all occur in previous studies (see above). As spectrum VI is new to this project, there are no previous results to compare against, but there exists new data from current DNS computations that can be used for comparison. Spectra V and VI are shown in comparison to the DNS-based results.

Comparison with LET2000

The LET2008 code is negligibly different than the LET2000 code and all expectations are that it should perform up to the same standard.

To demonstrate the current code's reliability in matching the earlier code, plots of the integral parameters, computed using the spectra I-IV, are given in figs. 3.3,3.4, and similar plots using a single initial energy spectrum, Spectrum V, and different viscosities are given in figs. 3.5, 3.6. All computations shown here use the same input parameters as those set by Quinn (see Appendix A of [101]).

For most parameters in figs. 3.3-3.6, the matching is fairly good. The dissipation rate $\varepsilon(t)$ and the skewness $S(t)$ consistently show the largest discrepancies between the two codes, but never more than 10%. The skewness of LET2008 is, in all cases, lower than that of LET2000. The lengthscales of $R_\lambda(0) \sim 2.58$ in fig. 3.5, also show growing deviations among the two computations but this seems to resolve as the Reynolds number is increased.

Comparison with DNS

As Spectra VI has been newly introduced for the current study, there are no historical measures to compare it against. However, recent work by Yoffe [114] has allowed some comparisons to be made against DNS. The following baseline results for spectra V and VI will be given for some viscosities in much the same manner as Quinn's Spectrum V, except in this case the viscosities will be $\nu = .1, .05, .01, .005$. These viscosities do not achieve the moderate Taylor-Reynolds numbers as given in Quinn as these were not available for comparison using the current DNS.

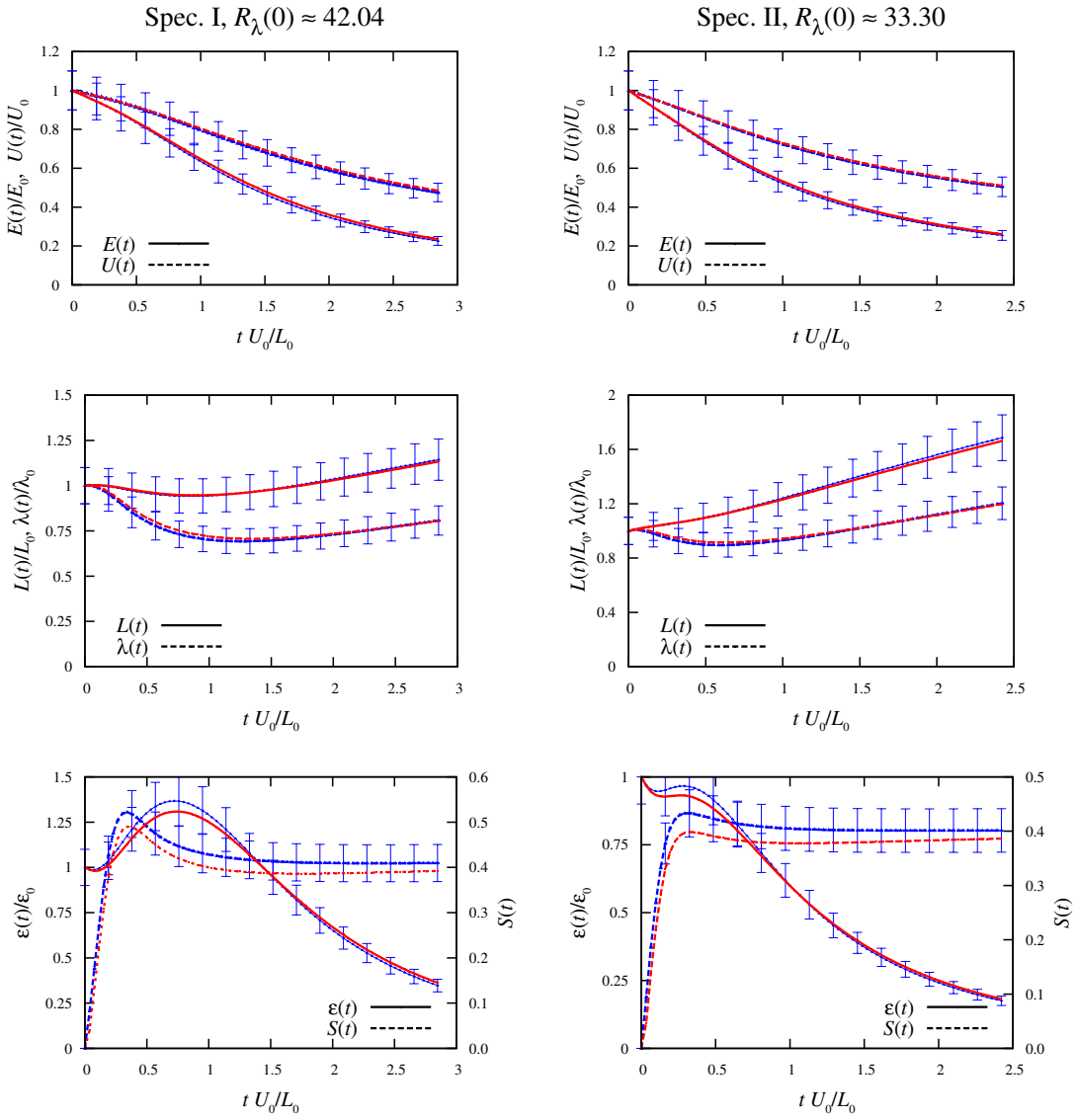

Figure 3.3: Comparison plots of integral parameters from the LET2000 (blue) and LET2008 (red) for LET computations of Spectrum I (left) and Spectrum II (right). The error-bars on the LET2000 plots represent ±10%; the LET2008 results typically fall well within these bounds. The 0-subscripts designate initial values for integral parameters, *e.g.* $E(0) \equiv E_0$.

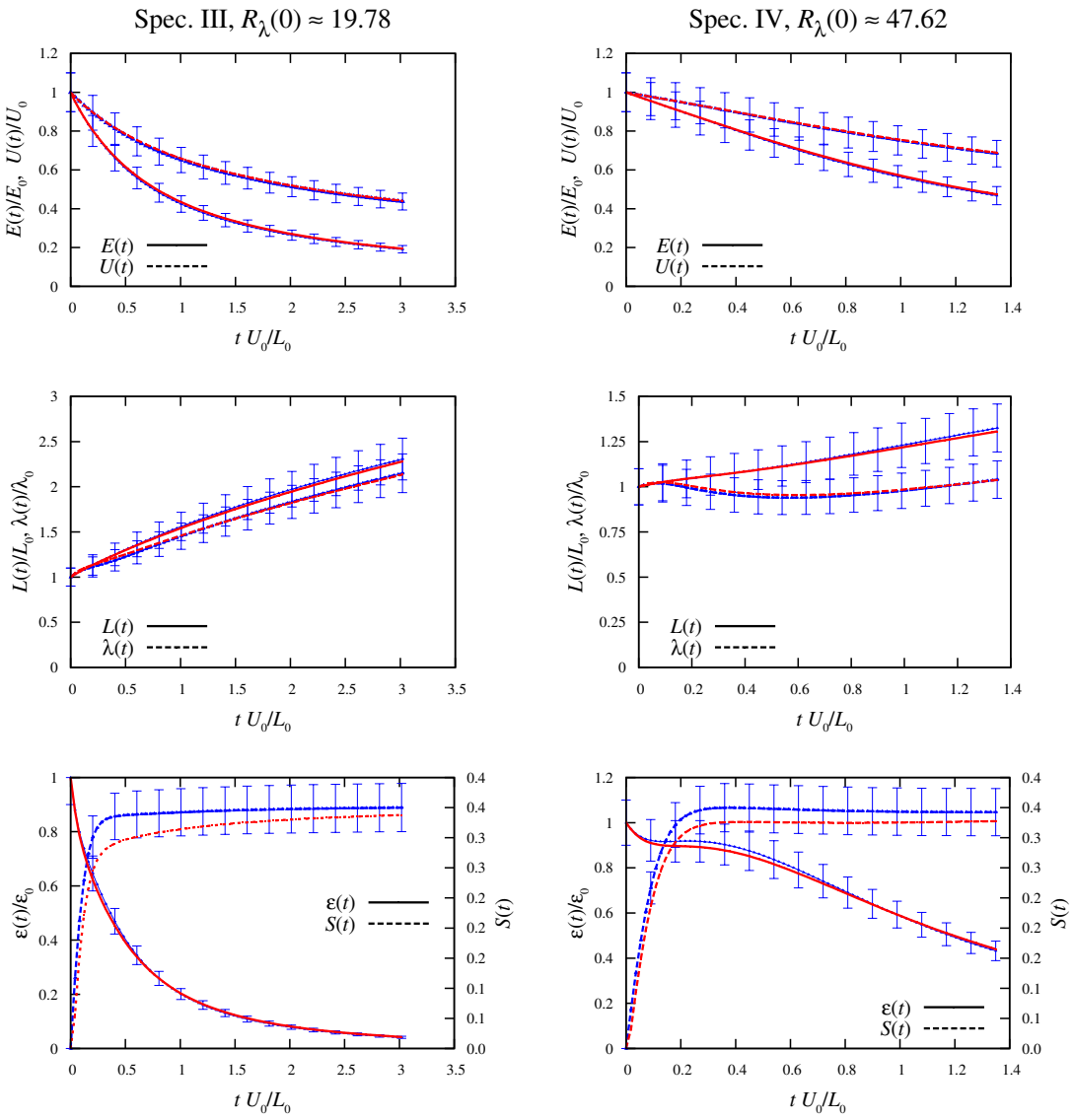

Figure 3.4: Comparison plots of integral parameters from the LET2000 (blue) and LET2008 (red) for LET computations of Spectrum III (left) and Spectrum IV (right). The error-bars on the LET2000 plots represent ±10%; the LET2008 results typically fall well within these bounds. The 0-subscripts designate initial values for integral parameters, *e.g.* $E(0) \equiv E_0$.

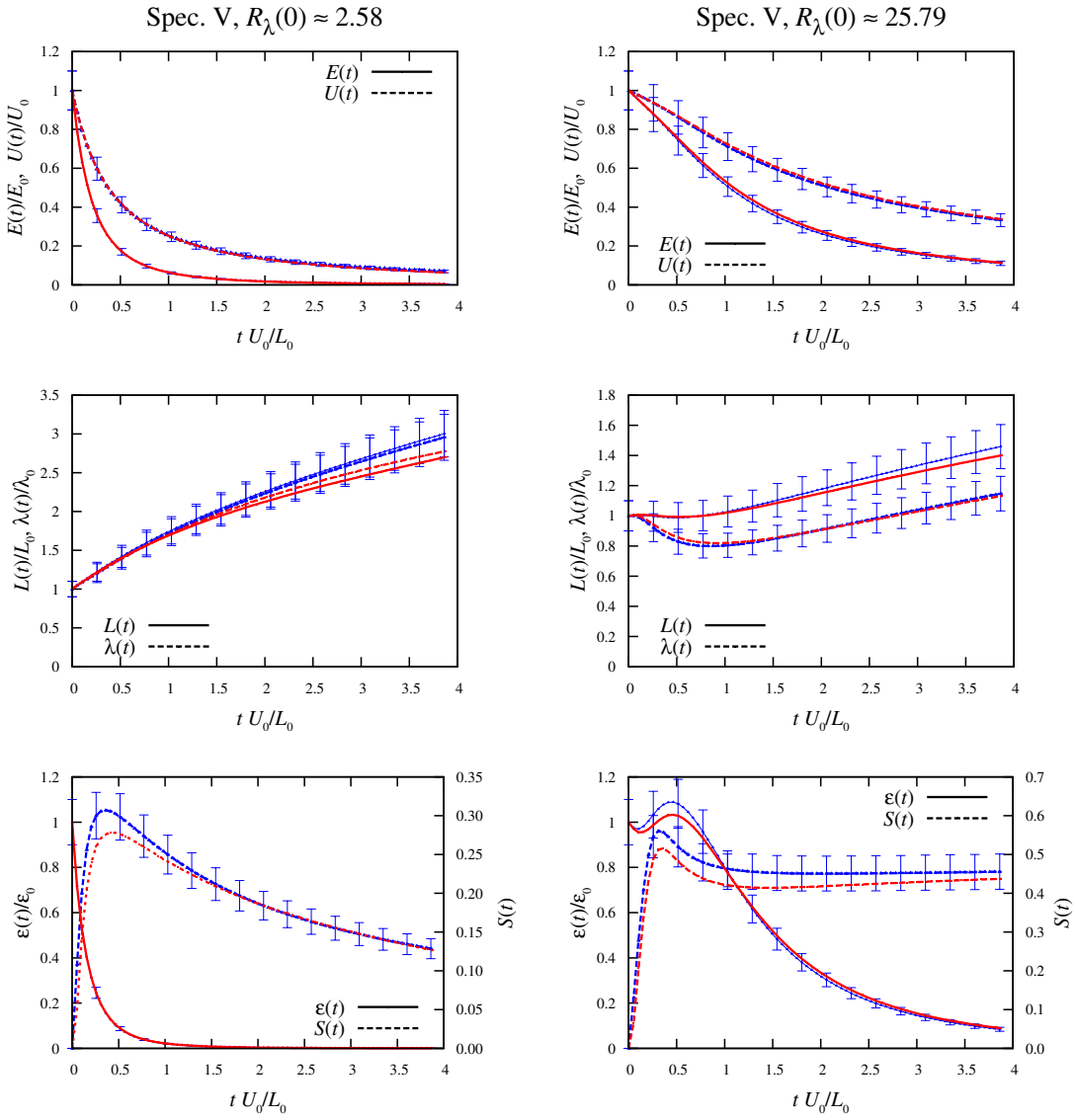

Figure 3.5: Comparison plots of integral parameters from the LET2000 (blue) and LET2008 (red) for LET computations of Spectrum V, $\nu = .1$ (left) and Spectrum V, $\nu = .01$ (right). The error-bars on the LET2000 plots represent $\pm 10\%$; the LET2008 results typically fall well within these bounds. The 0-subscripts designate initial values for integral parameters, *e.g.* $E(0) \equiv E_0$.

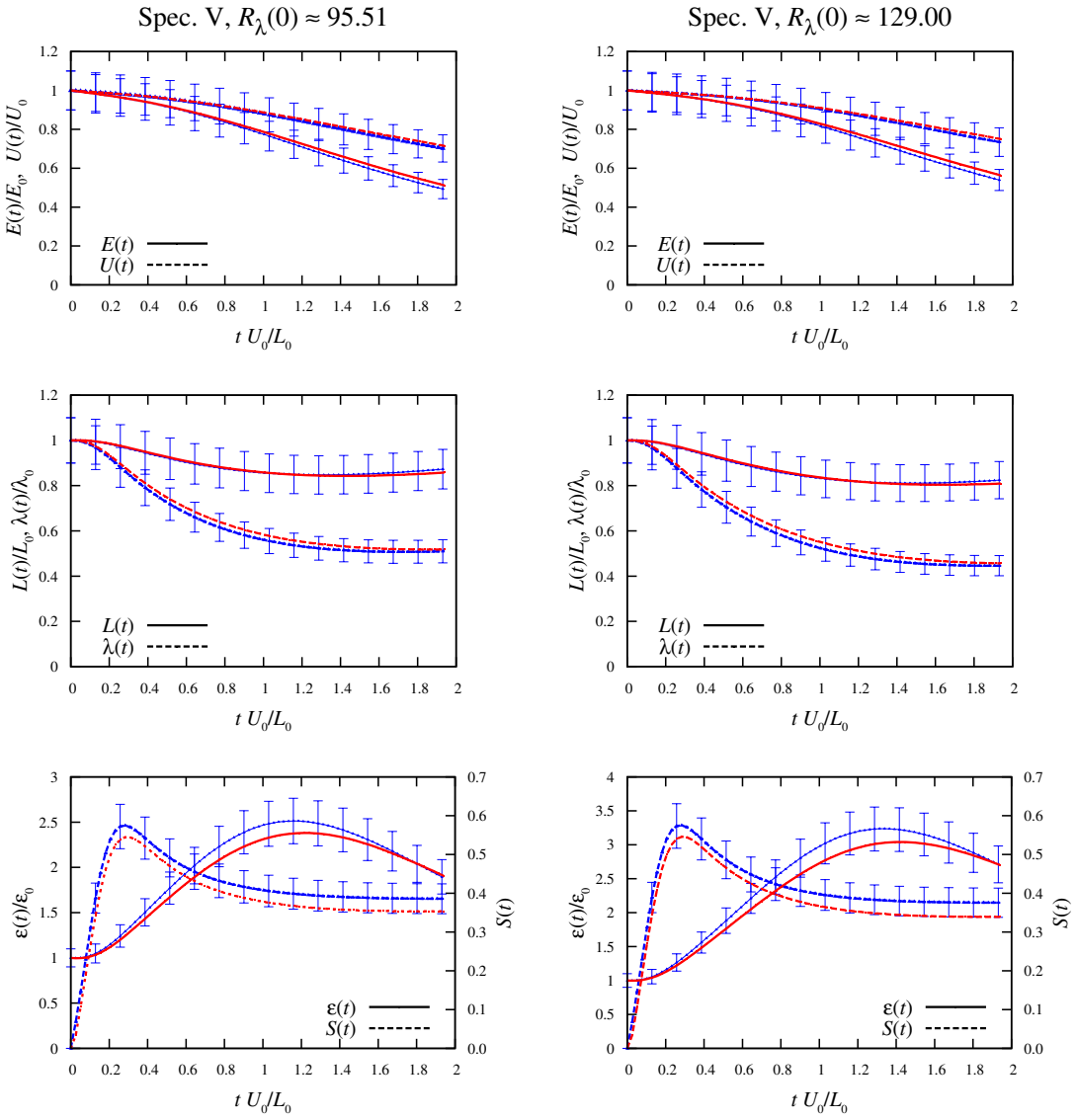

Figure 3.6: Comparison plots of integral parameters from the LET2000 (blue) and LET2008 (red) for LET computations of Spectrum V, $\nu = .0027$ (left) and Spectrum V, $\nu = .002$ (right). The error-bars on the LET2000 plots represent $\pm 10\%$; the LET2008 results typically fall well within these bounds. The 0-subscripts designate initial values for integral parameters, *e.g.* $E(0) \equiv E_0$.

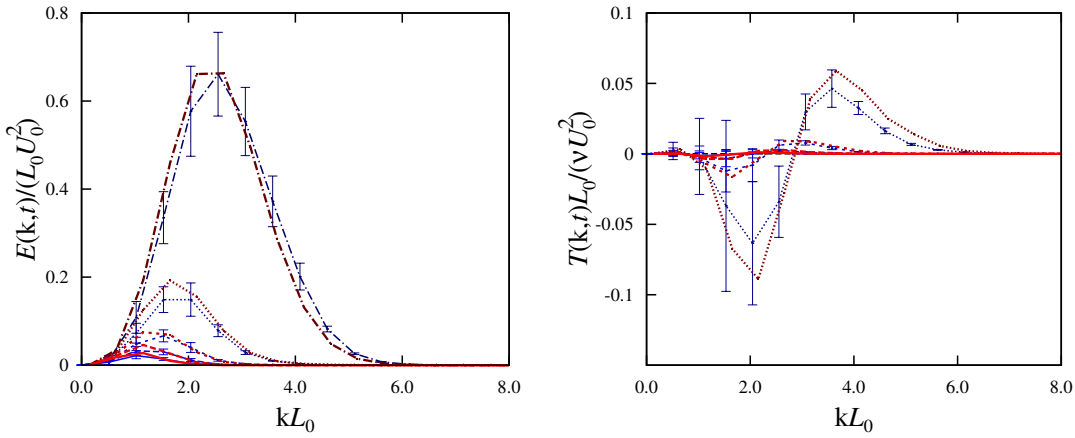

Figure 3.7: Comparison plots of energy (left) and transfer (right) spectra from the DNS (blue) and LET2008 (red) computations of Spectrum V, $\nu = 0.1$.

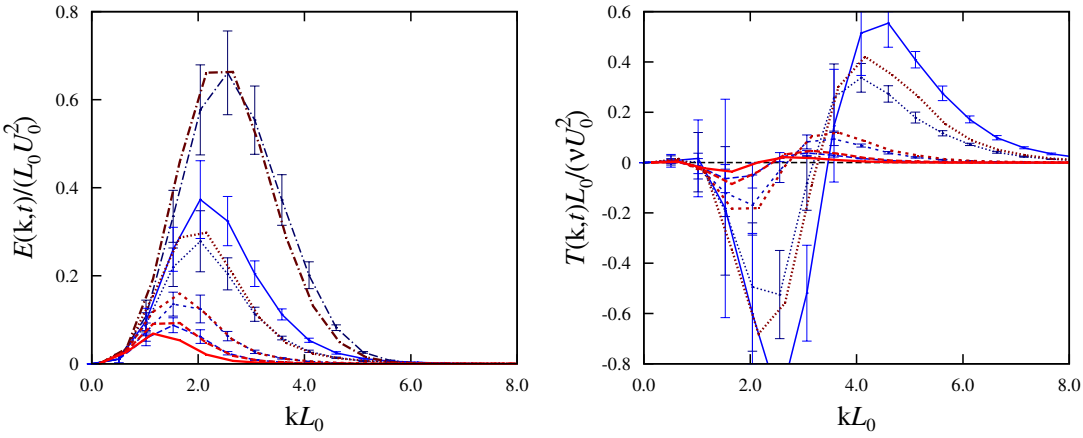

Figure 3.8: Comparison plots of energy (left) and transfer (right) spectra from the DNS (blue) and LET2008 (red) computations of Spectrum V, $\nu = 0.05$.

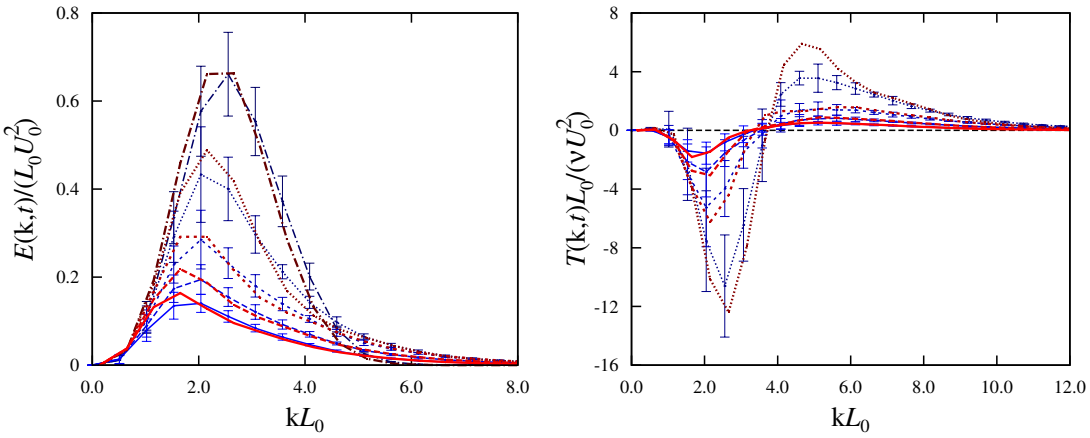

Figure 3.9: Comparison plots of energy (left) and transfer (right) spectra from the DNS (blue) and LET2008 (red) computations of Spectrum V, $\nu = 0.01$.

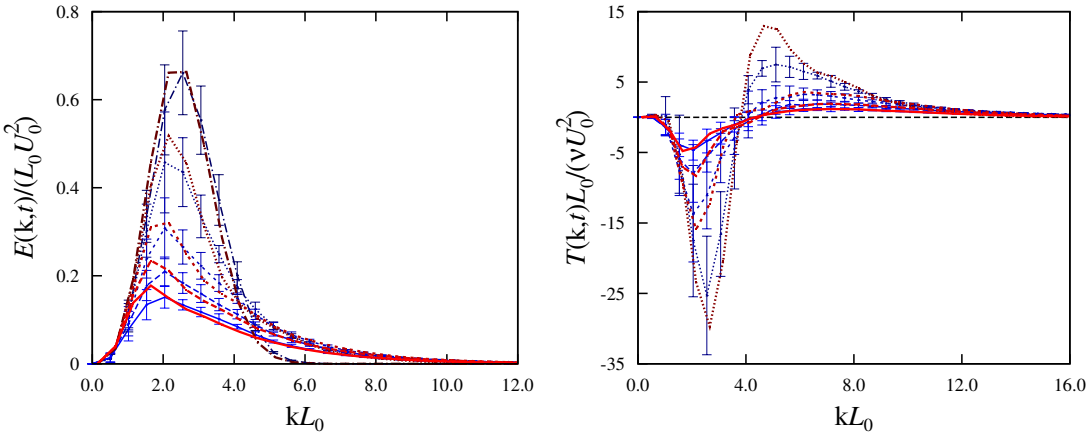

Figure 3.10: Comparison plots of energy (left) and transfer (right) spectra from the DNS (blue) and LET2008 (red) computations of Spectrum V, $\nu = 0.005$.

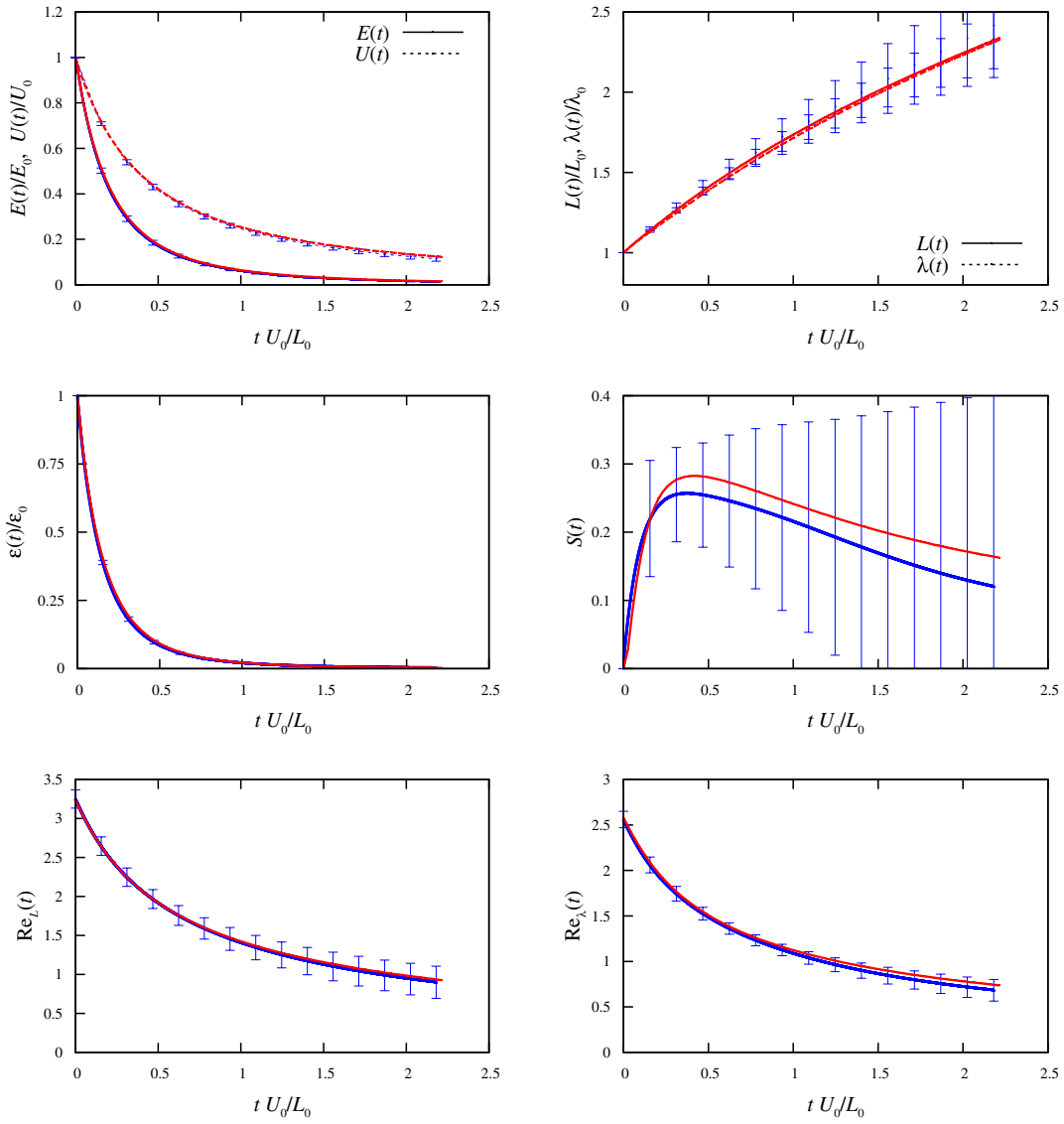

Figure 3.11: Comparison plots of integral parameters from the DNS (blue) and LET2008 (red) computations of Spectrum V, $\nu = 0.1$.

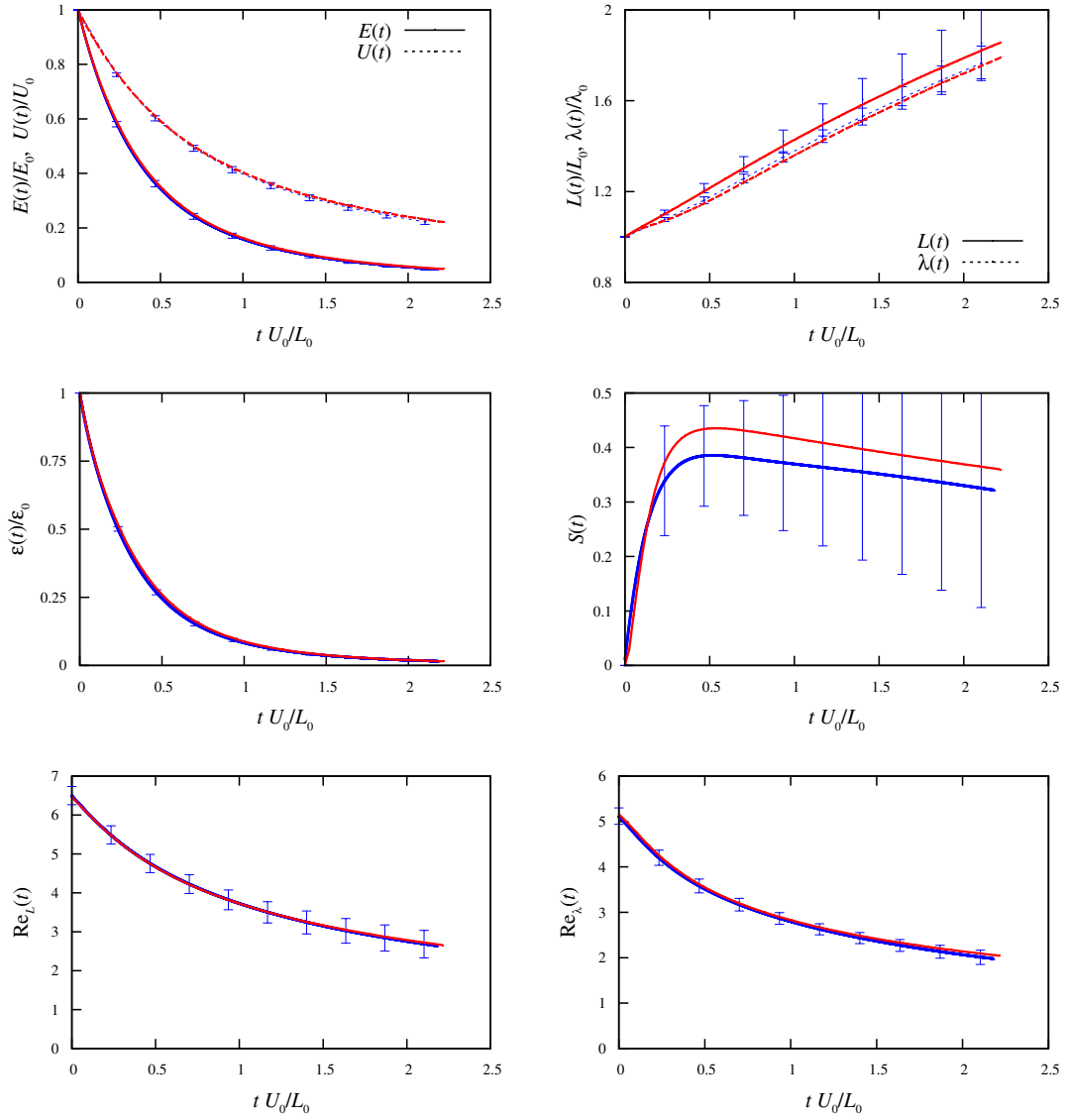

Figure 3.12: Comparison plots of integral parameters from the DNS (blue) and LET2008 (red) computations of Spectrum V, $\nu = 0.05$.

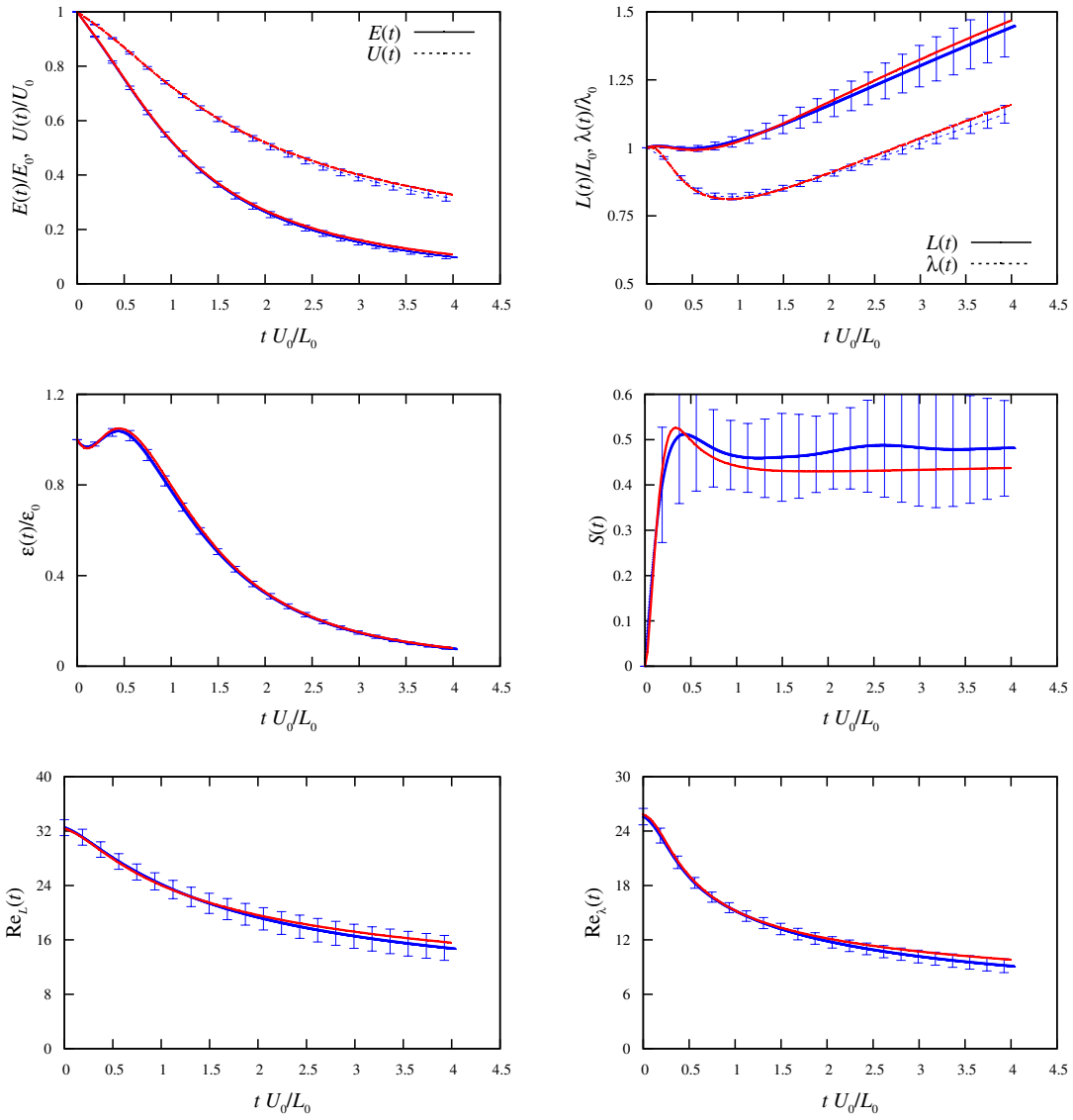

Figure 3.13: Comparison plots of integral parameters from the DNS (blue) and LET2008 (red) computations of Spectrum V, $\nu = .01$.

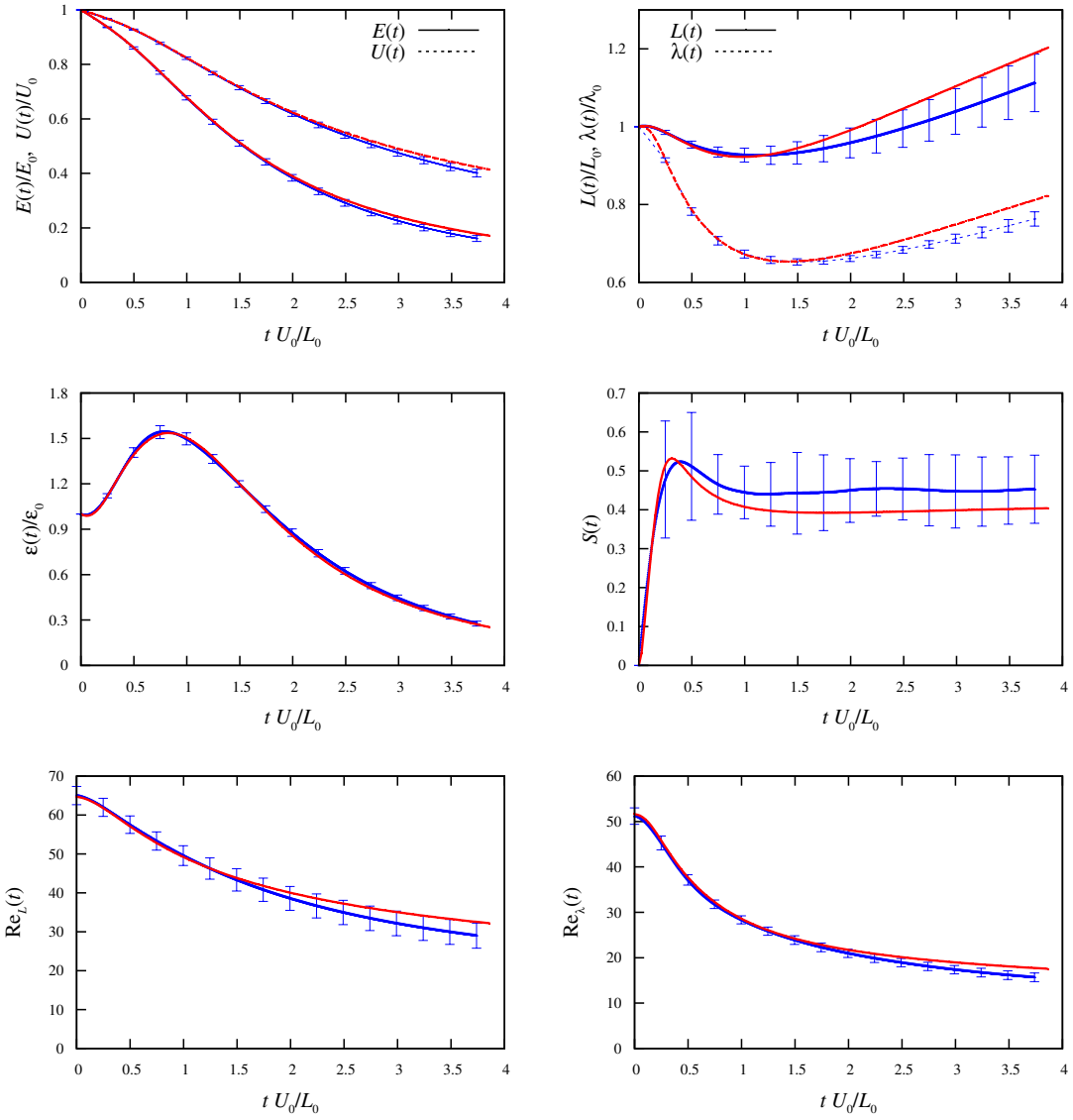

Figure 3.14: Comparison plots of integral parameters from the DNS (blue) and LET2008 (red) computations of Spectrum V, $\nu = 0.005$.

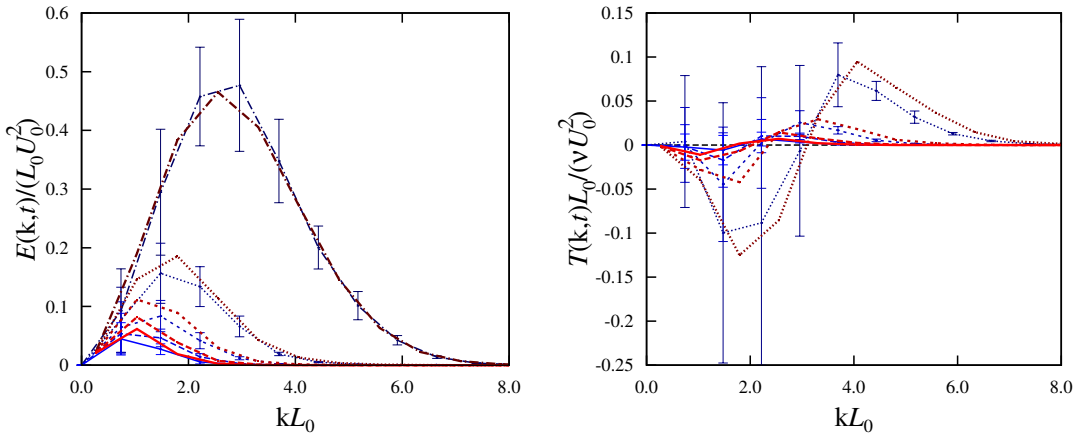

Figure 3.15: Comparison plots of energy (left) and transfer (right) spectra from the DNS (blue) and LET2008 (red) computations of Spectrum VI, $\nu = 0.1$.

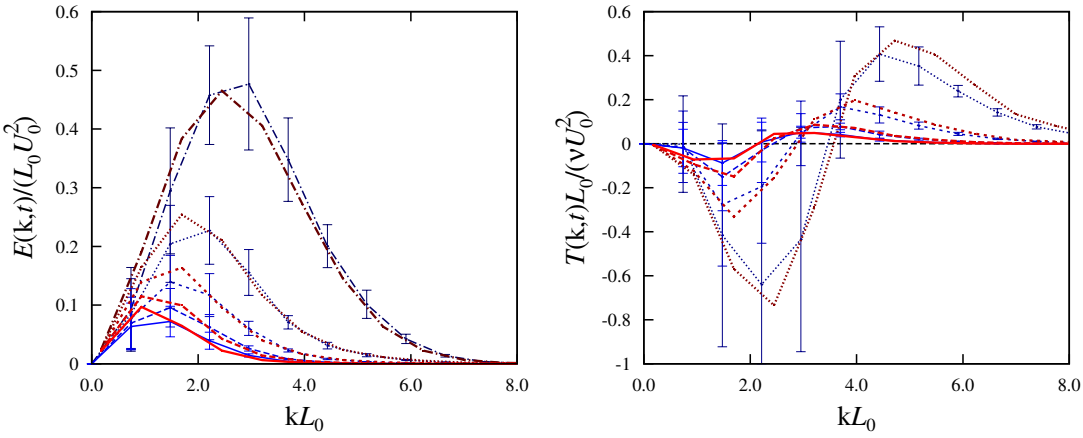

Figure 3.16: Comparison plots of energy (left) and transfer (right) spectra from the DNS (blue) and LET2008 (red) computations of Spectrum VI, $\nu = 0.05$.

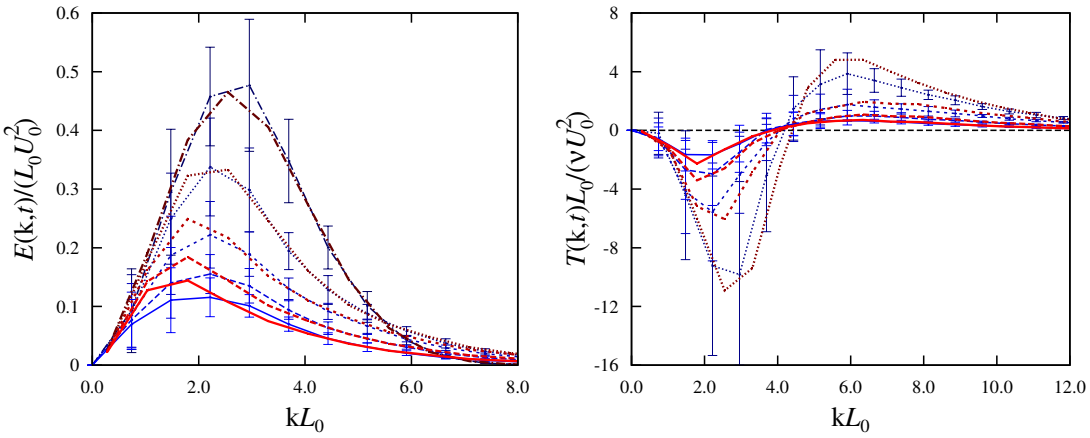

Figure 3.17: Comparison plots of energy (left) and transfer (right) spectra from the DNS (blue) and LET2008 (red) computations of Spectrum VI, $\nu = 0.01$.

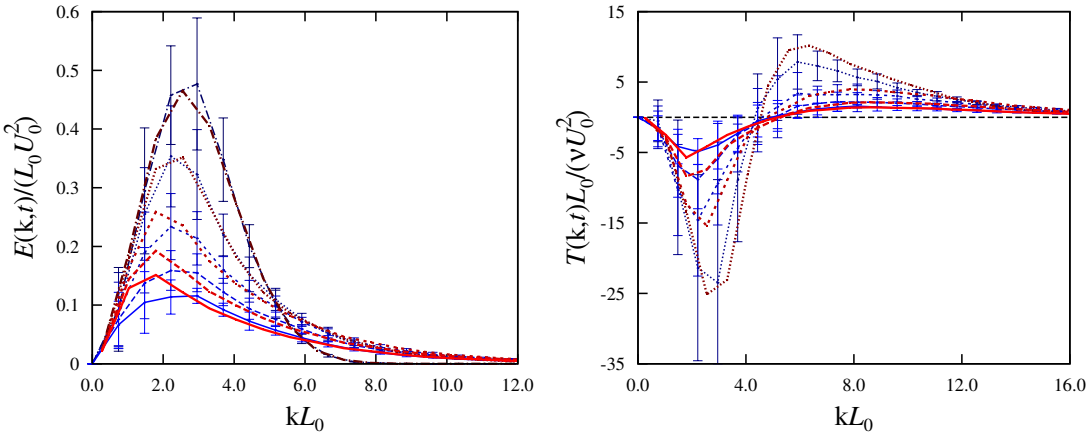

Figure 3.18: Comparison plots of energy (left) and transfer (right) spectra from the DNS (blue) and LET2008 (red) computations of Spectrum VI, $\nu = 0.005$.

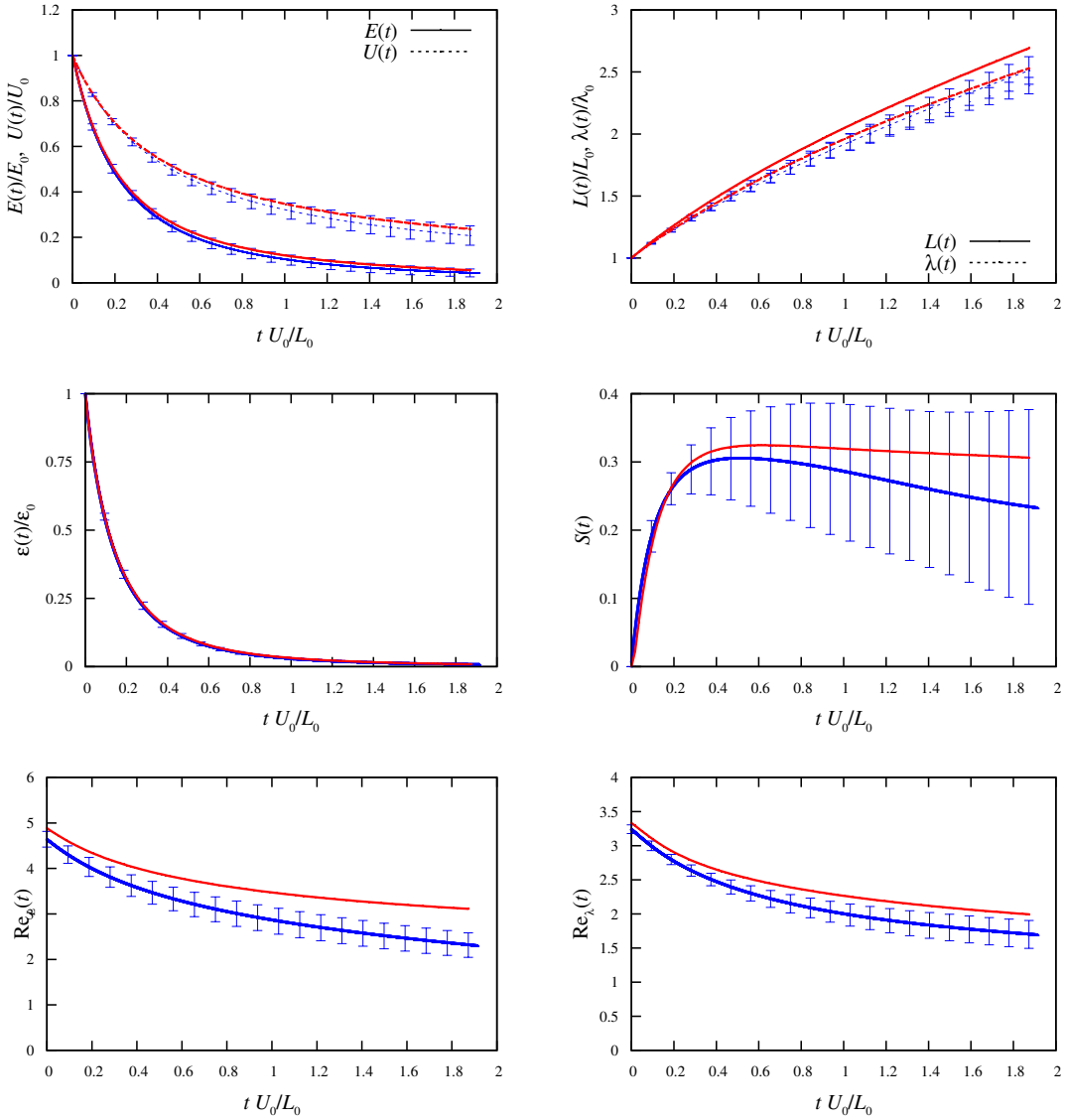

Figure 3.19: Comparison plots of integral parameters from the DNS (blue) and LET2008 (red) computations of Spectrum VI, $\nu = 0.1$.

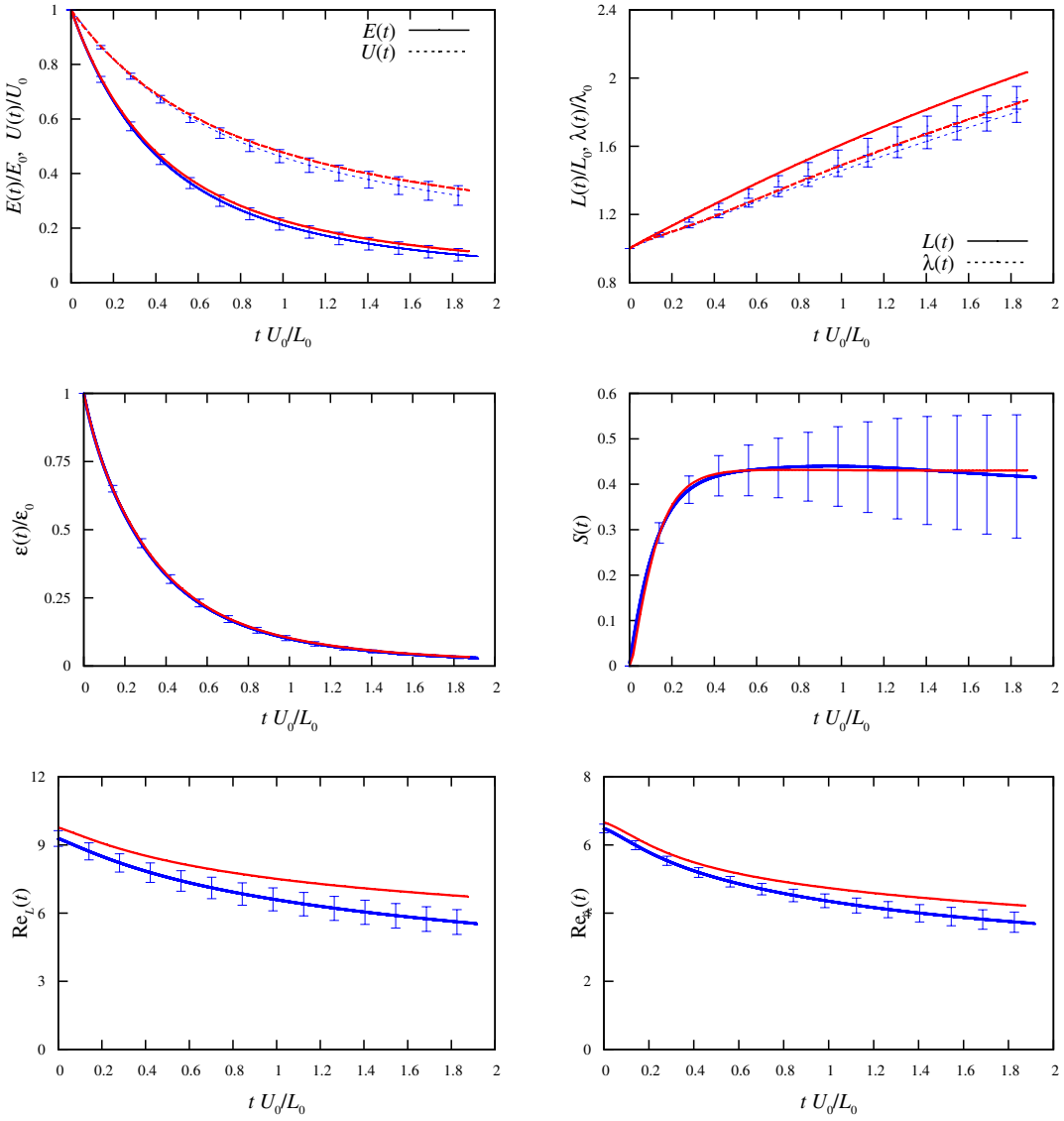

Figure 3.20: Comparison plots of integral parameters from the DNS (blue) and LET2008 (red) computations of Spectrum VI, $\nu = 0.05$.

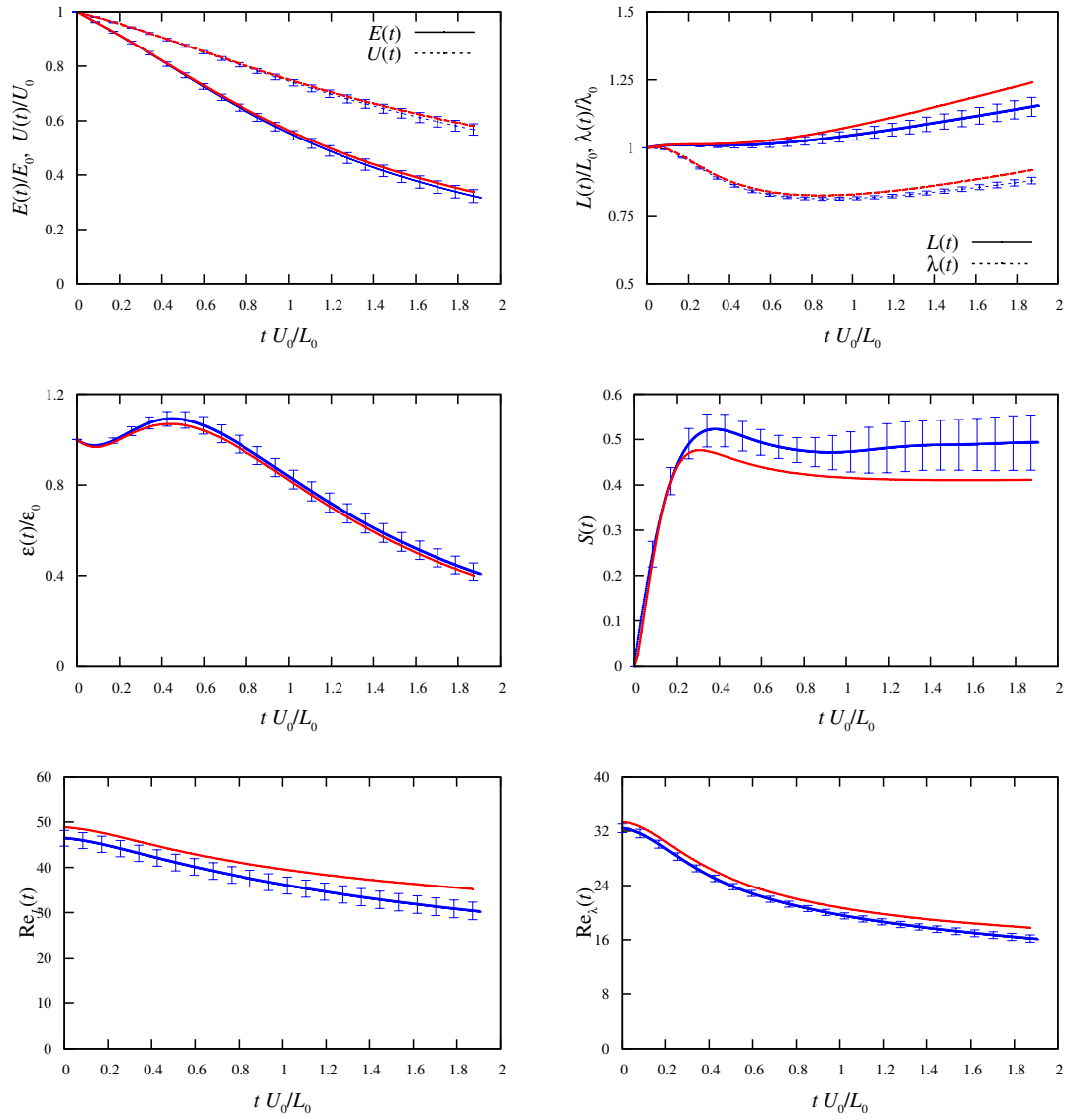

Figure 3.21: Comparison plots of integral parameters from the DNS (blue) and LET2008 (red) computations of Spectrum VI, $\nu = .01$.

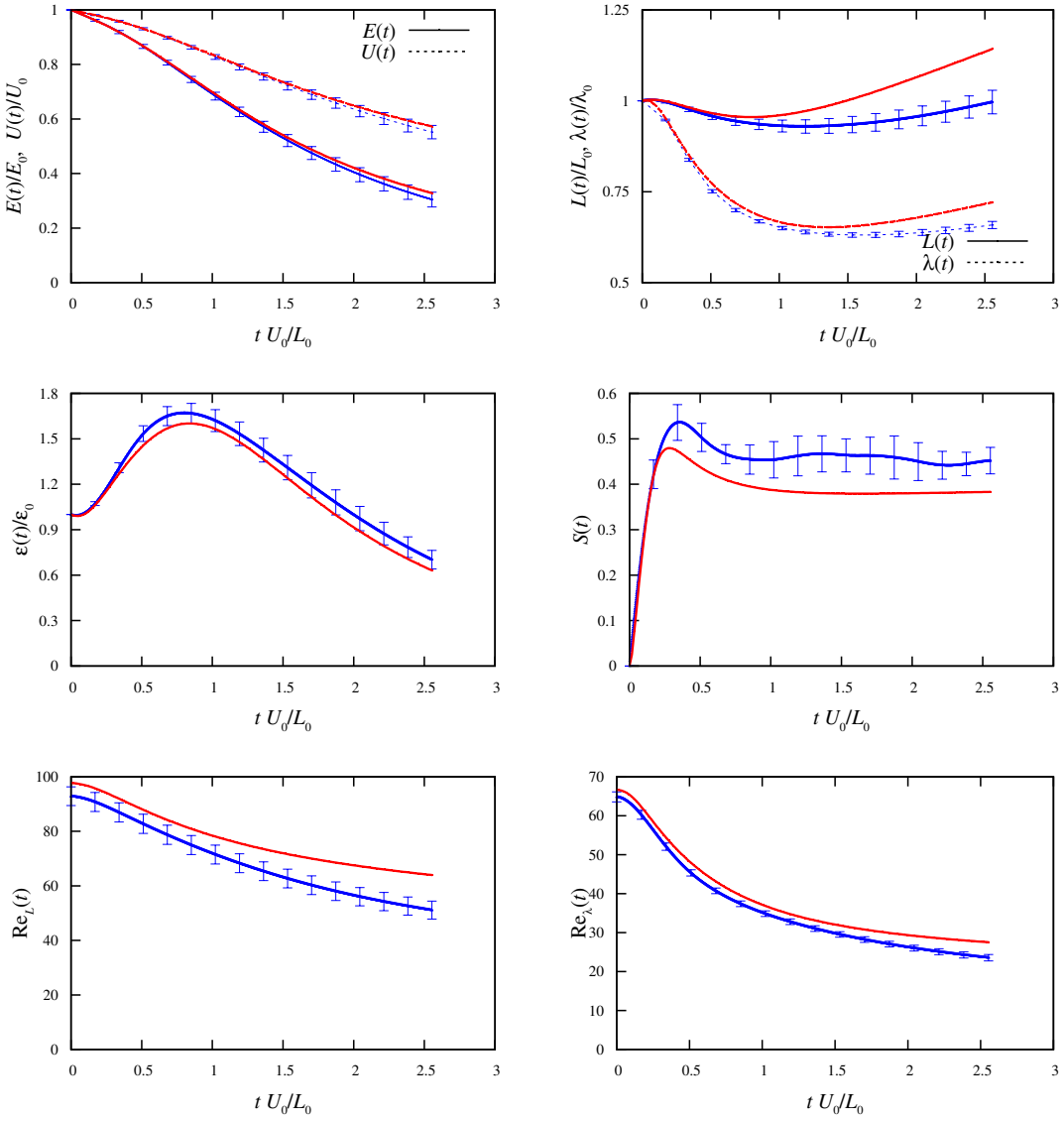

Figure 3.22: Comparison plots of integral parameters from the DNS (blue) and LET2008 (red) computations of Spectrum VI, $\nu = 0.005$.

3.3.4 Forced Turbulence with the LET

Forced turbulence was introduced to the LET in the work of Quinn, who also developed DNS forcing with which to compare the LET2000's results. The results compared well to those of the forced DNS computations, achieving a Taylor-Reynolds number of $R_\lambda \sim 230$.

The forcing routine which Quinn developed is completely reproduced in the current version. It consists of injecting energy at the low-k scales, typically k=1, such that the dissipation rate attains a steady-state with a constant value, $\varepsilon = 1m^2/s^3$. The routine operates by adding a fixed amount of energy per time, ΔE_f, to a chosen wavenumber, $\mathrm{k_f}$, in a single timestep Δt. The energy injection rate, ΔE_f, is chosen to fix the dissipation rate to a desired value given the relation,

$$\varepsilon(t) = \Delta E_\mathrm{f} \tag{3.23}$$

(see chapter appendix 3.C for this derivation). Then, for each timestep, the quantity $\Delta E_\mathrm{f} \Delta t$ is added to the wavemunber $\mathrm{k_f}$ in the energy spectrum.

It is important that implementation of the forcing routine occurs after the last iteration of the predictor-corrector routine, prior to advancing to the next timestep, $t_i + 1$. This means that for the LET code, all measurements of the correlator and P-transfer functions must be taken just before running the forcing as recording after the routine will give 'artificial' results that the system will not have been able to respond to when the measurement of these quantities is made.

It was mentioned above that the initial spectra are inconsequential to the steady-state energy spectra that the system settles to. For the purposes of comparison, Spectrum I was used as the initial energy spectrum. Quinn developed a DNS which used a forcing routine that was analogous to that used in the LET2000 code. Using the forced-DNS, the LET2000 code was shown to reasonably reproduce the same results.

In the following section, the results of the LET2008 computations for forced turbulence are presented.

Comparison with LET2000

The LET2000 was the first application of the LET model to forced turbulence and therefore the only available benchmark against which to test the current LET code. As with the decaying turbulence calculations, the LET2008 results were checked against the energy, dissipation, transfer, and flux spectra as well as the integral parameter calculations of the LET2000 code.

There was a second spectrum included in [101] that was used in the forced turbulence

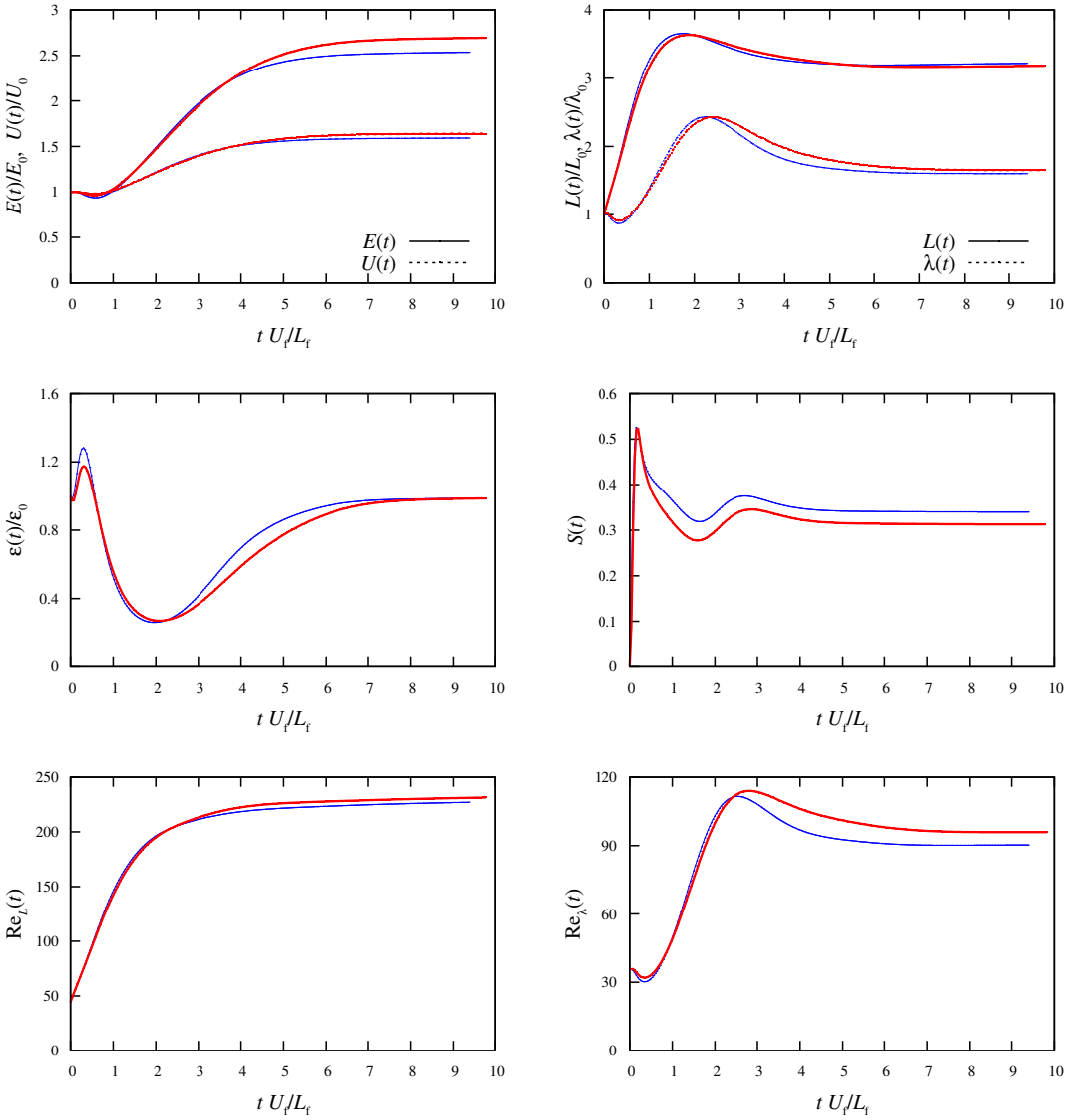

Figure 3.23: A comparison of integral parameters from the LET2000 (blue) and LET2008 (red) from forced computations of Spectrum I, $\nu = 0.01189$.

LET. This spectrum was tried in LET2008 however it was found to be unstable. A logarithmic wavestepping was used in LET2000 whereas linear-wavestepping is used in LET2008. Multiple resolutions in wavenumber and timesteps were attempted to reproduce the previous results. Higher Reynolds number calculations were obtained using Spectrum I and so further investigation in order to remedy the problems for the second forced spectrum was abandoned.

3.3.5 Memory Kernel Truncation in LET2008

A significant reduction in time occurs when using the memory-kernel truncation described earlier. As the current method is a further reduction from that of the THIT, it is necessary to determine how it differs from its predecessor. The following figures give examples the effects of the truncations on the skewness for decaying (fig. 3.24) and forced (fig. 3.25) turbulence using the LET2008 code.

The plots of the skewness $S(t)$ given in fig. 3.24 show how the LET2000 THIT scheme compares to the current version. The figure shows both schemes with various-sized memory kernels. In case of the smallest sized kernel (30 timesteps), the THIT performs no better than the LET2008-truncation with both deviating just prior to the 40^{th} timestep. However, in all other curves, the two schemes are indistinguishable according to their respective kernel sizes. Note that the figure exaggerates the differences; the inset shows the comparison of the LET2000-THIT and the LET2008 truncation, but at 30 timesteps and, at this scale, the differences are quite small.

While the truncation can save time, it does ignore information needed to correctly model the behaviour of a turbulent system. This becomes most apparent for cases of low Reynolds numbers where viscous effects are more important. For this reason, computations for decaying turbulence computed here using spectra V and VI, the truncation was only used when the viscosities were less than $\nu = .005$. In the results of the following chapters, the kernel was reduced to 50 timesteps where the viscosity met this criterion.

The truncations for forced turbulence, fig. 3.25, showed no noteworthy differences between the LET200 and LET2008 truncation schemes. There was a slight deviation for the memory kernels of 50 steps, but this deviation was never greater than 1% and tended to remain constant. Larger memory kernels made no significant improvements. Unlike the case for decaying turbulence, there seemed to be no significant dependence on the viscosity and the size of the memory kernel for the sizes (> 50 timesteps) used in this research. In the results given in the following chapters, the memory kernel was usually truncated to 50 timesteps for forced turbulence.

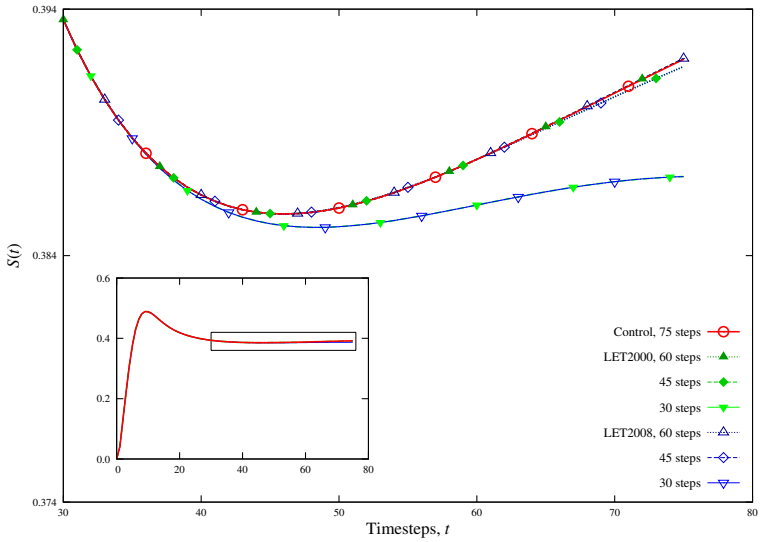

Figure 3.24: The effect on the skewness of memory-kernel truncation in the LET2008 compared to Time-History Integral Truncation used in LET2000 for decaying turbulence, using initial energy spectrum I. The red curve is the control skewness without any truncation. The inset shows the corresponding section of the total skewness where deviation is the largest.

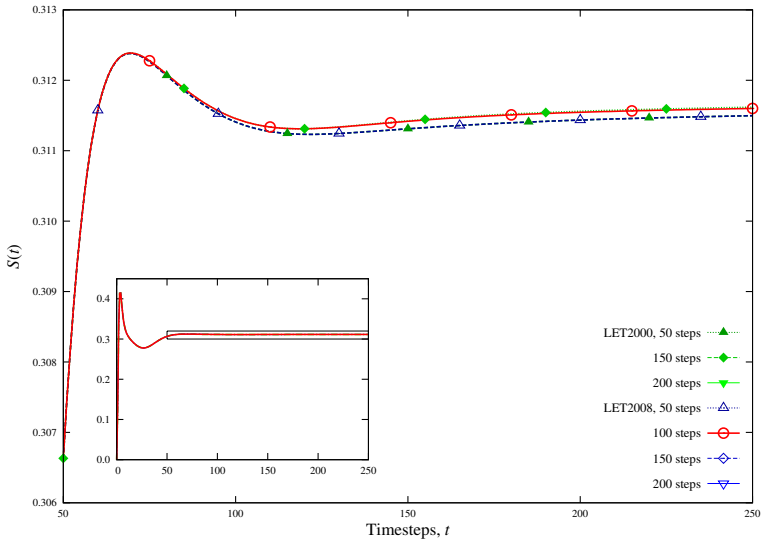

Figure 3.25: The effect on the skewness of memory-kernel truncation in the LET2008 compared to Time-History Integral Truncation used in LET2000 for decaying turbulence, using initial energy spectrum I. The red curve is the control skewness without any truncation. The inset shows the corresponding section of the total skewness where deviation is the largest.

3.4 Discussion

The LET theory of homogeneous isotropic turbulence has been outlined along with a method of numerical computation of its solution, the LET2008 code. Like its predecessor, LET2000, the current model is capable of computing both freely-decaying and forced turbulence.

3.4.1 Conclusions

The LET2008 has been evaluated against LET2000 and, in some cases, tested against DNS, specifically for the newly introduced Spectrum VI. It has been shown to satisfactorily reproduce the results of the predecessor code in the case of freely-decaying turbulence. Comparisons made between LET and DNS for Spectra V and VI show some reasonable similarities in the energy spectra but consistently show differences in the transfer spectra.

The current results for the forced turbulence benchmarks against the LET2000 code show some discrepancies, but qualitatively the codes compare well.

Lastly, the use of a new memory-kernel truncation matches the behaviour of an earlier truncation used by Quinn. The new truncation is relatively more efficient, and therefore faster than that used by Quinn.

3.4.2 Future Work

As the LET is a closure, one suggestion for future work would be to use the EDQNM for comparison. The use of EDQNM is well-documented, see for example [27, 115–119], and can provide a useful comparison to further check the LET against.

The usefulness of the LET is limited by the ability to compute solutions to it within a reasonable error and within a reasonable time. Using the results from [104, 105, 108], one could construct a computation for the single-time LET. This would retain the information of the two-time LET, but would do so at a smaller computational cost, in both memory and time, allowing higher Reynolds numbers to be attained. This is intriguing as no numerical computations have been made from these later analyses of the LET.

3.A Summary Derivation of the LET Equations

The starting point for the LET is the evolution equation for the two-time correlation tensor:

$$\begin{aligned}\Big(\partial_t + \nu \mathrm{k}^2\Big) C_{\alpha\alpha'}(\mathbf{k};t,t')\delta(\mathbf{k}+\mathbf{k}') &= \big\langle f_\alpha(\mathbf{k},t) u_{\alpha'}(\mathbf{k}',t')\big\rangle \delta(\mathbf{k}+\mathbf{k}') \\ &+ M_{\alpha\beta\gamma}(\mathbf{k}) \int d^3\mathrm{j}\, \big\langle u_\beta(\mathbf{j},t) u_\gamma(\mathbf{k}\text{-}\mathbf{j},t) u_{\alpha'}(\mathbf{k}',t')\big\rangle\end{aligned} \tag{3.24}$$

where $C_{\alpha\alpha'}(\mathbf{k};t,t')$ is defined below as

$$C_{\alpha\alpha'}(\mathbf{k};t,t')\delta(\mathbf{k}+\mathbf{k}') = \langle u_\alpha(\mathbf{k},t) u_{\alpha'}(\mathbf{k}',t')\rangle. \tag{3.25}$$

This equation is obtained directly from the Fourier-space NSE by multiplying it by $u_{\alpha'}(\mathbf{k}',t')$ and taking an ensemble average.

As the notation of the functions are complicated by multiple arguments, indices, and labels, the derivation will proceed using a reduced notation (as seen previously in section 2.2 of this thesis). The starting equation above, (3.24), in reduced notation is

$$\mathcal{L}_0 C_{\mathbf{k}} \delta_{\mathbf{k}+\mathbf{k}'} = \langle f_{\mathbf{k}} u_{\mathbf{k}'}\rangle \delta_{\mathbf{k}+\mathbf{k}'} + M_{\mathbf{k}} \langle u_{\mathbf{j}} u_{\mathbf{k}-\mathbf{j}} u_{\mathbf{k}'}\rangle \tag{3.26}$$

The velocity field is expanded perturbatvely using a bookkeeping-parameter, λ, and equated to a perturbative expansion of the NSE,

$$\begin{aligned} u_{\mathbf{k}} &= R^{(0)}_{\mathbf{k}} f_{\mathbf{k}} + \lambda R^{(0)}_{\mathbf{k}} M_{\mathbf{k}} \Big((u^{(0)}_{\mathbf{j}} + \lambda u^{(1)}_{\mathbf{j}} + \cdots)(u^{(0)}_{\mathbf{k}-\mathbf{j}} + \lambda u^{(1)}_{\mathbf{k}-\mathbf{j}} + \cdots)\Big) \\ &= R^{(0)}_{\mathbf{k}} f_{\mathbf{k}} + \lambda R^{(0)}_{\mathbf{k}} M_{\mathbf{k}} \big(u^{(0)}_{\mathbf{j}} u^{(0)}_{\mathbf{k}-\mathbf{j}}\big) + \lambda^2 R^{(0)}_{\mathbf{k}} M_{\mathbf{k}} \big(u^{(0)}_{\mathbf{j}} u^{(1)}_{\mathbf{k}-\mathbf{j}} + u^{(1)}_{\mathbf{j}} u^{(0)}_{\mathbf{k}-\mathbf{j}}\big) + \mathcal{O}(\lambda^3) \\ &= u^{(0)}_{\mathbf{k}} + \lambda u^{(1)}_{\mathbf{k}} + \lambda^2 u^{(2)}_{\mathbf{k}} + \mathcal{O}(\lambda^3). \end{aligned} \tag{3.27}$$

All terms may now be written in terms of the zeroth-order term defined as,

$$\begin{aligned} u^{(0)}_{\mathbf{k}} &= R^{(0)}_{\mathbf{k}} f_{\mathbf{k}} \\ &= \big[\partial_t + \nu \mathrm{k}^2\big]^{-1} f_{\mathbf{k}}. \end{aligned} \tag{3.28}$$

Substituting (3.27) for the velocity-field terms in the triple-moment of (3.26) leaves an expansion that is of even-orders in lambda,

$$\begin{aligned}\mathcal{L}_0 C_{\mathbf{k}}\delta_{\mathbf{k}+\mathbf{k}'} &= \langle f_{\mathbf{k}} u_{\mathbf{k}'}\rangle\delta_{\mathbf{k}+\mathbf{k}'} + \\ &+ \lambda^2\Big(M_{\mathbf{k}}\langle u^{(0)}_{\mathbf{j}} u^{(0)}_{\mathbf{k}-\mathbf{j}} u^{(1)}_{\mathbf{k}'}\rangle + M_{\mathbf{k}}\langle u^{(0)}_{\mathbf{j}} u^{(1)}_{\mathbf{k}-\mathbf{j}} u^{(0)}_{\mathbf{k}'}\rangle \\ &+ M_{\mathbf{k}}\langle u^{(1)}_{\mathbf{j}} u^{(0)}_{\mathbf{k}-\mathbf{j}} u^{(0)}_{\mathbf{k}'}\rangle\Big) + \mathcal{O}(\lambda^4); \end{aligned} \tag{3.29}$$

as the quantities $u^{(0)} \propto f$ are Gaussian-random, and correlations containing odd-numbers of them vanish accordingly. The term $\langle f_{\mathbf{k}} u_{\mathbf{k}'}\rangle\delta_{\mathbf{k}+\mathbf{k}'}$ will be left unexpanded and will be hereafter denoted as $\mathcal{W}(\mathrm{k})$.

For convenience, the remainder of this analysis will not work beyond second order; henceforth, $\lambda = 1$. The correlation equation may be summarised as

$$\mathcal{L}_0 C_{\mathbf{k}}\delta_{\mathbf{k}+\mathbf{k}'} = \mathcal{W}(\mathrm{k},t) + \mathcal{T}(\mathrm{k}) \tag{3.30}$$

where

$$\mathcal{T}(\mathrm{k}) \equiv M_{\mathbf{k}}\langle u^{(0)}_{\mathbf{j}} u^{(0)}_{\mathbf{k}-\mathbf{j}} u^{(1)}_{\mathbf{k}'}\rangle + M_{\mathbf{k}}\langle u^{(0)}_{\mathbf{j}} u^{(1)}_{\mathbf{k}-\mathbf{j}} u^{(0)}_{\mathbf{k}'}\rangle + M_{\mathbf{k}}\langle u^{(1)}_{\mathbf{j}} u^{(0)}_{\mathbf{k}-\mathbf{j}} u^{(0)}_{\mathbf{k}'}\rangle \tag{3.31}$$

Note that $\mathcal{W}(\mathrm{k},t)$ and $\mathcal{T}(\mathrm{k})$ are defined such that $2\pi\mathrm{k}^2\mathcal{W}(\mathrm{k},t) = W(\mathrm{k})$ and $2\pi\mathrm{k}^2\mathcal{T}(\mathrm{k}) = T(\mathrm{k})$ where $W(\mathrm{k})$ is the input energy term, and $T(\mathrm{k})$ is the inertial energy transfer term. For decaying turbulence $\mathcal{W}(\mathrm{k},t) = 0$; this will be taken for the remainder of this derivation.

Letting $\mathcal{T}(\mathrm{k})$ be the sum of three similar terms and then expanding all terms of $u^{(1)}$ in the triple-moments leaves

$$\begin{aligned}\mathcal{T}(\mathrm{k}) &= \mathcal{T}_1(\mathbf{k}) + \mathcal{T}_2(\mathbf{k}) + \mathcal{T}_3(\mathbf{k}) \\ &= M_{\mathbf{k}} R^{(0)}_{\mathbf{k}'} M_{\mathbf{k}'}\langle u^{(0)}_{\mathbf{j}} u^{(0)}_{\mathbf{k}-\mathbf{j}} u^{(0)}_{\mathbf{a}} u^{(0)}_{\mathbf{k}'-\mathbf{a}}\rangle \\ &+ M_{\mathbf{k}} R^{(0)}_{\mathbf{k}-\mathbf{j}} M_{\mathbf{k}-\mathbf{j}}\langle u^{(0)}_{\mathbf{j}} u^{(0)}_{\mathbf{a}} u^{(0)}_{\mathbf{k}-\mathbf{j}-\mathbf{a}} u^{(0)}_{\mathbf{k}'}\rangle \\ &+ M_{\mathbf{k}} R^{(0)}_{\mathbf{j}} M_{\mathbf{j}}\langle u^{(0)}_{\mathbf{a}} u^{(0)}_{\mathbf{j}-\mathbf{a}} u^{(0)}_{\mathbf{k}-\mathbf{j}} u^{(0)}_{\mathbf{k}'}\rangle \end{aligned} \tag{3.32}$$

As the $u^{(0)}$'s are Gaussian, the 4^{th}-order moments can be factorised into combinations of 2^{nd}-order moments. Using this and the definition of the zeroth-order correlator, $C^{(0)}_{\mathbf{k}}\delta_{\mathbf{k}+\mathbf{k}'} \equiv \langle u^{(0)}_{\mathbf{k}} u^{(0)}_{\mathbf{k}'}\rangle$, $\mathcal{T}_1$ may be written as

$$\begin{aligned}\mathcal{T}_1(\mathbf{k}) &= M_{\mathbf{k}} R^{(0)}_{\mathbf{k}'} M_{\mathbf{k}'}\big(C^{(0)}_{\mathbf{j}}\delta_{\mathbf{j}+\mathbf{k}-\mathbf{j}} C^{(0)}_{\mathbf{a}}\delta_{\mathbf{a}+\mathbf{k}'-\mathbf{a}} \\ &\quad + C^{(0)}_{\mathbf{j}}\delta_{\mathbf{j}+\mathbf{a}} C^{(0)}_{\mathbf{k}-\mathbf{j}}\delta_{\mathbf{k}-\mathbf{j}+\mathbf{k}'-\mathbf{a}} + C^{(0)}_{\mathbf{k}-\mathbf{j}}\delta_{\mathbf{k}-\mathbf{j}+\mathbf{a}} C^{(0)}_{\mathbf{j}}\delta_{\mathbf{j}+\mathbf{k}'-\mathbf{a}}\big). \end{aligned} \tag{3.33}$$

The first of these terms vanishes (as $M_{\mathbf{k}}\delta_{\mathbf{k}} = M(0) = 0$), and integrating over the dummy variable $\mathbf{a}$ leaves

$$\mathcal{T}_1(\mathbf{k}) = M_{\mathbf{k}} R^{(0)}_{\mathbf{k}'} M_{\mathbf{k}'} \left(C^{(0)}_{\mathbf{j}} C^{(0)}_{\mathbf{k}-\mathbf{j}} \delta_{\mathbf{k}+\mathbf{k}'} + C^{(0)}_{\mathbf{k}-\mathbf{j}} C^{(0)}_{\mathbf{j}} \delta_{\mathbf{k}+\mathbf{k}'} \right) \tag{3.34}$$

Applying this procedure to $\mathcal{T}_2$ and $\mathcal{T}_3$ gives

$$\begin{aligned} \mathcal{T}(\mathrm{k}) &= 2M_{\mathbf{k}} R^{(0)}_{\mathbf{k}'} M_{\mathbf{k}'} C^{(0)}_{\mathbf{j}} C^{(0)}_{\mathbf{k}-\mathbf{j}} \delta_{\mathbf{k}+\mathbf{k}'} \\ &+ 2M_{\mathbf{k}} R^{(0)}_{\mathbf{k}-\mathbf{j}} M_{\mathbf{k}-\mathbf{j}} C^{(0)}_{\mathbf{j}} C^{(0)}_{\mathbf{k}} \delta_{\mathbf{k}+\mathbf{k}'} \\ &+ 2M_{\mathbf{k}} R^{(0)}_{\mathbf{j}} M_{\mathbf{j}} C^{(0)}_{\mathbf{k}-\mathbf{j}} C^{(0)}_{\mathbf{k}} \delta_{\mathbf{k}+\mathbf{k}'} \end{aligned} \tag{3.35}$$

and hence

$$\begin{aligned} \mathcal{L}_0 C_{\mathbf{k}} \delta_{\mathbf{k}+\mathbf{k}'} &= 2M_{\mathbf{k}} R^{(0)}_{\mathbf{k}'} M_{\mathbf{k}'} C^{(0)}_{\mathbf{j}} C^{(0)}_{\mathbf{k}-\mathbf{j}} \delta_{\mathbf{k}+\mathbf{k}'} + \\ &+ 4M_{\mathbf{k}} R^{(0)}_{\mathbf{j}} M_{\mathbf{j}} C^{(0)}_{\mathbf{k}-\mathbf{j}} C^{(0)}_{\mathbf{k}} \delta_{\mathbf{k}+\mathbf{k}'} \end{aligned} \tag{3.36}$$

Integrating both sides over $\mathbf{k}'$

$$\mathcal{L}_0 C_{\mathbf{k}} = -2M_{\mathbf{k}} R^{(0)}_{\mathbf{k}} M_{\mathbf{k}} C^{(0)}_{\mathbf{j}} C^{(0)}_{\mathbf{k}-\mathbf{j}} + 4M_{\mathbf{k}} R^{(0)}_{\mathbf{j}} M_{\mathbf{j}} C^{(0)}_{\mathbf{k}-\mathbf{j}} C^{(0)}_{\mathbf{k}} \tag{3.37}$$

For the following steps, it will be more sensible to return to the full notation.

$$\begin{aligned} \mathcal{L}_0 C_{\alpha\omega}(\mathbf{k}; t, t') &= -M_{\alpha\beta\gamma}(\mathbf{k}) \int_{-\infty}^{\infty} d^3\mathrm{j} \\ &\left(2M_{\omega'\delta\epsilon}(\mathbf{k}) \int_0^{t'} ds\, R^{(0)}_{\omega\omega'}(\mathbf{k};\, t', s) C^{(0)}_{\beta\delta}(\mathbf{j}; t, s) C^{(0)}_{\gamma\epsilon}(\mathbf{k}-\mathbf{j}; t, s) \right. \\ &- \left. 4M_{\beta'\delta\epsilon}(\mathbf{j}) \int_0^{t} ds\, R^{(0)}_{\beta\beta'}(\mathbf{j};\, t, s) C^{(0)}_{\delta\omega}(\mathbf{k}; s, t') C^{(0)}_{\gamma\epsilon}(\mathbf{k}-\mathbf{j}; t, s) \right) \end{aligned} \tag{3.38}$$

The renormalisation comes in and it is simply to replace zero-order terms by their exact terms,

$$C^{(0)}_{\alpha\alpha'}(\mathbf{k};t,t') \;\rightarrow\; C_{\alpha\alpha'}(\mathbf{k};t,t') \tag{3.39}$$
$$R^{(0)}_{\alpha\alpha'}(\mathbf{k};\,t,t') \;\rightarrow\; R_{\alpha\alpha'}(\mathbf{k};t,t'). \tag{3.40}$$

The justification for this comes from diagrammatic re-summation as in the Wyld formalism (see section 2.2) or from power-series regression, for details see Leslie [49].

All tensors are isotropic and may be written in terms of a scalar function and an isotropic tensor,

$$C_{\alpha\alpha'}(\mathbf{k};t,t') = P_{\alpha\alpha'}(\mathbf{k})C(\mathrm{k};\,t,t'). \tag{3.41}$$

Applying this to (3.38) with the renormalisation gives

$$\begin{aligned}
\mathcal{L}_0 C_{\alpha\omega}(\mathbf{k};t,t') \;=\; & -2\int_{-\infty}^{\infty} d^3\mathrm{j} M_{\alpha\beta\gamma}(\mathbf{k})M_{\omega'\delta\epsilon}(\mathbf{k})P_{\omega\omega'}(\mathbf{k})P_{\beta\delta}(\mathbf{j})P_{\gamma\epsilon}(\mathbf{k}-\mathbf{j}) \times \\
& \int_0^{t'} ds\, R(\mathrm{k};\,t',s)C(\mathrm{j};\,t,s)C(|\mathbf{k}-\mathbf{j}|;\,t,s) \\
+ \;& 4\int_{-\infty}^{\infty} d^3\mathrm{j} M_{\alpha\beta\gamma}(\mathbf{k})M_{\beta'\delta\epsilon}(\mathbf{j})P_{\beta\beta'}(\mathbf{j})P_{\delta\omega}(\mathbf{k})P_{\gamma\epsilon}(\mathbf{k}-\mathbf{j}) \times \\
& \int_0^{t} ds\, R(\mathrm{j};\,t,s)C(\mathrm{k};\,s,t')C(|\mathbf{k}-\mathbf{j}|;\,t,s)
\end{aligned} \tag{3.42}$$

Taking the trace over tensor indices α and ω, and then contracting the tensors leaves

$$\begin{aligned}
\mathcal{L}_0 C(\mathrm{k};\,t,t') \;=\; & \int_{-\infty}^{\infty} d^3\mathrm{j} L(\mathbf{k},\mathbf{j})\Big(\int_0^{t'} ds\, R(\mathrm{k};\,t',s)C(\mathrm{j};\,t,s)C(|\mathbf{k}-\mathbf{j}|;\,t,s) \\
- \;& \int_0^{t} ds\, R(\mathrm{j};\,t,s)C(\mathrm{k};\,s,t')C(|\mathbf{k}-\mathbf{j}|;\,t,s)\Big).
\end{aligned} \tag{3.43}$$

The geometric factor, $L(\mathbf{k},\mathbf{j})$, referred to as the "L-coefficient", takes a scalar form with $\mu = \mathbf{k}\cdot\mathbf{j}/(\mathrm{kj})$,

$$L(\mathrm{k},\mathrm{j},\mu) = \frac{\mathrm{kj}(1-\mu^2)\big(\mu(\mathrm{k}^2+\mathrm{j}^2) - \mathrm{kj}(1+2\mu^2)\big)}{\mathrm{k}^2+\mathrm{j}^2-2\mu\mathrm{kj}}. \tag{3.44}$$

The calculation leading to this equation can be found in Leslie [49] and McComb[35].

Projecting onto a spherical-polar coordinate system with some rearrangement leaves

$$\begin{aligned}\partial_t C(\mathrm{k};\, t,t') &= -\nu \mathrm{k}^2 C(\mathrm{k};\, t,t') + \int_0^\infty d\mathrm{j}\, 2\pi \mathrm{j}^2 \int_1^{-1} d\mu L(\mathrm{k},\mathrm{j},\mu) \times \\ &\Big(\int_0^{t'} ds\, R(\mathrm{k};\, t',s) C(\mathrm{j};\, t,s) C(|\mathbf{k}-\mathbf{j}|;\, t,s) \\ &- \int_0^{t} ds\, R(\mathrm{j};\, t,s) C(\mathrm{k};\, s,t') C(|\mathbf{k}-\mathbf{j}|;\, t,s) \Big). \end{aligned} \tag{3.45}$$

This is the equation for the two-time correlation function as given in (3.3)-(3.5). Note that the single-time correlator equation is not simply to substitute $t' = t$ in the above equation; it follows from defining two NSEs with $u_\alpha(\mathbf{k},t)$ and $u_{\alpha'}(\mathbf{k}',t)$, summing and then averaging; the general procedure from above then applies.

3.B Derivation of the Energy Spectrum

The total kinetic energy (density) is formally obtained from the volume integral of the L^2-norm of the velocity field,

$$E(t) \equiv \frac{1}{2} \int_{\mathbf{x}\in\mathcal{V}} d\mathbf{x} \left(\mathbf{u}(\mathbf{x},t) \cdot \mathbf{u}(\mathbf{x},t) \right), \tag{3.46}$$

and the dissipation rate can be similarly defined

$$\varepsilon(t) \equiv \int_{\mathbf{x}\in\mathcal{V}} d\mathbf{x} \left(\mathbf{u}(\mathbf{x},t) \cdot \left(\nabla^2 \mathbf{u}(\mathbf{x},t) \right) \right). \tag{3.47}$$

These quantities would also be suitably averaged, time- or ensemble-averaged, so as to give the statistical quantities that are of interest in turbulence studies.

The spectral energy density, or energy spectrum, can be obtained from the velocity correlation function using the above formula for the average total kinetic energy, noting first the average of (3.46),

$$\left\langle E(t) \right\rangle = \frac{1}{2} \int_{\mathbf{x}\in\mathcal{V}} d\mathbf{x} \left\langle \mathbf{u}(\mathbf{x},t) \cdot \mathbf{u}(\mathbf{x},t) \right\rangle. \tag{3.48}$$

As incompressible fluids generally consider a constant mass, the above quantities in the

above equation assume the roles of kinetic energy density and velocity density. Using $\langle \mathbf{u} \cdot \mathbf{u} \rangle = 3\langle u^2 \rangle$, one can write the total kinetic energy as

$$\begin{aligned} \langle E(t) \rangle &= \langle u_\alpha(\mathbf{x}, t) u_\alpha(\mathbf{x}, t) \rangle \\ &= C_{\alpha\alpha}(\mathbf{0}; t, t) \end{aligned} \tag{3.49}$$

The separation vector $\mathbf{r} = \mathbf{0}$ since the velocities are correlated for a single point in space. Taking the Fourier transform gives

$$\begin{aligned} \langle E(t) \rangle &= \int d\mathbf{k} \langle u_\alpha(\mathbf{k}, t) u_\alpha(-\mathbf{k}, t) \rangle e^{-\mathbf{k}\cdot\mathbf{0}} \\ &= \int d\mathbf{k}\, C_{\alpha\alpha}(\mathbf{k}; t, t), \end{aligned} \tag{3.50}$$

and as this is isotropic turbulence, the correlation tensor can be separated into a scalar function and the isotropic projection tensor

$$\begin{aligned} \langle E(t) \rangle &= \int d\mathbf{k}\, P_{\alpha\alpha}(\mathbf{k}) C(\mathrm{k}; t, t) \\ &= 2 \int d\mathbf{k}\, C(\mathrm{k}; t, t). \end{aligned} \tag{3.51}$$

The last line has used the trace of the projection tensor. As the integral is over 3-dimensional wave-vector space, a simplification can be made by projecting the system unto a spherical-polar coordinate system where the isotropy ensures angular independence and the only spatial argument is the wavenumber,

$$\langle E(t) \rangle = 2 \int_0^\infty d\mathrm{k}\, 2\pi \mathrm{k}^2 C(\mathrm{k}; t, t). \tag{3.52}$$

Using the kinetic energy as the integral over spectral space of the energy spectrum, the energy spectrum can be defined according to the correlation function

$$E(\mathrm{k}, t) \equiv 4\pi \mathrm{k}^2 C(\mathrm{k}; t, t). \tag{3.53}$$

Multiplying $4\pi\mathrm{k}^2$ to the evolution equation for the single-time correlation function, (3.3), results in the spectral energy balance equation,

$$\partial_t \underbrace{4\pi \mathrm{k}^2 C(\mathrm{k};t,t')}_{E(\mathrm{k},t)} = -\underbrace{8\pi\nu \mathrm{k}^4 C(\mathrm{k};t,t)}_{D(\mathrm{k},t)} + \underbrace{8\pi \mathrm{k}^2 P(\mathrm{k};t,t)}_{T(\mathrm{k},t)}. \tag{3.54}$$

3.C Constant Dissipation Rate in Forced Turbulence

Consider the turbulent energy evolution equation

$$\partial_t E(\mathrm{k},t) = T(\mathrm{k},t) - D(\mathrm{k},t) + 4\pi \mathrm{k}^2 \,\mathrm{tr}\Big\{\langle f_\alpha(-\mathbf{k},t) u_\beta(\mathbf{k},t)\rangle\Big\} \tag{3.55}$$

where

$$f_\alpha(-\mathbf{k},t) = \Delta E_\mathrm{f} \frac{u_\alpha(-|\mathbf{k}| = \mathrm{k_f},t)}{2E_\mathrm{f}(t)}. \tag{3.56}$$

The wave-vector argument in the velocity specifies that the forcing is implemented if and only if $|\mathbf{k}| = \mathrm{k_f}$. Taking the trace and replacing the two-velocity correlation with a correlator gives

$$\partial_t E(\mathrm{k},t) = T(\mathrm{k},t) - D(\mathrm{k},t) + 4\pi \mathrm{k}^2 \Delta E_\mathrm{f} \frac{2C(\mathrm{k_f},t,t)}{2E_\mathrm{f}(t)}. \tag{3.57}$$

The condition that sets $|\mathbf{k}| = \mathrm{k_f}$ implies that $\mathrm{k}^2 = \mathrm{k_f^2}$, hence

$$\partial_t E(\mathrm{k},t) = T(\mathrm{k},t) - D(\mathrm{k},t) + \Delta E_\mathrm{f} \frac{E(\mathrm{k_f},t)}{E_\mathrm{f}(t)}. \tag{3.58}$$

Integrating over the entire wavenumber range results in

$$\partial_t E(t) = -\varepsilon(t) + \Delta E_\mathrm{f} \tag{3.59}$$

since by definition

$$\int_0^\infty d\mathrm{k}\, E(\mathrm{k_f},t) = \Delta E_\mathrm{f}(t). \tag{3.60}$$

Upon reaching a steady-state, the above equation becomes time-independent leaving the result that the dissipation rate is set by the rate of energy injection ΔE_f

$$\varepsilon(t) = \Delta E_\mathrm{f}. \tag{3.61}$$

Chapter 4

Further Investigation of Decaying and Forced Turbulence Using the LET

Building on the results of the LET2008 in its comparisons to earlier versions and DNS, it can be pushed further towards higher Reynolds numbers. Extensions to higher Reynolds numbers for both freely-decaying and forced turbulence are presented in this chapter, acquiring Taylor-Reynolds numbers of $R_\lambda(0) \sim 330$ ($R_\lambda(t_\mathrm{e}) \sim 60$) for decaying turbulence and $R_\lambda(t_\mathrm{e}) \sim 340$ for forced turbulence. The energy spectra for all computations were checked for their compatibility with the Kolmogorov inertial range and give mixed results. The free-decay LET shows an inertial range without Kolmogorov behaviour, however the forced computations show a definite Kolmogorov inertial range.

4.1 Decaying Turbulence

The goal of closure-based computations is to reproduce the observed, and in some cases the predicted, statistical behaviour of turbulence without the cost of solving the NSE explicitly. One such behaviour to reproduce is the Kolmogorov inertial range. Doing so typically requires a sufficiently small viscosity, and because of this a larger wavenumber range is needed. A common criterion for the wavenumber range is to ensure that the dissipation wavenumber, $\mathrm{k}_D(t) \equiv (\varepsilon(t)/\nu^3)^{1/4}$, is contained within the wavenumber range, hence the largest wavenumber set in the computation, k_top must be such that

$$\frac{\mathrm{k}_\mathrm{top}}{\mathrm{k}_D(t)} > 1 \quad \forall\, t. \tag{4.1}$$

The reason for this criterion is that the transfer of energy from low- to high-wavenumbers will move energy to as many wavenumbers as is possible where at the upper-limit of this range, they will be quickly dissipated. A wavenumber range that is truncated does not allow this to occur and energy will begin to grow in this upper end of the wavenumber range; this is more unphysical than the isotropic turbulence being modelled.

The time dependence in (4.1) has been made explicit as this value will change with time, and in some cases depending on the shape of the initial spectrum, the dissipation rate can become much larger than its initial value. As only the initial values are known *a priori*, this can make adequate spectral ranges difficult to predict and over-estimating the range can see computations becoming quickly intractable.

The need for larger spectral ranges can be somewhat accommodated in the current LET2008-code. However, it exceeds the ability of the current DNS used in this research as the grids are only of size 128^3. The results shown here require proper testing against a larger DNS grid to ensure reliability of the code for large Reynolds numbers. For the purposes of this research, the results made for high Reynolds numbers using the LET model will be given here and a follow-up study can test against them.

In the following pages, results for Spectra V and VI are given, each with $\nu = .001$ and $\nu = .0005$. The integral parameters are also given in the same manner as in previous figures.

4.1.1 Spectral Quantities

In this section the spectral quantities associated with both Spectra V and VI are given. The energy spectra are presented, in both the normalised and "compensated" forms. The results show evidence of an inertial range. Following the energy spectra, the dissipation and transfer spectra are presented. These give a direct view of the dynamics of the system.

The spectral quantities in freely-decaying turbulence are evolving in time and are presented to reflect this. Plots of these curves are given with times, normalised by the initial eddy-turnover time, $L(0)/U(0)$. The plots of the energy spectra are meant to demonstrate the existence of an inertial range, and the times chosen to show this correspond to the final eddy-turnovers. The figures of the dissipation and transfer spectra are presented differently showing evolution through the whole computation.

Energy Spectra

The energy spectra are plotted against wavenumbers normalised with respect to k_D, and presented in log-log scaling; this is particularly useful in presenting a Kolmogorov

inertial range where $E(\mathrm{k}) \sim \mathrm{k}^{-5/3}$ since log-log scaling shows power-law functions to be linear. Plots of this sort are seen in figs. 4.1 and 4.2.

Included in these plots are the energy spectra for $\nu = .002$. Quinn [101] produced similar results which compared well against DNS using the same parameters for spectrum V. Using these results offers consistency checks for the current computations. Additionally, they can help to identify a growing inertial range as the Reynolds number increases. There is a region of near constant slope that occurs in all three plots, growing wider as the viscosity is decreased; it is suspected to be the inertial range as given by the LET. The line $y \propto -(5/3)x$ is also included for comparison of the inertial range. One can argue that these plots do not display Kolmogorov behaviour. These results were also checked for the Kraichnan inertial range of $E(\mathrm{k}) \sim \mathrm{k}^{-3/2}$, associated with his Eulerian-DIA [49, 52] but it was found (results not included here) that the results were not consistent with this either.

A more revealing presentation is to use the so-called compensated energy spectrum, where the energy is specifically normalised in such a way to give a flat region for the inertial range,

$$E(\mathrm{k}, t) \quad \rightarrow \quad E(\mathrm{k}, t)\varepsilon(t)^{-2/3}k^{5/3}. \tag{4.2}$$

This is employed in figs. 4.3 and 4.4. It can be seen that the inertial range is a function of the wavenumber and shows a positive slope where a Kolmogorov inertial range would be constant. This misplaced inertial range seems to indicate an incompatibility of the LET with Kolmogorov's inertial range.

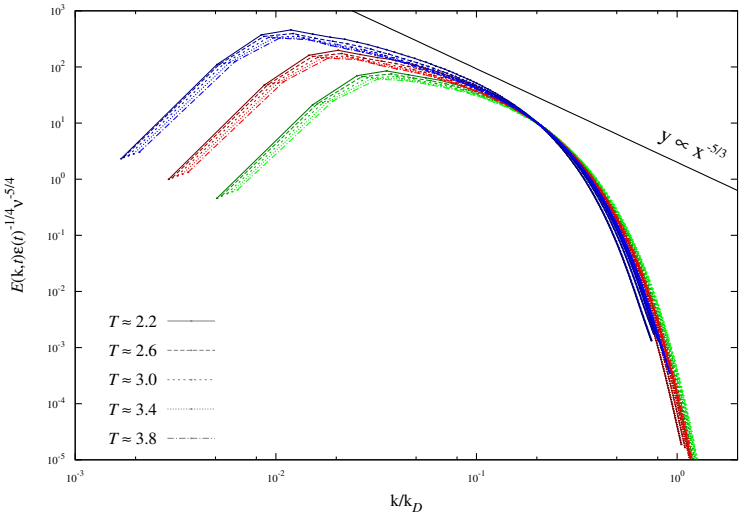

Figure 4.1: A log-log comparison of the normalised spectral energy curves for Spectrum V using viscosities $\nu = 0.0005, 0.001, 0.002$ (blue, red, green). The maximum wavenumbers for these computations are k_{top} = 220, 180, 150, respectively.

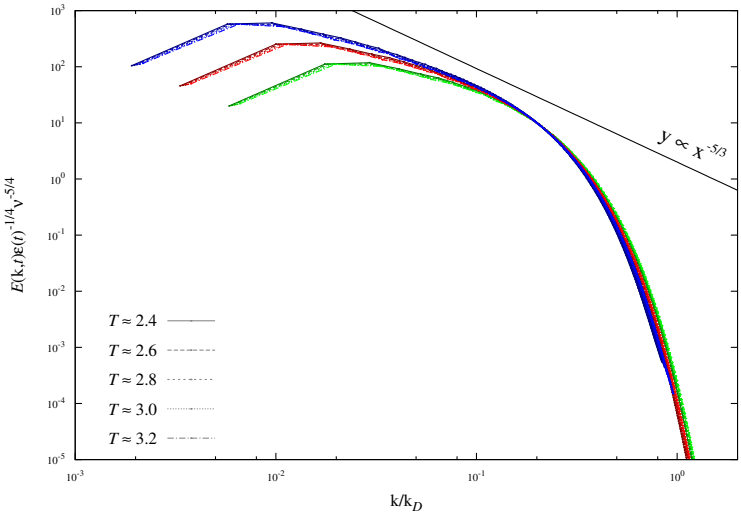

Figure 4.2: A log-log comparison of the normalised spectral energy curves for Spectrum VI using viscosities $\nu = 0.0005, 0.001, 0.002$ (blue, red, green). The maximum wavenumbers for these computations are k_{top} = 340, 200, 150, respectively.

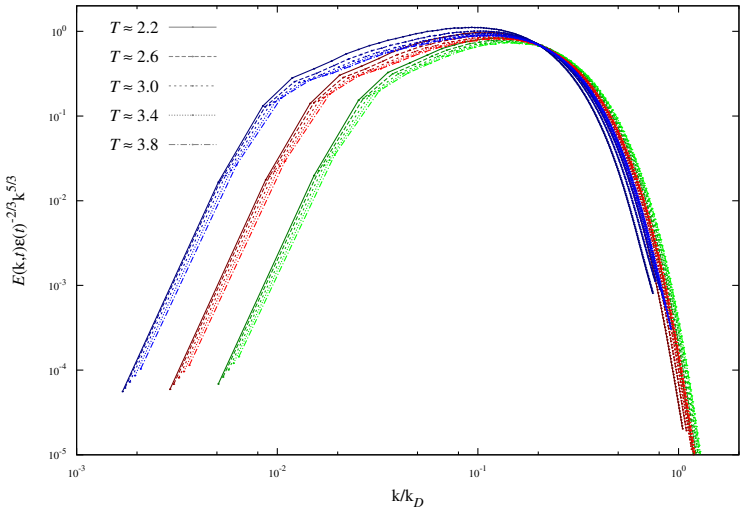

Figure 4.3: A log-log comparison of the compensated spectral energy curves for Spectrum V using viscosities $\nu = 0.0005, 0.001, 0.002$ (blue, red, green).

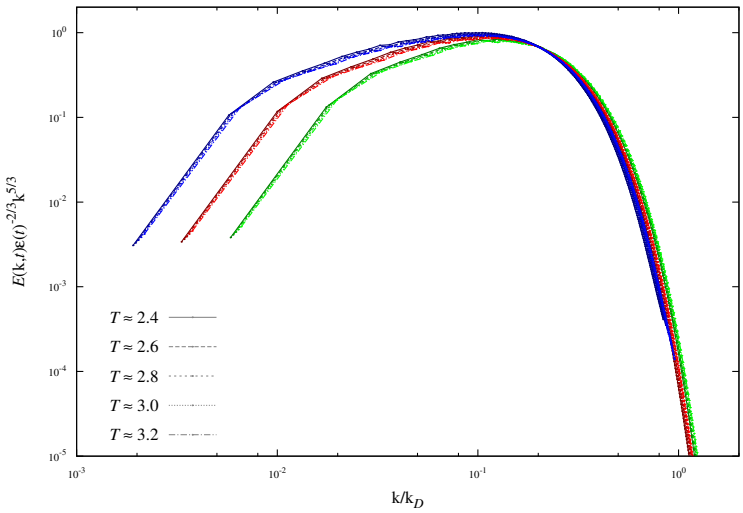

Figure 4.4: A log-log comparison of the compensated spectral energy curves for Spectrum VI using viscosities $\nu = 0.0005, 0.001, 0.002$ (blue, red, green).

Dissipation Spectra

Looking at the dissipation spectra provides some insight into the dynamic mechanisms affecting the energy spectrum. In figs. 4.5-4.8, the dissipation spectra are given. The figures display some common behaviours of the dissipation spectrum as it evolves through the turbulent processes. In each figure, one can see that a relatively narrow initial band of wavenumbers contains all of the energy. As time progresses, the peak of this band decreases and moves to larger wavenumbers while the band itself expands in width covering a larger region of wavenumber space. As the inertial mechanisms are instantiated, energy is transferred from low- to high-k in the energy cascade; thus, more energy reaches the dissipation scales and the dissipation spectrum grows.

As the the energy spreads, the more and more is placed into wavenumbers where the viscous forces are relatively strong and remove energy from the system. The dissipation rate reaches a peak where the rate of inertial transfer moves the most energy it is able to; then the spectrum reaches a what can be referred to as a decay-state where it follows a self-preserving decay as given in the early arguments of von Kármán [120]. The figures show that the LET demonstrates this quite well and regions of self-preserving decay can be identified in each plot.

Transfer Spectra

The transfer spectra likewise gives a measure of the dynamics in a turbulent system. The transfer spectra, as noted earlier, also provide a useful link for numerical comparisons in that it is directly related to one of the two principal quantities computed in the LET2008. Figures 4.9-4.12 show the transfer spectra associated with spectra V and VI.

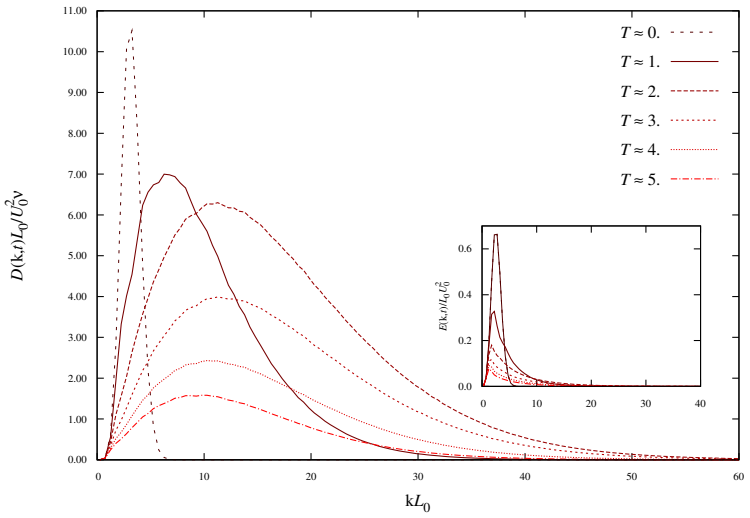

Figure 4.5: Plots of the dissipation spectrum for Spectrum V, $\nu = .001$, given in increments of the initial eddy-turnover time, T. The inset shows the normalised energy spectrum.

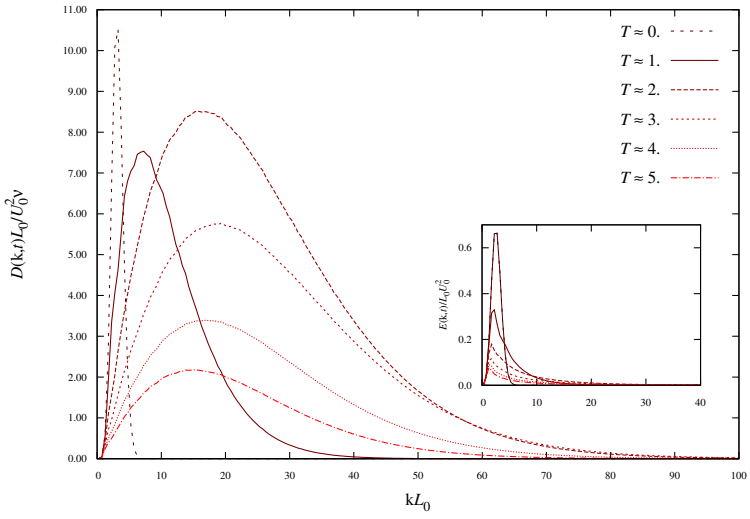

Figure 4.6: Plots of the dissipation spectrum for Spectrum V, $\nu = .0005$, given in increments of the initial eddy-turnover time, T. The inset shows the normalised energy spectrum.

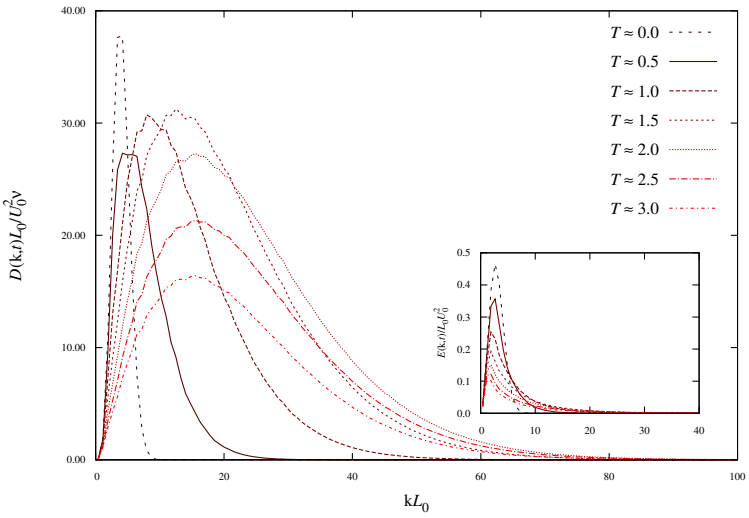

Figure 4.7: Plots of the dissipation spectrum for Spectrum VI, $\nu = .001$, given in increments of the initial eddy-turnover time, T. The inset shows the normalised energy spectrum.

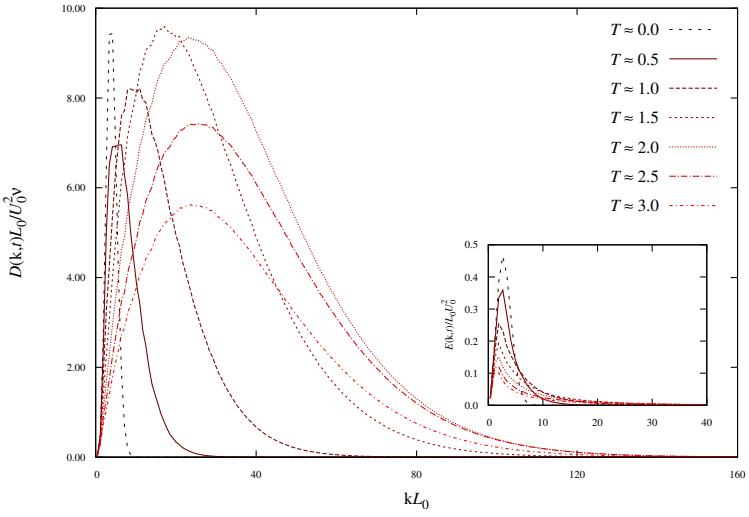

Figure 4.8: Plots of the dissipation spectrum for Spectrum VI, $\nu = .0005$, given in increments of the initial eddy-turnover time, T. The inset shows the normalised energy spectrum.

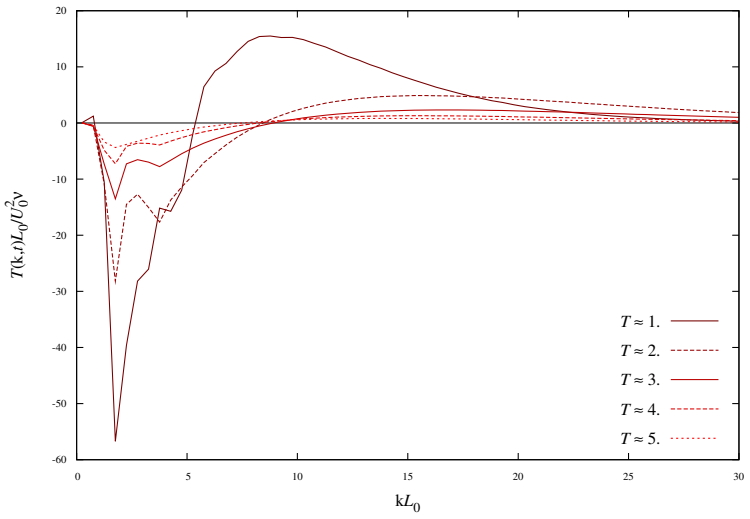

Figure 4.9: Plots of the transfer spectrum for Spectrum V, $\nu = .001$, given in increments of the initial eddy-turnover time, T.

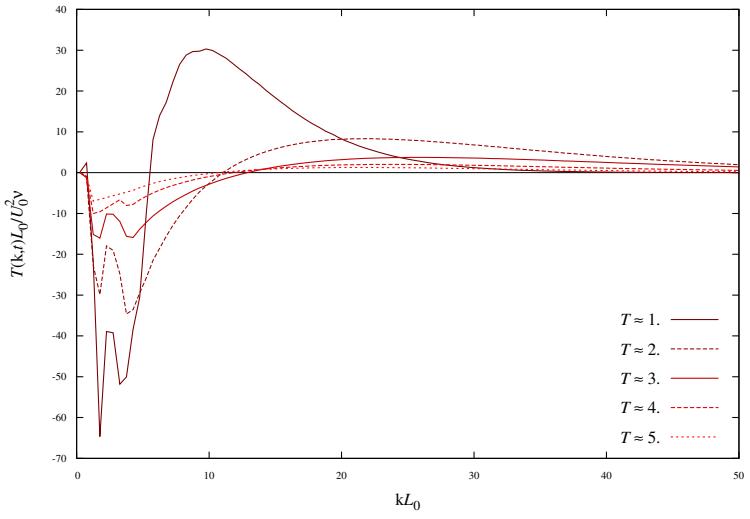

Figure 4.10: Plots of the transfer spectrum for Spectrum V, $\nu = .0005$, given in increments of the initial eddy-turnover time, T.

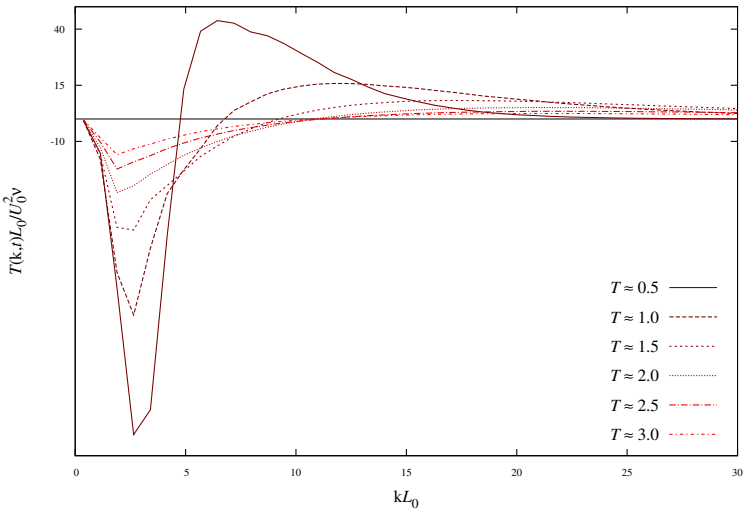

Figure 4.11: Plots of the transfer spectrum for Spectrum VI, $\nu = .001$, given in increments of the initial eddy-turnover time, T.

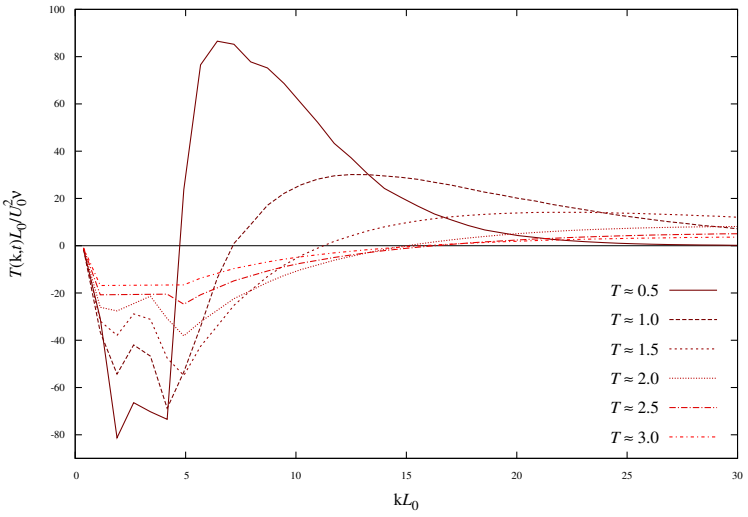

Figure 4.12: Plots of the transfer spectrum for Spectrum VI, $\nu = .0005$, given in increments of the initial eddy-turnover time, T.

4.1.2 Integral Parameters

The integral parameters for the decaying computations of spectra V and VI are given here. In the absence of comparable earlier LET computations or similar DNS computations, the following parameters are presented against computations of lower Reynolds numbers. Showing self-consistency of these parameters with respect to their lower-Re and tested counterparts, gives a qualitative measure of how the high-R computations are performing. This by no means validates these results, though it does give some reassurance that there are no drastic changes in the these parameter-curves as viscosity is decreased.

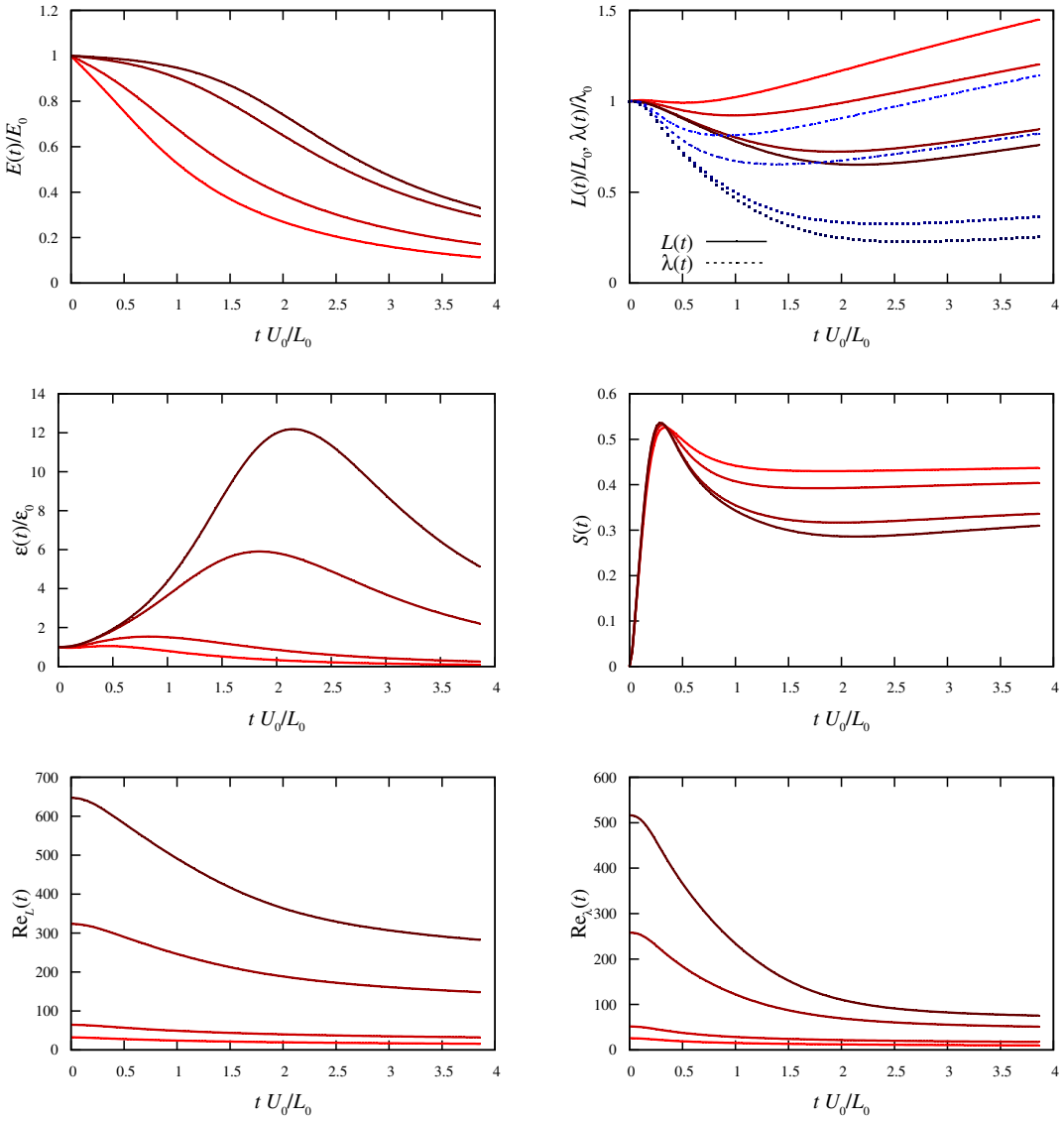

Figure 4.13: The integral parameters for Spectrum V against normalised time. Note the line-colour darkens as the viscosity decreases: ν = .01, .005, .001, .0005. The maximum wavenumbers for these computations are k_{top} = 50, 50, 180, 220, respectively.

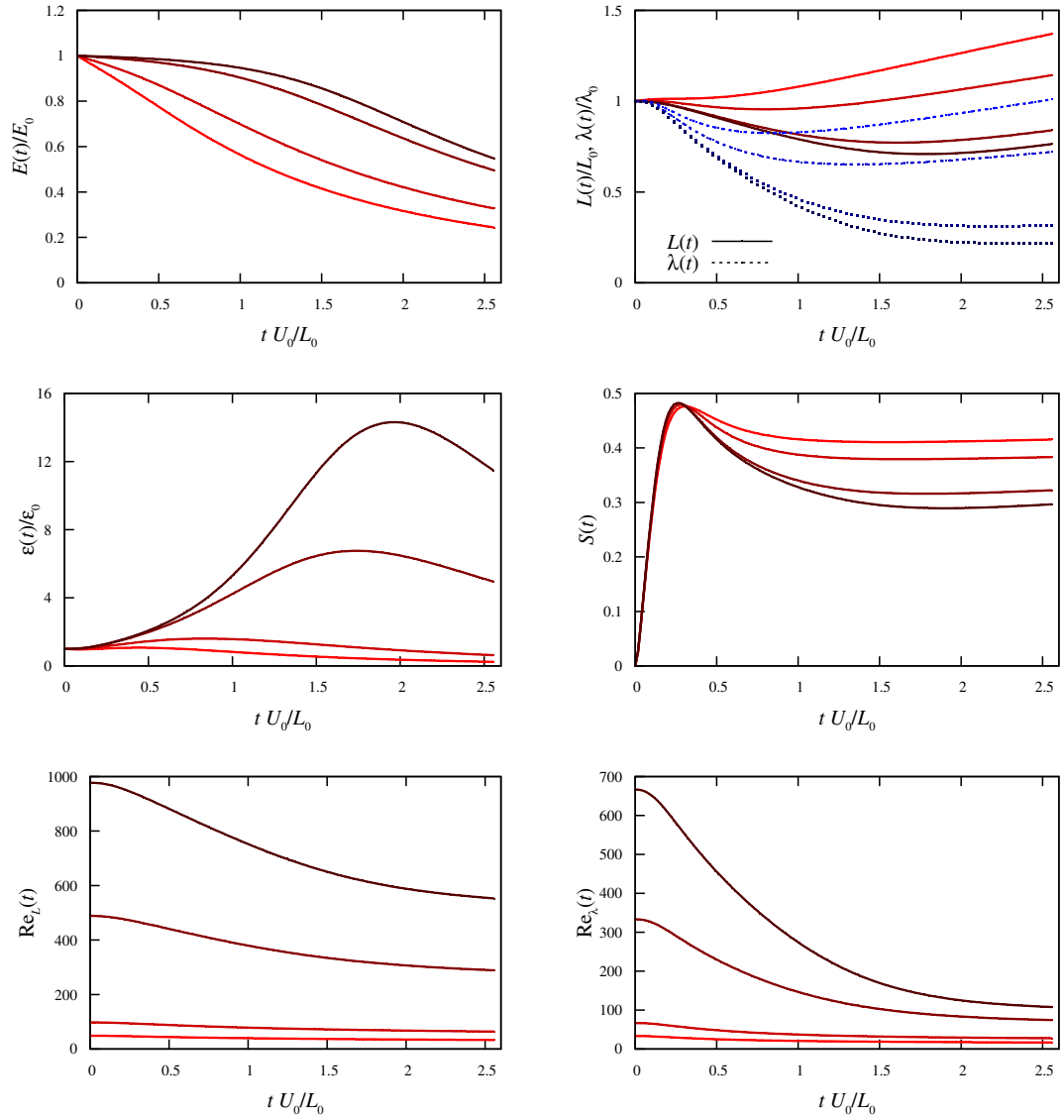

Figure 4.14: The integral parameters for Spectrum VI against normalised time. Note the line-colour darkens as the viscosity decreases: $\nu = .01, .005, .001, .0005$. The maximum wavenumbers for these computations are $k_{top} = 50, 60, 200, 360$, respectively.

4.2 Forced Turbulence

Without previously tested results to compare against, extending the the low-R results of LET2000 to higher Reynolds numbers requires some measure by which to check against to ensure the calculations remain useful. There are some qualitative checks which can be made, though none can be considered with the same weight of a DNS.

The first of which is to ensure that the dissipation rate remains constant when compared to previous or smaller-R_λ. This check is built into the computation and while it does not offer a physical measure it is reassuring that an initial condition will evolve to maintain this constraint.

The energy spectrum can be expected to roughly retain its shape, particularly in the low- and high-k regions, and the inertial range, if present, should be wider in those computations with larger Reynolds numbers. This can be best seen when using the compensated energy spectrum $E(\mathrm{k},t)\varepsilon^{-2/3}\mathrm{k}^{5/3}$. As seen in the previous section, the compensated energy spectrum will reach a plateau in the inertial range and have a maximum value of the Kolmogorov constant, which has a short range of 1.5-2.5 [121, 122]. The plateau also shows a broadening of the energy in the inertial range, which is expected according to the Kolmogorov theory [24].

A final and related check, is to examine the flux. When normalised by this dissipation rate, will be nearly unity [24, 35]. It will also show a slight plateau at this maximum, broadening in wavenumber space when viscosity is decreased.

Examining these properties of the current computation does not ensure correct behaviour of the numerical model nor the theory it represents, and it must be stressed that these results require further analysis against a more reliable measure provided by DNS or even experiment. It does give a qualitative assessment of the theory and allows further investigation to be more refined.

The following figures show plots of the energy and flux spectra for forced-turbulence computations according to the LET. The initial spectrum for both is Spectrum I. The viscosities used in the following results are $\nu = .002, .001$; these give evolved Taylor-Reynolds numbers of $R_\lambda \sim 235, 336$, respectively.

4.2.1 Spectral Quantities

The time dependence of forced turbulence results does not share the same importance as the case of free-decay, and so only the spectral quantities found in the steady-state are needed. In this section, the energy and flux spectra are presented for viscosities $\nu = .002,\ .001$. The quantities have been chosen to these forced computations as they contain more information about the system (see above) than can be obtained from the dissipation and transfer spectra, which were used for decaying turbulence.

Energy Spectra

As will be seen in the figure below, the energy spectra for these computations display a very definite inertial range that is compatible with the Kolmogorov theory. To illustrate this, the plots of the energy spectra are presented in the compensated energy spectrum format. As the energy spectrum is believed to follow the form $E(\mathrm{k}) = \alpha_{\mathrm{K}}\varepsilon^{2/3}\mathrm{k}^{-5/3}$ in this region, plotting with the compensated normalisation gives a value for the Kolmogorov constant α_{K}; it can be seen that $\alpha_{\mathrm{K}} \approx 2.3$ for $\nu = .002$ and $\alpha_{\mathrm{K}} \approx 2.$ for $\nu = .001$. These values are consistent with the range of values determined given above.

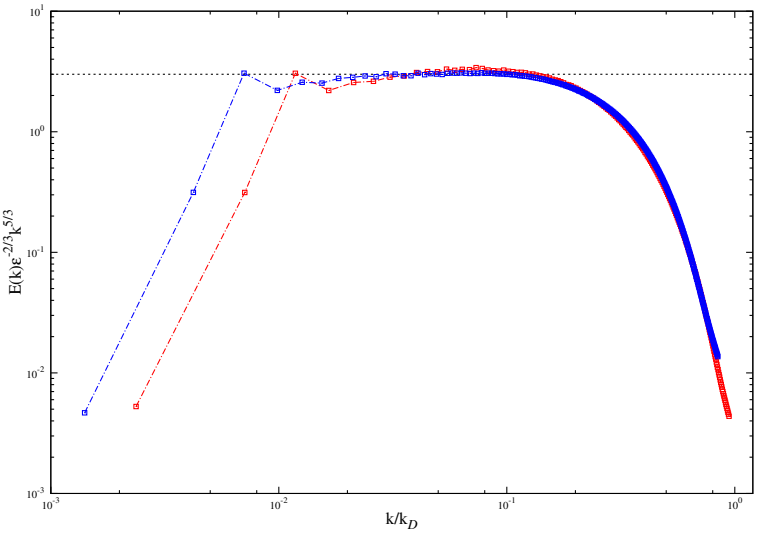

Figure 4.15: A comparison of compensated energy spectra for forced computations using viscosity $\nu = .002$ (red) and $\nu = .001$ (blue) under LET2008. The maximum wavenumbers for these computations are $\mathrm{k}_{\mathrm{top}} = 200$, 300, respectively.

Flux Spectra

The flux spectra for these computations are shown in fig. 4.16. The flux, $\Pi(\mathrm{k})$, is normalised by the dissipation rate, ε. Both computations show a plateau at unity, and the region of the plateau broadens when the viscosity is decreased from $\nu = .002$ to $\nu = .001$. One can see by inspection that the wavenumber region of this plateau corresponds to the same region given in the figure of the energy spectra in fig. 4.15.

The behaviour of the flux in the inertial range seems to satisfy the expected phenomenology associated with forced turbulence. It is difficult to detect from the figures, but there is a small part of the inertial range of the $\nu = .001$ result that is greater than unity. More than numerical errors, it is suspected that this is due to

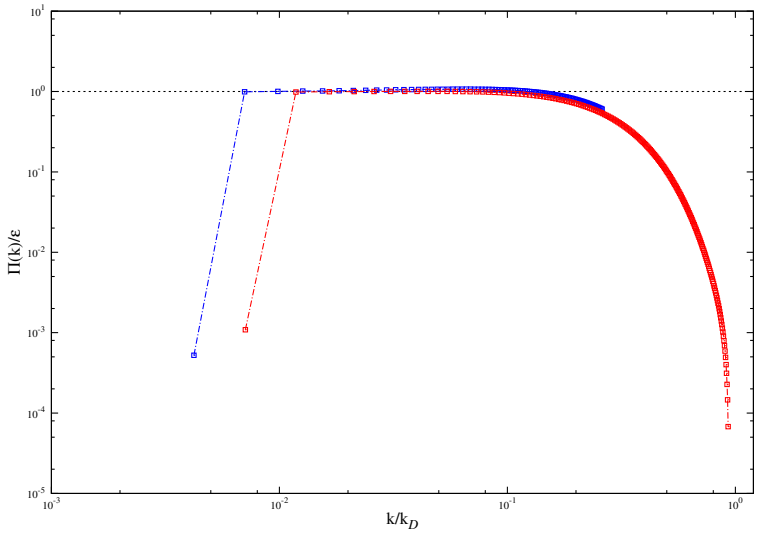

Figure 4.16: A comparison of flux spectra for forced computations using viscosity $\nu = .002$ (red) and $\nu = .001$ (blue) under LET2008. Normalising by the dissipation rate, ε, the flux should equal unity in the inertial range.

an insufficiently large wavenumber range. Noting the maximum wavenumber for this computation $\mathrm{k_{top}} = 150$, and using the fact that the dissipation rate is unity when evolved, the Kolmogorov criterion is not met,

$$\frac{\mathrm{k_{top}}}{\mathrm{k}_D} = 150\nu^{3/4} \approx .84 \tag{4.3}$$

At the time of writing, calculations with an increased maximum wavenumber are too large in terms of their memory requirements for the computers being used.

4.2.2 Integral Parameters

As with the computations for free-decay, the integral parameters are an important measure by which to examine the characteristic properties of a turbulent system. These are given in the figure below and show the computations' behaviour is consistent, and not behaving erratically. Note that the normalised dissipation rate $\varepsilon/\varepsilon_0 \sim 6$ for $\nu = .002$ and $\varepsilon/\varepsilon_0 \sim 12$ for $\nu = .001$. Using the fact that the initial energy spectrum is the same for both computations and the viscosities are different by a factor of 2, it can be shown that the final dissipation rates are equal.

Let quantities for $\nu = .002$ be associated with a subscript A, and those for $\nu = .001$ use B. From the figure, the normalised dissipation rates are different by a factor of 2

and since $\varepsilon(t) = 1$ is set by the forcing,

$$2\left(\int 2\nu_A \mathrm{k}^2 E_A(\mathrm{k},0)d\mathrm{k}\right)^{-1} = \left(\int 2\nu_B \mathrm{k}^2 E_B(\mathrm{k},0)d\mathrm{k}\right)^{-1}. \tag{4.4}$$

Since $E_A(\mathrm{k},0) = E_B(\mathrm{k},0)$ and $E(\mathrm{k},0) = 0$ for high values of k, the integrals can be factored away after some slight rearrangements leaving

$$2\nu_B = \nu_A. \tag{4.5}$$

This demonstrates that the dissipation rates of both computations are fixed to the same value ($\varepsilon = 1$) by the forcing, as they should be. This explains the different values of the dissipation rates in the figure and shows that the computation is consistent in maintaining the forcing.

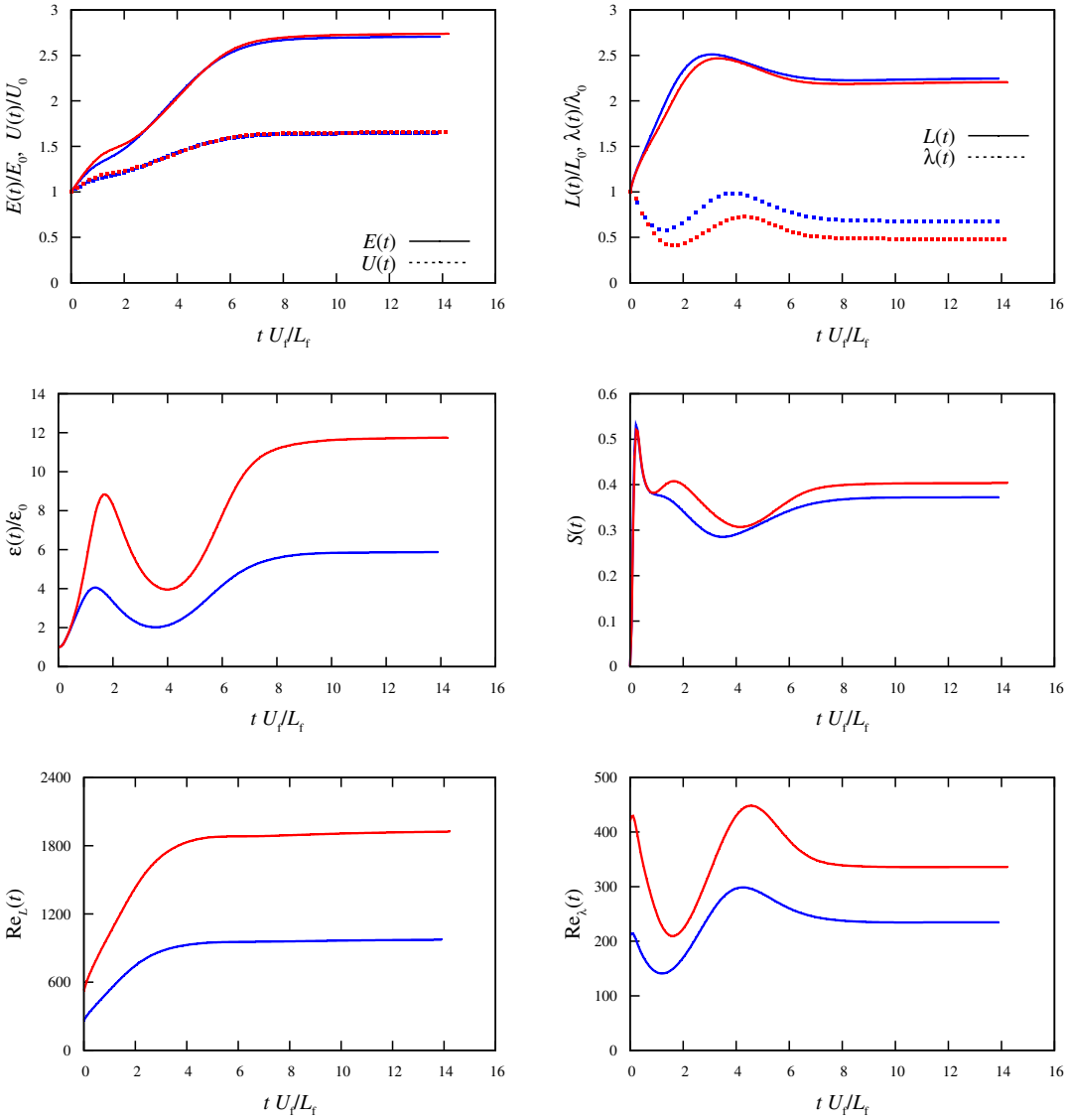

Figure 4.17: A comparison of integral parameters from the forced-LET2008 computations for $\nu = .002$ (blue) and $\nu = 0.001$, using initial Spectrum I.

4.3 Discussion

As the comparisons against previous codes have been successful, the original computations were extended for produce the higher Reynolds number results present here. This was done for both cases of free-decay and forced turbulence.

4.3.1 Conclusions

The results of the LET2008 computations for decaying turbulence show consistent behaviour of the code when extensions are made to higher Reynolds numbers. The initial Taylor-Reynolds numbers achieved for these computations are $R_\lambda \sim 260,520$ for Spectrum V and $R_\lambda \sim 330,660$ for Spectrum VI, using the viscosity values of .001, .0005, respectively; using the time of the maximum dissipation rate as an evolved time, these computations have Taylor-Reynolds numbers of $R_\lambda \sim 90,110$ for Spectrum V and $R_\lambda \sim 100,150$ for Spectrum VI. These results represent the highest values achieved for the LET using decaying turbulence. Previous studies show higher values of $R_\lambda \sim 1000$ but these computations were not run long enough (0.3 eddy turnover times) [35, 98, 100].

The results from the forced computations also achieved higher Taylor-Reynolds numbers for the LET,with the highest being $R_\lambda \sim 340$ for $\nu = .0005$. Note that the results for $\nu = .001$ produce a similar Taylor-Reynolds number to that found in Quinn, $R_\lambda \sim 230$; however, the results found there do not demonstrate a stationary final state as clearly as that presented here.

With regard to ability to show an inertial range, the current results present an ambiguous picture. On the one hand, the results for the decaying turbulence show an inertial range whose slope is greater than the Kolmogorov -5/3; yet the results for the forced computations show a pronounced inertial range giving a value for the Kolmogorov constant as ~ 2. This value is consistent with results found in the literature.

4.3.2 Future Work

Such equivocal results require further testing to determine whether the LET is an accurate portrayal of the current understanding of turbulence phenomenology. Having an analytic theory that can summarise the complexities of turbulent motion and give reasonable, reliable quantitative predictions would prove a great benefit to the understanding of turbulence by providing a useful shortcut that can correctly reproduce statistical turbulent behaviour. Comparisons against DNS data would allow such an assessment to be made.

Chapter 5

Evolved Time in Freely-Decaying Turbulence

The study of freely-decaying turbulence allows an insight into the nonlinear interaction that is unbiased by a mechanism of external forcing. However, when obtaining single values for time-dependent parameters that are meant to characterise the system there is some ambiguity as to when such parameters can be measured and give reliable data indicative of decaying turbulence. This chapter explores criteria for an appropriate time to measure time-dependent quantities for decaying turbulence, and determines a time based on the physical features of the system. This would allow meaningful comparisons to be made among measurements of freely-decaying turbulent systems.

5.1 Introduction

The following chapter investigates the normalised dissipation rate of forced and decaying homogeneous isotropic turbulence using the LET computational model. This requires a single measurement from several computations of different viscosities. Each measurement needs an evolved time at which the measurement can be made that indicates a fully turbulent system. In forced turbulence, it is not difficult to determine an evolved time as it naturally occurs when all quantities have reached a steady-state. For freely decaying turbulence however, it is a problem to determine such a time. To elucidate the need for an evolved time for decaying homogeneous isotropic turbulence, the following example is given.

5.1.1 Example: Measurement Time

In the study of dissipation, the subject of the next chapter, there are two quantities of interest,

$$C_\varepsilon \equiv \frac{\varepsilon L}{U^3}, \qquad C_\Pi \equiv \frac{\Pi_{\max} L}{U^3},$$

the normalised dissipation rate and maximum flux, respectively. Further explanation about these quantities can be found in the following chapter as the issue here is to determine when these values can be measured in freely-decaying turbulence. The figure below, fig. 5.1, shows plots of these quantities against the Taylor-Reynolds number, R_λ.

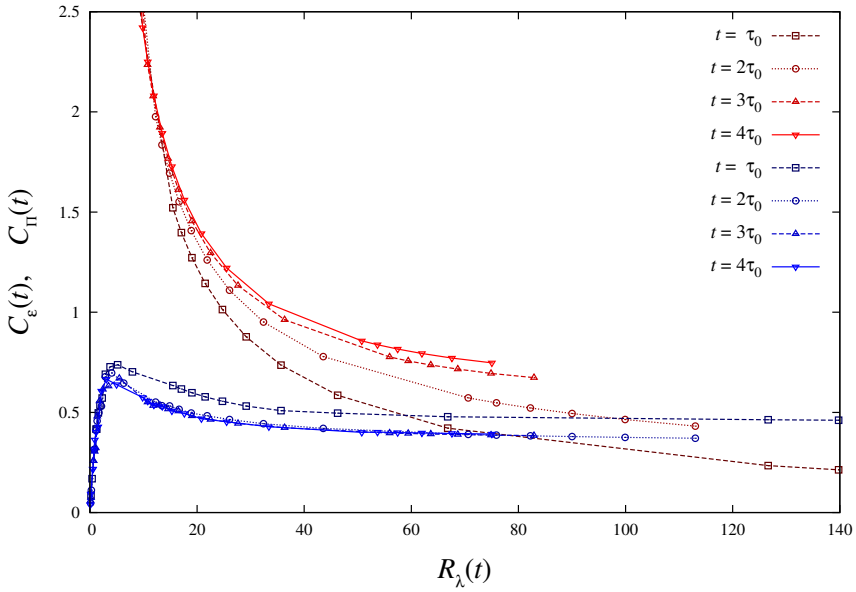

Figure 5.1: The normalised dissipation rate against Taylor-Reynolds number for decaying homogeneous turbulence. Evolved times are chosen using integer number of initial eddy turnover times, $\tau_0 = L(0)/U(0)$.

In the figure, C_ε and C_Π are given for various evolved times based on the characteristic time of the initial energy, $\tau_0 = L(0)/U(0)$. For decreasing $R_\lambda \lesssim 5$, the values of C_ε and C_Π tend to converge. With the exception of the earliest measurement at time $t = \tau_0$, the curves for C_Π are fairly well converged irrespective of the Reynolds number. However, as R_λ increases, and presumably C_ε asymptotes, the curves take different values within a range 0.2-1. Estimates for the dissipation rate give $C_\varepsilon \sim 0.5$ for forced turbulence [123–125], while for decaying turbulence this is found to be somewhat higher [125–127], $C_\varepsilon \sim .6 - 1$. No value for C_Π is given as this quantity has not been previously measured in this context. However, as will be seen in the next chapter, this value should asymptote like C_ε in the case for forced turbulence, $C_\Pi \sim 0.5$. The wide

spread given here for C_ε demonstrates the effect of the measurement time on the values obtained for C_ε in decaying turbulence.

For the measurement taken at $t = \tau_0$, the asymptotic value of the dissipation rate is rather low. This value is not entirely correct in that the turbulence is not developed so early in the computation. The computation must run for a certain amount of time before the system takes on a solution of the LET equations. Another problem is that the curves for the dissipation and flux intersect at this measurement time; it will be shown in the next chapter that this cannot happen in developed decaying turbulence. If the measurement is too late, then the system is no longer in a turbulent state since all such motion would be damped out by the viscosity.

Without looking at other parameters, there is no way of knowing how these chosen measurement times reflect the turbulence of the system. It would be better to have evolved times that are based on the intrinsic properties of a turbulent system.

5.1.2 Evolved Turbulence in Decaying Turbulence

A noteworthy paper looking into the normalised dissipation rate is given by Sreenivasan [126] who collected many results from contemporaries in the period 1942 to 1980. The results he presented were obtained from various wind-tunnel experiments looking into grid turbulence. The standard for evolved turbulence in the free-decay was the so-called "initial decay". There is little indication as to where this originated but a reasonable source to consult is Batchelor [25], who defines the initial period of decay rather loosely. The result presented therein is given in terms of the spatial coordinates used to measure the turbulent flow which can be reformulated for the time variable,

$$E \propto (x - x_0)^{-1} \xrightarrow[x=Ut]{} E \propto t^{-1}, \tag{5.1}$$

where x is the downstream coordinate in the direction of the mean velocity U. To contrast, the *final* period of decay is that which occurs at an adequately low Reynolds number so that the nonlinear term can be neglected, giving an energy spectrum whose decay is exponential,

$$E(\mathrm{k}, t) = E(\mathrm{k}, t_0) e^{-2\nu \mathrm{k}^2 (t - t_0)}. \tag{5.2}$$

Batchelor showed that this can be transformed back to real-space to give $E \propto t^{-5/2}$, though it should be noted that this depends on the shape of the energy spectrum at t_0; for example, using the initial spectra of Chapter 4 where $E(\mathrm{k}, t_0 = 0) \propto \mathrm{k}^n \exp(-c_3 \mathrm{k}^{c_4 = 2})$ would give a power-law decay of $E(t) \sim t^{-\frac{1}{2}(n+1)}$.

A more recent exposition of the stages of turbulent evolution involving freely-

decaying turbulence is given by Davidson [24]. By his account, there are four stages of evolution given for the case of decaying grid turbulence. The first stage identifies a fluid passing from the grid and transitioning to a turbulent state; this can be compared to Batchelor's description involving all points $x < x_0$ where x_0 designates the start of developed turbulence. Stage (ii) is developed turbulence, defined by a state where all lengthscales from the integral, L, to the Kolmogorov lengthscale η contain energy. This is the state to which Davidson describes as "the decay of *freely evolving turbulence*" (his italicisation) and claims is also referred to as the "asymptotic state". Davidson defines a third stage (iii) in which all the small scale motion has been depleted, and finally, the last stage (iv) corresponds to the final period of decay that Batchelor defines.

The decay of freely evolving turbulence that Davidson describes as stage (ii) is important to the current work. It is this stage, corresponding to the initial period of decay, that most early work had been done in revealing the so-called decay laws of turbulence. A well-known decay law has been derived by Kolmogorov [40] who found that the energy should decay as $t^{-10/7}$. This was an important result and found to be consistent with the decay of turbulence in the wind-tunnel experiments of his days. However, it later emerged that the reasoning that allowed this prediction was not always correct [42, 47, 128] and different values for the decay exponent were found [129, 130]. Subsequently, further studies were made using experiments, theoretical analysis, and simulations with the exponent lying somewhere in the range 1-1.7 [131].

In the few contemporary studies of the normalised dissipation rate for decaying turbulence involving numerical computation, there is one which gives the criteria used to determine the evolved time needed for measurement. Wang *et al* [127] determined an evolved decaying state has been reached when the total energy and dissipation rate decrease according to a power-law, which in their study was $t^{-1.47}$ for the energy. A more recent numerical study [125] which focused more on the normalised dissipation rate also used this as their criterion [132].

Two comments about the criterion described are that a decay exponent must first be determined and secondly that the total energy function must fit the power-law within a given tolerance to determine the time when the power-law decay starts. The first comment can be regarded as not so significant with the many data-fitting algorithms currently available, and the second can be addressed by noting that the tolerance can be fixed when further adjustments do not change the determined time. While neither of these issues present any major difficulty in determining an evolved time, it has been the purpose of this study to find a time that reflects the system's dynamics. The following section details the considerations made as to which parameters can be used to determine an evolved time and how they are used to do so.

5.2 Candidate Parameters

In order to determine an appropriate time at which to take a measurement, it is necessary to look at time evolution of the behaviour of the integral parameters. The main criteria needed with the candidate parameters are that they offer a time that is within the period of decay, which is taken to be stage (ii) in Davidson's nomenclature, and that these parameter values exist for both small and large Reynolds numbers. Secondary criteria would involve parameters that can be easily computed and those that can be directly measured in an experiment.

5.2.1 The Dissipation Rate and Spectrum

Turbulence is highly dissipative [133]. And the dissipation rate gives a measure of this, indicating a fully developed turbulent state with a pronounced peak. The maximum of ε then corresponds to the maximum turbulent intensity, signifying that the energy has reached well into the dissipation region of the wavenumber spectrum. As this time can easily be determined from the position of the peak, it is logical to use this in determining an evolved time. However, as an indicator of turbulent intensity, and in effect signalling the onset of stage (ii), it is too early for an evolved state that is indicative of decaying turbulence. Although the total energy is always decreasing, it is only after this point that it can show the characteristics of turbulent decay.

The time of peak dissipation, t_ε, can still be considered as it gives a reference time; one can use it to make measurements after a given time has elapsed. Noting that an estimate for the time it takes an eddy of low-wavenumber to breakdown is $\tau \equiv L/U$, gives the time for the transfer of the energy contained in the eddy to reach the higher wavenumbers of dissipation. An evolved time can be obtained by adding this characteristic time to the time of the maximum dissipation,

$$\begin{aligned} t_\mathrm{e} &= t_\varepsilon + L(t_\varepsilon)/U(t_\varepsilon) \\ &= t_\varepsilon + \tau_\varepsilon. \end{aligned} \tag{5.3}$$

This would provide a time that is later than the peak, carrying the measurement to a region where turbulent decay is occurring.

It must be noted that the peak does not exist for low Reynolds numbers. The fig. 5.2 shows various dissipation rates for computations performed using different viscosities. As can be seen in the figure of the dissipation rate, the shape of the plot changes with viscosity, most notably the emergence of the peak when viscosity is adequately low, $\nu < 0.015$. This is consistent with the turbulent phenomenology as the peak signifies the turbulent dissipation, where the energy is transferred by the nonlinearity from

the low- to high-wavenumbers, thus amplifying the dissipation by placing more energy into those wavenumbers where viscosity has a stronger effect. The lack of continuity

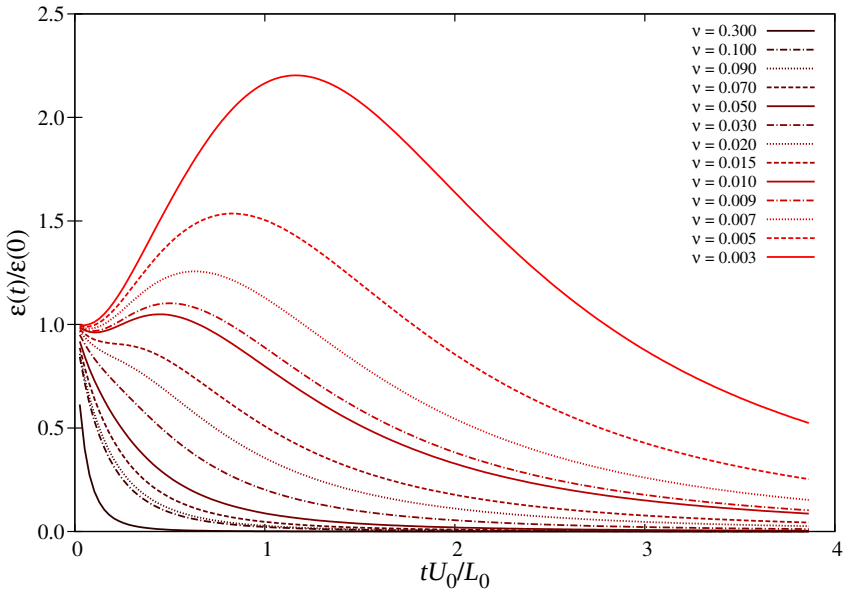

Figure 5.2: The normalised dissipation rate as a function of time, normalised by the initial timescale. Various dissipation rates, corresponding to different viscosities, show the emergence of a peak for sufficiently small viscosity.

with respect to viscosity of the dissipation rate is problematic. Note that for larger viscosities, the transfer mechanism will not be significant relative to the viscous forces, and in this case the observed peak will be slight or absent.

However, the dissipation rate also offers a power-law decay when the total energy follows a power-law since $d_t E = -\varepsilon$ and hence

$$E \sim t^n \Rightarrow \varepsilon \sim n t^{-n-1}. \tag{5.4}$$

This implies the need to know the value of the exponent n and then to fit the dissipation rate to this power law. One can rather ask what the reason is for this behaviour and look for some other means to determine the answer. Recalling that the definition for the dissipation rate in HIT is

$$\varepsilon(t) \equiv \int_0^\infty d\mathrm{k} 2\nu \mathrm{k}^2 E(\mathrm{k}, t), \tag{5.5}$$

it is useful to look into the dissipation spectrum for more insight via turbulent

phenomenology as it could provide a more continuous measure of an evolved time.

Considering the notion of self-similarity in decaying turbulence [27], one can look for the time where

$$D(\mathrm{k}, t_\mathrm{e}) > D(\mathrm{k}, t > t_\mathrm{e}) \quad \forall\, \mathrm{k}. \tag{5.6}$$

This is by no means a rigorous definition or requirement of self-similar decay with but it does given an indication of when the inertial mechanism is unable to transfer energy beyond a particular wavenumber, thereby signalling the onset of a decay period when wavenumbers in the decay spectrum can only decrease with time. Looking at the energy in the maximum wavenumber of a system can be indicative of the spread of energy and hence the onset of decay. For experiments, this maximum wavenumber corresponds to the smallest of scales measurable and is dependent on the measurement capabilities of the apparatus; likewise, in simulations, the maximum wavenumber is somewhat arbitrary and is chosen for the convenience of the computation. Using a standard quantity, such as the Kolmogorov dissipation wavenumber, that is independent of these considerations would be useful.

Considering the above arguments, the proposal is to use the time when $E(\mathrm{k}_D, t)$ reaches a maximum value, which can then be associated with the maximum spread of energy into the dissipation region, and therefore the start of the turbulent decay period. As k_D is time-dependent, a condition of taking the maximum value of this wavnumber which occurs when the dissipation rate peaks,

$$\mathrm{k}_D(t_\varepsilon) = \left(\varepsilon(t_\varepsilon)/\nu^3\right)^{1/4}. \tag{5.7}$$

An example of this can be seen in fig. 5.3 where the dissipation spectrum from an LET-computation is shown for various times. In the plot of the dissipation spectrum, the dark dashed-lines give the initial and final spectra (the peak of the initial has been cut-off for greater detail), and the light grey lines show the dissipation rate in 20 timestep increments. The inset shows the behaviour of the integral parameters $E(t)$ (yellow), $\varepsilon(t)$ (red), and $E(\mathrm{k}_D, t)$ (blue).

Initially $D(\mathrm{k}, t)$ is peaked at $\mathrm{k} \sim 3$, but then spreads out and becomes peaked at $\mathrm{k} \sim 10$. As it evolves, the inertial forces redistribute the energy among the wavenumbers, hence moving the peak and spreading the spectrum. This process continues through a peak in the dissipation rate, denoted by the green line in the spectrum and a similar green circle on the dissipation rate (inset).

Beyond the maximum in ε, the peak of the dissipation spectrum no longer grows but does continue to spread itself out until it reaches a point, denoted with the colour blue in the plots, where the transfer cannot move energy into higher wavenumbers faster than they can be destroyed by viscosity. The blue curve in the spectrum as well as

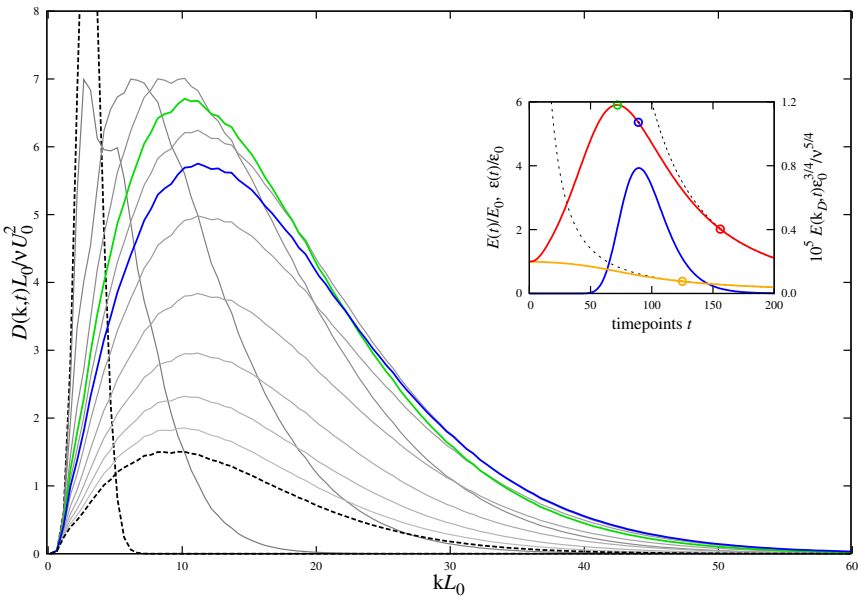

Figure 5.3: The normalised dissipation spectrum against normalised wavenumber with total energy (orange) and dissipation rate (red) against timesteps (inset). For this computation, $\nu = .001$. See text for more details.

the blue circle on the dissipation rate (inset) corresponds to this time. Furthermore, the inset shows the blue circle corresponding to the peak in $E(\mathrm{k}_D, t)$. Note that curves under the blue curve show a self-similar decay for the dissipation spectrum.

The inset shows the evolution of the energy (yellow) as well as the dissipation rate (red). Both of these curves have been fit to a power-law, $\propto t^n$, in their later stages. The exponent value for each has been determined to be -1.42 for $E(t)$ and -2.43 for $\varepsilon(t)$. When the fitted-curves are within 1% of their respective parent curves, a coloured circle has been placed. It can be seen in the inset plot, that point corresponding to the onset of the power-laws are later than those points given for the maximum of the dissipation rate and the onset of self-similarity in the dissipation spectrum. To make a comparison with Wang *et al* [127], their method would conclude that the latest point, red circle on the dissipation rate, is a sufficient time for a measurement.

While it has not been investigated here, the evolved time, t_D defined such that $E(\mathrm{k}_D, t_D)$ is a maximum may always be present and continuous throughout all R. It is thought that when the nonlinearity is activated, however small, a spreading of the energy and dissipation spectra occurs and $E(\mathrm{k}_D, t_D)$ has a maximum. It is possible to use an initial spectra where the $E(\mathrm{k}_D, 0)$ is also a (global) maximum, but this can be accounted for by noting that it should decay early, presumably before the second maximum $E(\mathrm{k}_D, t_D)$. A final comment is that while the generality of this method,

in terms of the phenomenology of homogeneous isotropic turbulence, is left to further investigation, it has been applied to the LET2008 results with Spectra V and VI, both of which have only a single maximum for $E(\mathrm{k}_D, t_D)$ that occurs throughout all Reynolds numbers considered.

5.2.2 The Maximum Energy Flux

Another parameter that has been useful in this research is the maximum of the energy flux, which was introduced earlier in §1.2.6,

$$\Pi_{\max}(t) \equiv -\int_0^{\mathrm{k}_0(t)} d\mathrm{j}\, T(\mathrm{j},t) \;=\; \int_{\mathrm{k}_0(t)}^{\infty} d\mathrm{j}\, T(\mathrm{j},t). \tag{5.8}$$

This definition is slightly different from that given previously in that for time-dependent turbulence the value of $\mathrm{k}_0(t)$ will also change with time; this dependence has been made explicit here. Similarly, $\Pi_{\max}$ can be defined,

$$\Pi_{\max}(t) \equiv \Pi\big(\mathrm{k}_0(t), t\big). \tag{5.9}$$

This quantity has some features that make it attractive as a candidate for an evolved time. Most notable is that it has a peak value which occurs early, giving an indication that the system has assumed an LET solution. As this quantity is a measure of the inertial transfer, it is expected to exist when the transfer is even weakly active, and therefore should exist for low- and large-R_λ computations. Figure 5.4 shows example plots of $\Pi_{\max}(t)$ against the timesteps for different viscosities.

The figure shows that for each curve and associated viscosity, there is a peak value for $\Pi_{\max}$ and the time of this peak, t_Π, increases with the decreasing viscosity. The 'rate', with respect to viscosity, at which the time of the peak increases is not as fast as that for the peak of the dissipation rate, see fig. 5.2. Furthermore, the height of the peak and the time when it occurs seem to become constant as the viscosity continues to decrease, for example when $\nu < .001$ in fig. 5.4; this is due to the same initial energy used in these computations.

A further comment that is fair to note about fig. 5.4 is that for curves where $\nu < .001$, some peculiar behaviour begins just prior to $t = L(0)/U(0)$. It is unknown at this time why this occurs and is pending further investigation. The focus here is the use of the early peak in this parameter to use as reference for measurements, and this is unaffected by the post-peak behaviour of $\Pi_{\max}$.

Because it is continuously present throughout a range of large and small viscosities, $\Pi_{\max}$ has a better status than that of the peak in the dissipation rate. Rather, the

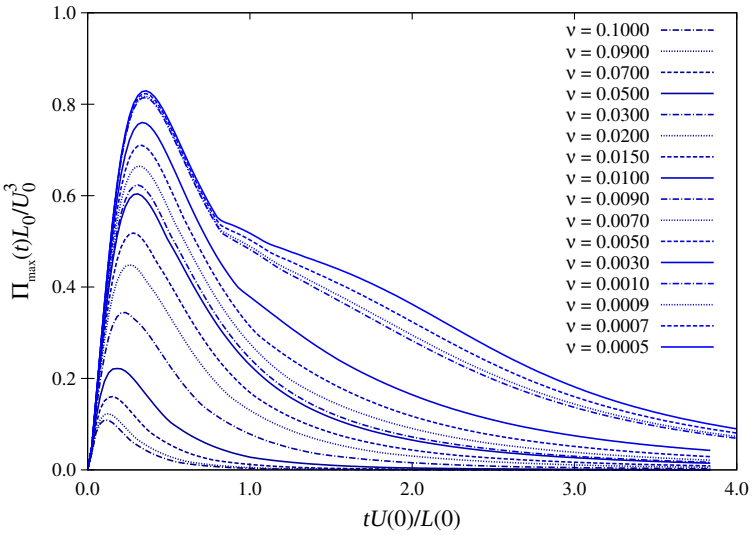

Figure 5.4: The normalised maximum flux as a function of time, normalised by the initial timescale. The various fluxes, corresponding to different viscosities, show a peak for all viscosities but also the convergence of the peak as viscosity is decreased.

behaviour of the peak when ν is sufficiently small is a cause for concern. As the peak of $\Pi_{\max}$ does not change appreciably when the viscosity is decreased beyond a given threshold, there is a greater chance that it will not capture the physical information that indicates fully-developed, freely-decaying turbulence.

Hybrid Time of t_Π and t_ε

Neither t_Π nor t_ε are suitable by themselves to give a reference time which can be used to measure turbulent parameters in a decaying turbulent system. The established criteria for a continuous evolved time amongst both small- and large-Reynolds numbers excludes t_ε, and the early onset of $\Pi_{\max}$ with uncertainties as to the number of τ_Π's needed eliminating these candidates for measurement times. While these parameters fail individually, together they might have something to offer.

The peak in the dissipation rate fails to appear when the viscosity prevents any noticeable transfer effects. The peak of $\Pi_{\max}$ occurs for (presumably) any viscosity, but is not suited to the desired purpose when ν is 'too' small. One might consider then that perhaps these two quantities could overlap in giving a evolved time. That is to say, t_Π reasonably coincides with t_ε for a critical viscosity when the peak in ε begins to appear. Figure 5.5 shows that this may be the case.

The range of overlapping viscosities is quite narrow and one would hope for more overlap between these two times. However, their separation is not so large and is within

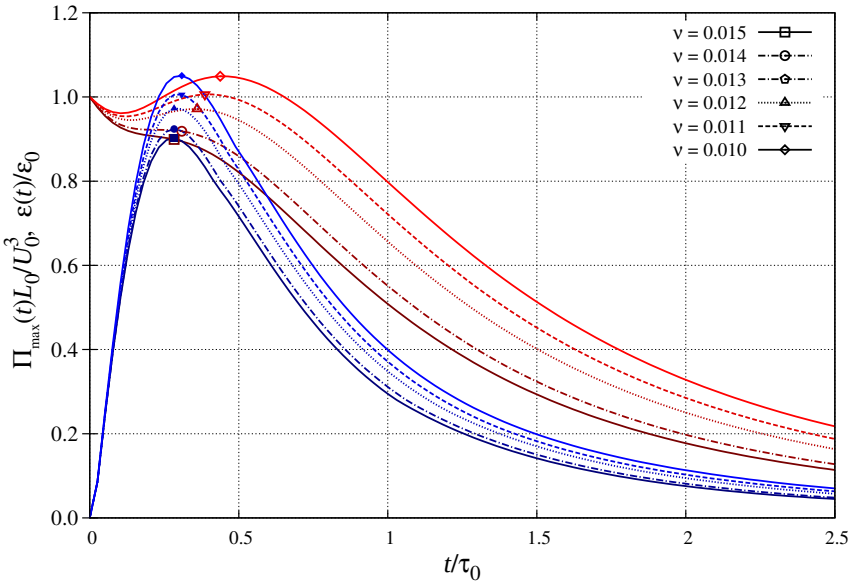

Figure 5.5: Curves of ε and $\Pi_{\max}$ against t, superimposed to show the near-coincidence of the peaks. Note that $\Pi_{\max}$ has been multiplied by a factor so the height of the peak is the same as that of ε.

5 computational timesteps, measuring 0.1 seconds in real-time which, for viscosity $\nu = .015$, is on the order of the viscous decay time criterion, $\delta t \sim 1/(\nu \mathrm{k}_D^2)$.

It is prudent to look at both ε and $\Pi_{\max}$, or rather C_ε and C_Π, as functions of the Reynolds number, specifically focusing on this range of viscosities. Going slightly further would be to see how the incremented evolved times, $t_\mathrm{e} + \tau_e$, differ in this range. If the difference is respectably small, then this hybrid time can be considered valid for obtaining measurements for decaying turbulence. Plots of C_ε and C_Π are shown in fig. 5.6.

The figure 5.6 shows the narrow range of viscosities where this change-over from t_Π to t_ε occurs for both C_ε and C_Π, which are plotted using $t_{\Pi|\varepsilon}$, $t_{\Pi|\varepsilon}+\tau_{\Pi|\varepsilon}$, and $t_{\Pi|\varepsilon}+2\tau_{\Pi|\varepsilon}$. Note that $t_{\Pi|\varepsilon}$ means that if a peak exists in the dissipation rate, the time associated with it, t_ε, will be used; otherwise, the time corresponding to the peak in the maximum energy flux, t_Π, will be used. This implies that small-R_λ uses t_Π and large-R_λ uses t_ε. In all plots of C_ε, the change-over seems indistinguishable from the rest of the curve; the plot for $C_\Pi(t_{\Pi|\varepsilon})$ shows a noticeable discontinuity near $R_\lambda = 16$. This seems to improve on the measurements incremented by $\tau_{\Pi|\varepsilon}$ and $2\tau_{\Pi|\varepsilon}$.

One might guess that continuity should be maintained by re-considering the results shown in fig. 5.1 where all points for C_ε aside from the initial value nicely converge for $R_\lambda < 15$ suggesting that the variability caused by the cross-over is 'tolerated' in

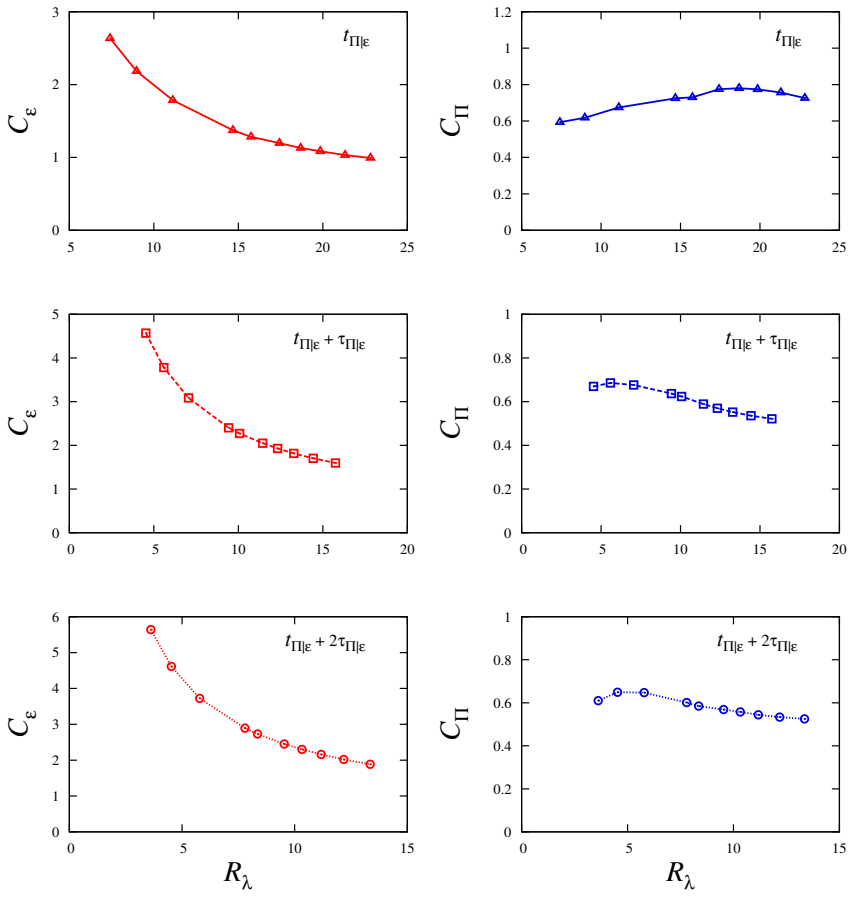

Figure 5.6: Plots of C_ε and C_Π against Taylor-Reynolds number. Each plot shows C_ε or C_Π measured at a given measurement time. The viscosities from largest to smallest are $\nu = .03, .025, .02 - .001(\Delta\nu = .002), .009, .008$.

the data. Similarly, all curves of C_Π excepting the initial again converge for all R_λ in fig. 5.1 so the same would be expected for C_Π as in C_ε. However, it should be noted that the scale for C_Π in this figure is much larger than for fig. 5.6 and, as a result, the discontinuity can be easily hidden. The disappearance of $t_{\Pi|\varepsilon}$ at large viscosities has made a quantitative measure of the overlap regions difficult, and so all evaluations were made by inspection. For the purposes of studying these quantities in the next chapter, the cross-over is acceptable.

5.2.3 Extension to Later Times

There are now two possible evolved times for use in measuring the dissipation rate and the maximum flux as functions of the Reynolds number for decaying turbulence. However, as has been argued in previous sections, to get into an developed decaying turbulent regime, one must move further in time beyond that given by either t_D or $t_{\Pi|\varepsilon}$. The proposal is to use t_D and $t_{\Pi|\varepsilon}$ as reference points such that the time of measurement is incremented by 1 and 2 eddy-turnover times, where the large-scale eddy-turnover times are defined at their respective evolved times,

$$\tau_e \equiv \frac{L(t_e)}{U(t_e)}. \tag{5.10}$$

The incremented evolved times to be tested are

$$t_{\Pi|\varepsilon},\ \ t_{\Pi|\varepsilon} + \tau_{\Pi|\varepsilon},\ \ t_{\Pi|\varepsilon} + 2\tau_{\Pi|\varepsilon},$$

and

$$t_D,\ \ t_D + \tau_D,\ \ t_D + 2\tau_D,$$

This has been used above for fig. 5.6.

The reason for choosing a characteristic time-scale based on the integral lengthscale is for practical reasons. The common interpretation of this estimate is that an eddy of size L will take roughly an amount of time $\tau = L/U$ to traverse the energy cascade, breaking down in the process, and finally reaching dissipative scales. In the spectral vocabulary, the energy contained in the small wavenumbers $\mathrm{k} \sim \pi/L$ will take roughly τ to reach the dissipation wavenumbers $\mathrm{k} \sim \mathrm{k}_D$. This represents one of the longer timescales attributed to turbulent systems; the expectation is that one or more increments should bring the measurement time sufficiently beyond the evolved times determined thus far. The evolved and incremental measurement times are indicated in figs. 5.7 and 5.8 by points on the time-dependent dissipation rate curve.

The first figure, 5.7, shows three different curves for three viscosities, $\nu = .05, .005, .0005$. The curve for $\nu = .0005$ is also accompanied with a line fitted to $y = mx^n$, which shows where the power-law decay behaviour begins for ε as this was the indication for developed turbulence as determined by Wang *et al* (see above). The second figure shows the same behaviour from Spectrum VI using slightly different viscosities (the smallest viscosity attainable with long time-domains of Spectrum VI is $\nu = .0006$). It can be seen from both figures that the measurement times $t_e + \tau_e$ both fall before the onset of the power-law decay, but $t_D + 2\tau_D$ is behind this point while $t_{\Pi|\varepsilon} + 2\tau_{\Pi|\varepsilon}$ arguably coincides with it.

There is now a set of six times which represent different stages of freely-evolving

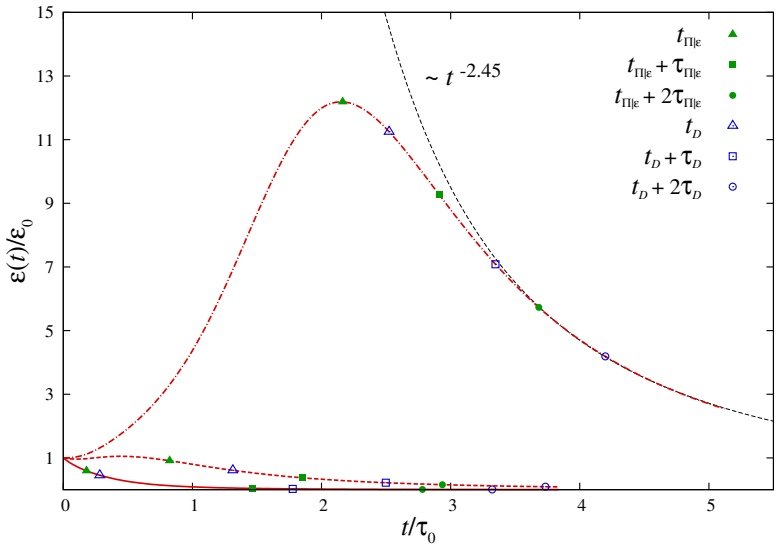

Figure 5.7: The normalised dissipation rate against normalised time for decaying turbulence using the LET2008 and Spectrum V. Evolved and measurement times are shown as filled and unfilled shapes respectively. Viscosities used are: $\nu = .05$ solid line, $\nu = .005$ dashed line, $\nu = .0005$ dash-dot line.

turbulence. It was argued earlier that times indicating turbulent decay must occur later than some of the times found in the current set and it has been found that the

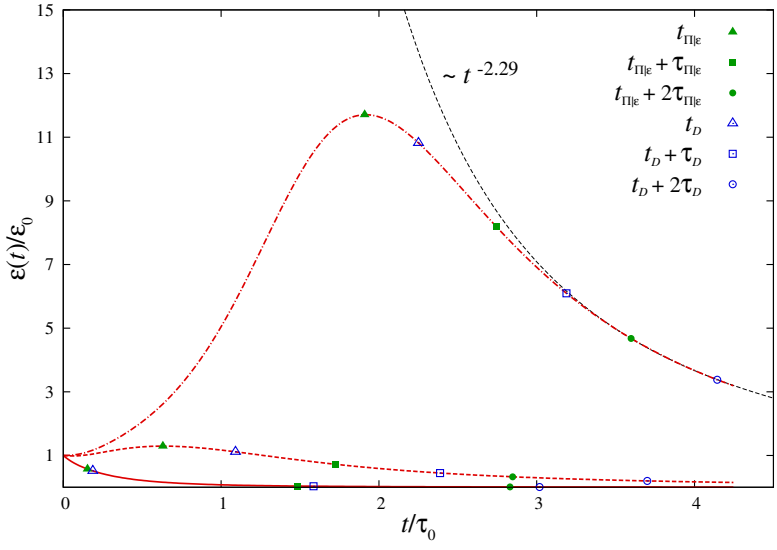

Figure 5.8: Same as in fig. 5.7, however using Spectrum VI and $\nu = .06$ solid line, $\nu = .006$ dashed line, $\nu = .0006$ dash-dot line.

latest times would agree with this. The following section will see the results of all six times put into practise and compared.

5.3 C_ε and C_Π Measurements Using the Newly Established Evolved-Times

It has been argued and demonstrated that the shape of parameter plots for C_ε and C_Π used to investigate the dissipation phenomenology are dependent upon the times used to measure these parameters. As the previous sections have detailed some methods determining evolved and measurement times, this section will see these methods put to use for LET computations.

The quantities C_ε and C_Π are shown with evolved and measurement times in figs. 5.9 and 5.10 for Spectra V and VI, respectively. It can be seen in both figures that the larger-R_L values for the normalised flux converge to the asymptotic value for all times considered. The main effect of the time appears to be at the Reynolds number where the curve converges to the asymptotic value. Note that measurement times $t_e \gtrsim \tau_{\Pi|\varepsilon}$ show little difference in $C_\Pi(t_e)$ in both figures, but the curves for C_ε have a stronger dependence on the time used.

The earliest values are also the lowest in terms of their asymptotic values, ~ 0.5, which is similar to that found in forced turbulence [123, 124]. The later values do show some convergence, similar to that of C_Π, though with more dispersion. The later times show an asymptotic value to be ~ 0.8 which compares better to the experimental values of ~ 1.1 in Sreenivasan [126] and the computational values of ~ 1.0 found in Bos *et al.* [125].

Figure 5.11 shows the same results presented differently to better compare the evolved and measurement times for t_D and $t_{\Pi|\varepsilon}$. It shows mostly the same information as the two previous figures, namely the convergence when using later times. The curves of Spectra V and VI are very similar though C_ε and C_Π are consistently larger for Spectrum VI. The differences in these quantities due to the small wavenumber exponent given in the initial energy spectra have not been explored in this study and little can be said for the comparison of Spectra V and VI in this figure.

An additional observation to make is rather than looking at C_ε, it may be useful to consider the behaviour of ε alone against the Reynolds number using the evolved times. Plots of this can be seen in figs. 5.12-5.15. The most apparent feature in the figures showing the dissipation rate is that at low Reynolds numbers, ε is either very large or very small depending on the time used for measurement. Curves using $t_{\Pi|\varepsilon}$ or t_D show that the low-R behaviour of ε to diverge whereas all later times show ε to

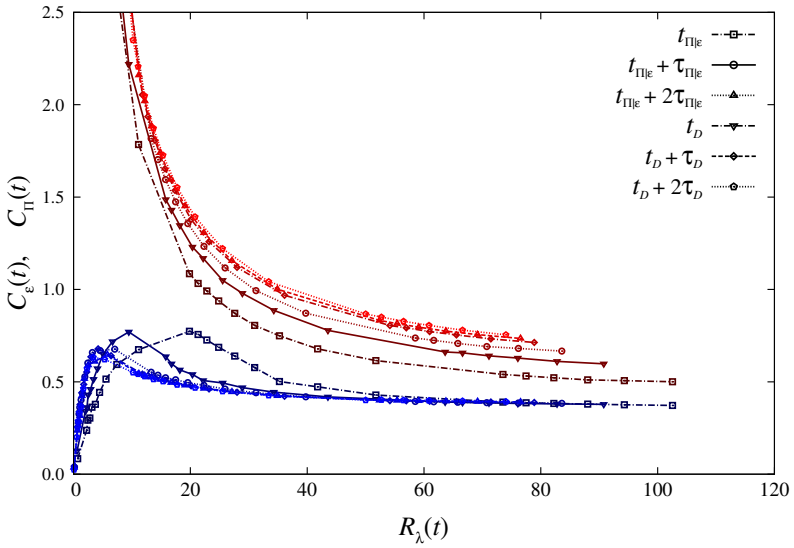

Figure 5.9: The normalised dissipation rate C_ε (red) and maximum energy flux C_Π (blue) against Reynolds number for decaying turbulence using the LET2008 and Spectrum V.

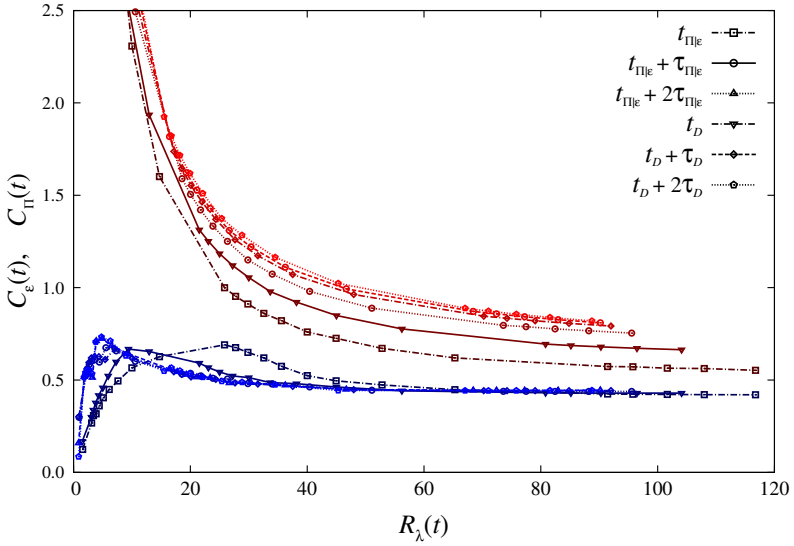

Figure 5.10: The normalised dissipation rate C_ε (red) and maximum energy flux C_Π (blue) against Reynolds number for decaying turbulence using the LET2008 and Spectrum VI.

shrink to zero as $R \to 0$.

Similar plots are seen for $\Pi_{\max}$, though the difference in these curves does not result

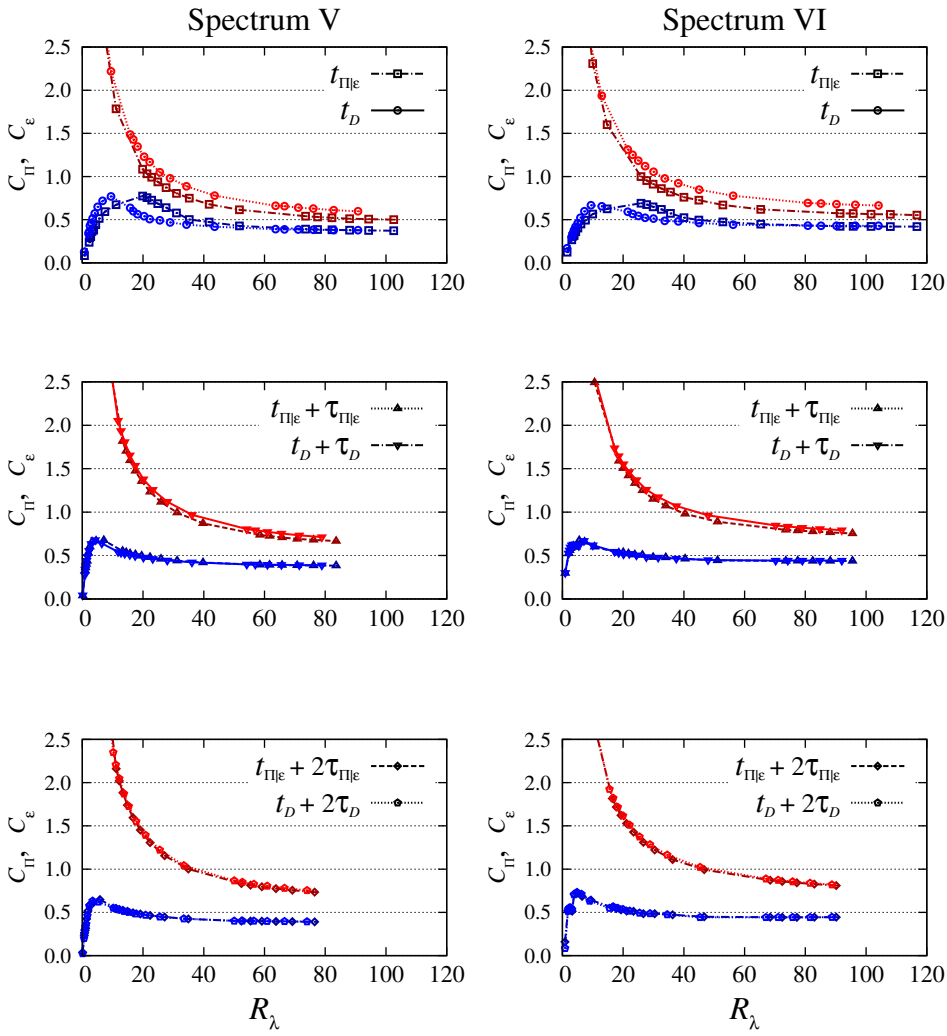

Figure 5.11: The normalised dissipation rate C_ε (red) and maximum energy flux C_Π (blue) against Reynolds number for decaying turbulence using the LET2008. Evolved (top two plots) and measurement times (bottom four plots) are shown.

in a divergence at low Reynolds numbers. What is remarkable about these curves is the existence of a peak for the early times $t_{\Pi|\varepsilon}$ and t_D that vanishes as the time increases. A similar peak is found in the low-R region of C_Π, however, it appears for all times used.

It is also of interest that while C_ε and C_Π show tolerance for differences in measurement times, the unnormalised quantities ε and $\Pi_{\max}$ are more sensitive in this respect. This suggests that there is some compensation in the combined terms of ε, L and U in C_ε that counters such differences. However some cases, for example

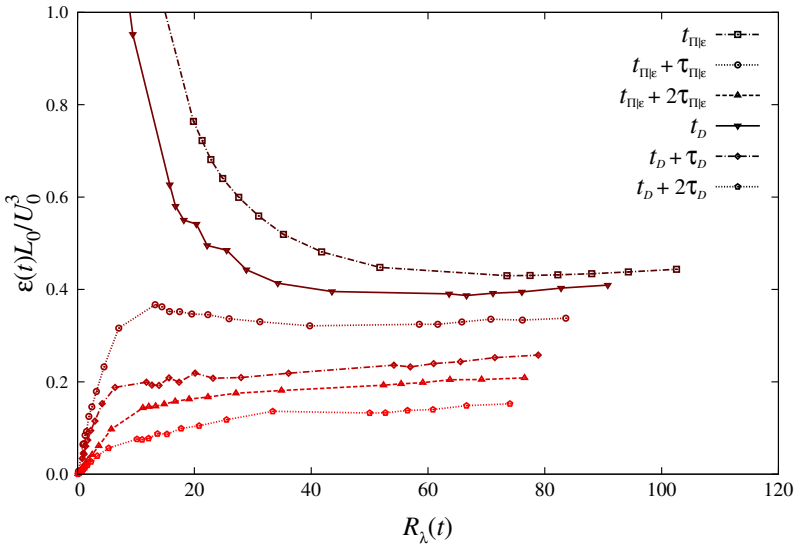

Figure 5.12: The dissipation rate $\varepsilon L_0/U_0^3$, normalised by the initial velocity and integral lengthscale, against the Taylor Reynolds number for decaying turbulence using the LET2008 and Spectrum V.

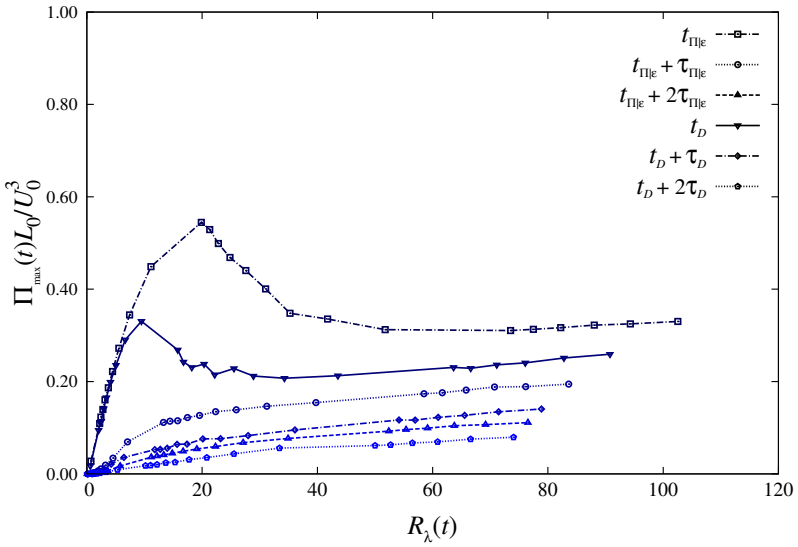

Figure 5.13: The maximum flux $\Pi_{\max} L_0/U_0^3$, normalised by the initial velocity and integral lengthscale, against the Taylor Reynolds number for decaying turbulence using the LET2008 and Spectrum V.

the later measurement times of $\Pi_{\max}$, show nearly the same shape of curve, possibly multiplied by a constant factor throughout. It is possible that this behaviour leads to

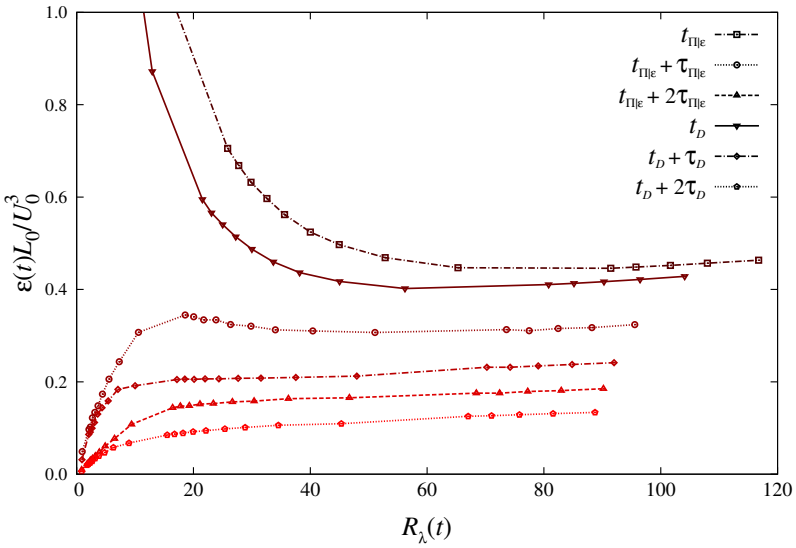

Figure 5.14: The dissipation rate $\varepsilon L_0/U_0^3$, normalised by the initial velocity and integral lengthscale, against the Taylor Reynolds number for decaying turbulence using the LET2008 and Spectrum VI.

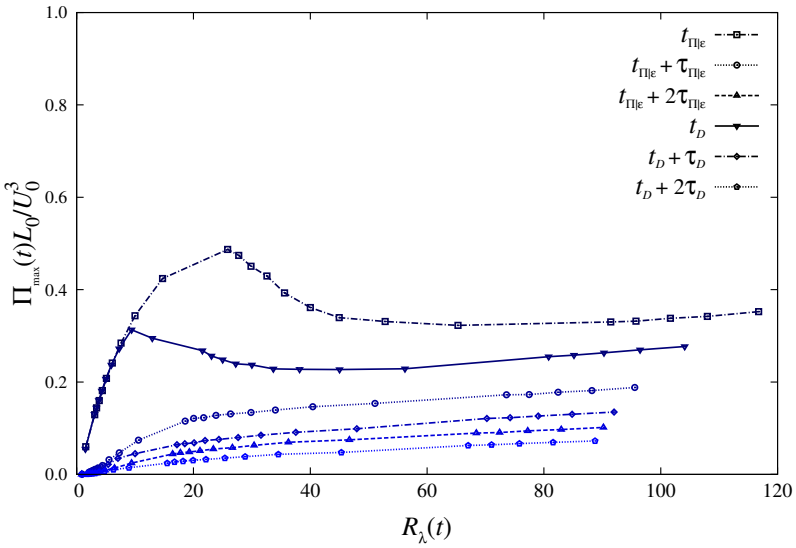

Figure 5.15: The maximum flux $\Pi_{\max} L_0/U_0^3$, normalised by the initial velocity and integral lengthscale, against the Taylor Reynolds number for decaying turbulence using the LET2008 and Spectrum VI.

the relatively early convergence of C_Π as time increases.

The reason for the divergent behaviour of ε for low-R is of some concern. It is clear

in the sense that computations when the viscosity is large will have a large dissipation rate early in the computation that decreases thereafter. This is also the case for when the dissipation rate as a function of time only has a peak value at t_ε, where ε measured after will be smaller. It is not known how this serves in the criterion for finding suitable measurement times as it is perhaps a subtle point as to whether the dissipation rate should diverge when $R \to 0$. To investigate this, one can consider the spectral energy balance equation (see (5.2)) with an assumption of negligibly weak inertial forces

$$\partial_t E(\mathrm{k}, t) \approx -2\nu \mathrm{k}^2 E(\mathrm{k}, t). \tag{5.11}$$

This reasonably describes a fluid at very low Reynolds numbers. A solution to this equation is

$$E(\mathrm{k}, t) = E(\mathrm{k}, 0) e^{-2\nu \mathrm{k}^2 t}. \tag{5.12}$$

For small Reynolds numbers, specifically large viscosities, the wavenumber of this system can be safely truncated and in extreme cases the shape of the energy spectrum can be approximated by its $\mathrm{k} \to 0$ behaviour, $E(\mathrm{k}, 0) \approx c_1 \mathrm{k}^n$ where for present purposes $n = 2, 4$. Using this and (5.12), one can evaluate ε analytically to find its viscosity and time dependence,

$$\begin{aligned} \varepsilon(t) &= \int_0^\infty d\mathrm{k}\; 2\nu \mathrm{k}^{2+n} c_1 e^{-2\nu \mathrm{k}^2 t} \\ &\sim \nu^{-(n+1)/2}\; t^{-(n+3)/2}. \end{aligned} \tag{5.13}$$

Since viscosity is considered to be large in the present argument, sufficiently early times ($t \approx 0$) will cause $\varepsilon(t)$ to diverge. However, in picking a reference time $t_e \neq 0$, viscosity can be increased to show that the dissipation rate $\varepsilon(t_e)$ will vanish as $R \to 0$. It is arguable then that the early curves for ε in figs. 5.12 and 5.14 are not sufficiently resolved for very small Reynolds numbers to show $\varepsilon \to 0$.

5.4 Discussion

A method has been presented for determining when measurements can be made on a freely-decaying turbulent system. The times determined here, $t_{\Pi|\varepsilon}$ and t_D, serve as indicators of a developed decaying turbulent system. These times approximate when turbulent activity is near its peak, measured by the peak value in the dissipation rate and by the maximum spread of energy in the dissipation spectrum. It has been noted that these times may be too early to designate a decaying turbulent system, and hence it would be better to use these times as a basis from which later times, such as the

eddy-turnover times $\tau_{\Pi|\varepsilon}$ and τ_D, can be determined.

The earlier time, $t_{\Pi|\varepsilon}$, is determined directly from the average dissipation rate or the time-derivative of the average total kinetic energy and can be easily measured in experiment and computation. As this time is based on the peak of the dissipation rate, it has been noted that this peak will not occur for sufficiently low Reynolds numbers and to supplement it, the peak in the maximum flux is used. The peak value of the flux also has problems in that it is too early in most cases except when the Reynolds number is low. The discontinuity of both the peak dissipation and peak flux has allowed for a hybrid time that shows potential for its use as an evolved time.

The other reference time, t_D, follows from the point at which the dissipation spectrum extendend to its maximum wavenumber. This was found to be equivalent to the time at which the energy spectrum at the dissipation wavenumber, $E(\mathrm{k}_D, t_D)$, obtains a maximum value. It is a requirement to measure to the energy spectrum which may not be as directly accessible in an experimental situation. An advantage of this time over the earlier reference time is that it is present throughout all Reynolds numbers though it is based on the assumption that the Kolmogorov wavenumber, k_D, or its inverse, the lengthscale η, is relevant for all fluid systems irrespective of Reynolds number.

These reference times can be used to determine an appropriate time to measure quantities meant to characterise the decaying system. It was found that the measurement times, $t_{\Pi|\varepsilon} + 2\tau_{\Pi|\varepsilon}$ and $t_D + 2\tau_D$, coincide better with the criterion of the dissipation rate behaving as a power-law with time as used by Wang *et al* [127].

5.4.1 Conclusions

Using the measurement times, $t_{\Pi|\varepsilon} + 2\tau_{\Pi|\varepsilon}$ and $t_D + 2\tau_D$, values for C_ε were found that were close to the values taken from other studies of decaying turbulence such as wind-tunnel experiments and numerical simulations. Though the values of C_ε at these times are slightly lower than those of the literature, there is some indication that these times and the criteria for determining them are appropriate.

It was also noted for computations using the latest measurement times, the individual quantities C_ε and C_Π do not differ appreciably. Because of its continuity throughout (presumably) all Reynolds numbers, the reference time of t_D will be used for measurements of C_ε and C_Π in the following chapter, specifically using $t_D + 2\tau_D$. The findings here indicate that this time is reasonable to make such measurements that depict a freely-decaying turbulent system.

5.4.2 Future Work

The issue of choosing an evolved time has been examined in some detail here, but much more remains to be done. The reference times are chosen based on the dynamics of the system, but the measurement times are not necessarily so. Adding multiples of eddy-turnover times was done somewhat arbitrarily and was justified through comparison with one other study. As the method developed here works by finding an onset time when decaying turbulent dynamics are expected, a resolution to this issue would be to come from the other direction and determine when this motion has finished. One estimate for this would be when the ratio of the maximum flux to the dissipation rate vanishes, $\Pi_{\max}(t_e)/\varepsilon(t_e) \to 0$. This would signify the inertial terms becoming negligible. This time might be too late, but noting that the value of C_Π did not change appreciably for $t > t_{\Pi|\varepsilon} + \tau_{\Pi|\varepsilon}$, a departure from this may mark the end when such measurements can be made.

It must also be considered that these times may not exist for all types of homogeneous isotropic turbulence and hence it would be informative to know where these criteria can be applied. The assumption that has been used here is that there is sufficient energy in the small wavenumbers to elicit a transfer of energy into the dissipation wavenumbers; this applies to both times. One can imagine that initial spectra with significant energy in the dissipation region give erroneous behaviour of these times. For example, it is possible to construct an initial spectrum at large Reynolds numbers such that $\varepsilon(0)$ or $E(\mathrm{k}_D, 0)$ is already a maximum value and as the system evolves no such maximum will occur again. More specific investigations might focus on how the evolved-time criteria proposed here are influenced by the shape of the initial energy spectrum.

A possible application of the evolved time is that it can be used to find a time where the turbulent quantities associated with decaying turbulence are qualitatively similar to those of steady turbulence, thereby allowing the use of freely-decaying turbulence to be meaningfully compared to forced turbulence. It was noted that value of the asymptote of C_ε is similar to that for forced computations; it will be shown in the following chapter that the the asymptotes of C_ε and C_Π coincide for forced turbulence. If such an evolved time were known where a decaying turbulent system effectively emulates a forced system, there is the possibility to study the effects of initial conditions in generating a developed turbulent state.

Chapter 6

Phenomenology of Turbulent Dissipation

It is well known that turbulence is a highly dissipative phenomenon. It is perhaps just as well known that this dissipation exists even when the viscosity is extremely small, and, in theory, taken to zero. This chapter discusses this anomalous dissipation and offers some interpretation of it based on the flux of energy from large to small scales. An equation for the normalised dissipation rate based on the spectral energy balance equation is derived here. This relationship can make some quantitative predictions distinguishing the behaviour of the dissipation rate in forced and decaying turbulence. It is demonstrated that this equation can be computed using the LET2008 developed in this thesis, the results of which are comparable to those given in the current literature.

6.1 Introduction to Turbulent Dissipation

A key feature of turbulence is that it is extremely dissipative [133]. Creating turbulence within a flow takes energy away from the transport of mass and momentum, which reduces the amount of fluid that can be moved through a confined space, producing what is call 'turbulent drag' [13]. There is a focus in this area that seeks to prevent or reduce this phenomenon by understanding how turbulence develops [134, 135] and how the working fluid interacts with an additive that effectively absorbs the fluid's ability to transition into a turbulent state [12, 136]. A better understanding of this behaviour could have practical benefits as well as improve the general understanding of turbulence itself.

To introduce this concept, an example is considered where the dissipation rate has been obtained for a variety of viscosities using the LET model in computing the free-decay of homogeneous isotropic turbulence. Plots of the dissipation rate against time

for several computations are shown in fig. 6.1 below. It can be noted that at the largest viscosities used, the dissipation rate follows a monotonic power-law decay. However, as the viscosity is decreased, the curve begins to deform, first acquiring an inflection point and then showing a slight peak. The peak becomes more pronounced as the viscosity decreases. It should be noted that the dissipation rate is normalised by its respective initial value, $\varepsilon(0)$, which in all cases uses the same initial spectrum thereby giving

$$\varepsilon(0) = \nu \left(\int_0^\infty d\mathrm{k}\; 2\mathrm{k}^2 E(\mathrm{k}, 0) \right) \quad \rightarrow \quad \nu \times \text{constant}. \tag{6.1}$$

This accounts for the seemingly large growth of the peak, but not immediately for its existence as it is this occurrence which is most interesting.

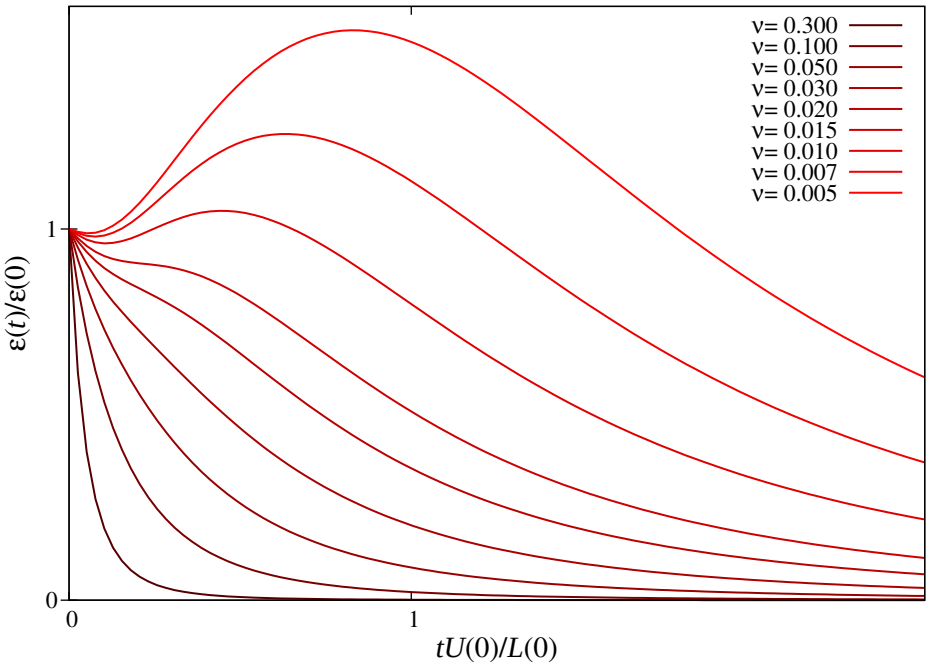

Figure 6.1: A plot of normalised dissipation rate curves, $\varepsilon(t)/\varepsilon(0)$, with various viscosities plotted against time.

The mechanism(s) believed to be driving such a phenomenon is not entirely clear. The figure shows that this maximum dissipation peak increases as the viscosity decreases in both its value and the time at which it occurs. These increases may be explained in the following way. Firstly it should be recalled that this dissipation rate can be obtained from the dissipation spectrum, which shows the energy spectrum weighted by the viscosity and a simple quadratic function of the wavenumber

$$\varepsilon \equiv \int d\mathrm{k}\, D(\mathrm{k}) = \int d\mathrm{k}\, 2\nu \mathrm{k}^2 E(\mathrm{k}). \tag{6.2}$$

The dissipation spectrum grows stronger as the wavenumber is increased, and above a particular wavenumber, k′, the energy spectrum becomes negligible, $E(\mathrm{k}') \approx 0$. As viscosity is decreased, the wavenumber k′ is increased, thereby suggesting that more of the wavenumber spectrum is accessible to the system. What this means in terms of the figure is that as the viscosity decreases and the wavenumber range grows, and the time it takes for the energy to move through the system from small wavenumbers to those where it is dissipated also increases.

It is helpful to consider another illustration. Figure 6.2 shows a plot of an energy spectrum $E(\mathrm{k})$ that has a peak in the low wavenumbers. This could be either the initial energy spectrum or the constant energy spectrum of a forced system. The energy spectrum is plotted against curves $y(\mathrm{k}) \propto \nu \mathrm{k}^2$ with various viscosities, ν. This has been done since the dissipation spectrum is similarly related to the energy spectrum via $D(\mathrm{k}) = 2\nu \mathrm{k}^2 E(\mathrm{k})$. Note that the dissipation term in the spectral Navier-Stokes equation is similarly $\nu \mathrm{k}^2 \mathbf{u}(\mathbf{k})$.

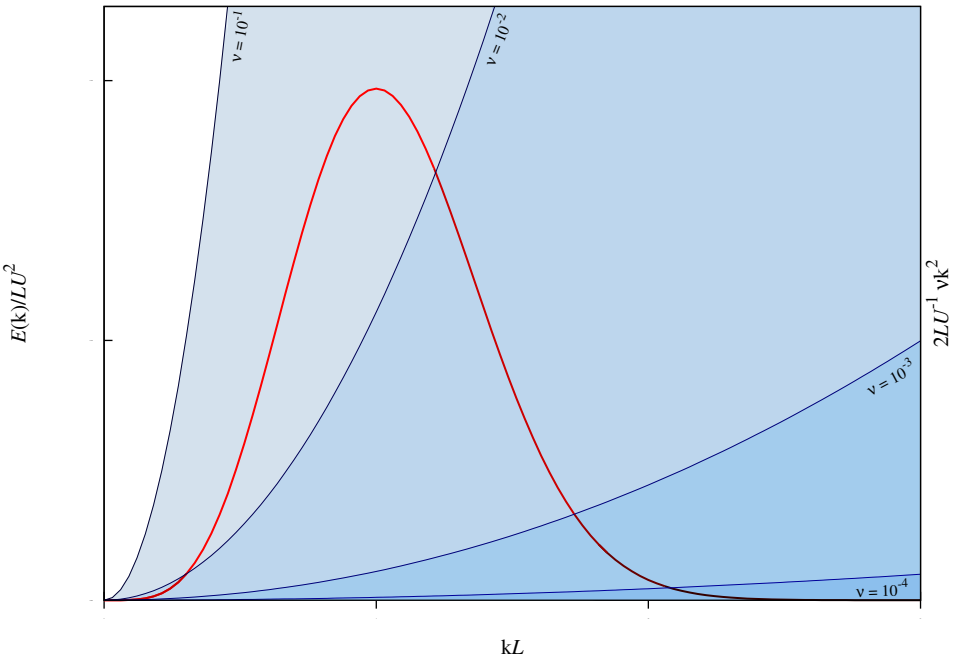

Figure 6.2: A plot of a normalised energy spectrum $E(\mathrm{k})$ superimposed onto curves $y(\mathrm{k}) \propto \nu \mathrm{k}^2$ against normalised wavenumber k.

The figure illustrates what may be called a region of dissipative influence for a

particular viscosity; the region begins at the boundary $y(\mathrm{k}) = 2(L/U)\nu\mathrm{k}^2$ and continues for higher wavenumbers. The largest viscosities show the spectrum to be completely contained within the region of influence. As viscosity is decreased, the slope of the region's boundary decreases and less of the peak of the energy spectrum is contained within the region. Indeed, as the viscosity is reduced further, the majority of the energy spectrum is outside of the region. As viscosity is let to vanish, $\nu \to 0$, then it can be seen that a large amount of energy remains outside the region of influence, which must be transferred giving rise to non-zero turbulent dissipation rate. Dissipation is still occurring but the viscosity is negligible and it may be considered to be completely absent. This is known as anomalous dissipation [137–141].

The information in fig. 6.2 is speculative and serves only to illuminate the current discussion. The part of the spectrum that lies to the left of the boundary represents the energy that can be transferred by the inertial-transfer mechanism. As the boundary is pushed to higher wavenumbers by decreasing the viscosity, there is a greater chance for the inertial mechanisms to activate, which will transfer energy throughout all wavenumbers. If there is more energy to be transferred rather than dissipated (which occurs in the low-k range), the flux of energy will increase. As the flux increases, it brings more energy to the dissipation range of wavenumbers, increasing the dissipation rate. So then, as viscosity is decreased, the amount of energy to be transferred is increased, increasing the flux and the dissipation rate. This was seen in fig. 6.1.

The purpose of this lengthy introduction is to present the reader with the notion of turbulent dissipation and the phenomenon of anomalous dissipation. These issues will be discussed in more precise language in the following sections.

6.2 The Dissipation Anomaly

Finite dissipation in the vanishing viscosity-limit has and still plays a fundamental role in the study of turbulence. It has been asserted as an empirical law [44] and has even come to be referred to as the 'Zeroth Law of Turbulence' [142, 143].

6.2.1 The Taylor Dissipation Rate

The quantity that is of greatest concern here is the normalised dissipation rate,

$$C_\varepsilon \equiv \frac{\varepsilon L}{U^3}. \tag{6.3}$$

This was first considered by Taylor [111] who defined it in terms of characteristic-time ratios:

$$\frac{\text{time scale of dissipative eddies}}{\text{time scale of energy-containing eddies}} = \frac{\varepsilon}{U^2} \Big/ \frac{U}{L}. \tag{6.4}$$

Taylor determined that this quantity should become independent of Reynolds number when R is large and C_ε becomes a constant.

Evidence was found supporting this, some of which was later compiled and published in Batchelor [25]. The impact of this result has proved fundamental to the study of turbulence. Heisenberg and Weisäcker, Onsager, and Kolmogorov are said to have independently developed what eventually became the well-known "five-thirds" law of Kolmogorov based on this phenomenology of turbulent dissipation [24, 25].

A major work in the normalised dissipation rate came from Sreenivasan [126] who collected and analysed relevant data from wind tunnel experiments, giving proof to the asymptotic behaviour of the dissipation rate. Sreenivasan also gave a simple formula showing the small-R behaviour to go as R^{-1}:

$$C_\varepsilon = \left(\frac{15\nu U^2}{\lambda^2}\right)\frac{L}{U^3} = \frac{15}{R}\left(\frac{L}{\lambda}\right)^2 \tag{6.5}$$

which was confirmed with the results given in his paper. Since then, there have been numerous additions to the documented evidence of this phenomenon, for example, [123–125, 138, 144–148].

6.2.2 Analytic Relations for the Dissipation Parameter

Given its importance in the study of turbulence, there is a body of work that is emerging which has sought to develop an analytic relationship tying the dissipation rate to its observed behaviour. Some notable approaches are presented below. This list considers only those results that have something directly in common with the work to be presented here.

Lohse, 1994

The work by Lohse [149] used an expression for the dissipation rate derived from mean-field closure that was developed and applied to the Navier-Stokes equation by Effinger and Grossmann [150]. Lohse was able to make some predictions and numerical calculations that showed the low-R behaviour of the dissipation rate to be $C_\varepsilon \sim R^{-1}$, as

$$C_\varepsilon = C_{\varepsilon,\infty}\left\{\left(\frac{3b^3}{8}\right)^{1/2} R_L^{-1} + \left(1 + \frac{3b^3}{8}R_L^{-2}\right)^{1/2}\right\}. \tag{6.6}$$

The constant b is the Kolmogorov constant. The predictions of this equation, though derived for steady turbulence, were compared to the data of Sreenivasan [126] and showed a sensible fit to the data. It is noteworthy that the lower bound of his prediction, obtained using a range of values for b, shows a reasonable fit to the current value of $C_\varepsilon \sim 0.5$.

Doering and Foias, 2002

Doering and Foais [151] rigorously determined upper- and lower-bounds on the dissipation rate and C_ε for stationary turbulence. The detailed introduction of their paper gives a short history of similar work. Only the upper bound is of concern here:

$$C_\varepsilon \leq \frac{A}{R_L} + B. \tag{6.7}$$

The constants, A and B, are determined by the low-wavenumber forcing used to maintain stationarity. Furthermore, they only depend on the shape of the forcing function, but not on its magnitude or the lengthscales associated with it. This work is quite general in its treatment of the Navier-Stokes equation as it does not specify homogeneity or isotropy.

This work was extended to plane-shear flows [152], body-forced turbulence [92, 153], and fractal-generated turbulence [154] by Doering and associates.

Bos *et al*, 2007

The work of Bos *et al* [125], investigated the dissipation rate using various methods of DNS, Large-eddy simulation (LES), and an EDQNM closure for both stationary and decaying turbulence. Their findings indicate that the asymptotic behaviour of the normalised dissipation rate is distinct for forced and decaying systems, most notably that the asymptotes for the decay computations are larger than those of the forced.

They provided arguments explaining that the separation observed was based on the time needed for the energy in the low-wavenumber regions to traverse the energy cascade into the dissipation region. An equation is constructed to demonstrate the phenomenology behind these results:

$$C_\varepsilon(t) = C_\varepsilon^F \left(1 + \frac{T_c}{t})\right)^{n+1}, \tag{6.8}$$

where the cascade time, T_c, the time it takes energy at L to reach η (given here as k_D), is

$$T_c \equiv \frac{L}{U}\left(1 + \left(\frac{\pi}{\mathrm{k}_D L}\right)^{-2/3}\right)^{n+1}. \tag{6.9}$$

The exponent $n+1$ found in both equations comes from the power-law exponent decaying energy, $E(t) \sim t^{-n}$. The quantity C_ε^F is described as the normalised dissipation rate of stationary turbulence. This result explains the increase of the C_ε found for decaying turbulence. This result does not explicitly show any dependence on Reynolds number, though they derive model equations where C_ε^F has a R_L^{-1}-dependence.

6.3 New Analysis of the Dissipative Anomaly

In this section, new results based on recent work of McComb [155] and further developed in McComb *et al* [156] are presented. The work derives an exact relation for the normalised dissipation rate from the spectral energy balance equation that can be associated with the equation derived by McComb. Furthermore, the relation shows that there will be a distinct difference between the normalised dissipation rate found in decaying turbulence as opposed to that found for stationary forced turbulence.

6.3.1 The Taylor Surrogate and Related Quantities

It will be useful to define a quantity that will be encountered frequently in this chapter. The 'Taylor surrogate' will be formally defined as

$$\xi(t) \equiv \frac{U(t)^3}{L(t)}. \tag{6.10}$$

It was originally used by Taylor when investigating the dissipation rate. Its intended function was, in effect, to normalise the dissipation rate, leading to the normalised dissipation rate:,

$$C_\varepsilon \equiv \frac{\varepsilon(t)}{\xi(t)}. \tag{6.11}$$

It is worth giving a few remarks about the Taylor surrogate. It is called a surrogate as it serves a place for the rate of energy transfer, or energy flux. But such a name might belie a more fundamental role.

As a rough estimate for the energy flux, the energy of an eddy of size comparagraphble to L would be proportional to U^2. The so-called 'eddy turnover time', or the time it takes an eddy of size L to transfer down the energy cascade can be estimated by L/U. As this line of reasoning is focused on the large scales, the energy flux from the large scales may be estimated by the surrogate:

$$\text{energy flux} \equiv \frac{\text{energy}}{\text{time}} \sim \left(U^2\right) / \left(\frac{L}{U}\right) \tag{6.12}$$

(these arguments follow from Davidson [24]). It will be found later that the maximum flux, which is obtained from the spectral flux,

$$\Pi_{\max}(t) \equiv \max\Big\{\Pi(\mathrm{k},t)\Big\}, \tag{6.13}$$

is related to the surrogate. The spectral flux is directly computed from the energy transfer spectrum

$$\Pi(\mathrm{k},t) \equiv -\int_0^{\mathrm{k}} d\mathrm{j}\, T(\mathrm{j},t) \;=\; \int_{\mathrm{k}}^{\infty} d\mathrm{j}\, T(\mathrm{j},t). \tag{6.14}$$

It describes the rate of net energy flowing through a particular wavenumber. The first equality relates the flow through the wavenumber to the transfer of energy from all lower wavenumbers, while the second equality describes the flow from k to all higher wavenumbers. As the flux is the flow of spectral energy through a wavenumber, the transfer spectrum may be written in terms of the flux,

$$T(\mathrm{k},t) = \frac{\partial\Pi(\mathrm{k},t)}{\partial\mathrm{k}}. \tag{6.15}$$

Given in this way and considering the shape of the transfer spectrum, one will find that the flux is always positive. An illustration of the flux is given in the fig. 6.3. It shows a typical example of the transfer spectrum with an established inertial range, implying a large Reynolds number. As the inertial range is shown as the nearly flat region where $T(\kappa,t) \approx 0$, this corresponds to the maximum of the flux.

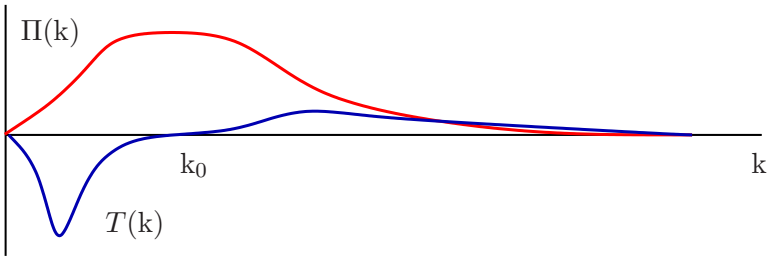

Figure 6.3: A schematic of energy flux, Π(k), red, and a typical transfer spectrum, T(k), blue.

A quantity similar to that of the normalised dissipation rate may be defined then for the maximum flux, the normalised 'flux':

$$C_\Pi \equiv \frac{\Pi_{\max}(t)}{\xi(t)}. \tag{6.16}$$

It will be shown that this parameter is equivalent or proportional (depending on whether forced or decaying turbulence is being considered) to the asymptotic value for the dissipation rate, $C_{\varepsilon,\infty}$ such that

$$\lim_{R\to\infty} C_\varepsilon = C_{\varepsilon,\infty}. \tag{6.17}$$

6.3.2 The Spectral Analysis of the Dissipation Rate

This section derives a result for the normalised dissipation rate that is central to this chapter.

Stationary Turbulence

The approach presented here follows McComb[155]. It can be explicitly shown that the injection and dissipation rates are equal to the rate of energy transfer when the Reynolds number is large. The spectral analysis for stationary turbulence is conceptually simple, and will serve as a starting point.

The starting point here is with the spectral energy balance equation:

$$\frac{\partial}{\partial t}E(\mathrm{k},t) = T(\mathrm{k},t) + W(\mathrm{k},t) - D(\mathrm{k},t). \tag{6.18}$$

This equation has been given previously in the first chapter of this thesis; the following points will summarise.

- The spectral energy density, $E(\mathrm{k},t)$, is proportional to the two-point correlation function
- the transfer spectral density function, $T(\mathrm{k},t)$, is effectively the triple correlation of the velocity fields
- $W(\mathrm{k},t)$ represents input energy due to coupling the external forcing with the velocity field
- $D(\mathrm{k},t)$ is the dissipation spectral density, which includes the viscosity in its definition.

The following definitions are given for the energy input rate and the dissipation rate,

respectively:

$$\int_0^\infty d\mathrm{k}\, W(\mathrm{k}) = w \tag{6.19}$$

$$\int_0^\infty d\mathrm{k}\, D(\mathrm{k}) = \varepsilon. \tag{6.20}$$

Under stationary turbulence, $\partial_t E(\mathrm{k}) = 0$, and integrating (6.18) over k, the conservation of energy ensures that the transfer function will vanish, leaving

$$w = \varepsilon. \tag{6.21}$$

The energy within the system is constant with its input balanced by its dissipation.

Energy production in turbulence occurs mainly at large scales and hence small wavenumbers [25]. Conversely, dissipative effects dominate at small scales and as seen above, at large wavenumbers. When the Reynolds number is large, the production and dissipation regions become separated and an inertial range emerges [155]. To specify the wavenumbers of the inertial range, they will be labelled by κ and the boundaries of the inertial range will be given as $\kappa_{\mathrm{bot}} \leq \kappa \leq \kappa_{\mathrm{top}}$. Under these conditions, the energy input rate and the dissipation rate are effectively confined to the low- and high-wavenumber regions respectively; hence, the following approximations can be made:

$$w \approx \int_0^{\kappa_{\mathrm{bot}}} d\mathrm{k}\, W(\mathrm{k}), \tag{6.22}$$

$$\varepsilon \approx \int_{\kappa_{\mathrm{top}}}^\infty d\mathrm{k}\, D(\mathrm{k}). \tag{6.23}$$

Now considering the energy transfer rate, or flux:

$$\Pi(\mathrm{k}) = \int_k^\infty d\mathrm{j}\, T(\mathrm{j}) = -\int_0^k d\mathrm{j}\, T(\mathrm{j}). \tag{6.24}$$

The energy in a wavenumber k equals the rate of energy flowing from it to all wavenumbers above it. Likewise, it is also equal to the negative rate of energy flowing into it from all wavenumbers below. Noting the shape of the transfer spectra and that when integrated over it will vanish, the flux is at its largest when it accounts for either 'half' of the transfer spectra. This entails that the flow of energy from the low

wavenumbers is as much as it can possibly be, or that the flow of energy into the large-wavenumbers is analogously as large as it can be. Wavenumbers that meet this criteria are considered to be members of the inertial range where scale invariance exists.

The flux is largest when the input range is balanced by the dissipation range since this is the maximum amount of energy that can flow into a wavenumber. When there is an inertial range present, the input range is always balanced by the dissipation within the inertial range by definition; hence the flux is maximal and constant in the inertial range:

$$\Pi(\kappa) = \Pi_{\max},$$

where κ is again used to denote a wavenumber in the inertial range. The recent high-resolution, large-Reynolds number work of Kaneda *et al* has very clear data to confirm this [145].

Taking the stationary case of (6.18) where the Reynolds number is large, and integrating along selected wavenumber ranges gives

$$\underbrace{\int_0^{\kappa_{\text{bot}}} d\mathrm{k}\, T(\mathrm{k})}_{-\Pi(\kappa_{\text{bot}}) = -\Pi_{\max}} + \underbrace{\int_0^{\kappa_{\text{bot}}} d\mathrm{k}\, W(\mathrm{k})}_{\approx w} = \underbrace{\int_0^{\kappa_{\text{bot}}} d\mathrm{k}\, D(\mathrm{k})}_{\approx 0} \tag{6.25}$$

and

$$\underbrace{\int_{\kappa_{\text{top}}}^{\infty} d\mathrm{k}\, T(\mathrm{k})}_{\Pi(\kappa_{\text{top}}) = \Pi_{\max}} + \underbrace{\int_{\kappa_{\text{top}}}^{\infty} d\mathrm{k}\, W(\mathrm{k})}_{\approx 0} = \underbrace{\int_{\kappa_{\text{top}}}^{\infty} d\mathrm{k}\, D(\mathrm{k})}_{\approx \varepsilon} \tag{6.26}$$

Hence, for large R, the dissipation rate is balanced by the rate of energy flux into the dissipation range, which is in turn balanced by the energy flux out of the energy-production range:

$$w = \Pi_{\max} = \varepsilon.$$

Considering the ratio of the dissipation rate and the maximum flux, this quantity diverges for low-R when the transfer spectral density, and thus the flux, are small. Furthermore, in the limit of infinite Reynold's number this value asymptotes to unity:

$$\lim_{\mathcal{R}\to\infty} \frac{\varepsilon}{\Pi_{\max}} = 1. \tag{6.27}$$

This relationship holds for large-to-infinite Reynolds numbers, which implies that it will do so for vanishing viscosity. Under these considerations the behaviour of the dissipation rate is not anomalous but is consistent with what should be expected for a

turbulent system containing a well-developed inertial range.

Decaying Turbulence

The original work by McComb [155] does not consider the case of freely-decaying turbulence in spectral space. However it can be shown with very simple arguments that the spectral analysis above can be generalised to the case of time-dependent turbulence. The inclusion of the nonzero time-derivative does have a distinct effect on the asymptotic dissipation rate as will be seen.

When the the system is not in a stationary state, $\partial_t E(\mathrm{k}, t) \neq 0$, whether under the influence of forcing or not, the behaviour of the maximum flux and dissipation are slightly altered. Focusing on the case of freely-decaying turbulence, the injection term is ignored and (6.18) becomes

$$\frac{\partial}{\partial t} E(\mathrm{k}, t) = T(\mathrm{k}, t) - D(\mathrm{k}, t). \tag{6.28}$$

It is important to note that while this equation is correct for all times, t, there are some equations to follow that are only valid for specific regions of time where turbulence can be reasonably assured to exist. Considering that the energy of the system is always decreasing, there will come a time when the system is no longer turbulent. This was the subject of the previous chapter, and the work of this chapter will implement it. Hence, when it becomes necessary to specify a dependence on the evolved time, the arguments of time-dependent quantities will use t_e to denote this.

Integrating over part of the wave-number spectrum, from k_0 to ∞ gives

$$\int_{\mathrm{k}_0}^{\infty} \partial_t E(\mathrm{k}, t_\mathrm{e})\, d\mathrm{k} = \Pi_{\max}(t_\mathrm{e}) - \int_{\mathrm{k}_0}^{\infty} D(\mathrm{k}, t_\mathrm{e})\, d\mathrm{k}. \tag{6.29}$$

This is an exact result, valid for all Reynolds numbers and therefore does not need to employ any limits. As before, one obtains an expression for $\Pi_{\max}$. However, the partial integration of the dissipation spectrum can be rewritten to include the dissipation rate without an approximation using

$$\int_{\mathrm{k}_0}^{\infty} D(\mathrm{k}, t_\mathrm{e})\, d\mathrm{k} = \varepsilon(t_\mathrm{e}) - \int_{0}^{\mathrm{k}_0} D(\mathrm{k}, t_\mathrm{e})\, d\mathrm{k}; \tag{6.30}$$

and hence the energy balance equation can be written

$$\int_{\mathrm{k}_0}^{\infty} \partial_t E(\mathrm{k}, t_\mathrm{e})\, d\mathrm{k} = \Pi_{\max}(t_\mathrm{e}) - \varepsilon(t_\mathrm{e}) + \int_0^{\mathrm{k}_0} D(\mathrm{k}, t_\mathrm{e})\, d\mathrm{k}. \tag{6.31}$$

With some re-arrangement the result becomes

$$\varepsilon(t_\mathrm{e}) = \dot{E}^+(t_\mathrm{e}) + \Pi_{\max}(t_\mathrm{e}) + \varepsilon^-(t_\mathrm{e}), \tag{6.32}$$

where

$$\dot{E}^+(t_\mathrm{e}) \equiv -\int_{\mathrm{k}_0}^{\infty} \partial_t E(\mathrm{k}, t_\mathrm{e})\, d\mathrm{k} \tag{6.33}$$

and

$$\varepsilon^-(t_\mathrm{e}) \equiv \int_0^{\mathrm{k}_0} D(\mathrm{k}, t_\mathrm{e})\, d\mathrm{k}, \tag{6.34}$$

have been introduced for convenience as these quantities no longer depend on spectral variables.

A key piece of information that distinguishes freely-decaying turbulence from the situation of forced turbulence is that the time-derivatives of the partial integrals over the energy spectrum in $\dot{E}^+(t_\mathrm{e})$ are negative for decaying turbulence, as the total energy is decreasing with time. This means that $\dot{E}^+(t_\mathrm{e})$ is strictly positive for an appropriately evolved time. The major implication is that now the ratio of the dissipation rate to the maximum flux is no longer unity in the infinite Reynolds number limit,

$$\lim_{\mathcal{R}\to\infty} \frac{\varepsilon(t_\mathrm{e})}{\Pi_{\max}(t_\mathrm{e})} > 1. \tag{6.35}$$

This is a strict inequality as $\dot{E}^+(t_\mathrm{e})$ cannot be zero for decaying turbulence. Multiplying this inequality by $\xi(t_\mathrm{e})/\xi(t_\mathrm{e})$ leads to a similar expression for the dissipation and flux parameters,

$$\lim_{\mathcal{R}\to\infty} \frac{C_\varepsilon(t_\mathrm{e})}{C_\Pi(t_\mathrm{e})} > 1. \tag{6.36}$$

In general,

$$\frac{\varepsilon(t_\mathrm{e})}{\Pi_{\max}(t_\mathrm{e})} = \frac{\dot{E}^+(t_\mathrm{e}) + \Pi_{\max}(t_\mathrm{e}) + \varepsilon^-(t_\mathrm{e})}{\Pi_{\max}(t_\mathrm{e})}, \tag{6.37}$$

which for the forced case is

$$\frac{\Pi_{\max}(t_\mathrm{e}) + \varepsilon^-(t_\mathrm{e})}{\Pi_{\max}(t_\mathrm{e})} = 1 + \frac{\varepsilon^-(t_\mathrm{e})}{\Pi_{\max}(t_\mathrm{e})}. \tag{6.38}$$

Hence, $\varepsilon > \Pi_{\max}$ and only when the second term on the RHS vanishes, which it does for forced turbulence in the limit of infinite R, will this equation be unity. This demonstrates that equation (6.32) formally contains the result (6.27). It can be multiplied by $1/\xi(t_{\rm e})$ to obtain an equation for the normalised dissipation rate,

$$C_\varepsilon(t_{\rm e}) = \frac{\dot{E}^+(t_{\rm e})}{\xi(t_{\rm e})} + C_\Pi(t_{\rm e}) + \frac{\varepsilon^-(t_{\rm e})}{\xi(t_{\rm e})}, \tag{6.39}$$

As was seen in both forced and decaying turbulence, the dissipation rate is intrinsically tied to the transfer of energy from the low-k region of the spectral energy. The next section re-examines these ideas in real-space with the Karman-Howarth equation.

6.3.3 The Dissipation Rate in Real Space

The previous treatment in spectral space provided a general result and some quantitative predictions about the change of the asymptotic behaviour of the dissipation and flux parameters from forced to decaying turbulence. However, it does not provide any relationship to the Reynolds number dependency that has been observed for the dissipation rate.

The arguments given above that describe the relationship between ε and $\Pi_{\max}$ may also be derived from the Karman-Howarth equation for both the decaying and stationary cases with the inclusion of a dependence on the Reynolds number. The following uses the same reasoning as can be found in [156], which is slightly different than McComb's earlier work [155]. However, the exposition of the material here is altered in that it focuses on the time-dependent case.

Decaying and Forced Turbulence

The Karman-Howarth equation can be used to derive an equation for the dissipation rate in homogeneous, isotropic turbulence (see chapter appendix),

$$\varepsilon(t) + \frac{3}{4}\frac{\partial}{\partial t}S_2(r,t) = -\frac{1}{4r^4}\frac{\partial}{\partial r}\Big(r^4 S_3(r,t)\Big) + \frac{3\nu}{2r^4}\frac{\partial}{\partial r}\Big(r^4\frac{\partial}{\partial r}S_2(r,t)\Big)., \tag{6.40}$$

where $S_n \equiv \big\langle \big(u_x(x+r) - u_x(x)\big)^n \big\rangle$ are the $n^{\rm th}$-order longitudinal velocity structure functions.

The original approach devised in [155] rescales the structure functions noting that the dimensionality is (velocity)^n,

$$S_n(r,t_{\rm e}) = U^n(t_{\rm e}) f_n(x,\tau). \tag{6.41}$$

The functions $f_n(x, t_e)$ are dimensionless functions of the dimensionless variables $x \equiv r/L(t_e)$ and $\tau \equiv tU(t_e)/L(t_e)$. Using this scaling of the structure functions is similar to the definitions of the non-dimensional longitudinal structure functions commonly found in homogeneous isotropic turbulence (see chapter appendix B). Furthermore, the time argument is specified as the evolved time and that the evolved scaled-time is $\tau_e \equiv t_e U(t_e)/L(t_e)$. It is relevant to point out here that the evolved time in forced turbulence is the time when quantities become stationary; in this case, all time arguments may be dropped and the scaling function $f_n(x)$ becomes dependent only on spatial variables.

Rewriting (6.40) using this rescaling produces

$$\begin{aligned} \varepsilon(t_e) &= -\frac{3}{4}\frac{U(t_e)^3}{L(t_e)}\frac{\partial}{\partial\tau}f_2(x,\tau)\Big|_{\tau=\tau_e} - \frac{1}{4x^4}\frac{U(t_e)^3}{L(t_e)}\frac{\partial}{\partial x}\Big(x^4 f_3(x,\tau_e)\Big) \\ &+ \frac{3\nu}{2x^4}\frac{U(t_e)^2}{L(t_e)}\frac{\partial}{\partial x}\Big(x^4\frac{\partial}{\partial x}f_2(x,\tau_e)\Big). \end{aligned} \tag{6.42}$$

Using the following definitions,

$$B_2(t_e) \equiv \frac{3}{4}\frac{\partial}{\partial\tau}f_2(x,\tau)\Big|_{\tau\equiv\tau_e} \tag{6.43}$$

$$A_3(t_e) \equiv -\frac{1}{4x^4}\frac{\partial}{\partial x}\Big(x^4 f_3(x,\tau_e)\Big) \tag{6.44}$$

$$A_2(t_e) \equiv \frac{3}{2x^4}\frac{\partial}{\partial x}\Big(x^4\frac{\partial}{\partial x}f_2(x,\tau_e)\Big), \tag{6.45}$$

and using the definitions of the surrogate, ξ, and the integral Reynolds number, R_L, (6.42) can be written

$$\frac{\varepsilon(t_e)}{\xi(t_e)} = \big(A_3(t_e) - B_2(t_e)\big) + \frac{A_2(t_e)}{R_L(t_e)}. \tag{6.46}$$

Thus, there is now an exact equation for the dissipation rate that takes into account the Reynolds number dependence,

$$C_\varepsilon(t_e) = \big(A_3(t_e) - B_2(t_e)\big) + \frac{A_2(t_e)}{R_L(t_e)}. \tag{6.47}$$

This is closely related to (6.39). It is also of interest to note that this takes exactly the same form as the upperbound of the dissipation rate as determined by Doering and Foias for the stationary case when $B_2(t_e) = 0$.

As in the spectral analysis, R_L is taken to be large which permits the negligence of

the last term, leaving the asymptotic value

$$\lim_{R_L\to\infty} C_\varepsilon(t_\mathrm{e}) = A_3(t_\mathrm{e}) - B_2(t_\mathrm{e}). \tag{6.48}$$

It was also pointed out that the terms involving the time-derivative will have a positive contribution to the asymptote. Noting the definition of B_2, its relationship to the second-order structure function is

$$B_2(t_\mathrm{e}) = \frac{3}{4}\frac{\partial}{\partial t} S_2(r,t)\bigg|_{t=t_\mathrm{e}}. \tag{6.49}$$

The significance of this is that the second-order structure function decreases with time in decaying turbulence, leaving this quantity to be negative; therefore, whatever the value determined for A_3, it will be larger by an amount determined from B_2. This can be compared to the asymptotic value of C_ε for forced turbulence which will be A_3 alone as in this case B_2 vanishes. This would reduce (6.47) to

$$C_\varepsilon = A_3 + \frac{A_2}{R_L}. \tag{6.50}$$

Taking the large-Reynolds number limit leads to the asymptotic value, $C_{\varepsilon,\infty}$, which is in fact A_3,

$$\begin{aligned} \lim_{R\to\infty} C_\varepsilon &= C_{\varepsilon,\infty} \\ &= A_3. \end{aligned} \tag{6.51}$$

Earlier arguments showed that the asymptote is actually the normalised flux; this allows the following identification:

$$C_{\varepsilon,\infty} = C_\Pi = A_3. \tag{6.52}$$

The real-space analysis gives the same result as that derived for the spectral case, namely that the finite dissipation rate is controlled by the inertial mechanisms.

It should be noted that (6.50) and (6.47) are still energy-balance equations. To see this, one can follow Tennekes and Lumley [26] and find an estimate for these results. One can write the characteristic times for the transfer, L/U and viscous dissipation, L^2/ν, of energy in the large scales, U^2; then the total rate at which energy is taken from the large scales is the sum of the rates of these two effects,

$$\frac{d}{dt}U^2 = \left(\sim U^2 \Big/ \frac{L}{U^2}\right) + \left(\sim U^2 \Big/ \frac{L^2}{\nu}\right). \tag{6.53}$$

Assuming that the bulk of the energy is contained in the large-scale structures and

using the identities $U^2 \sim E$ and $d_t E = -\varepsilon$, this result can be applied to the energy entering (as it is the negative of the energy leaving the large scales) into the viscous scales

$$\varepsilon = \left(\sim \frac{U^3}{L} \right) + \left(\sim \left(\frac{\nu}{UL} \right) \frac{U^3}{L} \right). \tag{6.54}$$

This qualitative estimate is similar to the result derived above. Additionally, one can note in passing that the form of (6.53) can be seen as the total differential operator acting on U^2 and being the sum of partial differentials of the different time-scales that U^2 is a function of,

$$\frac{d}{dt} U^2 = \frac{\partial}{\partial t_T} U^2 + \frac{\partial}{\partial t_D} U^2. \tag{6.55}$$

The variables t_T and t_D are the transfer and dissipation times respectively. This is only an observation and would require deeper analysis to demonstrate the validity of such a statement.

The Structure Functions and Reynolds Number Dependence

The formula for the structure function given by (6.41) can be generalised for any lengthscale and velocity. Using V and l to designate arbitrary velocity and lengscales, the structure functions may be written as

$$S_n(r, t_\mathrm{e}) = V^n(t_\mathrm{e}) f_n(x, \tau), \tag{6.56}$$

where the dimensionless variables are now $x \equiv r/l(t_\mathrm{e})$ and $\tau \equiv tV(t_\mathrm{e})/l(t_\mathrm{e})$. There are no assumptions to be made in writing this formula in these arbitrary variables, but once a choice is made, there are implications for the parameters A_2, B_2 and A_3.

To see how quantities can be affected by choice of lengthscale, one may consider using the Kolmogorov lengthscale. This can be done as there is freedom to choose any lengthscale and this lengthscale in particular is viscosity dependent, $\eta \sim \nu^{3/4}$. Note that this viscosity dependence is physically based and not due to an imposed definition. It is believed that eddies of size η are the smallest to exist before being destroyed by viscous forces.

Considering C_ε for forced turbulence and including the Kolmogorov lengthscale in the definition of S_n,

$$C_\varepsilon = A_3(\eta) \left(\frac{L}{\eta} \right) + A_2(\eta) \frac{\nu}{UL} \left(\frac{L}{\eta} \right)^2 \tag{6.57}$$

is divergent for $\nu \to 0$ ($R_L \to \infty$). To accept this infinity and accurately portray the physical system, the parameters A_2 and A_3 must have some ν-dependence that counters that from η. It can then be argued that A_2 and A_3 are themselves dependent on the

Reynolds number.

It cannot be demonstrated unequivocally that there is no other Reynolds dependency in C_ε aside from R^{-1}, however, given the formula derived here a choice must be made. The most natural choice is then $V = U$ and $l = L$. Similar decisions are needed in other equations given for C_ε. Doering and Foias [151] determined l to be the largest lengthscale delivered to the system via the forcing; judging from this it would seem that L is appropriate.

Quantitative Analysis of the Coefficients

In the spectral equation, expanded here as

$$C_\varepsilon(t_\mathrm{e}) = C_\Pi(t_\mathrm{e}) - \frac{L(t_\mathrm{e})}{U(t_\mathrm{e})^3}\int_{\mathrm{k}_0}^{\infty} \partial_t E(\mathrm{k}, t_\mathrm{e})\, d\mathrm{k} + \frac{L(t_\mathrm{e})}{U(t_\mathrm{e})^3}\int_0^{\mathrm{k}_0} D(\mathrm{k}, t_\mathrm{e})\, d\mathrm{k} \qquad (6.58)$$

$$= A_3(t_\mathrm{e}) - \quad B_2(t_\mathrm{e}) \quad + A_2(t_\mathrm{e})/R_L, \qquad (6.59)$$

one can identify those quantities which are analogous (if not equivalent) to the coefficient terms of (6.47). Since both derivations are based on energy balance equations, it is believed that these relationships hold. Note that in the real-space analysis, the identification of A_3 with the normalised flux C_Π required the limiting case of infinite Reynolds number, but the spectral analysis shows this to be an exact result. If this association is correct, then the connection between A_3 and C_Π in the real-space analysis is expected to hold.

One can find that the last term on the RHS of (6.58) can have a R_L^{-1}-dependence as written in (6.59) but requires some re-adjustment to obtain this.

$$\frac{L}{U^3}\int_0^{\mathrm{k}_0} D(\mathrm{k}, t_\mathrm{e})\, d\mathrm{k} = \frac{L}{U^3}\int_0^{\mathrm{k}_0} 2\nu\mathrm{k}^2 E(\mathrm{k}, t_\mathrm{e})\, d\mathrm{k} \qquad (6.60)$$

$$= \frac{1}{R_L}\left(\frac{L^2}{U^2}\int_0^{\mathrm{k}_0} 2\mathrm{k}^2 E(\mathrm{k}, t_\mathrm{e})\, d\mathrm{k}\right) \qquad (6.61)$$

This implies that

$$A_2 \equiv \left(\frac{L^2}{U^2}\int_0^{\mathrm{k}_0} 2\mathrm{k}^2 E(\mathrm{k}, t)\, d\mathrm{k}\right). \qquad (6.62)$$

The coefficients of the real-space equation of the normalised dissipation rate, (6.47), can be computed from a DNS computation where the structure functions can be

measured over the entire domain. The identification between the real- and spectral-space analyses allows these quantities to be computed in a much simpler manner. Such results can in fact be computed using the LET. Computations like this would allow both analyses to say something quantitative about the expected behaviour of normalised dissipation rate. The Reynolds number dependence of the coefficients can also be investigated using this analysis. The following section will see this put to use and display results of the coefficients.

6.4 Investigating Turbulent Dissipation Using the LET

The LET and an LET-based computational model were presented in earlier chapters and showed some success in depicting turbulent behaviour. While the higher Reynolds number computations of the decaying-LET were problematic in that they did not demonstrate a Kolmogorov inertial range, the lower-to-moderate Reynolds number computations found some support from similar DNS studies. The forced-LET also showed some evidence that it gives proper turbulent statistics, including a Kolmogorov inertial range. There is then some reason to believe that the LET-based model can be used to study the aspects of turbulent dissipation that have been outlined above.

The main quantities being investigated here are C_ε and C_Π, as well as their constituent parameters ε, $\Pi_{\max}$, and ξ. Given the preceding exposition on dissipation, there are some expectations regarding these parameters. The attributes of C_ε that are anticipated for both decaying and forced turbulence are the low-R divergence ($C_\varepsilon \sim R^{-1}$) and the large-$R$ asymptote. The small Reynolds number behaviour of both $\Pi_{\max}$ and C_Π is expected that they will vanish as $R \to 0$. For larger values of R, the spectral arguments of §6.3.2 suggest that they will asymptote with C_ε. For freely decaying turbulence, the asymptotic values of C_ε and C_Π should be separated by a finite amount whereas in forced turbulence they should be equivalent. The same belief is held for ε and $\Pi_{\max}$. The behaviour of ξ is also unknown, though like $\Pi_{\max}$, it might be expected to vanish at small values of R since $U \to 0$.

6.4.1 Decaying Turbulence

Chapter 5 noted that the time-dependence of the investigated parameters required a time in which measurements accurately represent a decaying turbulent system. It was decided that the evolved time being used to illustrate the LET results for decaying turbulence will be $t_D + 2\tau_D$. This choice places the measurement when both $E(t)$ and $\varepsilon(t)$ are in a power-law decay. This is consistent with contemporary results [125, 127] and possibly those of previous wind-tunnel experiments such as those noted in

Sreenivasan [126].

In the desire to check the results against a more accurate portrayal of a turbulent system, a subset of the results presented here have also been supported using DNS computations. It is only a subset in that the current capabilities of the DNS do not include the measurement times $t_D + 2\tau_D$ nor are they able to compute high-Reynolds number computations. The first of these is mitigated by using one of the evolved times, $t_{\Pi|\varepsilon}$, and shows agreement to the LET data to moderate Reynolds numbers, $R_L \sim 80$. The LET is able to reach higher Reynolds numbers and these results are shown separately.

Normalised Values: C_ε and C_Π

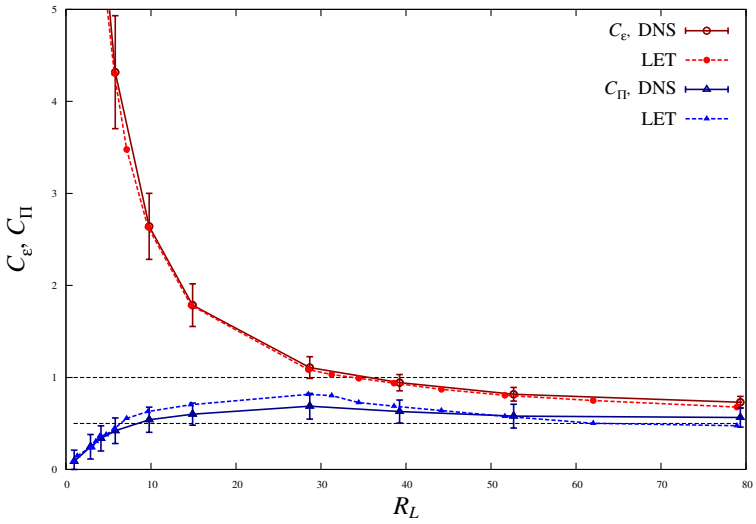

Figure 6.4: Comparison plots of C_ε and C_Π for decaying turbulence from Spectrum V using LET- and DNS-computed data, with the evolved time $t_{\Pi|\varepsilon}$ against integral lengthscale Reynolds numbers.

Figures 6.4 and 6.5 show the quantities C_ε and C_Π with both LET and DNS results. As noted, these plots have been taken at the evolved time $t_{\Pi|\varepsilon}$ and show very good agreement between the computations in the plot of C_ε for Spectrum V in fig. 6.4. The accompanying plot of C_Π in the same figure agrees reasonably well among LET and DNS, and within the error-bars of the DNS. While it is not clear that the asymptotic value has been reached in any of the computations, the value of C_ε corresponding to the highest R_L appears to be 0.7 in both cases; this seems appropriate to the values given in the literature, 0.8-1.1 (see above).

The asymptotic values produced by the LET for later measurement times and larger

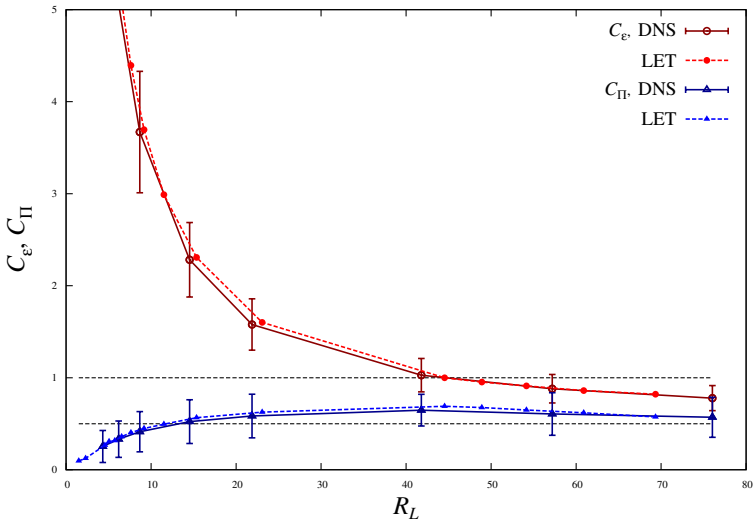

Figure 6.5: Comparison plots of C_ε and C_Π for decaying turbulence from Spectrum VI using LET- and DNS-computed data, with the evolved time $t_{\Pi|\varepsilon}$ against integral lengthscale Reynolds numbers.

Reynolds numbers, figs. 6.6 and 6.7, present a slightly different picture. In both figures, the asymptotic state is not clearly established at these Reynolds numbers, and therefore it cannot be said with certainty what the asymptotes are. The best that can be said for the earlier time, $t_{\Pi|\varepsilon}$, is that the values are approaching 0.6 and 0.7 for Spectrum V and VI, respectively. The later measurements using $t_D + 2\tau_D$ show these values to be elevated to $\sim$0.8 in both cases. These are closer to those given in the literature as might be expected given that the times used for these measurements are compatible with those in the literature.

The plots of C_Π can also be seen in these figures, but it shows more tolerance to the variability in the measurement times with a reasonable collapse of points onto the same curve for both spectra. In the plot of C_Π of Spectrum V, the curve tends to slowly decrease as R_L increases. Figure 6.7 shows a different scenario of C_Π looking arguably flat which is more apparent in the later time measurement. In both cases the value of the curve in the large-R_L regions appears to be in the range of 0.4-0.45;. This value is not significantly different from that of C_ε for forced turbulence (compare to fig. 6.17 of the next section).

Some further insight can be obtained by plotting these results on log-log coordinates, as in figs. 6.8 and 6.9. In both figures, the line $y \propto 1/x$ is given, and in both figures the low-R_L curves conform to this slope. This appears to demonstrate the R_L^{-1}-behaviour of C_ε as shown by Sreenivasan [126]. Using log-log coordinates here shows that there is not

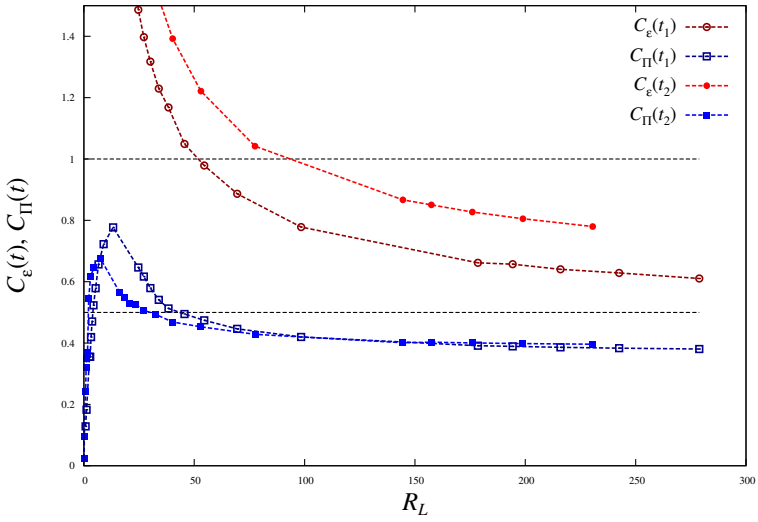

Figure 6.6: Plots of C_ε and C_Π for decaying turbulence from Spectrum V using the LET; two evolved times are compared, $t_1 = t_{\Pi|\varepsilon}$ and $t_2 = t_D + 2\tau_D$.

a significant part of these curves that suggests a unequivocal asymptote. Rather, the values of C_ε corresponding to the highest-R_L obtained in these computations indicate that C_ε is still transitioning from the R_L^{-1}-behaviour.

The plots of C_Π in log-log coordinates show some features that require further explanation. Most notable is the slope of the curve in the low-R_L region. For those plots corresponding to $t_{\Pi|\varepsilon}$, this slope appears to have a linear dependence on R_L, but this becomes ambiguous for the later time measurements. The later measurements also appear to be discontinuous in this region. The origin of these discontinuities is unknown at this time. One possibility to consider is that they may be related to the discrete wavenumbers used in these computations. The value of k_0 which is used to compute $\Pi_{\max}$ is confined to the lattice-spacing of the grid, and therefore introduces some discretisation errors when computed. The belief here is that the error is more significant at higher viscosities. A resolution to this would be to compute these values using a smaller lattice spacing. The lattice spacing used here is meant to be consistent throughout all computations and is thus fixed to unity as suggested in a previous chapter (see §3.4.2).

Unnormalised Values: $\varepsilon(R_L)$, $\Pi_{\max}(R_L)$, and $\xi(R_L)$

There is some understanding to be gained from the individual behaviours of the constituent quantities of the normalised quantities. As with C_ε and C_Π, the low-R_L plots of ε, $\Pi_{\max}$, and ξ obtained using LET2008 can be supported with DNS.

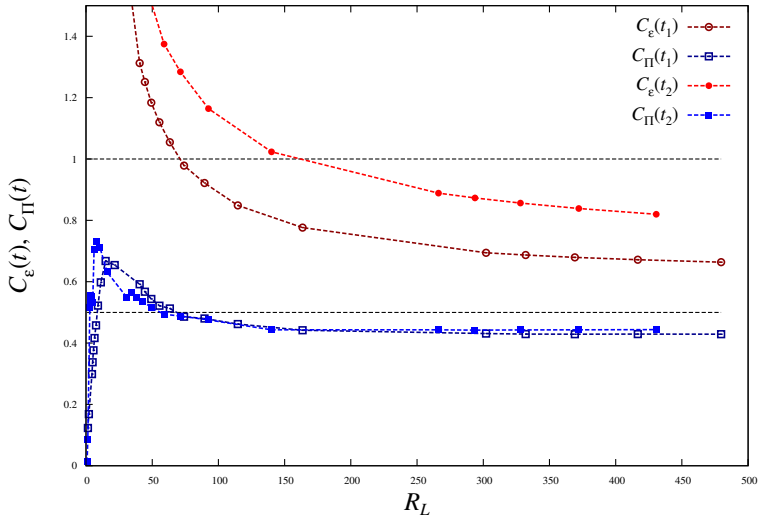

Figure 6.7: Plots of C_ε and C_Π for decaying turbulence from Spectrum VI using the LET; two evolved times are compared, $t_1 = t_{\Pi|\varepsilon}$ and $t_2 = t_D + 2\tau_D$.

These are shown in figs. 6.10 and 6.11. Again, in those plots of spectrum V, there is good agreement among the LET and DNS computations. The most noticeable discrepancies occur primarily with the $\Pi_{\max}(R_L)$, which suggests this as the reason for similar discrepancies seen earlier in fig. 6.4. As in the normalised case, the plots for quantities associated with Spectrum VI show very good agreement between LET and DNS.

It can be seen in these figures that the shape of $\varepsilon(R_L)$ resembles that of C_ε, as one might expect. The extent in Reynolds number is limited, so little can be said about the asymptotic behaviour of $\varepsilon(R_L)$ except that ε is always larger than $\Pi_{\max}$. This relationship is due to the spectral dynamics of a decaying turbulent system. Division by ξ will preserve this relationship, as seen in the figures for C_ε and C_Π.

When larger values of Reynolds number are used, as is the case in figs. 6.12 and 6.13, some slight changes occur. These plots also compare these parameters at the evolved and measurement times. In all cases, the asymptotic behaviour of all parameters is more apparent and there appears to be a trend in that all parameters increase with increasing R_L.

It was discussed in the previous chapter that the low-R behaviour of ε is drastically affected by when the measurement is made. It should be noted that in figs. 6.6 and 6.7 the value of C_ε in the low-R region for both times is quite large. The explanation for this is that ξ approaches zero faster than the dissipation rate does. This is consistent with the concept that viscous dissipation will be the dominant agent for low Reynolds

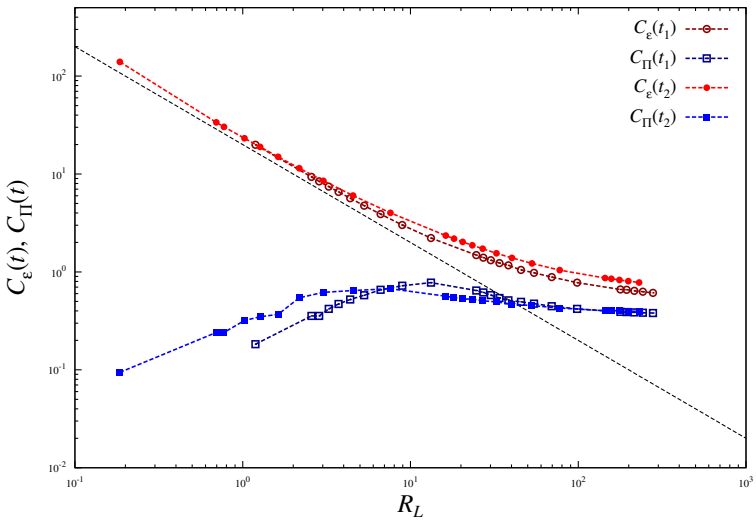

Figure 6.8: Log-log plots of C_ε and C_Π for decaying turbulence from Spectrum V using the LET; two evolved times are compared, $t_1 = t_{\Pi|\varepsilon}$ and $t_2 = t_D + 2\tau_D$.

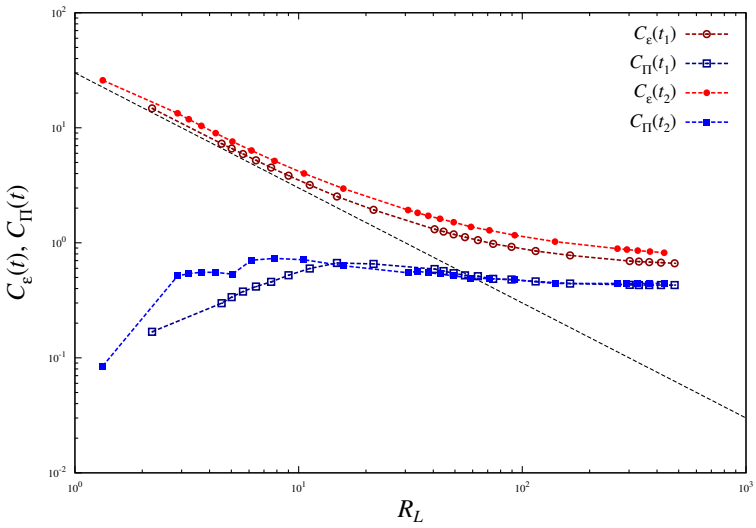

Figure 6.9: Log-log plots of C_ε and C_Π for decaying turbulence from Spectrum VI using the LET; two evolved times are compared, $t_1 = t_{\Pi|\varepsilon}$ and $t_2 = t_D + 2\tau_D$.

number systems. In a similar vein, but contrary in its approach to zero relative to the surrogate, the maximum flux approaches zero fast as the Reynolds number is decreased. Again, as viscous forces dominate, there is less likely to be any significant transfer of energy. Just beyond this range, the curves of $\Pi_{\max}$ and the dissipation rate are very similar in shape, looking to only be different by an additive constant. Such a result

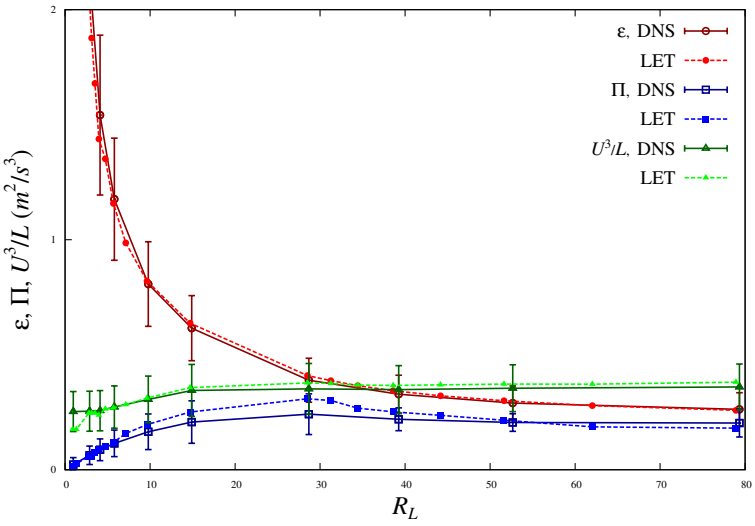

Figure 6.10: DNS/LET comparison plots of the time-dependent unscaled quantities $\varepsilon(R_L)$, $\Pi_{\max}(R_L)$, and $\xi(R_L)$ using Spectrum V, with evolved time $t_{\Pi|\varepsilon}$ against integral lengthscale Reynolds numbers.

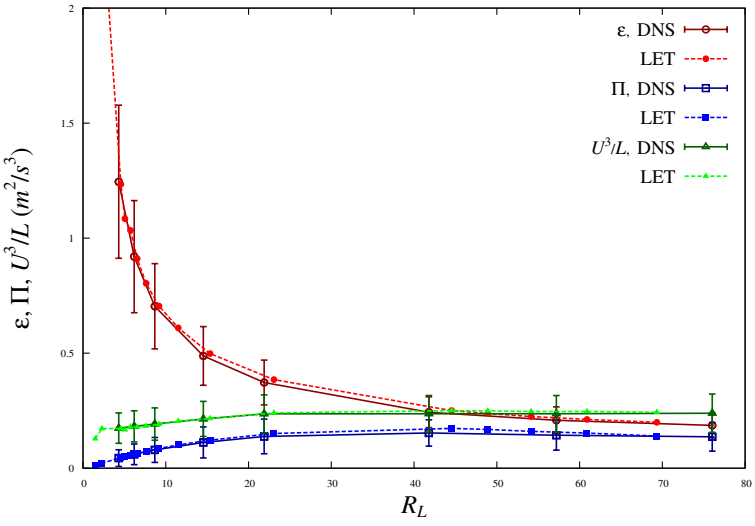

Figure 6.11: DNS/LET comparison plots of the time-dependent unscaled quantities $\varepsilon(R_L)$, $\Pi_{\max}(R_L)$, and $\xi(R_L)$ using Spectrum VI, with evolved time $t_{\Pi|\varepsilon}$ against integral lengthscale Reynolds numbers.

supports the claim that the dissipation rate is in effect controlled by the flux.

One final note concerning these results is that the log-log plots did not give any information that would be useful to the current understanding of these parameters. This

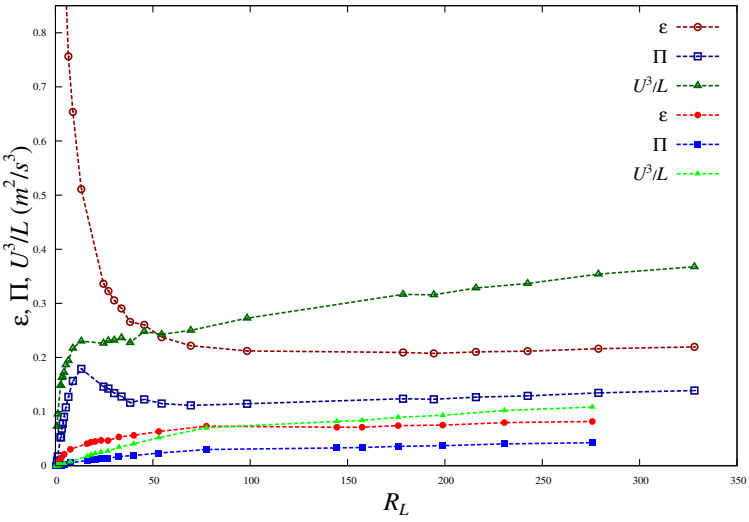

Figure 6.12: Plots of the time-dependent unscaled quantities $\varepsilon(R_L)$, $\Pi_{\max}(R_L)$, and $\xi(R_L)$ using the LET to compute Spectrum V, $t_1 = t_{\Pi|\varepsilon}$ and $t_2 = t_D + 2\tau_D$.

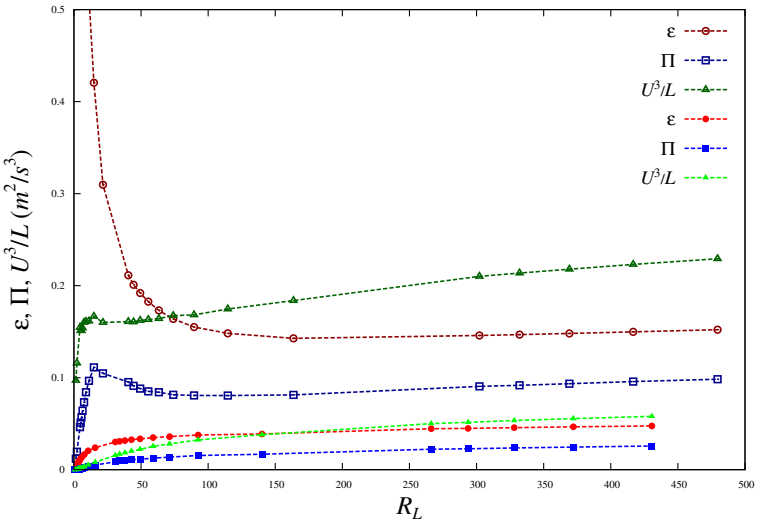

Figure 6.13: Plots of the time-dependent unscaled quantities $\varepsilon(R_L)$, $\Pi_{\max}(R_L)$, and $\xi(R_L)$ using the LET to compute Spectrum VI, $t_1 = t_{\Pi|\varepsilon}$ and $t_2 = t_D + 2\tau_D$.

is not to suggest that there is no use to plotting these parameters with this method. At this stage however, such results are pending further consideration and have been omitted from this thesis.

The Components A_2, A_3, and B_2

The coefficients given by (6.43)-(6.45) can be computed in both the LET and DNS computations. Looking at these can offer some clues as to which mechanisms play an important role in the Reynolds number dependence of C_ε. It was assumed that these

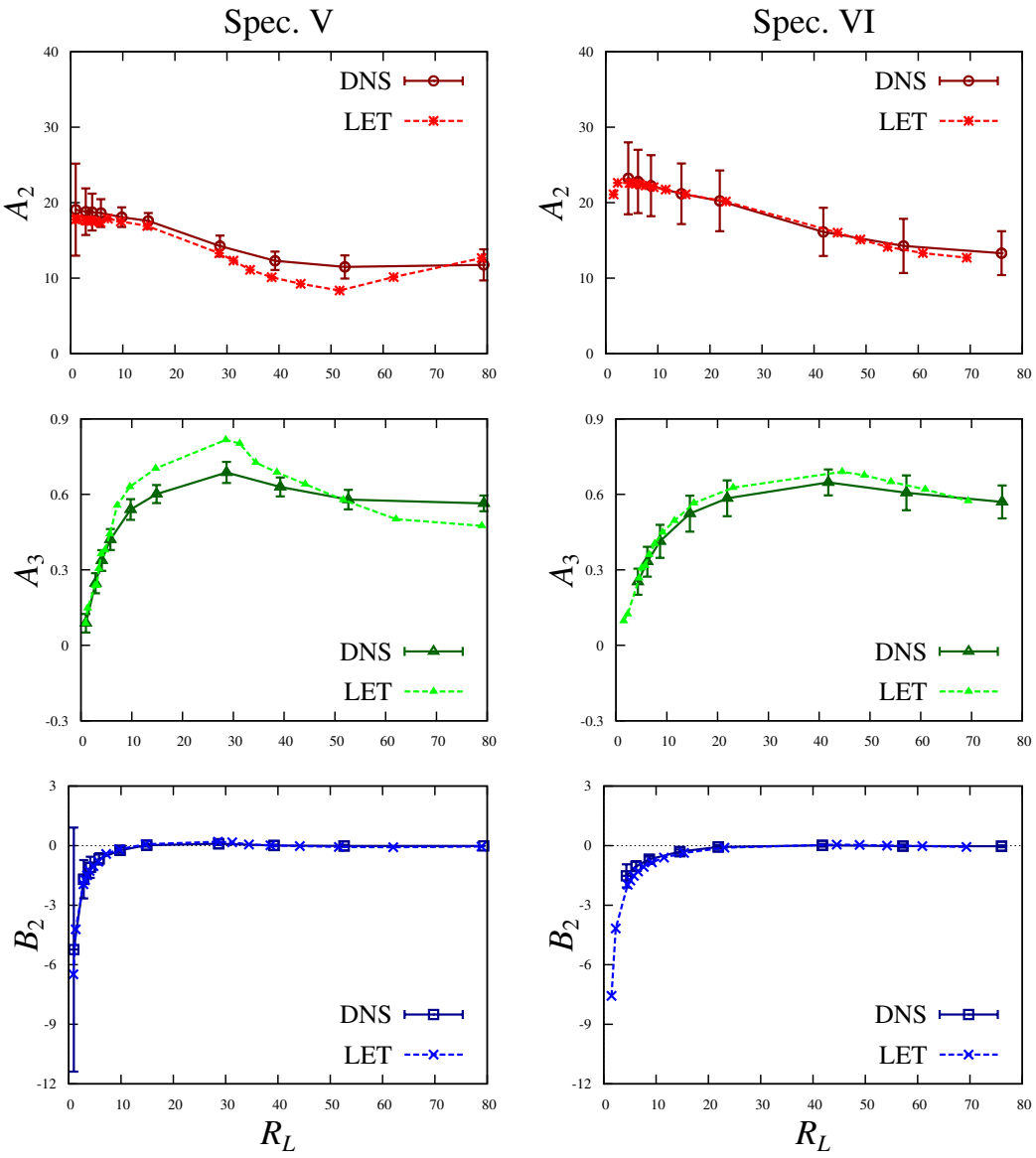

Figure 6.14: DNS/LET comparison plots of the time-dependent coefficients A_2, A_3, and B_2 using Spectrum V (left) and Spectrum VI (right), with evolved time $t_{\Pi|\varepsilon}$.

coefficients would have some dependence on the Reynolds numbers. This appears to be consistent with the results presented in figs. 6.14-6.16. The strongest dependencies

are found in the low-R behaviour of all plots and the large-R behaviour found in A_2.

The plots in fig. 6.14 give some indication of how these components behave for a small range of Reynolds numbers, comparing the results between the two computations (LET and DNS). As previously seen, the matching is quite decent for both spectra. The components A_3 and B_2 perform as expected; both have a transient part for low- to moderate Reynolds number but become a constant (or slowly varying) function of R_L. The behaviour of A_3 is exactly the same as C_Π by definition. The other quantity, A_2, displays no certain trends at such small values of R_L; the Reynolds number must be increased to obtain more detail. Figure 6.15 shows the components A_2, A_3, and B_2 in the extended range of Reynolds numbers seen in the earlier figures. While again A_3 and B_2 exhibit no significant departures from their suspected behaviours, the dependence of A_2 on the Reynolds number has a pronounced effect. The curves, again using two different times, show a strong dependence on R_L. The shape of the curve for A_2 suggests a Reynolds number dependent function of the form

$$A_2 = h_1 R_L^{-1} + h_2 + h_3 R_L. \tag{6.63}$$

Since this component contributes to C_ε as $A_2 R_L^{-1}$, this would leave the linear part of (6.63) to occur as a constant, h_3, and hence

$$C_\varepsilon = A_2/R_L + |B_2| + A_3 \xrightarrow[R_L\to\infty]{} h_3 + |B_2| + A_3. \tag{6.64}$$

It is surprising that there should be some additional increase in the asymptote of C_ε by a term

$$\varepsilon^- = \int_0^{\mathrm{k}_0} 2\mathrm{k}^2 E(\mathrm{k},t)\, d\mathrm{k} \xrightarrow[R_L\to\infty]{} 0. \tag{6.65}$$

To see this, consider that as turbulent activity is increased, the bulk of the energy in the dissipation spectrum is in the higher-wavenumbers, $k > \mathrm{k}_0$, hence ε^- should become vanishingly small in this limit. This issue has not been thoroughly explored as these are the most recent developments, however one can gain some information by using a different perspective. Plotting the components in log-log coordinates can help to probe this supposed linear-dependence. This is given in fig. 6.16. The dashed line in the plots of A_2 correspond to $y \propto x$, which in this case is a linear function of R_L. Immediately one can see that, according to these results, that the large-Reynolds number dependence of A_2 is not linear but a function of a lower order in R_L. This

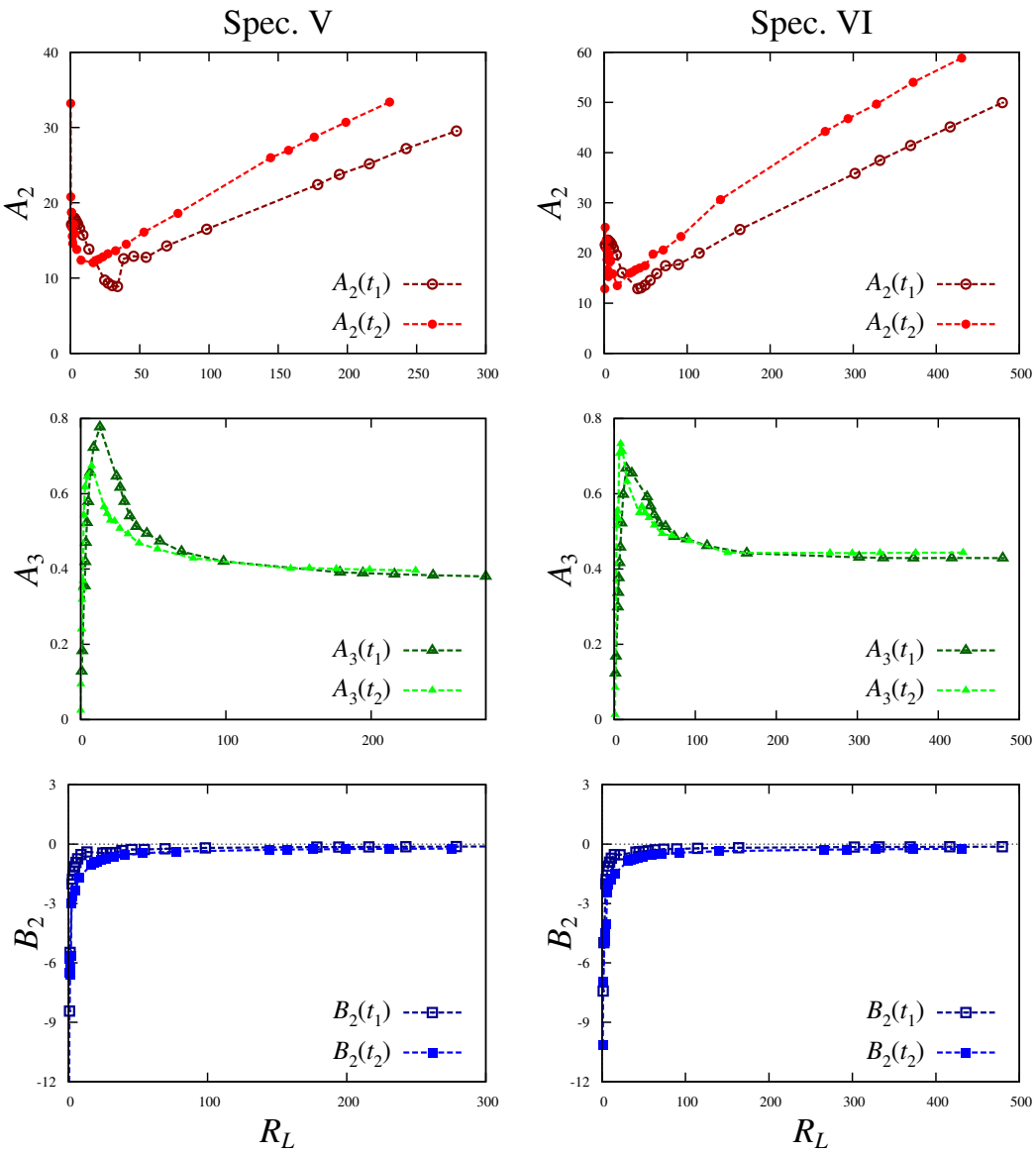

Figure 6.15: LET-plots of the time-dependent coefficients A_2, A_3, and B_2 using Spectrum V (left) and Spectrum VI (right); two evolved times are compared, $t_1 = t_{\Pi|\varepsilon}$ and $t_2 = t_D + 2\tau_D$.

would be compatible with the accepted phenomenology as described earlier since

$$\begin{aligned} C_\varepsilon &= A_2/R_L + |B_2| + A_3 \\ &= \frac{\left(h_1 R_L^{-1} + h_2 + h_3 R_L^q\right)}{R_L} + |B_2| + A_3 \xrightarrow[R_L\to\infty]{} |B_2| + A_3. \end{aligned} \tag{6.66}$$

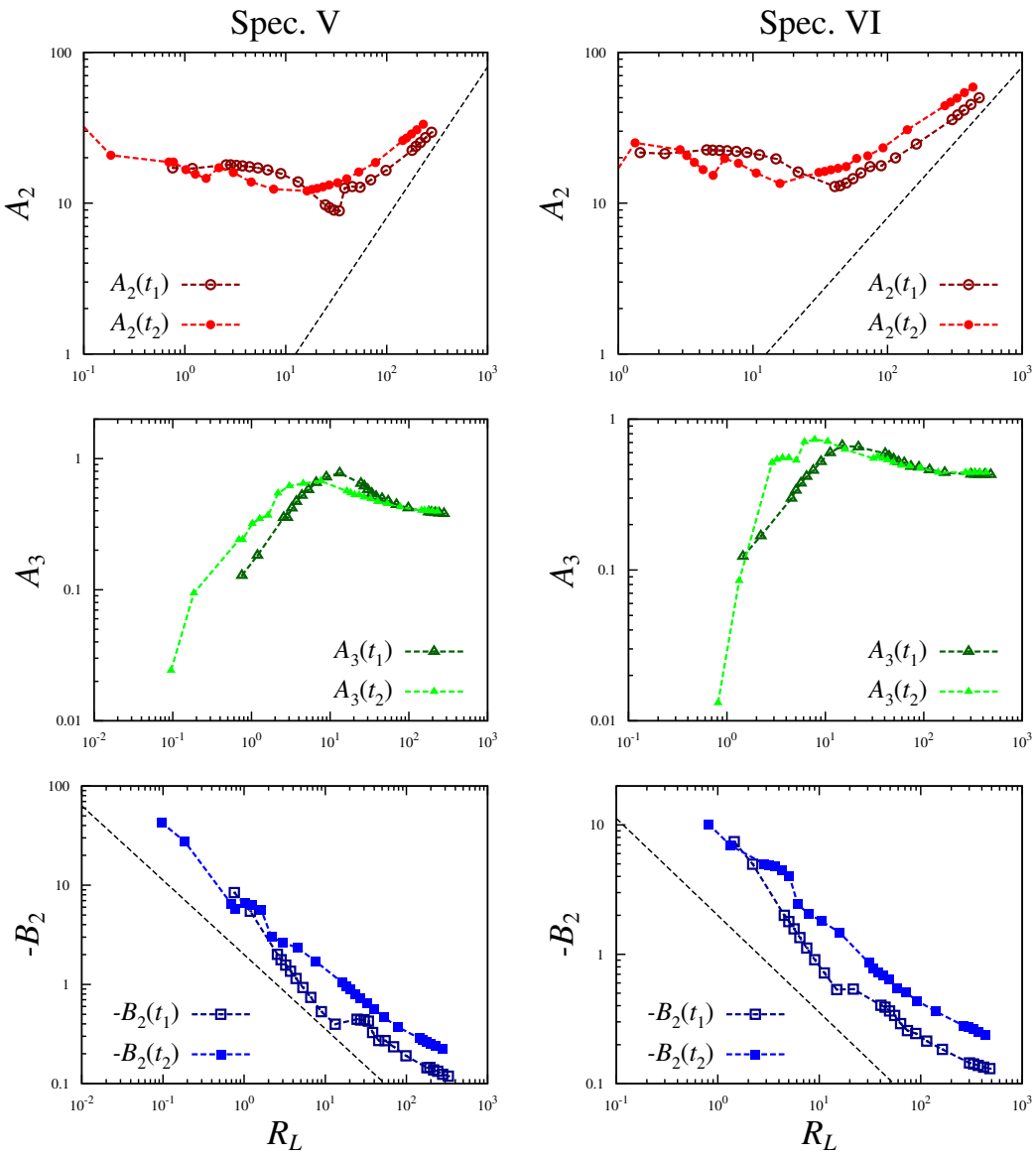

Figure 6.16: Log-log plots of the time-dependent coefficients A_2, A_3, and B_2 using the LET to compute Spectrum V (left) and Spectrum VI (right); two evolved times are compared, $t_1 = t_{\Pi|\varepsilon}$ and $t_2 = t_D + 2\tau_D$.

The quantity q is some positive (rational) exponent less than unity and will therefore allow for A_2/R_L to be a decreasing function of R_L that will vanish in the limit of infinite Reynolds number. While this subject is due more investigation it can be said that the behaviour of A_2 is connected with the decay of energy and will be much different when compared with stationary turbulence in the next section.

A final note about the R_L-dependence of B_2. In the figure, here plotting $-B_2$, there appears to be a case for arguing a $1/R_L$ dependence. It cannot be said with certainty that this is true for all Reynolds numbers as on closer inspection, there is a slight up-turn in the extreme end of the Reynolds number range.

6.4.2 The Dissipative Anomaly in Stationary Turbulence

Much of the current research looking into the normalised dissipation rate focuses on forced turbulence, and in order to make proper comparisons, the ideas expressed here should also be applied to it. It has been observed earlier that the present DNS does not yet incorporate stationary turbulence into its abilities, so the results obtained thus far and presented here are only those of the LET2008 computational model.

Normalised Quantities: C_ε and C_Π

The results for the normalised dissipation rate and maximal flux are seen in figs. 6.17 and 6.18 with the latter expressing these quantities in log-log coordinates. Some of the general features of C_ε and C_Π from the case of freely decaying turbulence are seen here. The value of C_ε is quite large for small Reynolds numbers and decays to a constant, expressing the "dissipation anomaly" result as Reynolds number increases. Noting the peak of C_Π in the small-R_L range, this is consistent with what has been seen in the case of computations of freely-decaying turbulence. The main feature that distinguishes the normalised dissipation rate of forced turbulence from that of decaying is the convergence of C_ε and C_Π for large Reynolds numbers. This is in particular a new result in showing the connection between the flux and the dissipation rate as both quantities are not considered together in the available literature. Again, this is anticipated from the phenomenology as the viscosity dissipates only what can be fed into it, and the rate of energy going into the dissipation range is directly controlled by the energy flux from the lower energy-containing wavenumbers. Thus the dissipation rate is limited by the rate of energy transfer. In contrast with the 'decaying' results, the dissipation rate is also limited by the time-derivative of the energy spectrum, increasing the asymptote of C_ε.

The coincidence of these curves is apparent but the possibility exists that it might not continue for larger Reynolds numbers. These results do not continue for large enough Reynolds numbers, which in the literature extends into three orders of magnitude. Furthermore, the asymptote is not clearly established by these computations though the amount of decrease seems to be slowing. The best that can be offered for an asymptotic value of C_ε is that it is near 0.4 (other research puts the value at 0.5). This is also similar to the value obtained for C_Π in the computations

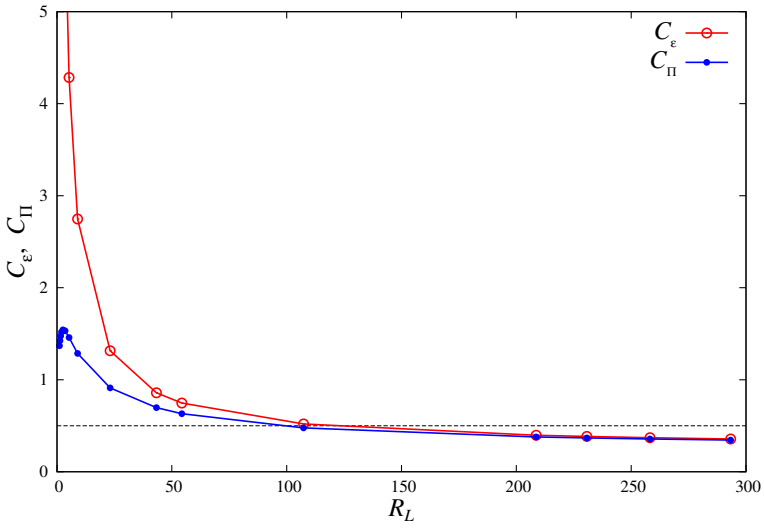

Figure 6.17: Plot of C_ε and C_Π for stationary, forced turbulence using the LET.

of the free decay, suggesting that it, and hence $\Pi_{\max}$, is not significantly affected by the decay of energy in the system. Current understanding supports this result of the inertial mechanism in that it is responsible for the exchange of energy throughout the fluid and in doing so conserves the total energy.

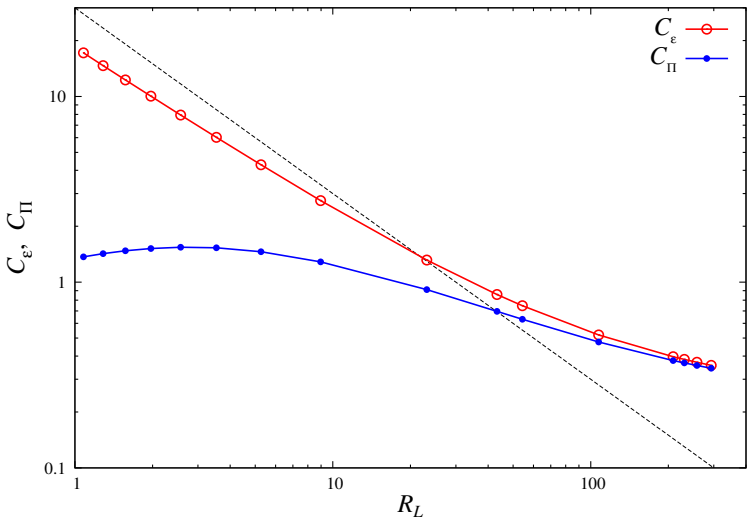

Figure 6.18: Log-log plot of C_ε and C_Π for stationary, forced turbulence using the LET.

The log-log plot of these quantities shows again that the Reynolds numbers are too low to detect an appreciable asymptote. It can also be see that these results demonstrate

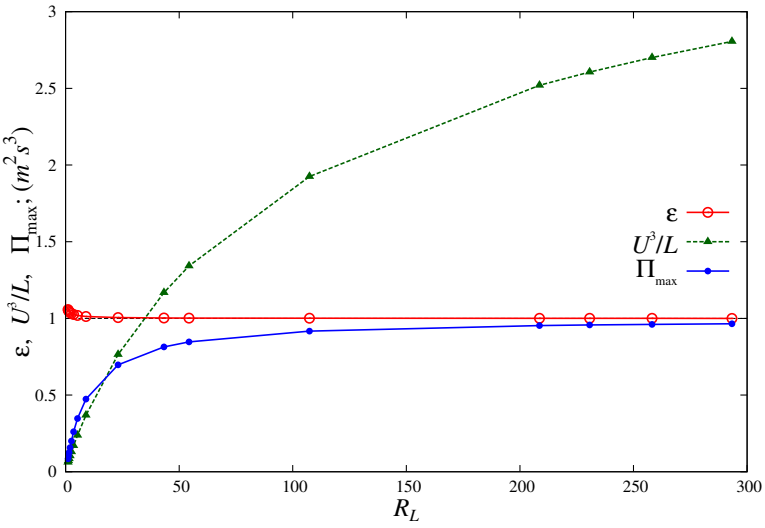

Figure 6.19: Plots of the time-dependent coefficients $\varepsilon(R_L)$, $\Pi_{\max}(R_L)$, and $\xi(R_L)$ using the LET.

slightly different picture from that of the expected and documented phenomenology. The low-R_L exponent of C_ε does not assume the predicted value of -1, but deviates from it with a fitted value of -.88 (not shown). It is not expected that this data suggest a new result but rather that this is an artifact of the LET2008 code. A similar flaw can be found in the plot of $\varepsilon(R_L)$ in fig. 6.20 where it is expected, by construction, that the dissipation rate is fixed to unity for all Reynolds numbers. This demonstrates the inability of the current LET model to accurately depict the physics of HIT at low-Reynolds numbers. Further tests were carried out with finer wavenumber and time resolutions but did not correct this artifact.

Unnormalised Quantities: ε, $\Pi_{\max}$ and ξ

The unnormalised quantities are also plotted for these computations and are given in fig. 6.19. As noted above, the small-R_L behaviour of ε is problematic but does assume a proper form, unity, as the Reynolds number is increased. Noting the shape of C_ε in fig. 6.17 and the constant dissipation rate, the picture offered in the current figure is that the low-R behaviour is determined by the surrogate, $\xi(R_L)$, which disappears at the origin. There is however no indication that the surrogate will stop growing, though further exploration of this is needed for assurance. One can argue that there is no justification that the present results show an asymptote of $\Pi_{\max}$ which could then be used to measure the behaviour of ξ against. The value of $\Pi_{\max}$ will only reach ε at $R_L \to \infty$, but to consider the asymptotic state of $\Pi_{\max}$ these quantities would be

expected to coincide more than what is seen here.

The Components A_2, A_3, and B_2

The components of C_ε as given by (6.42) show some differences when C_ε is obtained from forced turbulent computations. There is no term B_2 as this is identically zero for stationary turbulence. The shape of $A_3 = C_\Pi$ should also be unaffected, as discussed above. It is then A_2 which displays the most notable changes when a steady energy input is maintained.

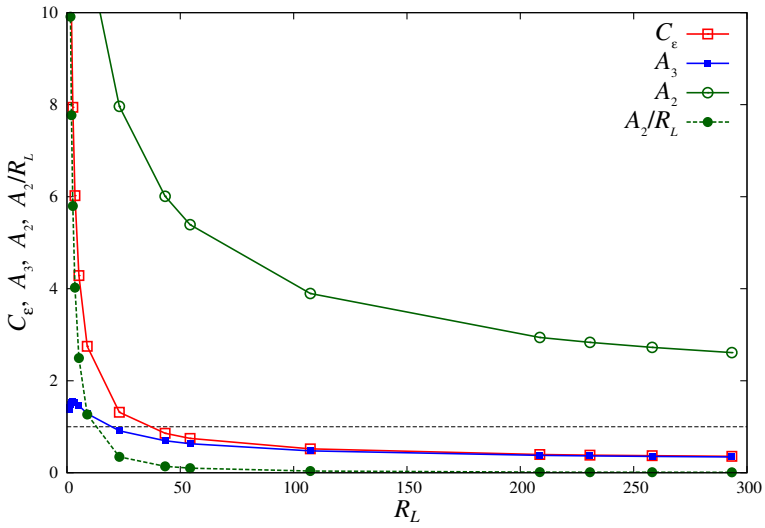

Figure 6.20: Plots of the coefficients A_2, A_3, and the quantities C_ε and A_2/R_L using the LET for stationary forced turbulence.

Figure 6.20 shows all the components of C_ε. The plot of A_2 here is very different from its time-dependent version in its dependence on the Reynolds number for forced turbulence. Rather than having a dependence on R_L with a positive non-unity exponent, the shape immediately shows that this exponent is negative and therefore A_2 decreases with increasing Reynolds number. Plotting A_2/R_L confirms that this influence on C_ε falls off quite rapidly.

To understand why this is so different from the results of freely decaying turbulence, it is worthwhile to discuss this in more detail. For stationary turbulence, the dissipation rate is fixed by the constant rate of energy being input into the lower wavenumbers. This means that $\varepsilon^+ + \varepsilon^-$ is also fixed. Arguing that $\varepsilon^+ \to \varepsilon$ in the limit of large Reynolds numbers implies that ε^- must vanish under the constraint of the constant dissipation rate.

For freely-decaying turbulence, there is no evidence to suggest that ε is fixed for

all Reynolds numbers. Evidence has been found in the current work suggesting that the unnormalised dissipation rate also increases, though this becomes noticeable only when the Reynolds numbers are quite large. Further investigation is needed to confirm this for the current results, specifically in the case of the LET.

The increasing dissipation rate can also be found in the so-called 'enstrophy catastrophe', where the enstrophy, $\frac{1}{2}\big\langle\big(\nabla\times\mathbf{u}(\mathbf{x},t)\big)^2\big\rangle$, diverges for infinite Reynolds number (and possibly finite time) [27]. The enstrophy is connected to the dissipation rate via $\varepsilon=\frac{1}{2}\nu\big\langle(\nabla\times\mathbf{u})^2\big\rangle$ and this further implies that

$$\frac{1}{2}\big\langle(\nabla\times\mathbf{u})^2\big\rangle=\int_0^\infty 2\mathrm{k}^2E(\mathrm{k},t)\,d\mathrm{k}, \tag{6.67}$$

is independent of viscosity. Hence the RHS must also diverge for $R_L\to\infty$, and therefore, in the finite-R_L case, the peak value of $\varepsilon(t)$ would grow (presumably) without bound as the Reynolds number grows.

Returning to the subject of $A_2(R_L)$, the implication is then that $\varepsilon^+ + \varepsilon^-$ must also increase with increasing Reynolds number when the turbulence is allowed to decay freely. The partial dissipation rate ε^+ might be expected to approach ε similar to the case of stationary turbulence but it is uncertain at this point how.

It is believed here that the primary factor responsible for this difference is the zero-crossing wavenumber, $\mathrm{k}_0(R_L)$. For systems with a fixed rate of energy injection, which is fixed in time but also for all Reynolds number considered, $\mathrm{k}_0(R_L)$ will also be fixed as the extent in wavenumber space of the input of energy is also fixed. To see this, one can consider the energy balance equation for stationary turbulence,

$$T(\mathrm{k})+W(\mathrm{k})=D(\mathrm{k}). \tag{6.68}$$

The antisymmetric shape of $T(\mathrm{k})$ includes a negative part, $\mathrm{k}<\mathrm{k}_0$, that must be completely accounted for by the energy input, or work, spectrum $W(\mathrm{k})$ to maintain the positivity of the dissipation spectrum $D(k)$ for all wavenumbers. This can be seen in fig. 6.21 below.

Hence, for $\mathrm{k}\le\mathrm{k}_0$

$$\big|T(\mathrm{k})\big|<W(\mathrm{k}). \tag{6.69}$$

As $W(k)$ is fixed in stationary turbulence for all R_L, k_0 must also be fixed, if not for all Reynolds numbers, at least beyond a particular value $R_L>R_L^{(\mathrm{c})}$. This is idealised in computations where $W(\mathrm{k})$ has an exact cut-off but this will not compromise the generality of the argument. It remains to be seen how these arguments can be extended to include decaying turbulence, and if so, how it can tie in the behaviour of A_2 as a

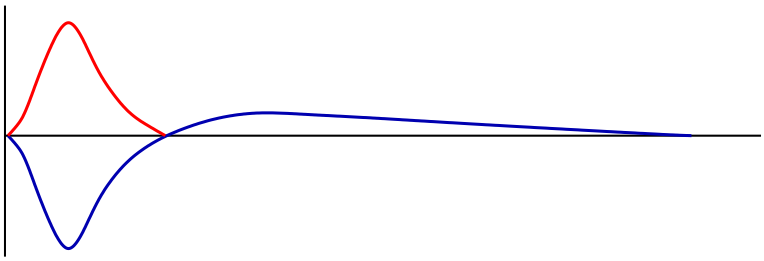

Figure 6.21: Schematic of the work and transfer spectra, $W(\mathrm{k})$ (red) and $T(\mathrm{k})$ (blue), respectively. For such an extreme case as this $D(\mathrm{k} \leq \mathrm{k}_0) = 0$.

function of R_L.

6.5 Discussion

An equation was obtained based on the spectral energy balance equation, giving the normalised dissipation rate C_ε as a function of the Reynolds number and the time in the case of decaying turbulence,

$$C_\varepsilon(R_L,t) = C_\Pi(R_L,t) + \frac{\dot{E}^+(R_L,t)}{\xi(R_L,t)} + \frac{\varepsilon^-(R_L,t)}{\xi(R_L,t)} \tag{6.70}$$

$$= A_3(R_L,t) - B_3(R_L,t) + \frac{A_2(R_L,t)}{R_L}. \tag{6.71}$$

This result is quite general and although its derivation and application used homogeneous, isotropic turbulence, these constraints are not necessary provided the pressure term in the Navier-Stokes equation can be effectively dealt with.

The spectral formulation developed here can be associated with that of McComb [155] (reproduced above in (6.69)). Provided this association is valid, then this formulation allows an equivalent computation to determine the coefficients derived in the McComb relation. As seen using the LET computational model, these coefficients can be directly computed.

6.5.1 Conclusions

It has been found that the values obtained for the normalised dissipation rate for decaying and forced turbulence are in agreement with those found in the available literature. For freely decaying turbulence, the asymptotic value of C_ε using the LET has been found to be 0.75 and 0.85 for initial Spectra V and VI, respectively. These values were obtained using the latest measure of evolved time established in the previous

chapter. Present data give a range for this value to be 0.8-1.1 (see above for references).

The value of C_ε found for forced turbulence is ~ 0.4, which is also compatible with established results. Similarly, the value of the normalised energy flux was obtained for decaying turbulence and found to be 0.4 and 0.45 for Spectra V and VI, respectively. One of the main results established here is the role of the energy transfer in the non-vanishing dissipation rate. This chapter illustrates that the energy transfer in the form of the flux is the driving influence to the asymptote of C_ε.

The real-space result, (6.70), shows an explicit Reynolds number dependence and it is only by association that the spectral result, (6.71), has a similar form. The results here demonstrate that the coefficents given in (6.70) are dependent on the Reynolds number; this dependence is even more pronounced in freely-decaying turbulence where the coefficient A_2 shows a power-law dependence for large Reynolds numbers.

6.5.2 Future Work

While (6.70) has been associated with the McComb's equation, (6.47), this association has not been demonstrated formally through an analytic proof. The spectral energy balance is claimed to be the Fourier transform of the Karman-Howarth equation [24], and while not demonstrated here it is believed that a more rigorous proof can be made to show that McComb's coefficients are exactly those terms found in the above equation, (6.70).

Using a computation that simulates the complete velocity field such as DNS, one can compute the structure functions $S_2(\mathrm{r}, t)$ and $S_3(\mathrm{r}, t)$. This would allow a direct quantitative measure on the Karman-Howarth result of McComb. The value of coefficients found in this manner can also be compared against those obtained using the methods developed here.

It must addressed that the LET2008 computations are not entirely sound for larger Reynolds numbers in the case of decaying turbulence; this can have implications when determining the proper behaviour of all coefficients. Therefore, more testing would be required to establish these results on more general grounds in terms of computational results. Earlier chapters also found the LET to give an inertial range incompatible with Kolmogorov's result for freely-decaying turbulence. Nonetheless, the data presented here agree with established results from the literature. Indeed the mechanism responsible for dissipation itself can be said to depend on the existence of an inertial range. One can suggest using such results to determine the effect of an 'incorrect' inertial range on the values obtained for the coefficients associated with C_ε.

As the main result of this chapter, the equation for the dissipation rate, (6.70), and the quantities associated with it, namely the coefficients A_2, B_2, and A_3, can be computed for presumably any given system. Future work would see these quantities related to the characteristic features of the system such as the initial energy or energy spectrum. It was claimed in Sreenivasan [123] that the asymptote was determined by the initial conditions and/or the forcing mechanism used. The results of Doering and Foias [151] are presented with the statement that the forcing is the primary influence on the Reynolds number-dependent shape of C_ε. The arguments and equation given here would allow such investigations to be carried out.

In tying the results to the arguments of the introduction, one can quantitatively examine the relationship between the energy in the low-k region, or large scales, of the energy spectrum. The shape of the initial or forced spectrum, or perhaps more importantly the distribution of energy among these wavenumbers, might be directly linked to the mechanisms found to be controlling the dissipation rate here. One could follow such arguments with those of Loitsianskii's [157] and Saffmann's [158] respective invariants to see how these quantities contribute to the behaviour of the dissipation rate.

As it has been developed here, the result above does not explicitly carry any information from the forcing, seemingly challenging the view expressed by Doering and Foias. However, the transfer spectrum would be heavily influenced by the forcing, and as demonstrated here this influence would then be felt in all the coefficients via their dependence on k_0. This would support the assertions made by Doering and Foias. It is believed that a direct connection can be established with the main result here and the upperbound on ε established in their paper. Further extensions could then be to use the results here to establish an equally rigorous bound for the time-dependent dissipation rate.

In the plots of C_Π in both decaying and stationary turbulence, one can find that there is a peak in the low-R region. This does not always exist in the unnormalised plots of $\Pi_{\max}$, and this appearance seems to be associated with the measurement time for the time-dependent computations. These findings are demonstrated in both the LET and DNS results. The belief is that this peak is associated with the initial energy spectrum similar to the peak of $\Pi_{\max}(t)$ (see fig. 5.4 in §5.2.2 of the previous chapter). This relationship between the initial energy spectrum and the occurrence of the peak in C_Π has not been established. Because it happens in the low-R regime, one may speculate that it indicates more accurately the emergence of the inertial interactions, suggesting a transition to turbulence. While the concept of turbulent transition seems vague in terms of HIT, this quantity can be sought in more conventional transition settings, such

as pipe flows, and may offer some insight into the mechanisms of turbulent transition.

6.A The Karman-Howarth Equation

First derived by von Kármán and Howarth in 1938[120], the Karman-Howarth equation has since become a fundamental equation in the study of homogeneous, isotropic turbulence. Any classic[25],[21] and contemporary[28],[24] texts which cover homogeneous, isotropic turbulence offer a derivation or summary derivation.

The starting point is to consider the Navier-Stokes equation for two spatial coordinates, $\mathbf{x}$ and $\mathbf{x}'$:

$$\partial_t u_\alpha(\mathbf{x},t) + \frac{\partial}{\partial \mathrm{x}_\gamma}\Big(u_\alpha(\mathbf{x},t)u_\gamma(\mathbf{x},t)\Big) = -\frac{1}{\rho}\frac{\partial}{\partial \mathrm{x}_\alpha}p(\mathbf{x},t) + \nu\frac{\partial^2}{\partial \mathrm{x}^2}u_\alpha(\mathbf{x},t) \tag{6.72}$$

$$\partial_t u_\beta(\mathbf{x}',t) + \frac{\partial}{\partial \mathrm{x}'_\gamma}\Big(u_\beta(\mathbf{x}',t)u_\gamma(\mathbf{x}',t)\Big) = -\frac{1}{\rho}\frac{\partial}{\partial \mathrm{x}'_\beta}p(\mathbf{x}',t) + \nu\frac{\partial^2}{\partial \mathrm{x}'^2}u_\beta(\mathbf{x}',t). \tag{6.73}$$

Both equations can be united into a single equation by summing and then averaging them, as in $\big\langle (6.72)\times u_\beta(\mathbf{x}',t) + (6.73)\times u_\alpha(\mathbf{x},t)\big\rangle$.

Since the space being considered is homogeneous, all quantities are functions of the distance between them. Writing $\mathbf{x}' = \mathbf{x} + \mathbf{r}$, changes the derivatives with respect to $\mathbf{x}$ and $\mathbf{x}'$. Replacing velocity-correlation functions with correlators leaves

$$\begin{aligned}\partial_t C_{\alpha\beta}(\mathbf{r};t) - \frac{\partial}{\partial \mathrm{r}_\gamma}\Big(C_{\alpha\gamma\beta}(\mathbf{r};t) - C_{\beta\gamma\alpha}(-\mathbf{r};t)\Big)\\ = -\frac{1}{\rho}\frac{\partial}{\partial \mathrm{r}_\gamma}\Big(\big\langle u_\beta(\mathbf{x}',t)p(\mathbf{x},t)\big\rangle\delta_{\gamma\beta} - \big\langle u_\alpha(\mathbf{x},t)p(\mathbf{x}',t)\big\rangle\delta_{\gamma\alpha}\Big) + 2\nu\frac{\partial^2}{\partial \mathrm{r}^2}C_{\alpha\beta}(\mathbf{r};t)\end{aligned} \tag{6.74}$$

It can be shown that under isotropy the pressure-velocity correlations will vanish [159]. Likewise, the triple-correlation is anti-symmetric under partiy, $C_{\beta\gamma\alpha}(-\mathbf{r};t) = -C_{\beta\gamma\alpha}(\mathbf{r};t)$. This leaves a much simpler equation to deal with,

$$\partial_t C_{\alpha\beta}(\mathbf{r};t) = \frac{\partial}{\partial \mathrm{r}_\gamma}\Big(C_{\alpha\gamma\beta}(\mathbf{r};t) + C_{\beta\gamma\alpha}(\mathbf{r};t)\Big) + 2\nu\frac{\partial^2}{\partial \mathrm{r}_\gamma^2}C_{\alpha\beta}(\mathbf{r};t). \tag{6.75}$$

By choosing a reference frame such that $\boldsymbol{u}(\mathbf{x}+\mathbf{r})\cdot\mathbf{r} = u_x(\mathbf{x}+\mathbf{r})\mathrm{r}$ with $\mathbf{r} = (\mathrm{r},0,0)$, one can make the following simplifications to the correlation functions without any loss of generality:

$$C_{\alpha\beta}(\mathrm{r},t) \;=\; U^3\bigg(f(\mathrm{r},t)\delta_{\alpha\beta} + \frac{\mathrm{r}}{2}f'(\mathrm{r},t)\delta_{\alpha\beta} - \frac{f'(\mathrm{r},t)}{2\mathrm{r}}\mathrm{r}_\alpha\mathrm{r}_\beta\bigg) \tag{6.76}$$

$$C_{\alpha\gamma\beta}(\mathrm{r},t) = U^3\Bigg(\frac{k(\mathrm{r},t)-\mathrm{r}k'(\mathrm{r},t)}{2\mathrm{r}^3}\mathrm{r}_\alpha\mathrm{r}_\beta\mathrm{r}_\gamma + \frac{2k(\mathrm{r},t)+\mathrm{r}k'(\mathrm{r},t)}{4\mathrm{r}}\big(\mathrm{r}_\alpha\delta_{\beta\gamma}+\mathrm{r}_\gamma\delta_{\alpha\beta}\big) - \frac{k(\mathrm{r},t)}{2\mathrm{r}}\mathrm{r}_\beta\delta_{\alpha\gamma}\Bigg). \tag{6.77}$$

The functions $f(\mathrm{r},t)$ and $k(\mathrm{r},t)$ are the logitudinal double- and triple-correlation functions

$$f(\mathrm{r},t) = \frac{1}{U(t)^2}\Big\langle\big(u_x(\mathrm{x}+\mathrm{r},t)u_x(\mathrm{x},t)\big)\Big\rangle, \tag{6.78}$$

$$k(\mathrm{r},t) = \frac{1}{U(t)^3}\Big\langle\big(u_x(\mathrm{x}+\mathrm{r},t)u_x(\mathrm{x},t)^2\big)\Big\rangle. \tag{6.79}$$

These nondimensional correlation functions are dependent only on the distance r between the points of measurement in a homogenous isotropic fluid.

Substituting these equations for the correlation functions into (6.75), and taking the trace over tensor indices, $\alpha=\beta$ returns

$$\partial_t\Bigg(\frac{U^2}{\mathrm{r}^2}\frac{\partial}{\partial\mathrm{r}}\big(\mathrm{r}^3 f\big)\Bigg) = \frac{U^3}{\mathrm{r}^2}\frac{\partial}{\partial\mathrm{r}}\Bigg(\frac{1}{\mathrm{r}}\frac{\partial}{\partial\mathrm{r}}\big(\mathrm{r}^4 k\big)\Bigg) + 2\nu\frac{U^2}{\mathrm{r}^2}\frac{\partial}{\partial\mathrm{r}}\Bigg(\mathrm{r}^2\frac{\partial}{\partial\mathrm{r}}\big(3f+\mathrm{r}f'\big)\Bigg). \tag{6.80}$$

Obtaining this result involves some nontrivial algebra which can be simplified by noting

$$C_{\alpha\alpha}(\mathrm{r},t) = \frac{U^2}{\mathrm{r}^2}\frac{\partial}{\partial\mathrm{r}}\big(\mathrm{r}^3 f\big), \tag{6.81}$$

$$\frac{\partial}{\partial\mathrm{r}_\gamma}C_{\alpha\gamma\alpha}(\mathrm{r},t) = \frac{U^3}{\mathrm{r}^2}\frac{\partial}{\partial\mathrm{r}}\Bigg(\frac{1}{\mathrm{r}}\frac{\partial}{\partial\mathrm{r}}\big(\mathrm{r}^4 k\big)\Bigg), \tag{6.82}$$

and using the spherical Laplacian

$$\frac{\partial^2}{\partial\mathrm{r}_\gamma^2} = \frac{1}{\mathrm{r}^2}\frac{\partial}{\partial\mathrm{r}}\mathrm{r}^2\frac{\partial}{\partial\mathrm{r}}. \tag{6.83}$$

Factoring out an r^{-2} term and integrating (6.85) over r gives

$$\partial_t\Big(U^2\mathrm{r}^3 f\Big) = \frac{U^3}{\mathrm{r}}\frac{\partial}{\partial\mathrm{r}}\big(\mathrm{r}^4 k\big) + 2\nu U^2\Bigg(\mathrm{r}^2\frac{\partial}{\partial\mathrm{r}}\big(3f+\mathrm{r}f'\big)\Bigg). \tag{6.84}$$

With a few further modifications, this becomes the celebrated Karman-Howarth equation,

$$\partial_t\big(U^2\mathrm{r}^4 f(\mathrm{r},t)\big) = U^3\frac{\partial}{\partial\mathrm{r}}\big(\mathrm{r}^4 k(\mathrm{r},t)\big) + 2\nu U^2\frac{\partial}{\partial\mathrm{r}}\big(\mathrm{r}^4 f'(\mathrm{r},t)\big). \tag{6.85}$$

The correlation functions can be related to the second- and third-order structure functions

$$\begin{aligned} S_2(\mathrm{r},t) &= \big\langle \big(u_x(\mathrm{x}+\mathrm{r},t)-u_x(\mathrm{x},t)\big)^2\big\rangle \\ &= \big\langle u_x(\mathrm{x}+\mathrm{r},t)^2+u_x(\mathrm{x},t)^2\big\rangle - 2\big\langle u_x(\mathrm{x}+\mathrm{r},t)u_x(\mathrm{x},t)\big\rangle \\ &= 2U(t)^2\big(1-f(\mathrm{r},t)\big) \end{aligned} \tag{6.86}$$

$$\begin{aligned} S_3(\mathrm{r},t) &= \big\langle \big(u_x(\mathrm{x}+\mathrm{r},t)-u_x(\mathrm{x},t)\big)^3\big\rangle \\ &= \big\langle u_x(\mathrm{x}+\mathrm{r},t)^3-u_x(\mathrm{x},t)^3\big\rangle + 3\big\langle u_x(\mathrm{x}+\mathrm{r},t)u_x(\mathrm{x},t)^2-u_x(\mathrm{x}+\mathrm{r},t)^2u_x(\mathrm{x},t)\big\rangle \\ &= 3\big\langle u_x(\mathrm{x}+\mathrm{r},t)u_x(\mathrm{x},t)^2+u_x(\mathrm{x}+\mathrm{r},t)u_x(\mathrm{x},t)^2\big\rangle \\ &= 6U(t)^3k(\mathrm{r},t). \end{aligned} \tag{6.87}$$

Substituting these into the Karman-Howarth equation gives

$$\partial_t\Big(U^2(t)-\frac{1}{2}S_2(\mathrm{r},t)\Big) = \frac{1}{6\mathrm{r}^4}\frac{\partial}{\partial \mathrm{r}}\big(\mathrm{r}^4S_3(\mathrm{r},t)\big) - \frac{\nu}{\mathrm{r}^4}\frac{\partial}{\partial \mathrm{r}}\big(\mathrm{r}^4\frac{\partial}{\partial \mathrm{r}}S_2(\mathrm{r},t)\big). \tag{6.88}$$

The mean velocity is related to the total (mean) kinetic energy, the time-derivative of which is directly proportional to the dissipation rate, hence the following relations can be made:

$$\partial_t U^2 = \frac{2}{3}\partial_t E = -\frac{2}{3}\varepsilon. \tag{6.89}$$

Inserting this into the (6.88) and some simple algebra reveals the result,

$$\varepsilon(t)+\frac{3}{4}\partial_t S_2(\mathrm{r},t) = -\frac{1}{4\mathrm{r}^4}\frac{\partial}{\partial r}\big[\mathrm{r}^4S_3(\mathrm{r},t)\big] + \frac{3\nu}{2\mathrm{r}^4}\frac{\partial}{\partial r}\big[\mathrm{r}^4\frac{\partial}{\partial r}S_2(\mathrm{r},t)\big]. \tag{6.90}$$

Chapter 7

Conclusions

The work detailed in this thesis covers various areas in turbulence research, beginning and ending on two largely different subjects: statistical closure formalisms and turbulent dissipation.

The first chapter introduces the main aspects of turbulence research that this work has been concerned with.

The second chapter details the need to deal with the Navier-Stokes equations in a statistical formalism that treats the closure problem found in nonlinear statistical equations. The formalisms presented there can define a foundation from which to construct or refine other renormalised perturbation theories.

One such theory, the Local energy transfer (LET) theory, is given in chapter 3. The numerical solution of the LET, resulting in the creation of the LET2008 code, is demonstrated there. Using such a computational model, the LET theory can be solved to obtain predictions for systems of freely-decaying and forced turbulence.

Chapter 4 extends the previous abilities of the LET by considering larger Reynolds numbers. These extensions provide a larger range of turbulent behaviours to observe, such as turbulent dissipation.

When investigating the quantities that demonstrate these behaviours, it was shown in chapter 5 that one needs to consider when to take measurements that appropriately characterise the turbulent dynamics of decaying systems.

The results of chapter 5 are then employed in chapter 6, where the LET2008 is used to investigate the phenomenon of turbulent dissipation.

Establishing such connections in seemingly disparate topics provides a theme of how important multiple perspectives are in turbulent research as well as establishing a few of the many attempts to approach this challenging subject.

More detailed summaries of the new work that has been developed in this thesis are given below.

7.1 Field-Theoretic Statistical Closures

Chapter 2 addresses the closure problem of a statistical treatment of homogeneous isotropic turbulence (HIT) and in doing so presents two formalisms. These formalisms which are based on techniques primarily developed for quantum field theory, have be applied to turbulence.

7.1.1 Wyld and MSR

The formalisms of Wyld and Martin, Siggia, and Rose (MSR) have been separated by the notion that Wyld's formalism is incorrect. However, it is stated in this chapter that Wyld's formalism has been misunderstood, and it is demonstrated that the result is equivalent to that obtained using the MSR formalism.

The work detailed in chapter 2 applies Wyld's formalism to the fully 3-D Navier-Stokes equations for incompressible HIT. It shows that using a different but equivalent version of the correlation equation aids in creating a consistent renormalisation procedure that explicitly obtains the exact (or renomalised) propagator equation introduced by Lee as well as reproducing the DIA equations.

The formalism of MSR is also presented along with its diagrammatic treatment of the Navier-Stokes equation. It is shown through a detailed analysis that the narrative of their paper is not clear when dealing with the NSE but their formalism does reproduce the diagrams of the primitive (or bare) correlator expansion.

The main conclusion to be drawn from this chapter is that the two formalisms produce the same set of results for the Navier-Stokes equations. This rectifies a long-standing debate which has discredited Wyld and possibly discouraged a relatively simpler but equivalent technique to be used.

While these claims are made, it must be observed that they have only been justified to fourth-order in the bare vertex expansion; future work should verify these claims to higher and even all orders if possible.

7.2 The Local Energy Transfer Theory

The LET is a closure theory for HIT which uses a fluctuation-dissipation relation to connect single- and two-time correlation functions. Chapters 3 and 4 give the re-development, testing, and implementation of a numerical solution of the LET in what

is called LET2008. This updated version of the LET code has been tested against previous LET results and DNS data for decaying turbulence up to moderate Reynolds numbers. The code can also be used for stationary turbulence, though the testing of this is made with comparisons to the previous version of the LET code.

Higher Reynolds numbers were attained with LET2008, the details are given in chapter 4. These are the largest Reynolds number achieved for the LET where the computation has been run for a sufficient amount of time enabling the development of an inertial range. The results for freely-decaying computations show an inertial range however the slope of this range, $\partial E(\mathrm{k}, t)/\partial \mathrm{k}$, is incompatible with the Kolmogorov prediction. In contrast, for similarly high Reynolds numbers, the results from forced-turbulence computations show that the LET does produce a Kolmogorov inertial range.

The contradictory results of the LET2008's inertial range require additional work to confirm these findings. A full assessment of the LET through similar calculations can be made to understand why such discrepancies exist. This could then be used to refine and improve the theory.

7.3 Turbulent Dissipation

The subject of turbulent dissipation is found in the chapters 5 and 6 of this thesis. An investigation has been undertaken that uses the LET to study turbulent dissipation in decaying and forced turbulence. Chapter 5 notes that in order to study this phenomenon appropriately, one must take measurements that accurately describe a freely-decaying turbulent system. The following chapter uses the methods of chapter 5 to compute the dissipation rate according to the LET.

7.3.1 Evolved Turbulence from Free-Decay

It is noted in chapter 5 that quantities of a time-dependent system, such as the dissipation rate $\varepsilon(t)$, can only be taken at a single time to have meaning when finding relationships between them and the Reynolds number, as is the case with the normalised dissipation rate, $C_\varepsilon(R)$.

The arguments presented in chapter 5 use what are considered common behaviours of freely-decaying turbulent fields to establish a time when the system is said to be sufficiently evolved into a turbulent state. These times can be used to measure the system or as references times from which to construct later times when measurements can be made.

The method developed here produces a measurement time that is based on the movement of energy through the wavenumber spectrum of a turbulent fluid. It fulfils a

criterion used for other studies of decaying turbulence that seeks to make a measurement when the total kinetic energy and dissipation rates show a power-law decay. This method has been briefly tested in noting that the values it gives for the normalised dissipation rate using the LET are acceptable with those obtained for experimental and numerical studies.

Future studies suggested for this would see this method applied to both experimental and numerical investigations where more realistic comparisons can be made.

7.3.2 Redefining the Dissipative Anomaly

In studying turbulent dissipation in chapter 6, the notion of anomalous dissipation was encountered. This phenomenon shows a non-vanishing dissipation rate exists when the viscosity is taken to be negligible.

An equation for the normalised dissipation rate is introduced in this chapter. This equation is based on the spectral energy balance equation and is an extension of the earlier work of McComb. It is applicable to both decaying and forced turbulence, and predicts a difference in behaviour of C_ε for decaying and forced systems.

The equation for the normalised dissipation rate can be computed using the LET, and provides a means to access the mechanisms behind the turbulent dissipation rate. The results of the chapter show the behaviour of these quantities as functions of Reynolds numbers. The explanations proposed suggest that the asymptotic behaviour of C_ε is a consequence of the rate of maximum energy flux and are augmented by the time derivative of spectral energy in decaying turbulence.

The conclusions of this chapter support the view of McComb that labelling such a phenomenon an anomaly is misleading as there is seemingly nothing anomalous about it. A clarification must therefore be made when using this phrase to refer to finite dissipation in the vanishing viscosity limit.

As the chapter primarily uses the LET to support its claims, additional work is required to confirm these results as the current use of DNS does not reach the Reynolds numbers and the performance of the LET at these Reynolds numbers is questionable. It was seen that the behaviour of the quantity A_2 has very different behaviour for forced and decaying turbulence, and this behaviour is significant at larger Reynolds numbers.

Bibliography

[1] K. R. Sreenivasan. Fluid turbulence. *Rev. Mod. Phys.*, 71:S383, 1999.

[2] A. Yaglom. The century of turbulence theory: The main achievements and unsolved problems. *New trends in turbulence Turbulence: nouveaux aspects*, pages 1–52.

[3] H. K. Moffatt. G. K. Batchelor and the homogenization of turbulence. *Annual Review of Fluid Mechanics*, 34(1):19–35, 2002.

[4] P. D. Stein and H. N. Sabbah. Turbulent blood flow in the ascending aorta of humans with normal and diseased aortic valves. *Circulation Research*, 39(1):58, 1976.

[5] M. X. Li, J. J. Beech-Brandt, L. R. John, P. R. Hoskins, and W. J. Easson. Numerical analysis of pulsatile blood flow and vessel wall mechanics in different degrees of stenoses. *Journal of Biomechanics*, 40(16):3715 – 3724, 2007.

[6] D. M. Sforza, C. M. Putman, and J. R. Cebral. Hemodynamics of cerebral aneurysms. *Annu. Rev. of Fluid Mech.*, 2008.

[7] A. Christen. *Atmospheric turbulence and surface energy exchange in urban environments*. Wepf, 2005.

[8] A. F. Tuck. *Atmospheric turbulence: a molecular dynamics perspective*. Oxford University Press, USA, 2008.

[9] T. N. Palmer and P. D. Williams. Introduction. Stochastic physics and climate modelling. *Philosophical Transactions of the Royal Society A: Mathematical, Physical and Engineering Sciences*, 366(1875):2419, 2008.

[10] S. P. Arya. *Air pollution meteorology and dispersion*. Oxford University Press Oxford., 1999.

[11] P. E. Dimotakis. Turbulent Mixing. *Annu. Rev. Fluid Mech*, 37:329–56, 2005.

[12] C. M. White and M. G. Mungal. Mechanics and Prediction of Turbulent Drag Reduction with Polymer Additives. *Annual Review of Fluid Mechanics*, 40:235–256, 2008.

[13] K. Kim, R. J. Adrian, S. Balachandar, and R. Sureshkumar. Dynamics of hairpin vortices and polymer-induced turbulent drag reduction. *Physical review letters*, 100(13):134504, 2008.

[14] M. S. Miesch and J. Toomre. Turbulence, Magnetism, and Shear in Stellar Interiors. *Annual Review of Fluid Mechanics*, 41:317–345, 2009.

[15] A. Brandenburg and A. Nordlund. Astrophysical turbulence. *Arxiv preprint arXiv:0912.1340*, 2009.

[16] A. R. Vasavada and A. P. Showman. Jovian atmospheric dynamics: An update after Galileo and Cassini. *Reports on Progress in Physics*, 68:1935, 2005.

[17] D. Grasso and H. R. Rubinstein. Magnetic fields in the early Universe. *Physics Reports*, 348:163–266, 2001.

[18] G. Gogoberidze, T. Kahniashvili, and A. Kosowsky. Spectrum of gravitational radiation from primordial turbulence. *Physical Review D*, 76(8):83002, 2007.

[19] H. Sohr. *The NavierStokes Equations An Elementary Functional Analytic Approach*. Birkhuser Verlag, 2001.

[20] C. Foias, O. Manley, R. Rosa, R. Temam, and C. Foias. Navier-Stokes equations and turbulence. *Physics Today*, 2001.

[21] L. D. Landau and E. M. Lifshitz. *Fluid Mechanics*. Pergamon Press, London, English edition, 1959.

[22] B.K. Shivamoggi. *Theoretical fluid dynamics*. Wiley-Interscience, 1998.

[23] P. G. Drazin and W. H. Reid. *Hydrodynamic stability*. Cambridge Univ Pr, 2004.

[24] P. A. Davidson. *Turbulence*. Oxford University Press, 2004.

[25] G. K. Batchelor. *The theory of homogeneous turbulence*. Cambridge University Press, Cambridge, 2nd edition, 1971.

[26] H. Tennekes and J. L. Lumley. *A first course in turbulence*. The MIT press, 1972.

[27] M. Lesieur. *Turbulence in fluids*. Springer Verlag, 1rst edition, 1990.

[28] S. B. Pope. *Turbulent flows*. Cambridge Univ Pr, 2000.

[29] O. Darrigol. *Worlds of flow: A history of hydrodynamics from the Bernoullis to Prandtl*. Oxford, 2001.

[30] G. Gallavotti. *Foundations of fluid dynamics*. Texts and Monographs in Physics, 2001.

[31] C. R. Doering. The 3D Navier-Stokes Problem. 2008.

[32] 2000. `http://www.claymath.org/millennium/Navier-Stokes_Equations/`.

[33] S. F. Edwards. The statistical dynamics of homogeneous turbulence. *J. of Fluid Mech.*, 18:239, 1964.

[34] P. Sagaut and C. Cambon. *Homogeneous turbulence dynamics*. Cambridge University Press, 2008.

[35] W. D. McComb. *The Physics of Fluid Turbulence*. Oxford University Press, 1990.

[36] C. Canuto, M. Y. Hussaini, A. Quarteroni, and T. A. Zang. *Spectral methods in fluid dynamics*. Springer New York, 1988.

[37] J. Mathews and R. L. Walker. *Mathematical methods of physics*. WA Benjamin New York, 1970.

[38] G. B. Arfken and H. J. Weber. *Mathematical methods for physicists*. Academic Pr, 2001.

[39] A. N. Kolmogorov. The local structure of turbulence in incompressible viscous fluid for very large reynolds numbers. *Proceedings of the Royal Society in London: Mathematical and Physical Sciences*, 434(1890):9, 1991.

[40] A. N. Kolmogorov. Dissipation of energy in the locally isotropic turbulence. *Proceedings of the Royal Society in London: Mathematical and Physical Sciences*, 434(1890):15, 1991.

[41] L. F. Richardson. *Weather Prediction by Numerical Process*. Cambridge University Press, 1922.

[42] L. Landau. On the problem of turbulence. *CR (Dokl.) Acad. Sci. URSS, n. Ser.*, 44:311–314, 1944.

[43] A. N. Kolmogorov. A refinement of previous hypotheses concerning the local structure of turbulence in a viscous incompressible fluid at high Reynolds number. *J. Fluid Mech.*, 13:82–85, 1962.

[44] U. Frisch. *Turbulence: The Legacy of A. N. Kolmogorov*. Cambridge University Press, Cambridge, 1995.

[45] JC Vassilicos. *Intermittency in turbulent flows*. Cambridge Univ Pr, 2001.

[46] M. D. Millionshchikov. On the theory of homogeneous isotropic turbulence. *Dokl. Akad. Nauk SSSR*, 32(9), 1941.

[47] I. Proudman and W. H. Reid. On the decay of a normally distributed and homogeneous turbulent velocity field. *Philosophical Transactions of the Royal Society of London. Series A, Mathematical and Physical Sciences*, 247(926):163–189, 1954.

[48] Y. Ogura. A consequence of the zero-fourth-cumulant approximation in the decay of isotropic turbulence. *J. of Fluid Mech.*, 16:33–40, 1963.

[49] D. C. Leslie. *Developments in the Theory of Turbulence*. Clarendon Press, 1973.

[50] R. H. Kraichnan. Relation of fourth-order to second-order moments in stationary isotropic turbulence. *The Physical Review*, 107(6):1485, 15 September 1957.

[51] R. H. Kraichnan. Irreversible statistical mechanics of incompressible hydromagnetic turbulence. *The Physical Review*, 109(5):1407, March 1958.

[52] R. H. Kraichnan. The structure of isotropic turbulence at very high reynolds numbers. *J. of Fluid Mech.*, 5:497, 1959.

[53] M. Beran. *Statistical Continuum Theories*. Interscience Publishers, 1968.

[54] S. Kida and S. Goto. A Lagrangian direct-interaction approximation for homogeneous isotropic turbulence. *J. of Fluid Mech.*, 345:307–345, 1997.

[55] J. A. Krommes. Fundamental statistical description of plasma turbulence in magnetic fields. *Physics Reports*, 360:1, 2002. Section 6.

[56] R. H. Kraichnan. Relation between Lagrangian and Eulerian Correlation Times of a Turbulent Velocity Field. *Phys. Fluids*, 7(1):142–143, 1964.

[57] R. H. Kraichnan. Isotropic turbulence and inertial-range structure. *Phys. Fluids*, 9(9):1728, 1966.

[58] P. C. Martin, E. D. Siggia, H. A. Rose. Statistical dynamics of classical systems. *Physical Review A*, 8(1):423, July 1973.

[59] H. W. Wyld. Formulation of the theory of turbulence in an incompressible fluid. *Annals of Physics*, 14:143, 1961.

[60] J. R. Herring. Self-consistent-field approach to turbulence theory. *Physics of Fluids*, 8:2219, 1965.

[61] J. R. Herring. Self-Consistent-Field Approach to Nonstationary Turbulence. *Physics of Fluids*, 9:2106, 1966.

[62] T. Nakano. A theory of homogeneous, isotropic turbulence of incompressible fluids* 1. *Annals of Physics*, 73(2):326–371, 1972.

[63] R. H. Kraichnan. Lagrangian-history closure approximation for turbulence. *Phys. Fluids*, 8(4):575, April 1965.

[64] S. A. Orszag. Analytical theories of turbulence. *J. of Fluid Mech.*, 41(02):363–386, 2006.

[65] Y. Kaneda. Renormalized expansions in the theory of turbulence with the use of the lagrangian position function. *J. of Fluid Mech.*, 107:131, 1981.

[66] Y. Kaneda. Renormalized expansions in the theory of turbulence with the use of the Lagrangian position function. *J. of Fluid Mech.*, 107:131–145, 2006.

[67] J. S. Frederiksen and A. G. Davies. Dynamics and spectra of cumulant update closures for two-dimensional turbulence. *Geophys. Astrophys. Fluid Dynamics*, 92:197, 2000.

[68] T. J. O'Kane and J. S. Frederiksen. The QDIA and regularized QDIA closures for inhomogeneous turbulence over topography. *J. Fluid Mech.*, 504:133, 2004.

[69] J. S. Frederiksen and A. G. Davies. The Regularized DIA Closure For Two-Dimensional Turbulence. *Geophys. Astrophys. Fluid Dynamics*, 98:203, 2004.

[70] J. S. Frederiksen and T. J. O'Kane. Inhomogeneous closure and statistical mechanics for Rossby wave turbulence over topography. *J. Fluid. Mech.*, 539:137–165, 2005.

[71] E. V. Teodorovich. On the yakhot-orszag theory of turbulence. *Fluid Dynamics*, 29(6):770, 1994.

[72] M. E. Peskin and D. V. Schroeder. *An introduction to quantum field theory*. Westview Pr, 1995.

[73]

[74] L. L. Lee. A formulation of the theory of isotropic hydromagnetic turbulence in an incompressible fluid. *Annals of Physics*, 32:292, 1965.

[75] J. Schwinger. On the Green's Functions of Quantized Fields: I. *Proceedings of the National Academy of Sciences of the United States of America*, 37(7):452, 1951.

[76] J. Schwinger. On the Green's Functions of Quantized Fields: II. *Proceedings of the National Academy of Sciences of the United States of America*, 37(7):455, 1951.

[77] J. Schwinger. The Theory of Quantized Fields. I. *Physical Review*, 82:914–927, 1951.

[78] R. V. Jensen. Functional integral approach to slassical statistical dynamics. *Journal of Statistical Physics*, 25(2):183, 1981.

[79] H. A. Rose. *Aspects of the statistical dynamics of classical systems*. PhD thesis, Harvard University, 1974.

[80] R. Phythian. The operator formalism of classical statistical dynamics. *Journal of Physics A: Mathematical and General*, 8:1423–1432, 1975.

[81] R. Phythian. Further application of the Martin, Siggia, Rose formalism. *Journal of Physics A: Mathematical and General*, 9:269–281, 1976.

[82] R. Phythian. The functional formalism of classical statistical dynamics. *Journal of Physics A: Mathematical and General*, 10:777–789, 1977.

[83] H. C. Andersen. Functional and graphical methods for classical statistical dynamics. I. A formulation of the Martin–Siggia–Rose method. *Journal of Mathematical Physics*, 41:1979, 2000.

[84] G. L. Eyink. Action principle in nonequilibrium statistical dynamics. *Physical Review E*, 54(4):3419–3435, 1996.

[85] G. L. Eyink. Turbulence noise. *Journal of Statistical Physics*, 83(5):955–1019, 1996.

[86] A. Berera and D. Hochberg. Galilean invariance and homogeneous anisotropic randomly stirred flows. *Physical Review E*, 72(5):57301, 2005.

[87] A. Berera and D. Hochberg. Gauge symmetry and Slavnov-Taylor identities for randomly stirred fluids. *Physical review letters*, 99(25):254501, 2007.

[88] A. Berera and D. Hochberg. Gauge fixing, BRS invariance and Ward identities for randomly stirred flows. *Nuclear Physics, Section B*, 814(3):522–548, 2009.

[89] J. Schwinger. Quantum electrodynamics. I. A covariant formulation. *Physical Review*, 74(10):1439–1461, 1948.

[90] F. J. Dyson. The S-matrix in quantum electrodynamics. *Physical Review*, 75(11):1736–1755, 1949.

[91] L. Machiels. Predictability of small-scale motion in isotropic fluid turbulence. *Physical Review Letters*, 79(18):3411–3414, 1997.

[92] C. R. Doering and N. Petrov. Low-wavenumber forcing and turbulent energy dissipation. *Progress in Turbulence*, pages 11–18, 2004.

[93] S. S. Schweber. Feynman and the visualization of space-time processes. *Reviews of Modern Physics*, 58(2):449–508, 1986.

[94] W. D. McComb. Local energy transfer. *Proceedings from the Royal Society in Edinburgh A*, 72:18, 1974.

[95] W. D. McComb. The inertial range spectrum from a local energy transfer theory of isotropic turbulence. *J.Phys.A*, 9:179, 1976.

[96] W. D. McComb. A theory of time dependent, isotropic turbulence. *J.Phys.A:Math.Gen.*, 11(3):613, 1978.

[97] W. D. McComb, V. Shanmugasundaram, and P. Hutchinson. Velocity derivative skewness and two-time velocity correlations of isotropic turbulence as predicted by the LET theory. *J. Fluid Mech.*, 208:91, 1989.

[98] W. D. McComb, M. J. Filipiak, and V. Shanmugasundaram. Rederivation and further assessment of the LET theory of isotropic turbulence, as applied to passive scalar convection. *J. Fluid Mech.*, 245:279–300, 1992.

[99] Davies A. G. Bell R. C. Frederiksen, J. S. Closure equations with non-gaussian restarts for truncated two-dimensional turbulence. *Physics of Fluids*, 6:31533163, 1994.

[100] W. D. McComb and V. Shanmugasundaram. Numerical calculations of decaying isotropic turbulence using the LET theory. *J. Fluid Mech.*, 143:95–123, 1984.

[101] A. P. Quinn. *Local Energy Transfer theory in forced and decaying isotropic turbulence*. PhD thesis, University of Edinburgh, 2000.

[102] W. D. McComb and A. P. Quinn. Two-point, two-time closures applied to forced isotropic turbulence. *Physica A Statistical Mechanics and its Applications*, 317:487–508, January 2003.

[103] W. D. McComb, 2010. Personal communication.

[104] M. Oberlack, W. D. McComb, and A.P. Quinn. Solution of functional equations and reduction of dimension in the local energy transfer theory of incompressible, three-dimensional turbulence. *Phys. Rev. E*, 63:026308–1, 2001.

[105] K. Kiyani and W. D. McComb. Time-ordered fluctuation-dissipation relation for incompressible isotropic turbulence. *Phys. Rev. E*, 70(6):066303, Dec 2004.

[106] R. V. R. Pandya. Simplification of local energy transfer theory of incompressible, isotropic, nonstationary turbulence. *Physical Review E*, 70(6):66307, 2004.

[107] R. V. R. Pandya. Model representation for self-consistent-field theory of isotropic turbulence. *Arxiv preprint cond-mat/0401227*, 2004.

[108] W. D. McComb and K. Kiyani. Eulerian spectral closures for isotropic turbulence using a time-ordered fluctuation-dissipation relation. *Phys. Rev. E*, 72(1):016309, Jul 2005.

[109] H. Lomax, T.H. Pulliam, D.W. Zingg, T.H. Pulliam, and D.W. Zingg. *Fundamentals of computational fluid dynamics*. Springer Berlin, 2001.

[110] T. J. Chung. *Computational fluid dynamics*. Cambridge University Press, 2002.

[111] G. I. Taylor. Statistical Theory of Turbulence. *Royal Society of London Proceedings Series A*, 151:421–444, September 1935.

[112] J. R. Herring and R. H. Kraichnan. Comparison of some approximations for isotropic turbulence. *Statistical models and turbulence*, pages 148–194, 1972.

[113] R. H. Kraichnan. Decay of isotropic turbulence in the Direct-Interaction Approximation. *Phys. Fluids*, 7(7):1030–1048, 1964.

[114] S. Yoffe, 2009-2010. Personal communication of DNS results.

[115] J. P. Bertoglio, K. Squires, and J. H. Ferziger. EDQNM closure: A homogeneous simulation to support it. A quasi-homogeneous simulation to disprove it. In *In Stanford Univ., Studying Turbulence Using Numerical Simulation Databases. Proceedings of the 1987 Summer Program p 53-62 (SEE N88-23086 16-34)*, pages 53–62, 1987.

[116] L. van Haren, C. Staquet, and C. Cambon. Decaying stratified turbulence: comparison between a two-point closure EDQNM model and direct numerical simulations. *Dynamics of Atmospheres and Oceans*, 23(1-4):217–233, 1996.

[117] O. Leuchter and C. Cambon. EDQNM and DNS predictions of rotation effects in strained axisymmetric turbulence. In *Symposium on Turbulent Shear Flows, 11 th, Grenoble, France*, pages 31–7, 1997.

[118] G. L. Eyink and D. J. Thomson. Free decay of turbulence and breakdown of self-similarity. *Physics of Fluids*, 12:477, 2000.

[119] M. Lesieur and S. Ossia. 3D isotropic turbulence at very high Reynolds numbers: EDQNM study. *Journal of Turbulence*, 1(7):1–25, 2000.

[120] T. von Kármán and L. Howarth. On the statistical theory of isotropic turbulence. *Royal Society of London Proceedings Series A*, 164, 1938.

[121] K. R. Sreenivasan. On the universality of the Kolmogorov constant. *Phys. Fluids*, 7:2778, 1995.

[122] P. K. Yeung and Y. Zhou. Universality of the Kolmogorov constant in numerical simulations of turbulence. *Phys. Rev. E*, 56:1746, 1997.

[123] K. R. Sreenivasan. An update on the energy dissipation rate in isotropic turbulence. *Phys. Fluids*, 10:528, 1998.

[124] B. R. Pearson, P.-Å . Krogstad, and W. van de Water. Measurements of the turbulent energy dissipation rate. *Physics of Fluids*, 14(3):1288–1290, 2002.

[125] W. J. T. Bos, L. Shao, and J.-P. Bertoglio. Spectral imbalance and the normalized dissipation rate of turbulence. *Physics of Fluids*, 19(4):045101, 2007.

[126] K. R. Sreenivasan. On the scaling of the turbulence energy dissipation rate. *Physics of Fluids*, 27:1048, 1984.

[127] L.-P. Wang, S. Chen, J. G. Brasseur, and J. C. Wyngaard. Examination of hypotheses in the kolmogorov refined turbulence theory through high-resolution simulations. part 1. velocity field. *J. of Fluid Mech. Digital Archive*, 309(-1):113–156, 1996.

[128] G. Birkhoff. Fourier Synthesis of Homogeneous Turbulence. In *Transactions of symposium in applied mathematics*, page 19. Interscience Publishers, 1954.

[129] G. Comte-Bellot and S. Corrsin. The use of a contraction to improve the isotropy of grid-generated turbulence. *J. of Fluid Mech.*, 25(04):657–682, 2006.

[130] P. G. Saffman. Note on decay of homogeneous turbulence. *Physics of Fluids*, 10(6):1349, 1967.

[131] V. Yakhot. Decay of three-dimensional turbulence at high reynolds numbers. *J. of Fluid Mech.*, 505:87, 2004.

[132] W. Bos, 2009. Personal communication.

[133] Z. Warhaft. Turbulence in nature and in the laboratory. *Proceedings of the National Academy of Sciences*, 99(Suppl 1):2481, 2002.

[134] B. Eckhardt, T. M. Schneider, B. Hof, and J. Westerweel. Turbulence transition in pipe flow. *Annu. Rev. of Fluid Mech.*, 2006.

[135] R. R. Kerswell. Recent progress in understanding the transition to turbulence in a pipe. *Nonlinearity*, 18(6):17, 2005.

[136] B. Hof, A. de Lozar, M. Avila, X. Tu, and T. M. Schneider. Eliminating Turbulence in Spatially Intermittent Flows. *Science*, 327(5972):1491, 2010.

[137] G. L. Eyink. Local 4/5-law and energy dissipation anomaly. *Nonlinearity*, 16:137–145, 2003.

[138] D. A. Donzis, K. R. Sreenivasan, and P. K. Yeung. Scalar dissipation rate and dissipative anomaly in isotropic turbulence. *J. of Fluid Mech.*, 532(-1):199–216, 2005.

[139] R. E. Seoud and J. C. Vassilicos. Dissipation and decay of fractal-generated turbulence. *Physics of Fluids*, 19(10):105108, October 2007.

[140] G. Falkovich and K. R. Sreenivasan. Lessons from hydrodynamic turbulence. *Physics Today*, page 43, April 2006.

[141] G. L. Eyink. Dissipative anomalies in singular Euler flows. *Physica D: Nonlinear Phenomena*, 237(14-17):1956–1968, 2008.

[142] G. Eyink. Zeroth Law of Turbulence. In *Physics of Hydrodynamic Turbulence Program, Institute for Theoretical Physics, Santa Barbara, CA. April 18,*, 2000.

[143] B. R. Pearson, T. A. Yousef, N. E. L. Haugen, A. Brandenburg, and P. A. Krogstad. The" zeroth law" of turbulence: Isotropic turbulence simulations revisited. *Arxiv preprint physics/0404114*, 2004.

[144] T. Gotoh, D. Fukayama, and T. Nakano. Velocity field statistics in homogeneous steady turbulence obtained using a high-resolution direct numerical simulation. *Physics of Fluids*, 14:1065, 2002.

[145] Y. Kaneda, T. Ishihara, M. Yokokawa, K. Itakura, and A. Uno. Energy dissipation rate and energy spectrum in high resolution direct numerical simulations of turbulence in a periodic box. *Physics of Fluids*, 15(2):L21–L24, 2003.

[146] P. Burattini, P. Lavoie, and R. A. Antonia. On the normalized turbulent energy dissipation rate. *Physics of Fluids*, 17(9):098103–+, September 2005.

[147] N. Mazellier and J. C. Vassilicos. The turbulence dissipation constant is not universal because of its universal dependence on large-scale flow topology. *Physics of Fluids*, 20(1):015101–+, January 2008.

[148] S. Goto and J. C. Vassilicos. The dissipation rate coefficient of turbulence is not universal and depends on the internal stagnation point structure. *Physics of Fluids*, 21(3):035104, 2009.

[149] D. Lohse. Crossover from high to low Reynolds number turbulence. *Physical review letters*, 73(24):3223–3226, 1994.

[150] H. Effinger and S. Grossmann. Static structure function of turbulent flow from the Navier-Stokes equations. *Zeitschrift für Physik B Condensed Matter*, 66(3):289–304, 1987.

[151] C. R. Doering and C. Foias. Energy dissipation in body-forced turbulence. *J. of Fluid Mech.*, 467:289–306, September 2002.

[152] C. R. Doering, B. Eckhardt, and J. Schumacher. Energy dissipation in body-forced plane shear flow. *J. of Fluid Mech.*, 494:275–284, 2003.

[153] B. Rollin, Y. Dubief, and C. R. Doering. Variation on the Kolmogorov Forcing: Asymptotic Dissipation Rate Driven by Harmonic Forcing. *Arxiv preprint arXiv:0903.1897*, 2009.

[154] A. Cheskidov, C. R. Doering, and N. P. Petrov. Energy dissipation in fractal-forced flow. *Journal of Mathematical Physics*, 48:065208, 2007.

[155] W. D. McComb. Taylors dissipation surrogate and its associated anomaly. *"Taylor's dissipation surrogate and its associated anomaly",submitted to J. Phys A*, 2009.

[156] W. D. McComb, A. Berera, M. Salewski, and S. Yoffe. An exact expression for the Reynolds number dependence of the energy dissipation rate in homogeneous, isotropic turbulence. *Arxiv preprint arXiv:1002.2131*, 2010.

[157] L. G. Loitsyanskii. Some basic laws for isotropic turbulent flow. *Trudy Tsentr. Aero.*, 1939.

[158] P. G. Saffmann. The large-scale structure of homogeneous turbulence. *J. Fluid Mech.*, 27:581–593, 19867.

[159] A. S. Monin and A. M. Yaglom. *Statistical fluid mechanics*. MIT Pr., 1987.